Springer Series in Materials Science 185

Vitaly Yu. Topolov
Paolo Bisegna
Christopher R. Bowen

Piezo-Active Composites

Orientation Effects and Anisotropy Factors

Springer

Springer Series in Materials Science

Volume 185

For further volumes:
http://www.springer.com/series/856

The Springer Series in Materials Science covers the complete spectrum of materials physics, including fundamental principles, physical properties, materials theory and design. Recognizing the increasing importance of materials science in future device technologies, the book titles in this series reflect the state-of-the-art in understanding and controlling the structure and properties of all important classes of materials.

Vitaly Yu. Topolov · Paolo Bisegna
Christopher R. Bowen

Piezo-Active Composites

Orientation Effects and Anisotropy Factors

Springer

Vitaly Yu. Topolov
Department of Physics
Southern Federal University
Rostov-on-Don
Russia

Christopher R. Bowen
Department of Mechanical Engineering
University of Bath
Somerset, Bath
UK

Paolo Bisegna
Department of Civil Engineering
and Computer Science
University of Rome "Tor Vergata"
Rome
Italy

ISSN 0933-033X ISSN 2196-2812 (electronic)
ISBN 978-3-642-38353-3 ISBN 978-3-642-38354-0 (eBook)
DOI 10.1007/978-3-642-38354-0
Springer Heidelberg New York Dordrecht London

Library of Congress Control Number: 2013942983

Printed on acid-free paper

Springer is part of Springer Science+Business Media (www.springer.com)

To our colleagues, friends and loved ones

Preface

… functional composites make use of a number of underlying ideas including connectivity patterns leading to field and force concentration; the use of periodicity and scale in resonant structures; the symmetry of composite structures and its influence on physical properties; polychromatic percolation and coupled conduction paths; varistor action and other interfacial effects; sum, combination, and product properties; coupled phase transformation phenomena; and the important role that porosity and inner composites play in composite materials.

R. E. Newnham

… The essence of science: ask an impertinent question, and you are on the way to a pertinent answer.

J. Bronowski

After the well-known discoveries of piezoelectricity (1880) and ferroelectricity (1921), new active dielectric materials with a high performance have been created to meet the many demands of modern applications. Among these materials one can highlight poled ferroelectric ceramics, composites based on ferroelectrics and thin ferroelectric films. Composites based on ferroelectrics (i.e., heterogeneous materials that contain two or more components and are characterized by ferro-, piezo-, pyroelectric, and other important properties) have been manufactured and studied since the late 1970s. These materials are characterized by various electromechanical properties and a remarkable ability to convert mechanical energy into electric energy and vice versa. Due to various adaptive characteristics and possibilities to vary and tailor their properties in external fields, composite materials have been regarded as an important group of smart materials. The complex and intricate interconnections between microstructure, composition, and physical properties of the ferroelectric composites stimulates studies to predict and interpret the properties and related parameters of these materials under various conditions. These studies need a multi-disciplinary effort of specialists working in such areas as solid-state physics, physics of active dielectrics, materials science, mechanics of heterogeneous media, mechanics of electro-elastic media, mechanical engineering, computational materials science, etc. These studies are impossible without a good

physics–mathematical basis and understanding the principles of modern materials science and mechanical engineering.

This monograph is devoted to the analysis of the *microgeometry—properties—anisotropy* relations in modern piezo-active composites, and this analysis broadens the well-known materials science concepts on the *composition—structure—properties* relations. The advantages of the piezoelectric performance of the composites are discussed in the context of the orientation effects, first studied for three main connectivity patterns (2–2, 1–3, and 0–3). A link between the orientation effects and the anisotropy of effective piezoelectric coefficients and electromechanical coupling factors is also discussed in this monograph. Its novelty consists of the first systematization of many authors' results on the orientation effects, the anisotropy of the piezoelectric properties and their role in forming the considerable hydrostatic piezoelectric coefficients, electromechanical coupling factors, and other parameters in the composites based on either ferroelectric ceramics or relaxor-ferroelectric single crystals.

To the best of our knowledge, there are few monographs concerned with the piezo-active composites and their effective properties. Moreover, the orientation effects were not described in these monographs. Two monographs devoted to methods for prediction of the effective electromechanical properties for some connectivity patterns of the two-component piezo-composites were written in Russian and published in the USSR (Khoroshun LP, Maslov BP, Leshchenko PV, (1989) Prediction of Effective Properties of Piezo-active Composite Materials. Naukova Dumka, Kiev) and Russia (Sokolkin YuV, Pan'kov AA, (2003) Electroelasticity of Piezo-composites with Irregular Structures. Fizmatlit, Moscow). The third monograph (Topolov VYu, Bowen CR, (2009) Electromechanical Properties in Composites Based on Ferroelectrics. Springer, London) is concerned with the prediction of the effective properties in the two- and three-component composites, and different analytical schemes of averaging the properties of these materials having different connectivity and microgeometric characteristics are given hereby for comparison. This monograph develops ideas of the previous book (2009) and enables us to fill a gap in the description of the orientation effects in novel anisotropic piezoelectric materials. This new publication may be also characterized as an international edition written by three specialists working in adjacent areas of science and engineering.

This monograph summarizes and generalizes a series of the authors' publications on the performance and anisotropic characteristics of the two- and three-component composites based on either the traditional ferroelectric ceramics or modern relaxor-ferroelectric single crystals. This monograph has been written on the basis of the authors' research results obtained at the Southern Federal University (Russia), University of Rome "Tor Vergata" (Italy), and University of Bath (UK). The academic style of presentation of the research results and the discussion about these results indicate that the present monograph would be useful to engineers, postgraduate students, researchers, and lecturers, i.e., to many specialists working in the field of ferro-, piezoelectric, and related materials, dealing with their effective electromechanical properties and applications. This monograph

will be of benefit to all specialists looking to understand the anisotropic electromechanical properties and related parameters of the piezo-active composites. Some chapters and sections of the monograph may be a basis for a university course devoted to piezo-active materials and their electromechanical properties.

Based on our knowledge, experience, and new research results, we hope that the twenty-first century termed *The Century of New Materials and Technologies*, will lead to the fruitful development of new scientific directions in the field of modern smart materials and structures.

Rostov-on-Don, Russia — Vitaly Yu. Topolov
Rome, Italy — Paolo Bisegna
Bath, UK — Christopher R. Bowen

References

1. Khoroshun LP, Maslov BP, Leshchenko PV (1989) Prediction of effective properties of piezo-active composite materials. Naukova Dumka, Kiev (in Russian)
2. Sokolkin YuV, Pan'kov AA (2003) Electroelasticity of piezo-composites with irregular structures. Fizmatlit, Moscow (in Russian)
3. Topolov VYu, Bowen CR (2009) Electromechanical properties in composites based on ferroelectrics. Springer, London

Acknowledgments

The authors are grateful to Prof. Dr. A. V. Turik, Prof. Dr. A. E. Panich, Prof. Dr. V. G. Gavrilyachenko, Prof. Dr. V. P. Sakhnenko, Prof. Dr. I. A. Parinov, Prof. Dr. A. A. Nesterov, Dr. A. A. Panich, Dr. V. V. Eremkin, Dr. V. G. Smotrakov, Dr. V. K. Dolya, Mr. A. A. Vorontsov, and Mr. S. E. Filippov (Southern Federal University, Russia), Prof. Dr. R. Stevens and Prof. Dr. A. Miles (University of Bath, UK), Prof. Dr. F. Maceri (University of Rome "Tor Vergata", Italy), Dr. S. A. Wilson (Cranfield University, UK), Prof. Dr. O. Kraft and Prof. Dr. M. Kamlah (Karlsruhe Research Centre, Germany), Prof. Dr. M. Lethiecq and Dr. F. Levassort (University of Tours, France), Prof. Dr. H. L. W. Chan (The Hong Kong Polytechnic University, P.R. China), Prof. Dr. J. H. Huang (Feng Chia University, Taiwan, Republic of China), Prof. Dr. W. Cao (The Pennsylvania State University, USA), Prof. Dr. A. Safari and Dr. E. K. Akdogan (Rutgers—The State University of New Jersey, USA), Prof. Dr. A. S. Sidorkin (Voronezh State University, Russia), Prof. Dr. L. N. Korotkov and Prof. Dr. S. A. Gridnev (Voronezh State Technical University, Russia), and Dr. A. V. Krivoruchko (Don State Technical University, Russia) for their interest in the research problems and for their interesting research results that have been taken into account at writing this book. Furthermore, the authors emphasize the vast geographic area wherein the piezo-active and related composites are studied or manufactured for various applications. The author Prof. Dr. C. R. Bowen would also like to thank past supervisors including Prof. Dr. B. Derby (University of Manchester, UK), Prof. Dr. N. Claussen (Technical University of Hamburg-Harburg, Germany), and Prof. Dr. R. Stevens (University of Bath, UK).

The authors express much thanks to Prof. Dr. C. Ascheron and Mrs. E. Sauer (Springer-Verlag, Heidelberg, Germany) for their effective and timely co-operation in the field of editing and producing this book. Special thanks are extended to Prof. Dr. C. Ascheron for his invitation to write a new monograph on the performance of modern piezo-active materials. The authors sincerely thank Ms. R. Garner, Mr. J. Thompson, and Mr. D. Barker (University of Bath, UK) for the technical help. Copyright permissions obtained from Springer (www.springer.com), Elsevier (www.elsevier.com), IOP Publishing (www.iop.org), AIP (www.aip.org), Taylor & Francis (www.informaworld.com), Wiley-VCH

(www.wiley-vch.de), and Nova Science Publishers (www.novapublishers.com) are acknowledged with due attention and gratitude.

Finally, financial support that promoted the fruitful research collaboration and writing this book is acknowledged with many thanks. Hereupon gratefully and proudly the authors mention the timely and effective support from the EPSRC (UK), National Physical Laboratory, QinetiQ (UK), Great Western Research (GWR, UK), University of Bath (UK), University of Rome "Tor Vergata" (Italy), and Southern Federal University (Russia). Prof. Dr. C. R. Bowen gratefully acknowledges support of ERC Advanced Fellowship (Project "NEMESIS", Grant Agreement No. 320963).

This work has been carried out with the financial support from the Ministry of Education and Science of Russia within the framework of the Federal Purposive Programme entitled "Studies and Working out on Priority Directions of the Development of the Research Complex of Russia" for 2007–2013. The aforementioned financial support from the Ministry of Education and Science of Russia is acknowledged by the author Prof. Dr. V. Yu. Topolov with sincere gratitude.

Contents

Chapter 1
The Piezoelectric Medium and Its Electromechanical Properties

An effect that links a mechanical action (mechanical stress or strain) with an electric response (electric field, displacement or polarisation) is *the piezoelectric effect* or, more exactly, the *direct piezoelectric effect* [1]. This effect was first studied by brothers P. Curie and J. Curie in experimental work (1880) on the behaviour of quartz single crystals (SCs) subjected to an external mechanical stress. At a later date, the *converse piezoelectric effect* was revealed in acentric dielectric SCs wherein an external electric field generated a mechanical response, i.e., a stress or strain of the sample [2, 3]; similar to electrostriction of dielectrics [3, 4]. The piezoelectric effect follows a linear relationship between electric and mechanical variables and originates from the displacement of ions of an acentric SC under an applied electric field [1–4]. This relationship means that there is change in the sign of the effect when the direction of the external electric field is switched in the piezo-active medium, unlike electrostriction which follows a quadratic effect [3, 4] and does not undergo switching with the electric field. Despite the linear character, the piezoelectric response of a SC sample is often intricate owing to various interconnections between the piezoelectric and other properties such as the elastic, dielectric (including pyro- and ferroelectric) and thermal properties [3]. The piezoelectric response of poled ferroelectric ceramic (FC) and composite samples are even more complicated in comparison to ferroelectric SCs due to microstructural, domain, orientation, intrinsic and extrinsic contributions, etc. [5–11].

Piezoelectricity was initially discovered as a physical phenomenon and has led to a range of new adapted materials and technologies in the past 130 years. It was a long and sometimes difficult path to improve the initially minor effect to a point where is was a real and even superior competitor to the electro-dynamic magnetic principal, which for a long time was the only effective way to transform electrical energy or signals into mechanical ones or vice versa [11]. In the history of piezoelectric materials there is the remarkable era concerned with the perovskite-type FC of $BaTiO_3$. After discovering the ferroelectric properties and ability to orient the ferroelectric domains within grains (or crystallites) of FC $BaTiO_3$ in an external electric field, a new way of producing the highly-effective piezoelectric materials was opened in the 1940s.

V. Yu. Topolov et al., *Piezo-Active Composites*,
Springer Series in Materials Science 185, DOI: 10.1007/978-3-642-38354-0_1,

Due to the domain-orientation effect, poled FC materials exhibit both ferroelectric and piezoelectric properties [2–4, 9, 11–13]. As noted by Haertling [14], this was a most startling discovery, because the prevailing opinion was that FCs could not be piezoelectrically active, because the sintered and randomly oriented crystallites would, on the whole, cancel out each other.

1.1 Piezoelectric Coefficients

A general consideration of the piezoelectric effect in dielectric SCs is carried out in terms of thermodynamic functions, such as Helmholtz free energy, Gibbs free energy, elastic Gibbs energy, and electric Gibbs energy [2–4]. Each of these functions has at least three arguments that characterise the mechanical, electric and thermal states of the SC. The first argument can be either mechanical stress σ_{kl} or mechanical strain ξ_{jr}, the second argument can be electric field $\boldsymbol{E}$ or electric displacement (electric flux density) $\boldsymbol{D}$, and the third argument can be temperature T or entropy S. Obviously, these arguments are represented as second-rank (σ_{kl} and ξ_{jr}), first-rank (E_k and D_j) and zeroth-rank (scalars T and S) tensors. It is also possible to develop additional arguments in terms of magnetic field $\boldsymbol{H}$ or magnetic induction $\boldsymbol{B}$ [5]. Based on the thermodynamic functions and relations between the arguments of the mechanical, electric and thermal states [2, 3], one can describe the linked "response – actions" in terms of ξ_{jr}, E_i and T as follows:

$$\sigma_{kl} = c^{E}_{kljr}\xi_{jr} - e_{ikl}E_i + \beta_{kl}\Delta T \tag{1.1}$$

$$D_i = e_{ikl}\xi_{kl} + \varepsilon^{\xi}_{if}E_f + p_i\Delta T \tag{1.2}$$

$$\Delta S = \beta_{jr}\xi_{jr} + p_iE_i + (\rho/T_0)c\Delta T \tag{1.3}$$

In (1.1)–(1.3) the constants written in the tensor form are elastic moduli at constant electric field (c^{E}_{kljr}), piezoelectric coefficients (e_{ikl}), coefficients of thermal stress (β_{kl}), dielectric permittivities at constant mechanical strain (ε^{ξ}_{if}), pyroelectric coefficients (p_i). There are scalars, namely, density (ρ), and specific heat (c) of the SC. Summing over the repeated subscripts [e.g., j, r and i in (1.1)] is to be performed from 1 to 3. The increments ΔT and ΔS in (1.1)–(1.3) denote differences $T - T_0$ and $S - S_0$, respectively, where T_0 is the initial temperature and S_0 is the initial entropy of the SC.

Linear relations from (1.1)–(1.3) hold in the case of relatively weak external fields. For example, the linear dependence $\sigma_{kl}(\xi_{jr})$ from (1.1) obeys Hooke's law in an anisotropic medium [12] at small ($< 1\%$) strains ξ_{jr}. The linear dependence $D_i(E_f)$ from (1.2) is valid at relatively low levels of electric field E_f applied to the dielectric SC. In a case of an acentric dielectric SC, the low level of electric field means that the E_f value is considered much smaller than the electric breakdown field. With regard to a ferroelectric SC , similar requirements concerning the linear

dependences $\sigma_{kl}(\xi_{jr})$ and $D_i(E_f)$ are possible, but the E_f range becomes narrower than that in the acentric linear dielectric SC. It is well known that in the presence of a low electric field E, the polarisation of a ferroelectric SC linearly depends on E [3, 4] so that domain-wall displacements are reversible and no nuclei of reoriented domains are formed. In this connection the electric field E_f is usually regarded to be a few times lower than the coercive field E_c which is determined from a ferroelectric hysteresis loop [3, 4, 6].

Using Eqs. (1.1)–(1.3), one can determine a set of isothermal constants (measured at $T = \text{const}$) of the piezoelectric SC. An analogous set of adiabatic constants (measured at $S = \text{const}$) can also be derived using the thermodynamic functions and a combination of three arguments including ΔS (for example, ξ_{jr}, E_i and ΔS). According to experimental data, the difference between the related isothermic and adiabatic constants of the piezoelectric SCs is approximately 1 % or less [3, 5]. Based on this observation, the effect of thermal fields on the elastic and electric responses of the piezoelectric SCs is often neglected, and the description of the piezoelectric effect is carried out in terms of (1.1) and (1.2) at $\Delta\mathrm{T} = 0$. Equations (1.1) and (1.2) are written in the matrix form [2, 3] as follows:

$$\sigma_p = c^E_{pq}\xi_q - e_{fp}E_f \tag{1.4}$$

$$D_k = e_{kl}\xi_l + \varepsilon^{\xi}_{kr}E_r, \tag{1.5}$$

and the conventional transition from two subscripts to one subscript follows Vogt's rule [2–4, 12].

Equations (1.4) and (1.5) represent the first pair of piezoelectric equations that link two variables, mechanical strain ξ and electric field E. The first term in the right part of (1.5), $P_k = e_{kl}\xi_l$, describes the piezoelectric polarisation produced by an external mechanical strain as a result of the *direct* piezoelectric effect. In contrast to this, the *converse* piezoelectric effect is described by the $e_{fp}E_f$ term in (1.4), and the sequence of subscripts (*fp, f*) differs from the sequence (*kl, l*) at the direct piezoelectric effect.

From the thermodynamic treatment of the interrelations between the electric and elastic fields [2, 3], the converse and direct piezoelectric effects can also be described by the three following pairs of equations:

$$\xi_p = s^E_{pq}\sigma_q + d_{fp}E_f \tag{1.6}$$

$$D_k = d_{kl}\sigma_l + \varepsilon^{\sigma}_{kr}E_r \tag{1.7}$$

in variables of mechanical stress σ and electric field E,

$$\xi_p = s^D_{pq}\sigma_q + g_{fp}D_f \tag{1.8}$$

$$E_k = -g_{kl}\sigma_l + \beta^{\sigma}_{kr}D_r \tag{1.9}$$

in variables of mechanical stress σ and electric displacement D, and

$$\sigma_p = c^D_{pq}\xi_q - h_{fp}D_f \tag{1.10}$$

$$E_k = -h_{kl}\xi_l + \beta^\xi_{kr}D_r \tag{1.11}$$

in variables of mechanical strain ξ and electric displacement D. Superscripts σ and D denote measurement conditions at σ= const and D = const, respectively. Dielectric impermittivities β^σ_{kr} and β^ξ_{kr} are determined [2, 3] from equalities $\beta^\sigma_{kr}\varepsilon^\sigma_{rv} = \delta_{kv}$ and $\beta^\xi_{kr}\varepsilon^\xi_{rv} = \delta_{kv}$, and elastic moduli c^E_{pq} or c^D_{pq} and elastic compliances s^E_{pq} or s^D_{pq} are related by conditions $c^E_{pq}s^E_{qr} = \delta_{pr}$ and $c^D_{pq}s^D_{qr} = \delta_{pr}$, where δ_{kv} is the Kronecker symbol. Thus, Eqs. (1.4)–(1.11) contain four types of piezoelectric coefficients, namely e_{kl}, d_{kl}, g_{kl}, and h_{kl}, and in each pair of Eqs. (1.4)–(1.11), there is a term corresponding to the direct piezoelectric effect and a term corresponding to the converse piezoelectric effect. Each piezoelectric coefficient characterises the relationship between components of two fields that are described by first- and second-rank tensors, and all the piezoelectric coefficients from (1.4)–(1.11) are defined to be components of the third-rank tensors, but written in the matrix form (i.e., with two subscripts) [2–5] only. These individual piezoelectric coefficients can be used to aid in the selection of piezoelectric materials for specific applications. For example, for an actuator application [4] it may be necessary to select materials with a high strain per unit applied electric field (i.e., with large values of $|d_{kl}|$). For a pressure sensor, the electric field generated per unit mechanical stress is more likely to be important (i.e., with large values of $|g_{kl}|$).

The interrelationships of the piezoelectric coefficients d_{kl}, e_{kl}, g_{kl}, and h_{kl} follow from the thermodynamic description [2, 3] and are expressed by the following equalities:

$$d_{fp} = \varepsilon^\sigma_{fk}g_{kp} = e_{fq}s^E_{qp} \tag{1.12}$$

$$e_{fp} = \varepsilon^\xi_{fk}h_{kp} = d_{fq}c^E_{qp} \tag{1.13}$$

$$g_{fp} = \beta^\sigma_{fk}d_{kp} = h_{fq}s^D_{qp} \tag{1.14}$$

$$h_{fp} = \beta^\xi_{fk}e_{kp} = g_{fq}c^D_{qp} \tag{1.15}$$

The piezoelectric coefficients from (1.12)–(1.15) are also involved in relations [2, 3] between dielectric or elastic constants measured on different conditions:

$$\varepsilon^\sigma_{kr} - \varepsilon^\xi_{kr} = d_{kf}e_{rf} \tag{1.16}$$

$$\beta^\xi_{kr} - \beta^\sigma_{kr} = g_{kf}e_{rf} \tag{1.17}$$

$$c^D_{pq} - c^E_{pq} = e_{fp}h_{fq} \tag{1.18}$$

$$s^D_{pq} - s^E_{pq} = d_{fp}g_{fq} \tag{1.19}$$

As is seen from (1.12)–(1.19), there are close connections between the elastic, piezoelectric and dielectric constants of a piezoelectric medium. These connections

enable us to term the sets of the elastic, piezoelectric and dielectric constants as *electromechanical constants*. These constants characterise *electromechanical properties* in a variety of piezo-active materials, such as piezoelectric or ferroelectric SCs, poled FCs, thin ferroelectric films, piezo-active composites, etc.

As follows from (1.1), (1.2) and (1.4)–(1.11), the piezoelectric properties are described by third-rank tensors and are represented in the matrix form, as 3×6 or 6×3 matrices. Tables of the matrices of the piezoelectric coefficients related to acentric SCs, poled FCs, composites, and piezoelectric textures (i.e., to various piezoelectric media) have been collected in a series of monographs [2–5, 12]. The piezoelectric effect is detected in 20 symmetry classes (point groups) and 3 limiting symmetry classes (Curie groups). The symmetry classes that obey the conditions for the piezoelectric effect [3, 12] are 1 (triclinic system), 2 and m (monoclinic system), 222 and $mm2$ (orthorhombic system), 3, 32 and $3m$ (trigonal or rhombohedral system), 4, 422, $4mm$, $\bar{4}$, and $\bar{4}2m$ (tetragonal system), 6, 622, $\bar{6}$, and $\bar{6}m2$ (hexagonal system), and 23 and $\bar{4}3m$ (cubic system). The Curie groups that satisfy conditions for the piezoelectric texture [3, 12] are ∞, $\infty\, mm$ and $\infty/2$.

Below we give some examples of the matrix representation of the piezoelectric coefficients d_{fp}:

$$\| d \| = \begin{pmatrix} 0 & 0 & 0 & 0 & d_{15} & 0 \\ 0 & 0 & 0 & d_{15} & 0 & 0 \\ d_{31} & d_{31} & d_{33} & 0 & 0 & 0 \end{pmatrix},$$ $4mm$, $6mm$ and $\infty\, mm$ classes (3 independent non-zero constants),

$$\| d \| = \begin{pmatrix} 0 & 0 & 0 & 0 & d_{15} & -2d_{22} \\ -d_{22} & d_{22} & 0 & d_{15} & 0 & 0 \\ d_{31} & d_{31} & d_{33} & 0 & 0 & 0 \end{pmatrix},$$ $3m$ class (4 independent non-zero constants),

$$\| d \| = \begin{pmatrix} 0 & 0 & 0 & 0 & d_{15} & 0 \\ 0 & 0 & 0 & d_{24} & 0 & 0 \\ d_{31} & d_{32} & d_{33} & 0 & 0 & 0 \end{pmatrix},$$ $mm2$ class (5 independent constants),

$$\| d \| = \begin{pmatrix} 0 & 0 & 0 & d_{14} & 0 & d_{16} \\ d_{21} & d_{22} & d_{23} & 0 & d_{25} & 0 \\ 0 & 0 & 0 & d_{34} & 0 & d_{36} \end{pmatrix},$$ 2 class (8 independent constants),

$$\| d \| = \begin{pmatrix} d_{11} & d_{12} & d_{13} & 0 & d_{15} & 0 \\ 0 & 0 & 0 & d_{24} & 0 & d_{26} \\ d_{31} & d_{32} & d_{33} & 0 & d_{35} & 0 \end{pmatrix},$$ m class (10 independent constants).

It should be added that in the 1 class, the $\| d \|$ matrix comprises the largest number of independent constants, i.e., $d_{11}, d_{12}, \ldots, d_{16}, d_{21}, d_{22}, \ldots, d_{26}, d_{31}, d_{32}, , , , , d_{36}$, or 18 constants.

Irrespective of symmetry of the piezoelectric medium, the same form of the matrix representation with the same zero and non-zero pattern of the matrix elements and with the same number of independent constants, is valid to characterise the piezoelectric coefficients g_{fp}. As for e_{fp} and h_{fp}, the matrix representation of these

piezoelectric coefficients is also similar. However the structure of $\| d \|$ (or $\| g \|$) differs from the structure of $\| e \|$ (or $\| h \|$) for the following symmetry classes: 3, 32, $3m$, $\bar{6}$, and $\bar{6}m2$ [2, 3, 12].

The conditions for measuring the piezoelectric coefficients are associated with the electric and mechanical variables from (1.4)–(1.11). If the direct piezoelectric effect is considered, then the piezoelectric coefficients of the medium are measured [3] using the following relations:

(1) $P_k = d_{kl}\sigma_l$ (for d_{kl}),
(2) $E_k = -g_{kl}\sigma_l$ (for g_{kl}),
(3) $E_k = -h_{kl}\xi_l$ (for h_{kl}), and
(4) $P_k = e_{kl}\xi_l$ and $E = 0$ (for e_{kl}).

We remind that $P_k = D_k$ at $E_k = 0$, and the polarisation P_k is determined from a surface density of electric charge on a sample face [3]. In the case of the converse piezoelectric effect, the following relations are taken into account:

(1) $\xi_p = d_{fp}E_f$ (for d_{fp}),
(2) $\xi_p = g_{fp}D_f$ (for g_{fp}),
(3) $\sigma_p = -h_{fp}D_f$ (for h_{fp}), and
(4) $\sigma_p = -e_{fp}E_f$ (for e_{fp}).

As follows from the above-given conditions, it is relatively easy to measure e_{kl} and h_{kl} as constants of the direct piezoelectric effect and d_{kl} as a constant of the converse piezoelectric effect [3].

1.2 Electromechanical Coupling Factors

In Sect. 1.1 various sets of electromechanical constants of the piezoelectric medium have been introduced. The elastic, piezoelectric and dielectric constants enable us to estimate the effectiveness of the conversion of electric energy into mechanical energy and vice versa. From the analysis of the energy conversion [2, 13] in a piezoelectric medium, the effectiveness strongly depends on differences between dielectric permittivities from (1.16) or differences between elastic compliances from (1.19), and these differences strongly depend on the piezoelectric effect. In a general form, the effectiveness of the energy conversion is described by an electromechanical coupling factor (ECF) [2, 3, 5, 6, 13]

$$k = w_{piezo}/\sqrt{w_{el}w_{mech}} \tag{1.20}$$

and is expressed in terms of volume densities of piezoelectric (or mutual) energy $w_{piezo} = \sigma_i d_{mi} E_m/2$, electric energy $w_{el} = E_l \varepsilon^{\sigma}_{lr} E_r/2$, and mechanical energy $w_{mech} = \sigma_p s^{E}_{pq} \sigma_q/2$. The k^2 value calculated from (1.20) characterises [2–5, 9, 13] a ratio of stored mechanical energy to electric energy input (when a portion of

electric energy is applied to the piezoelectric sample) or a ratio of stored electric energy to mechanical energy input (when a portion of mechanical energy is applied to the piezoelectric sample). The k^2 value also characterises a measure of the magnitude of the piezoelectric transducer bandwidth [2]. The absolute ECF value depends [2, 4, 9, 13] on the vibration mode, measurement methodology, sample shape, and the electromechanical constants of the piezoelectric medium. As a rule, two kinds of ECFs are considered as follows: the static ECF determined from equations of the state of the piezoelectric medium and the dynamic (effective) ECF related to the individual piezoelectric element [9, 13]. It is obvious that the ECFs strongly depend on the orientation of the external electric or mechanical field applied to the piezoelectric element and on the symmetry of its properties.

The poled FC element with a remanent polarisation vector $\boldsymbol{P}_r \parallel OX_3$ (∞mm symmetry) is characterised by three independent piezoelectric coefficients, d_{31}, d_{33} and d_{15}. These constants are linked to the ECFs as follows:

$$k_{33} = d_{33}/(\varepsilon_{33}^{\sigma}\, s_{33}^{E})^{1/2} \tag{1.21}$$

(ECF at the longitudinal oscillation mode, or simply, longitudinal ECF),

$$k_{31} = d_{31}/(\varepsilon_{33}^{\sigma}\, s_{11}^{E})^{1/2} \tag{1.22}$$

(ECF at the transverse oscillation mode) and

$$k_{15} = d_{15}/(\varepsilon_{11}^{\sigma}\, s_{55}^{E})^{1/2} \tag{1.23}$$

(ECF at the shear oscillation mode). Since an equality $s_{55}^{E} = s_{44}^{E}$ holds [2–5] in a poled FC medium, expression (1.23) is often given by $k_{15} = d_{15}/(\varepsilon_{11}^{\sigma} s_{44}^{E})^{1/2}$. For various piezo-active materials the ECF is represented in the general form as $k_{ij} = d_{ij}/(\varepsilon_{ii}^{\sigma} s_{ij}^{E})^{1/2}$, and hereby it is sufficient to require $d_{ij} \neq 0$ at a specific oscillation mode. Due to equalities $s_{22}^{E} = s_{11}^{E}$ and $d_{24} = d_{15}$, which are valid for any poled FC [2–5], relations

$$k_{32} = k_{31} \text{ and } k_{24} = d_{15} \tag{1.24}$$

are also valid. It should be noted that a violation of conditions (1.24) may be accounted for by a symmetry of the piezoelectric medium. For example, in a case of $mm2$ symmetry class, we should distinguish s_{22}^{E} and s_{11}^{E}, d_{24} and d_{15}, etc. As a consequence, we get $k_{32} \neq k_{31}$ and $k_{24} \neq d_{15}$.

Along with the ECFs from (1.21)–(1.24), the following ECFs are wide-spread [2, 4, 9, 10, 13] and often measured on poled FC and piezo-active composite samples:

$$k_t = e_{33}/(c_{33}^{D}\varepsilon_{33}^{\xi})^{1/2} \tag{1.25}$$

(ECF at the thickness oscillation mode, or simply, thickness ECF),

$$k_p = k_{31}[2/(1-\sigma_E)]^{1/2} \tag{1.26}$$

(ECF at the planar oscillation mode, or simply, planar ECF) and

$$k_h = d_h/(\varepsilon_{33}^{\sigma} s_h^E)^{1/2} \tag{1.27}$$

(hydrostatic ECF). In (1.26) σ_E is the Poisson's ratio at electric field E = const, and in (1.27) d_h and s_h^E are the hydrostatic piezoelectric coefficient and hydrostatic elastic compliance at E = const, respectively. Data on the ECFs from (1.21)–(1.27) are useful to characterise piezoelectric materials for active elements of electromechanical transducers and hydrophones.

1.3 Electromechanical Properties of Relaxor-Ferroelectric Single Crystals

Relaxor-ferroelectric perovskite-type solid solutions are materials with one of the following general formulae: $(1-x)Pb(B_1, B_2)O_3 - xPbTiO_3$ or $(1-x-y)Pb(B_1, B_2)O_3 - xPb(B_1', B_2')O_3 - yPbTiO_3$. These complex perovskites $Pb(B_1, B_2)O_3$ [or $Pb(B_1', B_2')O_3$] are disordered compounds that contain ions of metals from the following groups: B_1 (or B_1') = Mg, Zn, Ni, Fe, Sc, Yb, and In (low valence) and B_2 (or B_2') = Nb, Ta and W (high valence) [15, 16]. A combination of metal ions with low and high valences results in physical properties that distinguish $Pb(B_1, B_2)O_3$ from "normal" (ordered or regular) perovskite-type ferroelectrics such as $PbTiO_3$, $BaTiO_3$ or $KNbO_3$. The complex perovskites $Pb(B_1, B_2)O_3$ exhibit a broad and frequency-dispersive dielectric maxima and contain polar nanoregions (with ferro- or antiferroelectric ordering) in a non-polar phase over a wide temperature range [15, 16]. These materials are characterised by a relaxation dielectric polarisation and are termed *relaxors* or *ferroelectric relaxors* [15–17].

The perovskite-type solid solutions of $(1-x)Pb(B_1, B_2)O_3 - xPbTiO_3$ combine the physical properties of the relaxor-type and "normal" ferroelectric components, and, as a rule, excellent electromechanical properties are observed near the morphotropic phase boundary (MPB) [15, 18, 19]. To achieve a high piezoelectric activity in SC samples, the relaxor-ferroelectric solid solutions are often engineered by compositional adjustment with a corresponding decrease in Curie temperature of the paraelectric-to-ferroelectric phase transition [15, 19, 20], and specific domain-engineered structures are formed in an electric field [19, 20]. In the last decade, there has been significant interest in domain-engineered SCs of $(1-x)Pb(Mg_{1/3}Nb_{2/3})O_3 - xPbTiO_3$ (PMN–xPT) and $(1-x)Pb(Zn_{1/3}Nb_{2/3})O_3 - xPbTiO_3$ (PZN–xPT) with molar concentrations x taken in the vicinity of the MPB. As follows from numerous experimental and theoretical studies, the engineered non-180° domain structures [19–21], intermediate ferroelectric phases [18, 22] and domain-orientation processes [23–26] play an important role in the relaxor-

Table 1.1 Experimental values of elastic compliances s_{ab}^E (in 10^{-12} Pa^{-1}), piezoelectric coefficients d_{ij} (in pC / N) and dielectric permittivities $\varepsilon_{pp}^{\sigma}$ of $[001]_c$-poled domain-engineered PMN–xPT and PZN–xPT and single-domain $PbTiO_3$ SCs ($4mm$ symmetry) at room temperature

SC	s_{11}^E	s_{12}^E	s_{13}^E	s_{33}^E	s_{44}^E	s_{66}^E	d_{31}	d_{33}	d_{15}	$\varepsilon_{11}^{\sigma}/\varepsilon_0$	$\varepsilon_{33}^{\sigma}/\varepsilon_0$
PMN–0.33PT [27]	69.0	–11.1	–55.7	119.6	14.5	15.2	–1,330	2,820	146	1,600	8,200
PMN–0.30PT [28]	52.0	–18.9	–31.1	67.7	14.0	15.2	–921	1,981	190	3,600	7,800
PMN–0.28PT [29]	44.57	–28.91	–13.91	34.38	15.22	16.34	–569	1,182	122	1,672	5,489
PZN–0.045PT [30]	82.0	–28.5	–51.0	108	15.6	15.9	–970	2,000	140	3,100	5,200
PZN–0.07PT [31]	85.9	–14.1	–69.0	142	15.9	14.1	–1,204	2,455	176	3,000	5,622
PZN–0.08PT [31]	87.0	–13.1	–70.0	141	15.8	15.4	–1,455	2,890	158	2,900	7,700
$PbTiO_3$ [32]	6.70	–2.00	–579	28.8	13.2	7.60	–26.9	143	60.2	140	125

ferroelectric SCs exhibiting outstanding electromechanical properties. Due to these and other phenomena, the domain-engineered PMN–xPT and PZN–yPT SCs poled along the certain crystallographic directions (often along $[001]_c$, $[011]_c$ or $[111]_c$ of the perovskite unit cell) [15, 19] exhibit very high piezoelectric activity and significant electromechanical coupling [16, 19, 21, 23].

Full sets of electromechanical constants of some domain-engineered relaxor-ferroelectric SCs with compositions near the MPB are given in Table 1.1. Typical values of $|d_{3j}| \sim 10^3$ pC / N in the domain-engineered PMN–xPT and PZN–xPT SCs (Table 1.1) are larger than the $|d_{3j}|$ of regular ferroelectric single-domain $PbTiO_3$ SC [32] and conventional FC based on $Pb(Zr_{1-x}Ti_x)O_3$ [4, 9, 10, 14]. As follows from results of work [22], the piezoelectric coefficient d_{31} in the $[001]_c$-poled heterophase PZN–0.08PT SC can be approximately 12,000 pC / N due to the electric-field-induced phase transition and the presence of an intermediate monoclinic phase.

Results of experimental research [16, 20] suggest that relatively high piezoelectric strains (over 0.5 %) are achieved in the $[001]_c$-poled domain-engineered PZN–xPT SCs under an electric field $\boldsymbol{E} \parallel [001]_c$. At room temperature these SCs are charcterised by $3m$ symmetry in the single-domain state and by $4mm$ symmetry in the polydomain state wherein the spontaneous polarisation vectors of the non-180° domains are parallel to the $[111]_c$, $[\bar{1}11]_c$, $[1\bar{1}1]_c$, and $[\bar{1}\bar{1}1]_c$ directions of the perovskite unit cell [15, 19, 33]. Important interconnections between the structure and properties in the PMN–xPT and PZN–yPT SCs have been reviewed by Noheda [18]. The high piezoelectric activity in these materials is associated with a polarisation rotation induced by the electric field $\boldsymbol{E}$ [23, 25]. This rotation between the single-domain states in the tetragonal ($4mm$) and rhombohedral ($3m$) phases of the ferroelectric nature can be implemented in different ways that form the intermediate monoclinic phases [18] and complex heterophase states [22] near the MPB.

The outstanding electromechanical propertie of the domain-engineered PMN–xPT and PZN–xPT SCs near the MPB (Table 1.1), large absolute values of ECFs etc. [19–21] enable us to characterise these materials as excellent candidates for advanced piezoelectric sensors, large-strain actuators, highly sensitive medical ultrasonic transducers, hydrophones, ultrasonic imaging devices, and other piezo-technical devices. In Chaps. 3–5 of this monograph we will describe the possibilities and advantages of using the relaxor-ferroelectric SCs as piezo-active components in novel high-performance composites. We will demonstrate potential improvements in the piezoelectric performance of the composites in comparison to the performance of conventional FC/polymer composites, and the formation of important volume-fraction dependences of the effective electromechanical properties and other important parameters for many piezo-technical applications. Additionally we analyse the key role of the relaxor-ferroelectric SC component in forming the large anisotropy of the piezoelectric properties in the composites.

1.4 Electromechanical Properties of Poled Ferroelectric Ceramics

After the discovery of piezoelectric properties in ceramic (polycrystalline) $BaTiO_3$ and $Pb(Zr_{1-x}Ti_x)O_3$ with the perovskite structure [3, 4, 9, 13, 14], the FC materials have been important objects of research and a key material of choice in various applications [2, 4, 9, 13]. The poled FCs (also termed *piezo-ceramics*) [9, 17] exhibit piezoelectric, dielectric, elastic, thermal, etc. properties that can be comparable to those in the related ferroelectric SC. Since the 1980s FCs have been of interest as highly-effective components of piezo-active composite materials [4, 5, 10]. Undoubtedly, due to their remarkable electromechanical properties, the FCs have been the most vast and widespread group of modern smart materials [4, 10, 14], i.e., materials that undergo transformations through physical interactions.

Equations (1.4)–(1.11) are often used to describe the linear behaviour of the poled FCs and piezo-active composites [5, 10] under weak electric and mechanical fields. The linear description provides a reasonable approximation of the functional characteristics of FCs at low levels of applied electric field and stress, but becomes increasingly inaccurate as these levels increase [34]. Non-linear behaviour of the electromechanical properties in various perovskite-type FCs is observed above the *threshold* values [34] of the electric field E_{thr} and mechanical stress σ_{thr}. Experimental data [34] show that $E_{thr} \approx 10$ kV / m is typical of "soft" PZT FCs (i.e., Pb(Zr, Ti)O_3-type ceramics with low coercive field E_c) and $E_{thr} \approx 300$ kV/m is achieved in well-aged "hard" PZT FCs (i.e. those with large E_c values). Moreover, non-linearity of mechanical properties in both the "soft" and "hard" PZT FCs becomes evident at the mechanical-stress level exceeding $\sigma_{thr} \approx 20$ MPa [34].

The hysteresis and non-linear behaviour of the electromechanical properties in ferroelectric SCs and ceramics are related to the reorientation of the spontaneous

polarisation vectors $\boldsymbol{P}_s$ of domains under the external electric field [3, 4, 13, 34]. A comparative analysis of the linear and non-linear properties in $BaTiO_3$FCs was carried out within the framework of the model of a polydomain grain in an effective medium [35, 36]. Results of the modelling of piezoelectric behaviour of the perovskite-type FC using *the effective medium method* (EMM) and its impact on electromechanical properties led to the conclusion that the non-linear behaviour is a result of 90° domain-wall displacement of the FC grains. These displacements as a result of an applied field become an important extrinsic factor that influences the piezoelectric coefficients d_{fp} of the FC at different poling states. For the fully poled $BaTiO_3$ FC, the aforementioned contributions from the 90° domain-wall displacements to d_{31} and d_{33} attain 68 and 64 % [36], respectively, at room temperature. Subsequent averaging procedures facilitate the consideration of *the hierarchy-of-properties chain* of "single-domain SC – polydomain SC – FC" in the presence of the 90° domain-wall displacements ($BaTiO_3$) or on condition of the motionless 90° domain walls ($PbTiO_3$) [37–42]. Authors of work [39–42] systematised the factors that influence the piezoelectric properties in the perovskite-type FCs and studied the correlation between the microstructure, domain-wall displacements and electromechanical properties in the FCs.

Knowledge of the full sets of the electromechanical constants of FC materials allows the appropriate material selection for various piezo-technical applications and offers a route to using the FCs as piezo-active components for composite materials. Electromechanical constants are often measured using standard methods [9, 13, 43, 44] at room temperature and with weak electric fields. The majority of the FCs are manufactured using the perovskite-type solid solutions [4, 13–15, 17] with compositions varied and tailored to improve specific properties and their anisotropy. Attempts to classify the FCs on directions of application and specific parameters have been made in a few papers [9, 14, 45]. From the classification scheme [25] and by considering the conventional perovskite-type FCs based on $Pb(Zr_{1-x}Ti_x)O_3$, it is possible to identify materials that are stable with regard to electric and mechanical actions, materials with high dielectric permittivity $\varepsilon_{33}^{\sigma}$, materials having high sensitivity with respect to mechanical stress fields (high piezoelectric coefficients g_{fp}), materials with the large piezoelectric anisotropy d_{33}/d_{31}, materials with high stability to the resonance frequency, materials with low dielectric permittivity $\varepsilon_{33}^{\sigma}$, and high-temperature materials (high Curie temperature T_C). Following the classification method [9], the $Pb(Zr_{1-x}Ti_x)O_3$-based FCs are divided into four groups with specific performances. These groups are related to molar concentrations of Ti from ranges $0 \leq x \leq 0.1$, $0.1 \leq x \leq 0.4$, $0.4 \leq x \leq 0.6$, and $0.6 \leq x \leq 1$, and some advantages of each group are mentioned [9] in connection with a variety of piezo-technical applications.

Examples of the poled FCs (piezo-ceramics) and full sets of their room-temperature electromechanical constants involved in (1.6) and (1.7) are given in Table 1.2. Any differences between the individual constants of the materials with the same composition (e.g., $BaTiO_3$ and $(Pb_{0.9625}La_{0.025})(Ti_{0.99}Mn_{0.01})O_3$ FCs from Table 1.2) are caused by technological, microstructural and poling factors, the selection of a composition in the proximity of the MPB, fluctuations of the composition over samples

Table 1.2 Elastic compliances s_{pq}^{E} (in 10^{-12}Pa^{-1})[a], piezoelectric coefficients d_{ij} (in pC / N) and dielectric permittivities $\varepsilon_{kk}^{\sigma}$ of perovskite-type FCs (on data of measurements at room temperature)

FC	s_{11}^{E}	s_{12}^{E}	s_{13}^{E}	s_{33}^{E}	s_{44}^{E}	d_{31}	d_{33}	d_{15}	$\frac{\varepsilon_{11}^{\sigma}}{\varepsilon_0}$	$\frac{\varepsilon_{33}^{\sigma}}{\varepsilon_0}$
$BaTiO_3$ (I) [46]	8.55	–2.61	–2.85	8.93	23.3	–79	191	270	1,623	1,900
$BaTiO_3$ (II) [13]	9.1	–2.7	–2.9	9.5	22.8	–78	190	260	1,450	1,700
$(Ba_{0.917}Ca_{0.083})TiO_3$ [13, 47]	8.63	–2.62	–2.71	9.10	22.2	–55.4	140	242	1,300	1,160
TBK-3 [5]	8.26	–2.37	–2.39	8.41	22.7	–48.7	121	207	1,160	1,160
TBKS [5]	8.40	–2.22	–2.20	8.61	20.4	–21.2	69.4	93.1	458	400
NBS-1 [5]	11.6	–3.15	–3.48	12.9	29.0	–79.5	213	223	1,090	1,310
ZTS-19 [5]	15.1	–5.76	–5.41	17.0	41.7	–126	307	442	1,350	1,500
ZTS-24 [48]	11.3	–3.9	–5.1	13.5	38	–90	205	390	1,020	850
ZTSNV-1 [48]	15.3	–5.3	–5.5	16.6	47.2	–169	354	672	2,020	2,470
PZT-4 [13]	12.3	–4.03	–5.35	15.6	39.1	–124	291	496	1,440	1,280
PZT-5 [13]	16.3	–5.67	–7.17	18.7	47.4	–170	373	583	1,730	1,700
PZT-5H [49]	10.8	–3.28	–3.41	11.6	28.3	–128	315	482	2,640	2,490
PZT-7A [50]	10.7	–3.22	–4.62	13.9	39.5	–60.2	151	364	843	427
Navy Type VI [51]	16.7	–4.84	–8.50	20.8	43.5	–275	594	739	2,890	3,670
PZ 27 [52, 53]	16.9	–6.32	–8.56	22.5	43.9	–174	419	515	1,800	1,770
PZ 34 [52, 53]	7.71	–1.54	–3.99	13.0	17.0	–3.92	59.1	39.2	191	196
PCR-1, hp[b] [45]	12.5	–4.4	–5.8	15.9	38.8	–95	220	420	1,130	650
PCR-7, hp [45]	17.2	–7.2	–6.7	17.3	42.4	–280	610	760	2,970	3,500
PCR-7M, hp [45]	17.5	–6.7	–7.9	19.6	43.8	–350	760	880	3,990	5,000
PCR-8, hp [45]	12.5	–4.6	–5.2	15.6	35.3	–130	290	410	1,380	1,400
PCR-8, ct [45]	13.3	–4.8	–4.4	14.5	39.5	–125	280	458	1,320	1,300

(continued)

Table 1.2 (continued)

FC	s_{11}^E	s_{12}^E	s_{13}^E	s_{33}^E	s_{44}^E	d_{31}	d_{33}	d_{15}	$\frac{\varepsilon_{11}^\sigma}{\varepsilon_0}$	$\frac{\varepsilon_{33}^\sigma}{\varepsilon_0}$
PCR-13, ct [45]	10.4	–3.7	–2.1	11.3	28.5	–65	140	200	870	780
PCR-21, hp [45]	11.8	–4.5	–3.9	12.6	40.8	–109	250	370	1,400	1,350
PCR-63, hp [45]	9.8	–3.5	–2.7	9.8	24.1	–60	140	166	960	1,170
PCR-73, hp [45]	17.9	–6.8	–9.6	23.5	43.7	–380	860	980	4,750	6,000
$Pb(Zr_{0.54}Ti_{0.46})O_3$ [13]	11.6	–3.33	–4.97	14.8	45.0	–60.2	152	440	990	450
$Pb(Zr_{0.52}Ti_{0.48})O_3$ [47]	13.8	–4.07	–5.80	17.1	48.2	–93.5	223	494	1,180	730
$(Pb_{0.94}Sr_{0.06})\cdot(Ti_{0.47}\cdot Zr_{0.53})O_3$ [47]	12.3	–4.05	–5.31	15.5	39.0	–123	289	496	1,475	1,300
Modified $PbTiO_3$ (I) [54]	7.50	–1.51	–1.10	8.00	17.9	–4.40	51.0	53.0	228	177
Modified $PbTiO_3$ (II) [55]	7.7	–1.7	–1.2	8.2	19	–6.8	56	68	240	190
$(Pb_{0.9625}La_{0.025})\cdot\cdot(Ti_{0.99}Mn_{0.01})O_3$ [56]	7.20	–1.42	–1.73	7.62	15.8	–4.15	47.2	53.0	223	168
$(Pb_{0.85}Nd_{0.10})(Ti_{0.99}\cdot\cdot Mn_{0.01})O_3$ [56]	6.84	–1.50	–1.83	7.27	16.4	–5.42	56.8	79.5	313	252
$(Pb_{0.855}Nd_{0,11})(Ti_{0,94}\cdot\cdot Mn_{0,02}In_{0,04})\cdot O_3$ [56]	6.77	–1.55	–1.79	7.29	16.0	–6.40	57.9	86.4	318	248
PMN–0.35PT [57]	13.2	–3.96	–6.05	14.7	33.4	–133	270	936	4,610	3,270

[a] In the poled state of any FC (∞mm symmetry, the poling axis is parallel to the co-ordinate axis OX_3), elastic compliance s_{66} is determined [2, 3, 9, 12, 13] as follows: $s_{66} = 2(s_{11}^E - s_{12}^E)$.

[b] FC samples of the PCR type have been manufactured using either the conventional technology (ct) or hot pressing (hp). PCR is the abbreviation for the group "piezoelectric ceramics from Rostov-on-Don" (Russia) [45]

and a variation in the mobility of the domain walls. These factors can influence the domain structures in FC grains, heterophase states and electromechanical properties [9, 47, 48] of the FC sample as a whole. For example, changes in volume fractions of the 90° domains or in the mobility of the 90° domain walls in the grains of the $PbTiO_3$-type FCs significantly affect their piezoelectric properties and the anisotropy of the piezoelectric coefficients d_{3j} and ECFs k_{3j} [37–40, 58].

1.5 Electromechanical Properties of Piezo-Active Composites

Composites can be defined as heterogeneous systems that consist of two or more components that differ in chemical composition and properties and are separated by distinct interfaces [5]. Each composite material is characterised by the following features [5, 10]:

(1) the typical size of the separate structural elements are small in comparison with the whole composite sample (i.e., there is an element of micro-inhomogeneity) and
(2) the typical sizes of the structural elements are greater than the size of their individual atoms or molecules so that each component of the composite sample is regarded as a continuous medium. As a result, to describe the composite properties it is possible to consider the physical laws and equations suitable for continuous media.

Each component of the composite represents a set of the structural elements with equal physical constants. These elements can be distributed regularly (uniformly) or irregularly and can have a specific, random or variable shape. The composite as a whole can be described using a set of microgeometrical characteristics, for example, connectivity, volume fraction of the components, their spatial distribution, etc. [5, 10, 48, 49].

The piezo-active composites (often termed *piezo-composites*) form an important group of modern smart materials. This group is vast due to the large number of components that may be involved in the design of the composites. Among the wide range of piezo-active components to be considered, ferroelectrics (FCs and SCs) play a leading role [4, 5, 10]. Moreover, modern processing technologies enable the synthesis of a variety of ferroelectric SCs, FCs, ferroelectric films, and nano-sized ferroelectrics. The ferroelectric properties of these systems are generally related to the change of the spontaneous polarisation vector in an external electric field (domain switching).

Piezo-active composites are of great interest due to the ability to vary and tailor the microgeometry, effective physical properties, their anisotropy, and hydrostatic and other parameters across a wide range [5, 10, 59–61]. These significant variations appear upon combining different components [5, 10], for example,

(1) FC and polymer (the latter can be either piezo-passive or piezo-active),

(2) ferroelectric SC and FC, or
(3) ferroelectric SC and polymer.

In various compositions (1)–(3) at least one of the components always exhibits piezoelectric properties. The presence of one or more piezoelectric components enables a set of parameters or properties to be attained that are not specific to the separate components, and this synergy is important for many practical transducer applications [10, 60, 61]. The piezo-active composites based on ferroelectrics form the final link in hierarchy-of-properties chains [10, 39] of "single-domain SC → polydomain SC → FC → composite" and "single-domain SC → polydomain SC → heterophase SC → composite".

The structure criteria play an important role in classification schemes applied to the piezo-active composites, and these materials are usually classified according to the following concepts [5, 10, 59]:

(1) connectivity of the structural elements,
(2) relative size and shape of the structural elements and
(3) features of the arrangement of structural elements.

The well-known classification of the two-component composites with planar interfaces was first put forward by Newnham et al. [62]. This classification is concerned with so-called *connectivity* of each component. Connectivity is regarded as one of the main characteristics of the microstructure and expressed by the numbers of dimensions (or co-ordinate axes) in which each component is continuously distributed between limiting surfaces of the composite sample. The distribution of a self-connected state of a component can take place along zero, one, two, or three co-ordinate axes, i.e., connectivity $\alpha = 0, 1, 2,$ or 3 for component 1 and connectivity $\beta = 0, 1, 2,$ or 3 for component 2. The connectivity of a two-component composite is written in a general form [10, 59, 62] of $\alpha{-}\beta$ where the connectivity of the piezoelectric or most piezo-active component takes the first position (α). In the case of $\alpha \leq \beta$, the n-component composites are described by $(n + 3)!\,/\,(3!\,n!)$ connectivities [62], for $n = 2$ the number of connectivities is 10. It is also possible to introduce 10 alternative connectivities $\alpha{-}\beta$ at $\alpha \geq \beta$.

The concept of connectivity [62] is fundamental in developing an understanding of the electromechanical interaction between components within piezo-composites, in the study of the distribution of internal electric and mechanical fields and in the interpretation of experimental or calculated data related to composites with specific connectivity. The connectivity of the piezo-composites is crucial in influencing the piezoelectric response and electromechanical coupling of these materials. Moreover, after publishing the pioneering paper [62], connectivities $\alpha{-}\beta$, $\alpha{-}\beta{-}\gamma$, etc. or related connectivity patterns are almost always mentioned when the research is devoted to the composites based on ferroelectrics or related materials. Particular examples that have been experimentally studied include piezo-composites with connectivities 0–3, 1–3, 2–2, 2–3, 3–1, 3–2, and 3–3 [5, 10, 48, 49, 51–53, 59–61]).

Equations (1.4)–(1.19) are valid for the composites containing at least one piezoelectric component under the action of a weak external field. The ability of

(1.4)–(1.19) to predict and describe the electromechanical properties of piezo-active composites is reasonable in cases when these properties can be regarded as effective (or overall), i.e., characterising the response of the composite sample as a whole. The effective electromechanical properties and related parameters enable us to move away from the properties of the individual components, the specifics of microgeometry and other features of heterogeneous materials and to estimate the potential advantages and applications of these materials.

The problem of predicting the effective physical properties is of interest to many specialists undertaking theoretical and experimental studies of these heterogeneous materials. A formulation of the related problem on the effective electromechanical properties in a piezo-active composite is given in monograph [5]. If the averaged components of the electric field $< E_f >$ and the mechanical strain $< \xi_q >$ in a macroscopic region of the composite sample are independent of co-ordinates x_j ($j = 1, 2$ and 3), then Eqs. (1.4) and (1.5) for the piezoelectric medium can be written for the piezo-active composite as

$$< \sigma_p > = c^{*E}_{pq} < \xi_q > - e^*_{fp} < E_f > \tag{1.28}$$

$$< D_k > = e^*_{kl} < \xi_l > + \varepsilon^{*\xi}_{kr} < E_r > \tag{1.29}$$

In (1.28) and (1.29) elastic moduli c^{*E}_{pq}, piezoelectric coefficients e^*_{fp} and dielectric permittivities $\varepsilon^{*\xi}_{kr}$ constitute the full set of effective electromechanical constants[1] that are determined [5] by taking into account equations of electric and mechanical equilibrium and boundary conditions at the surface of the macroscopic region in the heterogeneous medium. The determination of the effective electromechanical properties of the piezo-active composite is concerned with an averaging of a series of vector and tensor components of the electric and mechanical fields, for example, ξ_q, E_f, σ_p, and D_k. This averaging is performed on volume fractions of the composite components ($n = 1, 2, \ldots$), for which the full sets of electromechanical constants, such as $c^{(n),E}_{pq}$, $e^{(n)}_{fp}$ and $\varepsilon^{(n),\xi}_{kr}$ [see the similar electromechanical constants in (1.4) and (1.5)] or other electromechanical constants involved in (1.6)–(1.11), are known.

In the focus of the problem of the prediction of effective properties of composites there is a method of homogenisation of properties [5, 10, 63]. Based on the detailed analysis of results concerning composite materials and their effective properties, Khoroshun et al. [5] placed emphasis on two main scientific directions in modern mechanics of piezo-active composites. The first direction represents the mechanics of the composites having regular (periodic) structures [52, 53, 61, 63]. The second direction is related to the mechanics of stochastically heterogeneous materials,

[1] Hereafter we use asterisk (*) to denote the effective (average) properties of the ferroelectric polydomain single crystal, FC (polycrystal) and composite. These properties are often determined in the so-called long-wave approximation [10], for instance, in the case when the wavelength of an external field is much longer than the thickness of the separate domain in the single-crystal sample, of the layer in the composite sample, etc.

including the piezo-active composites with arbitrary connectivity, shape and distribution of structural elements [5].

The first direction deals with periodic solutions of equations of mechanics of micro-inhomogeneous media in which the regular distribution of the structural elements is present. As a rule, such solutions are applicable to the matrix piezo-active composites with inclusions having the appropriate shape, e.g., spheroids. The accompanying method, termed *the method of regularisation of structure* [5], is often applied to the piezo-active composites with a certain disorder in the shape and distribution of the structural elements. In this method the real composite sample is substituted by a model material with regularly distributed structural elements having the appropriate shape [10, 52, 53, 63]. In such a model material, a periodic representative volume element is chosen and analysed using the appropriate micromechanical methods, including *the finite-element method* (FEM) [64, 65].

The second direction implies using random functions [5] to describe the effective properties of the piezo-active composite with a stochastic structure. These properties are regarded as randomly varied ones over the composite sample, and the homogenisation can be performed with regard to mathematical features of the random functions. This approach is suitable for the prediction of the effective properties without essential restrictions of the shape, distribution of inclusions and the connectivity of the composite as a whole.

A considerable amount of research is devoted to 0–3 composites [10, 48, 49, 52, 65, 66] that contain a system of isolated piezoelectric inclusions embedded in a large matrix (being either piezo-passive or piezo-active). It is often assumed that the inclusions have the shape of a spheroid [65, 66] or a rectangular parallelepiped [52, 67] and are aligned regularly in the matrix. An electromechanical interaction between each inclusion and the surrounding matrix is taken into account in connection with internal electric and mechanical fields and boundary conditions for the specific shape of the inclusion.

In *the matrix method,* references [52, 67] put forward an approach to predict the electromechanical properties of 0–3 FC / polymer composites. The theoretical description is based on the matrix approach [68] previously applied to the 2–2 composite system. This approach is useful to perform an averaging procedure for a 0–3 composite with a regular distribution of parallelepiped-like inclusions. The method developed by Levassort et al. [52] has been successfully extended to 3–3 and 1–3 FC / polymer piezo-composites [10, 53, 67] with planar interfaces.

Many publications on 0–3 composites are concerned with a piezoelectric ellipsoidal inclusion problem [10, 49, 50, 69–71]. This problem stems from the classical Eshelby analysis [72, 73] of the stress and strain fields in and around an elastic ellipsoidal inclusion. Work on the coupled electric and mechanical fields in heterogeneous materials implied the application of the equivalent inclusion method [72, 73] for the description of the effective properties in the piezo-active composites, poled FCs and piezo-active materials with pores or cracks, etc. [10, 48–50]. The nature of the inclusion in the 0–3 composite can be either piezo-active or piezo-passive, and no restrictions on its symmetry are introduced [48, 49, 66, 69–71]. The matrix can be either piezo-active (transversely isotropic) or piezo-passive (isotropic).

The analysis of the coupled electromechanical behaviour of an "inclusions – matrix" system is based on knowledge of the Eshelby tensors. These tensors represent the strain and electric fields that are induced in the inclusion due to a constraint of the matrix in the external fields. The Eshelby tensors are expressed in the explicit form for the following inclusion shapes [74, 75]: spheroid, elliptical cylinder, rod, penny, and ribbon-like. All of the inclusions are assumed to be aligned along the axis of anisotropy, i.e., along the poling axis in the transversely isotropic medium. As in the classical work by Eshelby [72, 73], the Eshelby tensors related to the piezo-active composite [74, 75] depend on the shape of the inclusion and on the properties in the matrix. Further averaging of the electromechanical properties is often carried out according to a self-consistent scheme. The main variants of this scheme are concerned with the EMM [76, 77] and the *effective field method* (EFM, also termed *the mean field method*) [49, 77].

In the EMM the inclusion is regarded as a region in a continuous medium (i.e., in a matrix containing an ensemble of similar inclusions). The effective properties in this medium are found using the Eshelby tensors for the specified shape of the inclusions, and calculations are performed within the framework of iterative (self-consistent) procedures.

The application of the EFM to piezo-active composites stems from the Mori – Tanaka method [78] based on the concept of an average stress in the matrix containing the inclusions with so-called *eigenstrains*. The eigenstrains represent the strains appearing in a stress-free region, similar to the spontaneous strains in the ferroelectric or ferroelastic phases. According to the EFM concept, the inclusion interacts with the matrix subjected to an action of an external electric and mechanical field. Due to the presence of the ensemble of similar inclusions in the matrix, the field can be regarded as an effective field that acts on each inclusion therein. This means that the effective (or average) electric and mechanical field in the composite sample play a key role in forming the overall effective electromechanical properties. In the last decades the EFM approach has been one of the most powerful and most suitable methods [49, 77, 79] for studying the overall behaviour of piezo-active composites and for predicting their effective electromechanical properties in a wide volume-fraction range.

The effective electromechanical properties of the 0–3 composite with spheroidal inclusions can be also determined using the dilute concentration limit (or dilute solution) [50, 77, 79], the differential scheme [79] and the conditional moments method [5]. These methods are based on different averaging procedures and take into account features of the arrangement of the inclusions and their electromechanical interaction.

The determination of the effective properties of the piezo-active composites with arbitrary connectivity is often carried out by means of the FEM [64, 65, 80–86]. This method employs numerical modelling techniques that take into account boundary conditions for electric and mechanical fields in a composite system. The model of the composite is based on the representative unit cell being the periodic representative volume element, and this element is assumed to be characteristic of the whole composite structure. Periodic boundary conditions are enforced on the boundary of the representative unit cell. The latter is discretised using tetrahedral or hexahedral

elements in 3D problems, or using triangular or quadrilateral elements in 2D problems. The unknown displacement and electric-potential fields are interpolated using suitable shape functions: usually, linear or quadratic Lagrangian shape functions are adopted. Computations for diverse average strain and electric fields imposed to the representative unit cell are performed. Direct or iterative solvers can be used to solve the resulting linear system of equations. After solving the electroelastic equilibrium problem, the effective electromechanical constants of the composite are computed column-wise, by averaging the resulting local stress and electric-displacement fields over the representative unit cell.

An important advantage of the FEM approach is the lack of restrictions on connectivity of the composite, sizes of the inclusions and their spatial distribution, the number of the components and their properties. Trends in the study of the piezo-active composites and related materials show that the FEM approach and related finite-element software become increasingly more widespread in mechanical-engineering, smart-materials and piezo-technical applications (transducers, sensors, actuators, hydrophones, acoustic antennae, etc.). However, advances in numerical techniques do not exclude the development of analytical methods for two-index connectivity patterns such as 0–3, 1–3 and 2–2 (see, for instance, monographs [5, 10, 48, 63]).

1.6 Conclusion

In this chapter we have considered the electromechanical properties and related characteristics of the piezoelectric medium. In the last decades the most important piezoelectric materials have been poled FCs, relaxor-ferroelectric SCs with engineered domain structures and piezo-active composites that consist of at least one of the aforementioned components. The use of the highly-effective relaxor-ferroelectric SCs with compositions near the MPB is of significant interest due to their excellent electromechanical properties compared to those of the conventional FCs with the same perovskite-type structure. The excellent electromechanical properties of the relaxor-ferroelectric SCs in the domain-engineered / heterophase states are concerned with large values of the piezoelectric coefficients d_{ij}, ECFs k_{ij} and elastic compliances s^E_{ab}. Undoubtedly, these SCs are to be regarded as highly effective components of modern piezo-active composite materials, and their effectiveness for many composite piezo-technical applications strongly depend on the performance of the SC components therein.

The electromechanical properties of the poled FC and composite materials are regarded as "effective properties" in accordance with features of the microstructure, domain structure, arrangement of components, connectivity, etc. The piezo-active composites based on ferroelectrics have been the final link in the hierarchy-of-properties chains of "single-domain SC → polydomain SC → FC → composite" and "single-domain SC → polydomain SC → heterophase SC → composite", and this makes composites a unique range of materials whose effective properties can be tailored in wide ranges due to a range of factors.

Examples of the full sets of electromechanical constants of the $[001]_c$-poled domain-engineered relaxor-ferroelectric SCs (Table 1.1) and poled FCs (Table 1.2) suggest that these materials can be used as components of modern piezo-active composites and the anisotropy of the properties of these components may be of value in piezo-technical applications. A review of methods applied for the prediction of the effective electromechanical properties in the piezo-active composites enables us to choose the method(s) suitable for the specific microgeometry and connectivity patterns of the composites studied. As follows from numerous literature data, no systematic study of the orientation and related effects in the piezo-active composites has been undertaken.

References

1. Levanyuk AP, Sannikov DG (1994) Piezoelectrics. In: Prokhorov AM (ed) Physics encyclopaedia, vol 4. Bolshaya Rossiyskaya Entsiklopedia, Moscow, pp 188–189 (in Russian)
2. Ikeda T (1990) Fundamentals of piezoelectricity. Oxford University Press, Oxford, New York, Toronto
3. Zheludev IS (1971) Physics of crystalline dielectrics, Vol. 2. Electrical properties. Plenum, New York
4. Uchino K (1997) Piezoelectric actuators and ultrasonic motors. Kluwer, Boston
5. Khoroshun LP, Maslov BP, Leshchenko PV (1989) Prediction of effective properties of piezo-active composite materials. Naukova Dumka, Kiev (in Russian)
6. Turik AV (1970) Elastic, piezoelectric, and dielectric properties of single crystals of $BaTiO_3$ with a laminar domain structure. Sov Phys–Solid State 12:688–693
7. Aleshin VI (1990) Domain-orientation contribution into constants of ferroelectric polydomain single crystal. Zh Tekh Fiz 60:179–183 (in Russian)
8. Topolov VYu (2003) Domain wall displacements and piezoelectric activity of $KNbO_3$ single crystals. J Phys Condens Matter 15:561–565
9. Gorish AV, Dudkevich VP, Kupriyanov MF, Panich AE, Turik AV (1999) Piezoelectric device-making. Physics of ferroelectric ceramics, Vol. 1. Radiotekhnika, Moscow (in Russian)
10. Topolov VYu, Bowen CR (2009) Electromechanical properties in composites based on ferroelectrics. Springer, London
11. Siffert P, (2008) Foreword. In: Heywang W, Lubitz K, Wersing W (eds.) Piezoelectricity. Evolution and future of a technology. Springer, Berlin, p V
12. Newnham RE (2005) Properties of materials. Anisotropy, symmetry, structure. Oxford University Press, New York
13. Berlincourt DA, Cerran DR, Jaffe H (1964) Piezoelectric and piezomagnetic materials and their function in transducers. In: Mason W (ed) Physical acoustics. Principles and methods. vol 1. Methods and devices. Pt A. Academic Press, New York, pp 169–270
14. Haertling G (1999) Ferroelectric ceramics: history and technology. J Am Ceram Soc 82:797–818
15. Cross LE (2008) Relaxor ferroelectrics. In: Heywang W, Lubitz K, Wersing W (eds) Piezoelectricity. Evolution and future of a technology. Springer, Berlin, pp 131–156
16. Park S-E, Hackenberger W (2002) High performance single crystal piezoelectrics: applications and issues. Curr Opin Solid State Mater Sci 6:11–18
17. Smolensky GA, Bokov VA, Isupov VA, Krainik NN, Pasynkov RE, Sokolov AI, Yushin NK (1985) Physics of ferroelectric phenomena. Nauka, Leningrad (in Russian)
18. Noheda B (2002) Structure and high-piezoelectricity in lead oxide solid solutions. Curr Opin Solid State Mater Sci 6:27–34

19. Park S-E, Shrout TR (1997) Ultrahigh strain and piezoelectric behavior in relaxor based ferroelectric single crystals. J Appl Phys 82:1804–1811
20. Park S-E, Shrout TR (1997) Relaxor based ferroelectric single crystals for electro-mechanical actuators. Mater Res Innovations 1:20–25
21. Dammak H, Renault A-É, Gaucher P, Thi MP, Calvarin G (2003) Origin of the giant piezoelectric properties in the [001] domain engineered relaxor single crystals. Jpn J Appl Phys Pt 1(42):6477–6482
22. Topolov VYu, Turik AV (2002) An intermediate monoclinic phase and electromechanical interactions in $x\mathrm{PbTiO_3} - (1-x)\mathrm{Pb}(\mathrm{Zn_{1/3}Nb_{2/3}})\mathrm{O_3}$ crystals. Phys Solid State 44:1355–1362
23. Fu H, Cohen RE (2000) Polarization rotation mechanism for ultrahigh electromechanical response in single-crystal piezoelectrics. Nature 403:281–283
24. Davis M (2007) Picturing the elephant: giant piezoelectric activity and the monoclinic phases of relaxor-ferroelectric single crystals. J Electroceram 19:23–45
25. Noheda B, Cox DE, Shirane G, Park S-E, Cross LE, Zhong Z (2001) Polarization rotation via a monoclinic phase in the piezoelectric $92\%\mathrm{PbZn_{1/3}Nb_{2/3}O_3}$-$8\%\mathrm{PbTiO_3}$. Phys Rev Lett 86:3891–3894
26. Wada S, Tsurumi T (2002) Domain switching properties in PZN-PT single crystals with engineered domain configurations. Key Eng Mater 214–215:9–14
27. Zhang R, Jiang B, Cao W (2001) Elastic, piezoelectric, and dielectric properties of multidomain $0.67\mathrm{Pb}(\mathrm{Mg_{1/3}Nb_{2/3}})\mathrm{O_3} - 0.33\mathrm{PbTiO_3}$ single crystals. J Appl Phys 90:3471–3475
28. Zhang R, Jiang W, Jiang B, Cao W (2002) Elastic, dielectric and piezoelectric coefficients of domain engineered $0.70\mathrm{Pb}(\mathrm{Mg_{1/3}Nb_{2/3}})\mathrm{O_3} - 0.30\mathrm{PbTiO_3}$ single crystal. In: Cohen RE (ed) Fundamental physics of ferroelectrics. American Institute of Physics, Melville, pp 188–197
29. Liu G, Jiang W, Zhu J, Cao W (2011) Electromechanical properties and anisotropy of single- and multi-domain $0.72\mathrm{Pb}(\mathrm{Mg_{1/3}Nb_{2/3}})\mathrm{O_3} - 0.28\mathrm{PbTiO_3}$ single crystals. Appl Phys Lett 99:162901–3P
30. Yin J, Jiang B, Cao W (2000) Elastic, piezoelectric, and dielectric properties of $0.955\mathrm{Pb}(\mathrm{Zn_{1/3}Nb_{2/3}})\mathrm{O_3} - 0.045\mathrm{PbTiO_3}$ single crystals. IEEE Trans Ultrason Ferroelectr Freq Control 47:285–291
31. Zhang R, Jiang B, Cao W, Amin A (2002) Complete set of material constants of $0.93\mathrm{Pb}(\mathrm{Zn_{1/3}Nb_{2/3}})\mathrm{O_3} - 0.07\mathrm{PbTiO_3}$ domain engineered single crystal. J Mater Sci Lett 21:1877–1879
32. Fesenko EG, Gavrilyachenko VG, Semenchev AF (1990) Domain structure of multiaxial ferroelectric crystals. Rostov University Press, Rostov-on-Don (in Russian)
33. Liu T, Lynch CS (2003) Ferroelectric properties of [110], [001] and [111] poled relaxor single crystals: measurements and modeling. Acta Mater 51:407–416
34. Hall DA (2001) Review. Nonlinearity in piezoelectric ceramics. J Mater Sci 36:4575–4601
35. Rödel J, Kreher WS (2000) Self-consistent modeling of non-linear effective properties of polycrystalline ferroelectric ceramics. Comput Mater Sci 19:123–132
36. Rödel J, Kreher WS (2003) Modeling of linear and nonlinear behavior of polycrystalline ferroelectric ceramics. J Eur Ceram Soc 23:2297–2306
37. Turik AV, Topolov VYu, Aleshin VI (2000) On a correlation between remanent polarization and piezoelectric coefficients of perovskite-type ferroelectric ceramics. J Phys D Appl Phys 33:738–743
38. Topolov VYu, Bondarenko EI, Turik AV, Chernobabov AI (1993) The effect of domain structure on electromechanical properties of $\mathrm{PbTiO_3}$-based ferroelectrics. Ferroelectrics 140:175–181
39. Turik AV, Topolov VYu (1997) Ferroelectric ceramics with a large piezoelectric anisotropy. J Phys D Appl Phys 30:1541–1549
40. Topolov VYu, Turik AV, Chernobabov AI (1994) On the mechanism of high piezoelectric anisotropy in lead titanate-based ferroelectrics. Crystallogr Rep 39:805–809
41. Bondarenko EI, Topolov VYu, Turik AV (1990) The effect of 90° domain wall displacements on piezoelectric and dielectric constants of perovskite ceramics. Ferroelectrics 110:53–56
42. Bondarenko EI, Topolov VYu, Turik AV (1991) The role of 90° domain wall displacements in forming physical properties of perovskite ferroelectric ceramics. Ferroelectr Lett Sect 13:13–19

43. Ruschmeyer K, Helke G, Koch J, Lubitz K, Möckl T, Petersen A, Riedel M, Schönecker A (1995) Piezokeramik: Grundlagen, Werkstoffe. Applikationen, Expert-Verlag, Renningen-Malmsheim
44. Algueró M, Alemany C, Pardo L, González AM (2004) Method for obtaining the full set of linear electric, mechanical and electromechanical coefficients and all related losses of a piezoelectric ceramic. J Am Ceram Soc 87:209–215
45. Dantsiger AYa, Razumovskaya ON, Reznitchenko LA, Grineva LD, Devlikanova RU, Dudkina SI, Gavrilyatchenko SV, Dergunova NV, Klevtsov AN (1994) Highly effective piezoceramic materials (Handbook). Kniga, Rostov-on-Don (in Russian)
46. Bechmann R (1956) Elastic, piezoelectric, and dielectric constants of polarized barium titanate ceramics and some applications of the piezoelectric equations. J Acoust Soc Am 28:347–350
47. Jaffe B, Cook WR, Jaffe H (1971) Piezoelectric ceramics. Academic Press, London
48. Luchaninov AG (2002) Piezoelectric effect in non-polar heterogeneous ferroelectric materials. Volgograd State Academy of Architecture and Construction, Volgograd (in Russian)
49. Huang JH, Kuo W-S (1996) Micromechanics determination of the effective properties of piezoelectric composites containing spatially oriented short fibers. Acta Mater 44:4889–4898
50. Dunn ML, Taya M (1993) Electromechanical properties of porous piezoelectric ceramics. J Am Ceram Soc 76:1697–1706
51. Ritter T, Geng X, Shung KK, Lopath PD, Park S-E, Shrout TR (2000) Single crystal PZN/PT - polymer composites for ultrasound transducer applications. IEEE Trans Ultrason Ferroelectr Freq Control 47:792–800
52. Levassort F, Lethiecq M, Millar C, Pourcelot L (1998) Modeling of highly loaded 0–3 piezoelectric composites using a matrix method. IEEE Trans Ultrason Ferroelectr Freq Control 45:1497–1505
53. Levassort F, Lethiecq M, Certon D, Patat F (1997) A matrix method for modeling electroelastic moduli of 0–3 piezo-composites. IEEE Trans Ultrason Ferroelectr Freq Control 44:445–452
54. Ikegami S, Ueda I, Nagata T (1971) Electromechanical properties of $PbTiO_3$ ceramics containing La and Mn. J Acoust Soc Am 50:1060–1066
55. Xu Y (1991) Ferroelectric materials and their applications. North-Holland, Amsterdam, London, New York, Toronto
56. Nagatsuma K, Ito Y, Jyomura S, Takeuchi H, Ashida S (1985) Elastic properties of modified $PbTiO_3$ ceramics with zero temperature coefficients. In: Taylor GW (ed) Ferroelectricity and related phenomena, vol 4. Piezoelectricity, Gordon and Breach Science Publishers, New York, pp 167–176
57. Levassort F, Thi MP, Hemery H, Marechal P, Tran-Huu-Hue L-P, Lethiecq M (2006) Piezoelectric textured ceramics: effective properties and application to ultrasonic transducers. Ultrasonics 44 Suppl 1:e621–e626
58. Topolov VYu, Turik AV, Chernobabov AI (1999) Evaluation of nontrivial behaviour of electromechanical coupling factors in $PbTiO_3$-type ferroelectric ceramics. J Eur Ceram Soc 19:1213–1217
59. Newnham RE (1997) Molecular mechanisms in smart materials. Mater Res Soc Bull 22(5):20–34
60. Gururaja TR, Safari A, Newnham RE, Cross LE (1988) Piezoelectric ceramic-polymer composites for transducer applications. In: Levinson LM (ed) Electronic ceramics: Properties, devices, and applications. Marcel Dekker, New York, pp 92–128
61. Akdogan EK, Allahverdi M, Safari A (2005) Piezoelectric composites for sensor and actuator applications. IEEE Trans Ultrason Ferroelectr Freq Control 52:746–775
62. Newnham RE, Skinner DP, Cross LE (1978) Connectivity and piezoelectric-pyroelectric composites. Mater Res Bull 13:525–536
63. Sokolkin YuV, Pan'kov AA (2003) Electroelasticity of piezo-composites with irregular structures. Fizmatlit, Moscow (in Russian)
64. Topolov VYu, Bisegna P (2010) Anisotropic piezoelectric properties of 1–3 ceramic / polymer composites comprising rods with elliptic cross section. J Electroceram 25:26–37

65. Topolov VYu, Bisegna P, Bowen CR (2011) Analysis of the piezoelectric performance of modern 0–3-type composites based on relaxor-ferroelectric single crystals. Ferroelectrics 413:176–191
66. Glushanin SV, Topolov VYu, Krivoruchko AV (2006) Features of piezoelectric properties of 0–3 $PbTiO_3$-type ceramic / polymer composites. Mater Chem Phys 97:357–364
67. Levassort F, Topolov VYu, Lethiecq M (2000) A comparative study of different methods of evaluating effective electromechanical properties of 0–3 and 1–3 ceramic / polymer composites. J Phys D Appl Phys 33:2064–2068
68. Akcakaya E, Farnell GW (1988) Effective elastic and piezoelectric constants of superlattices. J Appl Phys 64:4469–4473
69. Benveniste Y (1992) The determination of the elastic and electric fields in a piezoelectric inhomogeneity. J Appl Phys 72:1086–1095
70. Wang B (1992) Three-dimensional analysis of an ellipsoidal inclusion in a piezoelectric material. Int J Solids Struct 29:293–308
71. Dunn ML, Taya M (1993) An analysis of piezoelectric composite materials containing ellipsoidal inhomogeneities. Proc Roy Soc (Lon) Pt A 443:265–287
72. Eshelby J (1957) The determination of the elastic field of an ellipsoidal inclusion, and related problems. Proc Roy Soc (Lon) Pt A 241:376–396
73. Eshelby J (1959) The elastic field outside an ellipsoidal inclusion. Proc Roy Soc (Lon) Pt A 252:561–569
74. Huang JH, Yu S (1994) Electroelastic eshelby tensors for an ellipsoidal piezoelectric inclusion. Compos Eng 4:1169–1182
75. Mikata Y (2001) Explicit determination of piezoelectric Eshelby tensors for a spheroidal inclusion. Int J Solids Struct 38:7045–7063
76. Nan C-W (1994) Effective-medium theory of piezoelectric composites. J Appl Phys 76:1155–1163
77. Fakri N, Azrar L, El Bakkali L (2003) Electroelastic behavior modeling of piezoelectric composite materials containing spatially oriented reinforcements. Int J Solids Struct 40:361–384
78. Mori T, Tanaka K (1973) Average stress in matrix and average elastic energy of materials with misfitting inclusions. Acta Metall 21:571–574
79. Dunn ML (1993) Micromechanics of coupled electroelastic composites: effective thermal expansion and pyroelectric coefficients. J Appl Phys 73:5131–5140
80. Berger H, Kari S, Gabbert U, Rodríguez-Ramos R, Bravo-Castillero J, Guinovart-Díaz R (2005) A comprehensive numerical homogenization technique for calculating effective coefficients of uniaxial piezoelectric fibre composites. Mater Sci Eng A 412:53–60
81. Pettermann HE, Suresh S (2000) A comprehensive unit cell model: a study of coupled effects in piezoelectric 1–3 composites. Int J Solids Struct 37:5447–5464
82. Bowen CR, Perry A, Stevens R, Mahon S (2001) Analytical and numerical modelling of 3–3 piezoelectric composites. Integr Ferroelectr 32:333–342
83. Kara H, Perry A, Stevens R, Bowen CR (2002) Interpenetrating PZT / polymer composites for hydrophones: models and experiments. Ferroelectrics 265:317–332
84. Jayasundere N, Smith BV (1993) Dielectric constant for binary piezoelectric 0–3 composite. J Appl Phys 73:2462–2466
85. Poizat C, Sester M (2001) Homogénéisation périodique de composites piézoélectriques 0–3: influence de la distribution. Revue des Composites et des Matériaux Avancés 11:65–74
86. Kar-Gupta R, Venkatesh TA (2005) Electromechanical response of 1–3 piezoelectric composites: effect of poling characteristics. J Appl Phys 98:054102

Chapter 2
Orientation Effects in Single-Domain Single Crystals

2.1 Single-Domain $0.67Pb(Mg_{1/3}Nb_{2/3})O_3 - 0.33PbTiO_3$

Full sets of electromechanical constants of perovskite-type relaxor-ferroelectrics of solid solutions of PMN–xPT and PZN–xPT are often measured on polydomain or domain-engineered SC samples (see for instance, Refs. [1–6]). The full set of room-temperature electromechanical constants related to the single-domain state was first measured [7] on PMN–0.33PT SCs. This particular composition is very close to the MPB [8], and single-domain SCs at $x = 0.33$ are characterised by rhombohedral 3 m symmetry [9]. Based on experimental data [7] of the single-domain PMN–0.33PT SC, their piezoelectric coefficients d_{3j} ($j = 1$ and 3) [9, 10], dielectric permittivity $\varepsilon^{\sigma}_{33}$ and ECF k_{33} [9] were calculated along arbitrary directions of the crystallographic axes, and also the spontaneous polarisation vector $\boldsymbol{P}_s$. The further study and generalisation of the orientation dependences of the electromechanical properties of the single-domain PMN–0.33PT SCs has been carried out in work [11].

Now we consider some features of the orientation dependences of the piezoelectric coefficients and ECFs of the aforementioned SC. It is assumed that the spontaneous polarisation vector $\boldsymbol{P}_s$ of the single-domain sample is parallel to the $[001]_{rh}$ direction (Fig. 2.1a) and is connected with the rectangular co-ordinate system $(X_1X_2X_3)$ of the SC sample, where subscript "*rh*" denotes "rhombohedral". The $[001]_{rh}$ direction coincides with the $[111]_c$ direction in the cubic (perovskite) unit cell, $OX_3||[111]_c$, and the subscript "*c*" denotes "cubic". An arbitrary SC orientation due to the transformation of the co-ordinate axes $(X_1X_2X_3) \rightarrow (X'_1X'_2X'_3)$ (Fig. 2.1b) is described in terms of the well-known Euler angles φ, ψ and θ [12]. Taking into account this transformation, we represent the electromechanical constants of the SC sample in $(X'_1X'_2X'_3)$ as tensor components

$$\varepsilon^{\sigma'}_{mn} = r_{mp}r_{nq}\varepsilon^{\sigma}_{pq},\ d'_{efg} = r_{ej}r_{fk}r_{gl}d_{jkl} \quad \text{and} \quad s^{E'}_{rtuv} = r_{ra}r_{tb}r_{uc}r_{vd}s^{E}_{abcd}. \qquad (2.1)$$

In (2.1) the terms $\varepsilon^{\sigma}_{pq}$, d_{jkl} and s^{E}_{abcd} are tensor components of dielectric permittivities (second rank), piezoelectric coefficients (third rank) and elastic compliances

V. Yu. Topolov et al., *Piezo-Active Composites*,
Springer Series in Materials Science 185, DOI: 10.1007/978-3-642-38354-0_2,

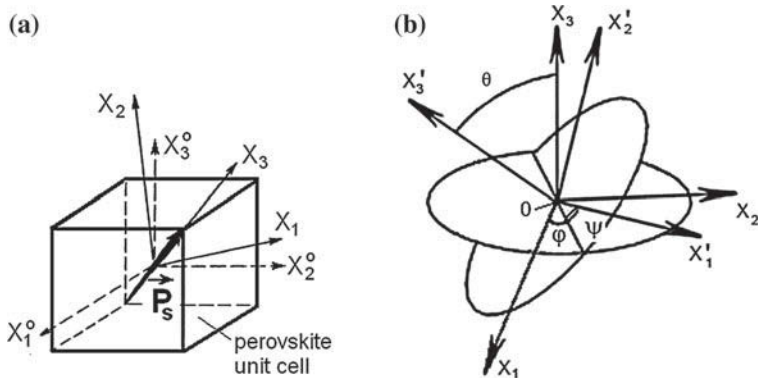

Fig. 2.1 Orientation of the domain with respect to the main crystallographic axes OX_j and perovskite unit-cell axes OX_j° **a** and interconnections between the axes of co-ordinate systems $(X_1X_2X_3)$ and $(X_1'X_2'X_3')$ **b**. $\boldsymbol{P}_s$ is the spontaneous polarisation vector in the rhombohedral phase, φ, ψ and θ are Euler angles

(fourth rank), respectively, and r_{mp} are elements of the rotation matrix

$$\|r\| = \begin{pmatrix} \cos\psi\cos\varphi - \sin\psi\cos\theta\cos\varphi & \cos\psi\sin\varphi + \sin\psi\cos\theta\cos\varphi & \sin\psi\sin\theta \\ -\sin\psi\cos\varphi - \cos\psi\cos\theta\sin\varphi & -\sin\psi\sin\varphi + \cos\psi\cos\theta\cos\varphi & \cos\psi\sin\theta \\ \sin\theta\sin\varphi & -\sin\theta\cos\varphi & \cos\theta \end{pmatrix}$$

that depends [12] on the above-mentioned Euler angles. We also highlight that a summation over the repeated subscripts [for instance, p and q in the $\varepsilon_{mn}^{\sigma\prime}$ formula from (2.1)] is performed from 1 to 3 in accordance with the Einstein summation notation at operations over tensor components.

After the transformation $(X_1X_2X_3) \rightarrow (X_1'X_2'X_3')$ in accordance with (2.1), we use the conventional two-index form [12–15] for the notation of the electromechanical constants as written, for example, in Table 2.1. Based on the electromechanical constants from (2.1), it is possible to determine the orientation dependences of the

Table 2.1 Room-temperature elastic compliances s_{ab}^E (in 10^{-12}Pa^{-1}), piezoelectric coefficients d_{ij} (in pC/N) and dielectric permittiivities ε_{pp}^σ of the single-domain PMN–0.33PT SC (3*m* symmetry). Data from experimental work [7] ([9] in parentheses) are related to the main crystallographic axes OX_j shown in Fig. 2.1a

s_{11}^E	s_{12}^E	s_{13}^E	s_{14}^E	s_{33}^E	s_{44}^E	s_{66}^E
62.16	−53.85	−5.58	−166.24	13.34	510.98	232.02
(62.2)	(−53.8)	(−5.6)	(−166.2)	(13.3)	(511.0)	(232.0)
	d_{15}	d_{22}	d_{31}	d_{33}	$\varepsilon_{11}^\sigma/\ \varepsilon_0$	$\varepsilon_{33}^\sigma/\ \varepsilon_0$
	4,100	1,340	−90	190	3,950	640

remaining piezoelectric coefficients (g'_{ij}, e'_{ij} and h'_{ij}), ECFs k'_{ij} [1] etc. Examples of the orientation dependences of the piezoelectric coefficients and ECFs of the single-domain PMN–0.33PT SC are shown in Figs. 2.2 and 2.3.

The orientation dependences of the electromechanical properties of the SC from the 3*m* symmetry class are characterised by the following important features [11].

1. Electromechanical constants Π'_{33} are independent of the Euler angle φ, where $\Pi = d, e, g, h, k, s^E$, and ε^σ.
2. There are two variants of periodicity on the Euler angle ψ. First, for Π'_{3j} with $j = 1; 2$,

$$\Pi'_{31}(\varphi, \psi, \theta) = \Pi'_{32}(\varphi, \psi + 90^\circ, \theta) \text{ and } \Pi'_{32}(\varphi, \psi, \theta) = \Pi'_{31}(\varphi, \psi + 90^\circ, \theta), \tag{2.2}$$

and second,

$$\Pi'_{33}(\varphi, \psi, \theta) = \Pi'_{33}(\varphi, \psi + 90^\circ, \theta). \tag{2.3}$$

3. Periodicity on the Euler angle φ is a result of the presence of a three-fold axis in the 3*m* symmetry class [15]. As a consequence, the following equality holds:

$$\Pi'_{3j}(\varphi, \psi, \theta) = \Pi'_{3j}(\varphi + 120^\circ, \psi, \theta), \tag{2.4}$$

where $j = 1$, 2 and 3.

4. The piezoelectric coefficients d'_{3j} show a periodical dependence as follows:
   (i) at $\theta = 90^\circ$, independently of φ and ψ, the sum of the piezoelectric coefficients (i.e., the analogue of the hydrostatic piezoelectric coefficient d_h of the poled FC [14]) obeys a condition

$$d'_{31}(\varphi, \psi, 90^\circ) + d'_{32}(\varphi, \psi, 90^\circ) + d'_{33}(\varphi, \psi, 90^\circ) = 0, \tag{2.5}$$

   (ii) at $\varphi = 0$, $\psi = 45^\circ + 90^\circ p$ ($p = 1$, 2 and 3) and independently of θ, condition

$$d'_{31}(0, \psi, \theta) = d'_{32}(0, \psi, \theta) \tag{2.6}$$

   is valid,
   (iii) at $\varphi > 0$, $\psi = 45^\circ + 90^\circ p$ ($p = 1$, 2 and 3) and $\theta = 90^\circ$, an equality

$$d'_{31}(\varphi, \psi, 90^\circ) = d'_{32}(\varphi, \psi, 90^\circ) \tag{2.7}$$

   holds, and
   (iv) at $\varphi = 30^\circ + 60^\circ q$ ($q = 1$, 2, 3, 4, and 5), $\theta = 90^\circ$ and independently of ψ, condition

[1] It should be added that examples of the orientation dependence of ECFs k'_{ij},thickness-mode ECF k'_t and planar-mode ECF k'_p for the single-domain $KNbO_3$ SC in the ferroelectric *mm*2 phase were discussed by Nakamura and Kawamura [13].

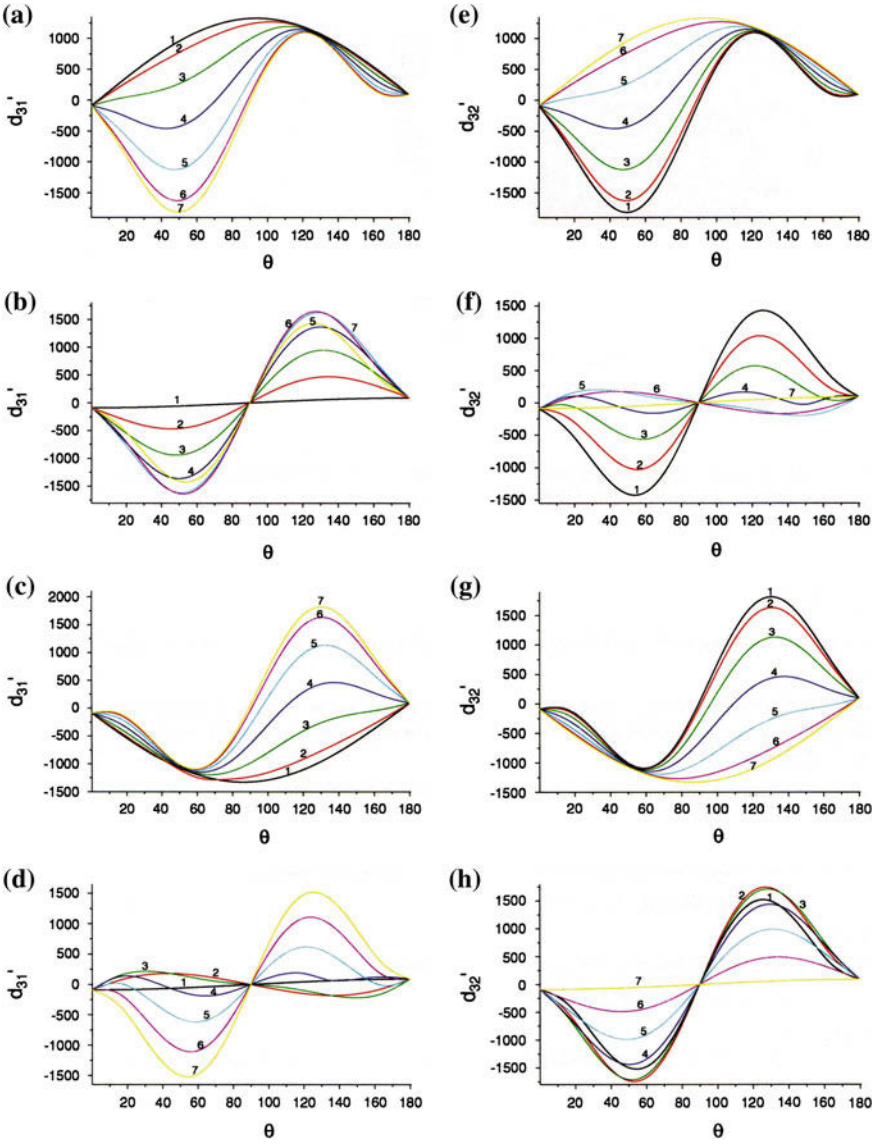

Fig. 2.2 Piezoelectric coefficients $d'_{3j}(\varphi, \psi, \theta)$ (d'_{3j} in pC/N, and φ, ψ and θ in degrees) calculated for the single-domain PMN–0.33PT SC: **a** $j = 1$ and $\varphi = 120°p$, **b** $j = 1$ and $\varphi = 30° + 120°p$, **c** $j = 1$ and $\varphi = 60° + 120°p$, **d** $j = 1$ and $\varphi = 90° + 120°p$, **e** $j = 2$ and $\varphi = 120°p$, **f** $j = 2$ and $\varphi = 30° + 120°p$, **g** $j = 2$ and $\varphi = 60° + 120°p$, **h** $j = 2$ and $\varphi = 90° + 120°p$, and **i** $j = 3$, no dependence on ψ. In graphs **a–h**, curves 1, 2, 3, 4, 5, 6, and 7 are related to $\psi = 0, 15, 30, 45, 60, 75,$ and $90°$, respectively, and $p = 0, 1, 2,$ and 3 (reprinted from paper by Topolov [11], with permission from IOP Publishing)

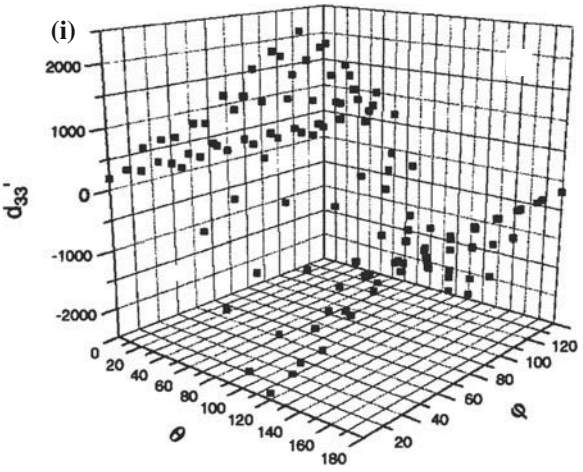

Fig. 2.2 (continued)

$$d'_{31}(\varphi, \psi, 90^\circ) = d'_{32}(\varphi, \psi, 90^\circ) = d'_{33}(\varphi, \psi, 90^\circ) = 0 \tag{2.8}$$

holds, i.e., no piezoelectric response is registered along the OX'_3 axis. Condition (2.8) can be regarded as a specific case of validity of condition (2.5).

An analysis of conditions (2.2)–(2.4) and (2.6)–(2.8) enables us to consider electromechanical constants Π'_{3j} of the single-domain PMN–0.33PT SC in the following ranges of the Euler angles:

$$0 \le \varphi \le 120^\circ,\ 0 \le \psi \le 90^\circ \quad \text{and} \quad 0 \le \theta \le 180^\circ. \tag{2.9}$$

Equations (2.2)–(2.9) suggest that the periodicity of the orientation dependence $\Pi'_{3j}(\varphi, \psi, \theta)$stems from features of the crystal structure of the $3m$ symmetry class [11] and should be taken into consideration in piezoelectric applications.

Comparing the curves in Figs. 2.2 and 2.3 at the corresponding fixed φ angles, one can conclude that the transformation of the curves $d'_{3j} \rightarrow k'_{3j}$ is mainly due to the influence of elastic compliances $s^{E\prime}_{rt}(\varphi, \psi, \theta)$ of the single-domain SC. Dielectric permittivities $\varepsilon^{\sigma\prime}_{pq}(\varphi, \psi, \theta)$ influence the orientation dependence of ECFs $k'_{3j}(\varphi, \psi, \theta)$ to a lesser degree and may be due to the lower rank of the $\varepsilon^{\sigma}_{pq}$ tensor in comparison to the rank of the s^E_{rt} tensor. In general, the comparative analysis of graphs from Figs. 2.2 and 2.3 enable us to conclude that the anisotropy of d'_{3j} and k'_{3j} can be varied within specific ranges. These ranges mainly depend on the anisotropy of d_{3j} and s^E_{rt} which are related to the main crystallographic axes (see Table 2.1).

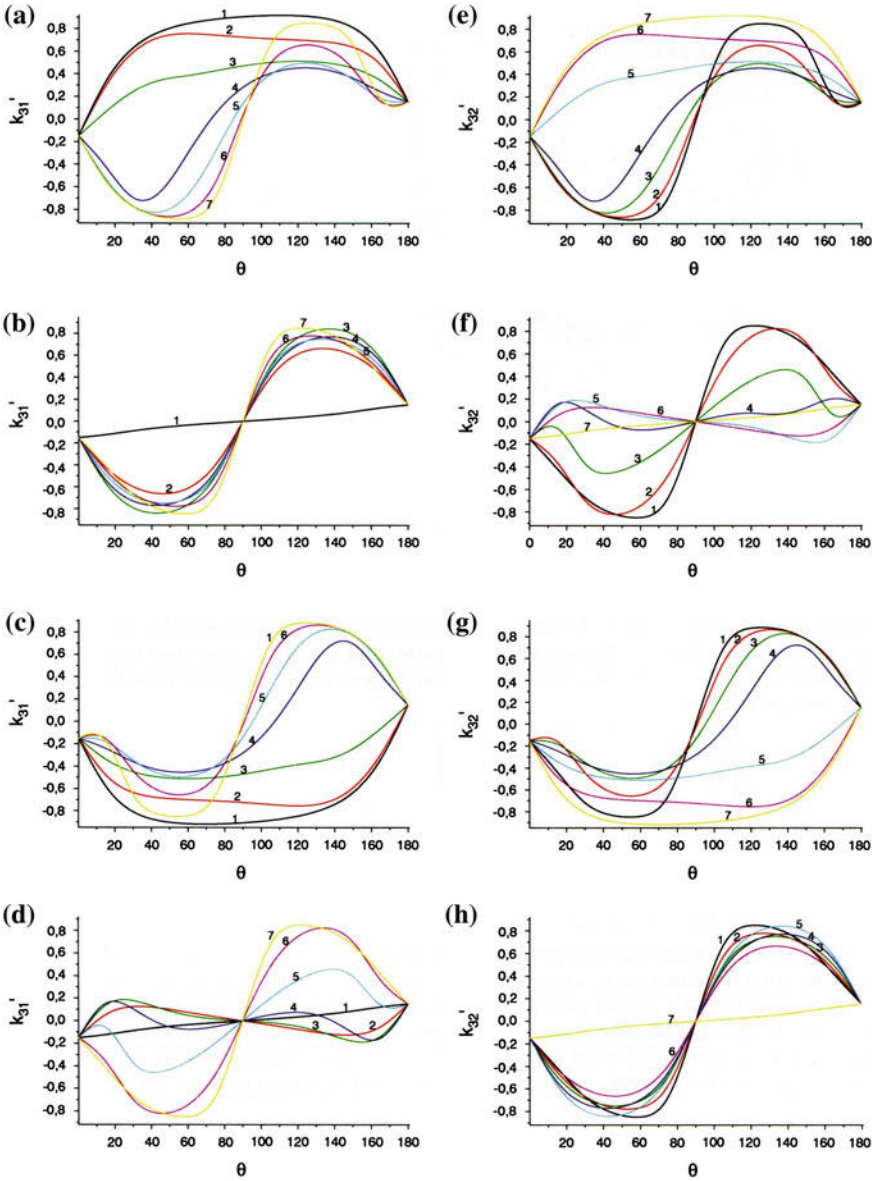

Fig. 2.3 ECFs $k'_{3j}(\varphi, \psi, \theta)$ (φ, ψ and θ in degrees) calculated for the single-domain PMN–0.33PT SC: **a** $j = 1$ and $\varphi = 120° p$, **b** $j = 1$ and $\varphi = 30° + 120° p$, **c** $j = 1$ and $\varphi = 60° + 120° p$, **d** $j = 1$ and $\varphi = 90° + 120° p$, **e** $j = 2$ and $\varphi = 120° p$, **f** $j = 2$ and $\varphi = 30° + 120° p$, **g** $j = 2$ and $\varphi = 60° + 120° p$, **h** $j = 2$ and $\varphi = 90° + 120° p$, and **i** $j = 3$, no dependence on ψ. In graphs **a–h**, curves 1, 2, 3, 4, 5, 6, and 7 are related to $\psi = 0$, 15, 30, 45, 60, 75, and 90°, respectively, and $p =$ 0, 1, 2, and 3 (reprinted from paper by Topolov [11], with permission from IOP Publishing)

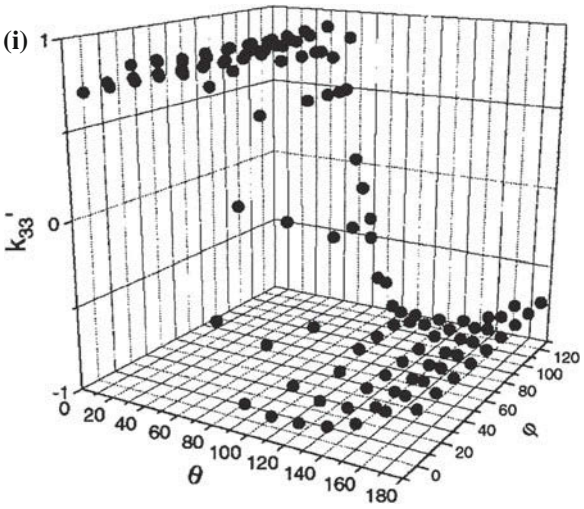

Fig. 2.3 (continued)

2.2 Polydomain $0.67Pb(Mg_{1/3}Nb_{2/3})O_3 - 0.33PbTiO_3$

Polydomain states (multidomains, domain-engineered states) are often formed in bulk relaxor-ferroelectric SC samples [1, 2] when the electric poling direction is not along the spontaneous polarisation vectors of the separate domain types. It is assumed that the $(001)_c$ cut of the rhombohedral PMN–xPT SC, poled along the $[001]_c$ perovskite unit-cell direction, is split into 71°(109°) domains that are mechanical twin components distributed regularly over the sample. Spontaneous polarisation vectors $\boldsymbol{P}_{si}$ in these domains (Fig. 2.4) are given in the coordinate system $(X_1^\circ X_2^\circ X_3^\circ)$ by $\boldsymbol{P}_{s1}(P, P, P)$, $\boldsymbol{P}_{s2}(P, -P, P)$, $\boldsymbol{P}_{s3}(-P, -P, P)$, and $\boldsymbol{P}_{s4}(-P, P, P)$. The 71°(109°) domains are separated by the planar $\{100\}_c$-type domain walls [1, 16, 17] that are permissible according to work [18, 19]. Based on the aforementioned domain arrangement, we consider two examples of the effective (average) electromechanical properties in polydomain PMN–0.33PT SCs.

2.2.1 Two Domain Types

We consider a laminar domain structure that is characterised by two domain types with $\boldsymbol{P}_{s1}(P, P, P)$ and $\boldsymbol{P}_{s2}(P, -P, P)$ (see the vector orientations in Fig. 2.4). These domains are regularly distributed over the SC sample and are separated by stress-free domain walls with normal vectors $\boldsymbol{n}_i || [001]_c$. We assume that the volume fractions of the domains with $\boldsymbol{P}_{s1}$ and $\boldsymbol{P}_{s2}$ equal h and $1 - h$, respectively. The electromechanical

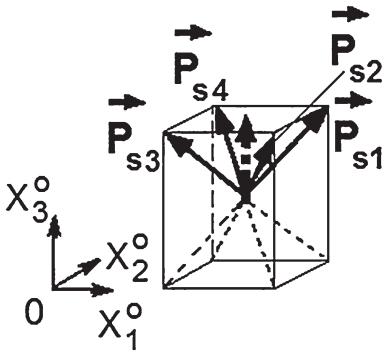

Fig. 2.4 Schematic of 71° (109°) domain types in the $[001]_c$-poled rhombohedral SC. Axes of the co-ordinate system $(X_1^\circ X_2^\circ X_3^\circ)$ are parallel to the crystallographic axes of the perovskite unit cell. The resulted (average) spontaneous polarisation vector (see the dotted arrow) is parallel to $OX_3^\circ || [001]_c$

properti of the *i*th domain type are determined in the $(X_1^\circ X_2^\circ X_3^\circ)$ system in accordance with (2.1), and the rotation matrices are

$$\|r\| = \begin{pmatrix} 1/\sqrt{2} & -1/\sqrt{2} & 0 \\ 1/\sqrt{6} & 1/\sqrt{6} & -2/\sqrt{6} \\ 1/\sqrt{3} & 1/\sqrt{3} & 1/\sqrt{3} \end{pmatrix}$$

for $i = 1$ and

$$\|r\| = \begin{pmatrix} 1/\sqrt{2} & 0 & -1/\sqrt{2} \\ 1/\sqrt{6} & 2/\sqrt{6} & 1/\sqrt{6} \\ 1/\sqrt{3} & -1/\sqrt{3} & 1/\sqrt{3} \end{pmatrix}$$

for $i = 2$.

Averaging the electromechanical properties in this laminar domain structure is carried out using the matrix approach developed in works [14, 20–22]. A full set of the effective elastic compliances $s_{rt}^{E*}(h)$, piezoelectric coefficients $d_{fj}^*(h)$ and dielectric permittivities $\varepsilon_{pq}^{\sigma *}(h)$ of the polydomain SC is calculated [11] at $0 < h < 1$. We remind that the aforementioned effective properties in the polydomain state are determined in the long-wave approximation [14, 20] so that the wavelength of an external field is much longer than the thickness of the individual domains of the SC sample.

Based on the volume-fraction dependences of the effective electromechanical properties, ECFs $k_{3j}^*(h)$ and the remaining effective constants of the polydomain SC are determined. Minima of $|d_{3j}^*(h)|$ and $|k_{3j}^*(h)|$ are observed at $h = 0.5$, i.e., at equal volume fractions of the 71° (109°) domains. The largest values of $|d_{3j}^*(h)|$ and $|k_{3j}^*(h)|$ are related to single-domain states, i.e., $h = 0$ or $h = 1$. The same volume-fraction dependence [11] holds true for the laminar domain structure with $\boldsymbol{P}_{s1}$ (volume fraction h) and $\boldsymbol{P}_{s4}$ (volume fraction $1 - h$), while the spontaneous polarisation vector $\boldsymbol{P}_s^*$ of the polydomain SC has only one component depending on h, and this

component is related to one of the non-poling directions, OX_1° or OX_2°. We note that the relatively low piezoelectric activity of the polydomain SC (spontaneous polarisation vectors $\boldsymbol{P}_{s1}$ and $\boldsymbol{P}_{s2}$ or $\boldsymbol{P}_{s1}$ and P_{s4}) is a result of the re-distribution of internal electric and mechanical stress fields [11] and may be associated with clamping of the non-180° domains in the presence of the domain walls with $\boldsymbol{n}_i || [001]_c$.

2.2.2 Four Domain Types

The next example of the effective electromechanical properties is related to the domain structure with four $\boldsymbol{P}_{si}$ orientations (Fig. 2.4). Similar domain structures are often observed [2–4] in domain-engineered PMN–xPT and PZN–xPT SC samples poled along the OX_3° direction. To define the volume fractions v_i of the four domain types, we represent v_i in terms of two parameters, t and n, as follows:

$$v_1 = tn,\ v_2 = t(1-n),\ v_3 = (1-t)(1-n), \quad \text{and} \quad v_4 = (1-t)n \tag{2.10}$$

The effective electromechanical properties of the polydomain SC are calculated [11] on the basis of a two-step averaging procedure described in paper [23]. Graphs of $d_{3j}^*(t, n)$ and $k_{3j}^*(t, n)$, which characterise the piezoelectric activity and electromechanical coupling of the polydomain SC along the poling axis OX_3°, are shown in Fig. 2.5. As in the case of the two domain types (see Sect. 1.2.1), the present domain structure (Fig. 2.4) provides a decrease in both $|d_{3j}^*(t, n)|$ and $|k_{3j}^*(t, n)|$ at $t \to 0.5$ and/or $n \to 0.5$. A comparison of graphs of $d_{33}^*(t, n)$ (Fig. 2.5c) and $k_{33}^*(t, n)$ (Fig. 2.5d) enables us to conclude that elastic compliance $s_{33}^{E*}(t, n)$ and dielectric permittivity $\varepsilon_{33}^{\sigma*}(t, n)$ slightly influence ECF $k_{33}^*(t, n)$. As a consequence, the piezoelectric coefficient $d_{33}^*(t, n)$ plays a key role in forming this electromechanical coupling. However, $d_{33}^*(t, n)$ (Fig. 2.5c) decreases in a fairly narrow range which may be due to the orientation of the domain walls [11] in the polydomain state.

According to the room-temperature data [4] of PMN–0.33PT SC poled along the $[001]_c$ axis ($4mm$ symmetry), experimental values of the piezoelectric coefficients are $d_{31,exp}^* = -1{,}330$ pC/N and $d_{33,exp}^* = 2{,}820$ pC/N. The macroscopic $4mm$ symmetry means that the four domain types shown in Fig. 2.4 would be present in the SC sample and volume fractions of these domain types are equal. The significant discrepancy between the calculated value of $d_{33}^*(0.5, 0.5) \approx 300$ pC/N (see Fig. 2.5c) and the above-given experimental $d_{33,esp}^*$ value is in good agreement with one of the conclusions of work [10] and could be due to the presence of an intermediate ferroelectric monoclinic phase [24, 25] near the MPB, by the non-180° domain coexistence [26] or by displacements of interfaces [24, 27] that separate two coexisting phases under the external electric field $\boldsymbol{E} || [001]_c$. Unfortunately, the lack of experimental data on the interconnections between the electromechanical properties of the single-domain and polydomain PMN–xPT SCs do not enable a comparison of the different results to any great degree. However some results of the present study are important for an

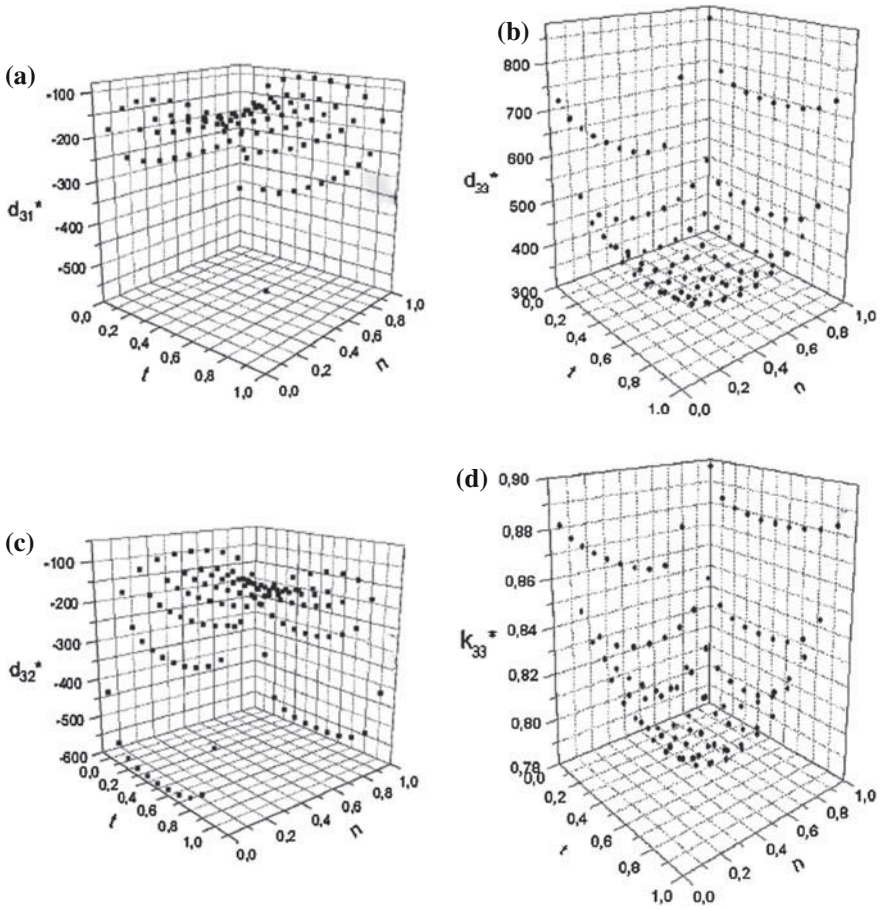

Fig. 2.5 Effective piezoelectric coefficients $d_{3j}^*(t, n)$ (in pC/N, graphs **a–c**) and ECF $k_{33}^*(t, n)$ (graph **d**) of the polydomain PMN–0.33PT SC (reprinted from paper by Topolov [11], with permission from IOP Publishing). The domain arrangement is shown in Fig. 2.4

interpretation of the complex links between the electromechanical properties in the SC and composite samples based on SCs that can be either polydomain or single-domain. Data on $d_{3j}^*(t, n)$ (Fig. 2.5a–c) are to be taken into account in the study of the anisotropy of the effective electromechanical properties of the composites based on SCs.

2.3 Single-Domain $(1-x)Pb(Zn_{1/3}Nb_{2/3})O_3 - xPbTiO_3$

Relaxor-ferroelectric PZN–xPT SCs are of great interest due to their various heterophase states [25, 28–31] and their outstanding electromechanical properties [16, 24, 26, 32] near the MPB ($x \approx 0.08$–0.09). The electromechanical constants of PZN–xPT SCs were determined for $0.045 \leq x \leq 0.12$ [3, 6, 33–37] on samples with engineered domain structures and in the single-domain state (Table 2.2). Electromechanical constants measured on single-domain SC samples are known, e.g., for PZN–0.09PT (intermediate monoclinic phase) and PZN–0.12PT (tetragonal 4*mm* phase). As is seen even for compositions away from the MPB, some discrepancies exist between the sets of electromechanical constants (see for instance, data for $x = 0.12$ in Table 2.2). These discrepancies can be accounted for by the poling conditions and heterogeneity of the SC samples.

The orientation dependences of the piezoelectric coefficients $d'_{3j}(\varphi, \psi, \theta)$ and $g'_{3j}(\varphi, \psi, \theta)$ and dielectric permittivity $\varepsilon^{\sigma\prime}_{33}(\varphi, \psi, \theta)$ of single-domain monoclinic PZN–0.09PT SCs were analysed by Topolov [38]. Results from these orientation dependences were first systematised on the basis of a group of criteria and compared with known experimental data. Based on the criteria from work [38], the description of periodic and other changes in the piezoelectric and dielectric properties of a low-symmetry single-domain sample was carried out in terms of the Euler angles. Specific features of the dielectric anisotropy and high piezoelectric activity in the single-domain state were considered. The dielectric anisotropy (see data on $\varepsilon^{\sigma}_{pp}$ at $x = 0.09$ from Table 2.2) influences the piezoelectric sensitivity of the single-domain PZN–0.09PT SC at various orientations of its crystallographic axes.

Table 2.2 Elastic compliances s^E_{ab}(in 10^{-12} Pa^{-1}), piezoelectric coefficients d_{ij} (in pC/N) and dielectric permittiivities $\varepsilon^{\sigma}_{pp}$ of single-domain PZN–xPT SCs

x	s^E_{11}	s^E_{12}	s^E_{13}	s^E_{33}	s^E_{44}	s^E_{66}	d_{31}
0.12 [33, 34]	20.1	−4.6	−18.2	54.5	19.5	17.2	−207
0.12 [36][a]	22.4	−3.53	−20.95	58	–	27.86	−217
0.12 [35]	18.0	−0.185	−19.1	52.8	27.0	45.5	−130
0.09 [26][b]	–	–	–	–	–	–	120
x	d_{32}	d_{33}	d_{15}	d_{24}	$\varepsilon^{\sigma}_{11}/\varepsilon_0$	$\varepsilon^{\sigma}_{22}/\varepsilon_0$	$\varepsilon^{\sigma}_{33}/\varepsilon_0$
0.12 [33, 34]	−207	541	653	653	10,000	10,000	750
0.12 [36][a]	−217	576	–	–	–	–	870
0.12 [35]	−130	326	946	946	6,160	6,160	566
0.09 [26][b]	−270	250	3,200	950	9,000	21,000	800

[a] In work [36] electromechanical properties of the single-domain $BiScO_3 - PbTiO_3$ SC are compared to the properties of the single-domain PZN-0.12PT SC, however no full set of electromechanical constants of PZN-0.12PT SC is present. The SCs of $BiScO_3 - PbTiO_3$ and PZN-0.12PT are characterised by tetragonal symmetry

[b] No full set of elastic constants of the single-domain PZN-0.09PT SC is known from literature data. To characterise the piezoelectric and dielectric properties of the monoclinic single-domain PZN-0.09PT SC, Dammak et al. [26] used the matrices that have forms [15] similar to those in the ferroelectric *mm*2 phase [39] of the single-domain $KNbO_3$ SC

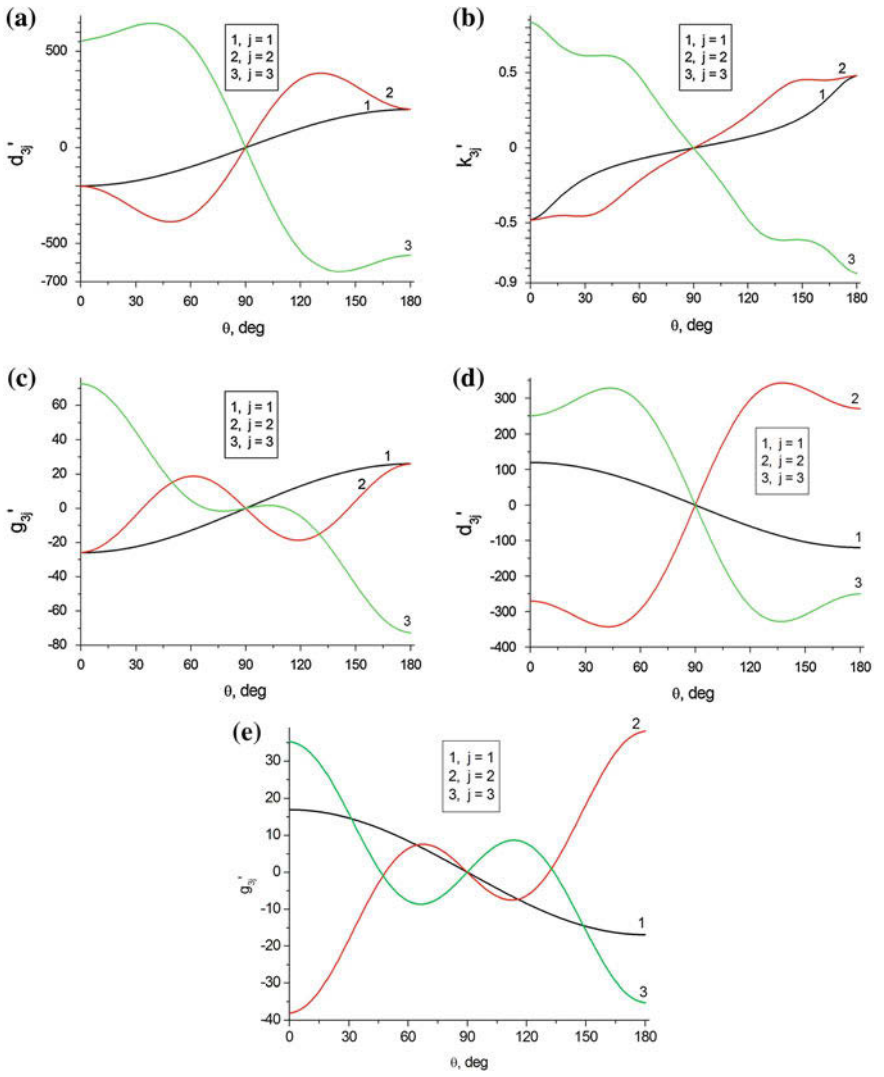

Fig. 2.6 Piezoelectric coefficients $d'_{3j}(\theta)$ (in pC/N, graphs **a** and **d**) and $g'_{3j}(\theta)$ (in $mV \cdot$m / N, graphs **c** and **e**) and ECFs $k'_{3j}(\theta)$ (graph **b**) of single-domain PZN–xPT SCs at $\varphi = \psi = 0°$: **a–c**, x = 0.12 and **d** and **e**, x = 0.09. Calculations for x = 0.12 and x = 0.09 were performed using data from [36] and [26], respectively (see Table 2.2)

As follows from work [11, 38], the electromechanical properties are represented by subscripts $i3$ and $3j$ and are highly dependent on the Euler angle θ (Fig. 2.1b) that directly links the spontaneous polarisation vector $\boldsymbol{P}_s$ to the OX_3 axis. Taking into account the key role of the piezoelectric coefficients d_{3j} in various piezoelectric applications [13–16, 40–42], we consider examples of the orientation dependences

of the piezoelectric coefficients d'_{3j} and g'_{3j} and ECFs k'_{3j} on θ (Fig. 2.6). It should be noted that max $d'_{33}(\theta)$ and min$d'_{3j}(\theta)$ are achieved in both cases (Fig. 2.6a and d) irrespective of symmetry of SCs, and the condition $|d'_{33}(\theta)| > d'_{33}(0°)$ is valid due to the effect of the large shear piezoelectric coefficients d_{15} and d_{24} (see Table 2.2). The distinctions between the curves of $g'_{3j}(\theta)$ related to $x = 0.12$ (Fig. 2.6c) and $x = 0.09$ (Fig. 2.6e) stem from the anisotropy of the piezoelectric coefficients d_{3j} and dielectric permittivities $\varepsilon^{\sigma}_{pp}$ of the studied single-domain SCs.

Comparing the graphs of $d'_{3j}(\theta)$ to $g'_{3j}(\theta)$ (cf. Fig. 2.6a, c and Fig. 2.6d, e), one can observe an interesting feature of the orientation dependence of the piezoelectric response: the condition sgn $d'_{33}(\theta)$=–sgn $g'_{33}(\theta)$ holds in certain ranges of the Euler angle θ. Such a discrepancy of signs is due to the influence of dielectric permittivity $\varepsilon^{\sigma\prime}_{23}(\theta)$ on the piezoelectric coefficient $g'_{33}(\theta)$ [see for instance, Eqs. (1.12) and (1.14)]. This influence becomes considerable when $|\varepsilon^{\sigma\prime}_{23}| \sim \varepsilon^{\sigma\prime}_{pp}$ ($p = 1, 2$ and 3) and, therefore, an interconnection between $d'_{33}(\theta)$ and $g'_{33}(\theta)$ becomes more complicated, depending on the balance of some components of $\varepsilon^{\sigma\prime}_{pq}(\theta)$.

2.4 Single-Domain xPb(In$_{1/2}$Nb$_{1/2}$)O$_3$ – yPb(Mg$_{1/3}$Nb$_{2/3}$)O$_3$ – (1 –x–y)PbTiO$_3$

The ternary system of relaxor-ferroelectric solid solutions of $x\text{Pb}(\text{In}_{1/2}\text{Nb}_{1/2})\text{O}_3 - y\text{Pb}(\text{Mg}_{1/3}\text{Nb}_{2/3})\text{O}_3 - (1-x-y)\text{PbTiO}_3$ (PIN–x–y) with a perovskite-type structure is of interest due to the considerable piezoelectric activity and anisotropy of the electromechanical properties. The full sets of electromechanical constants of the single-domain PIN–x–y SCs have been measured at room temperature (Table 2.3). Despite the relatively small difference in the composition, these SCs are related to different symmetry classes (3m for PIN–0.24–0.49 [43], $mm2$ for PIN–0.27–0.40 [44] and 4mm for PIN–x–y, without the definitive chemical composition [45]) and show clear distinctions in the anisotropy of the electromechanical properties. It should be added that the PIN–0.24–0.49 SCs maintain the single-domain state without an electric bias field [43].

The very large piezoelectric coefficients d_{15} and d_{24} (approximately 11.7–13 times more than the longitudinal piezoelectric coefficient d_{33}) in the single-domain PIN–0.27–0.40 SC are of value to study the effect of the orientation of crystallographic axes on the piezoelectric performance and related parameters. The coercive field E_c of PIN–x–y SC is on the order of 10 kV/cm [45] which is a few times higher than E_c of the neighbouring rhombohedral compositions and tetragonal PMN–xPT SCs [46]. The strong shear-mode piezoelectric effect and electromechanical coupling in the single-domain PIN–x–y SC [45] along with the large E_c value is of interest for piezo-technical applications such as actuators and transducers which are exploited in a relatively wide range of electric fields E.

Examples of the orientation dependences (Fig. 2.7) suggest that a similarity between the $d'_{3j}(\theta)$ and $k'_{3j}(\theta)$ curves is observed for the single-domain PIN–x–y SCs from various symmetry classes. Such orientation behaviour is accounted for by

Table 2.3 Room-temperature elastic compliances s^E_{ab} (in 10^{-12} Pa^{-1}), piezoelectric coefficients d_{ij} (in pC/N) and dielectric permittivities ε^σ_{pp} of single-domain PIN–0.24–0.49 [43], PIN–0.27–0.40 [44] and PIN–*x*–*y* [45] SCs

Composition	s^E_{11}	s^E_{12}	s^E_{13}	s^E_{14}	s^E_{23}	s^E_{23}	s^E_{33}	s^E_{44}
PIN–0.24–0.49	11.62	−7.81	−1.10	22.17	11.62	−1.10	6.05	93.33
PIN–0.27–0.40	9.20	−8.38	5.64	0	21.2	−14.4	16.8	78.1
PIN–*x*–*y*	17.1	−3.3	−14.2	0	17.1	−14.2	41	55.0
Composition	s^E_{55}	s^E_{66}	d_{15}	d_{22}	d_{24}	d_{31}	d_{32}	d_{33}
PIN–0.24–0.49	93.33	38.86	2,015	−490	2,015	−21	−21	75
PIN–0.27–0.40	316	15.5	4,550	0	4,100	153	–346	350
PIN–*x*–*y*	55.0	25.0	2,350	0	2,350	–200	–200	530
Composition	$\frac{\varepsilon^\sigma_{11}}{\varepsilon_0}$	$\frac{\varepsilon^\sigma_{22}}{\varepsilon_0}$	$\frac{\varepsilon^\sigma_{33}}{\varepsilon_0}$					
PIN–0.24–0.49	5,800	5,800	650					
PIN–0.27–0.40	8,070	30,000	1,500					
PIN–*x*–*y*	15,000	15,000	1,090					

the leading role of the piezoelectric properties and their anisotropy in forming the orientation dependence of ECF $k'_{3j}(\theta)$ (Fig. 2.7b, d and f). The role of symmetry of the relaxor-ferroelectric SCs is also to be taken into account by interpretation of the orientation effects and the anisotropy of d'_{3j}, k'_{3j} etc. Moreover, lowering the symmetry gives rise to a more complex link between the $d'_{3j}(\theta)$ and $k'_{3j}(\theta)$ curves (see for instance, Fig. 2.7a and b). This link is predominantly concerned with the anisotropy of the elastic and dielectric properties in the low-symmetry phases. As in Fig. 2.6, max $d'_{33}(\theta)$ and min $d'_{3j}(\theta)$ are achieved (Fig. 2.7a, c and e) irrespective of the symmetry class and is a result of the strong shear piezoelectric effect ($d_{15} > d_{33}$, see Table 2.3).

2.5 Conclusion

In this chapter important examples of the orientation dependences of the piezoelectric coefficients and ECFs are considered for ferroelectric-relaxor SCs in the single-domain state. Volume-fraction dependences of the piezoelectric properties are analysed for the polydomain relaxor-ferroelectric SCs. The non-monotonic orientation dependences of the piezoelectric coefficients d'_{3j} and g'_{3j} and ECFs k'_{3j} are analysed in terms of the Euler angles φ, ψ and θ.

Variants of periodicity of the electromechanical properties are explained by taking into consideration unit-cell symmetry elements. The role of the shear piezoelectric effect due to the large piezoelectric coefficients d_{15} and d_{24} is discussed in the context of the non-monotonic orientation dependence of d'_{3j}.

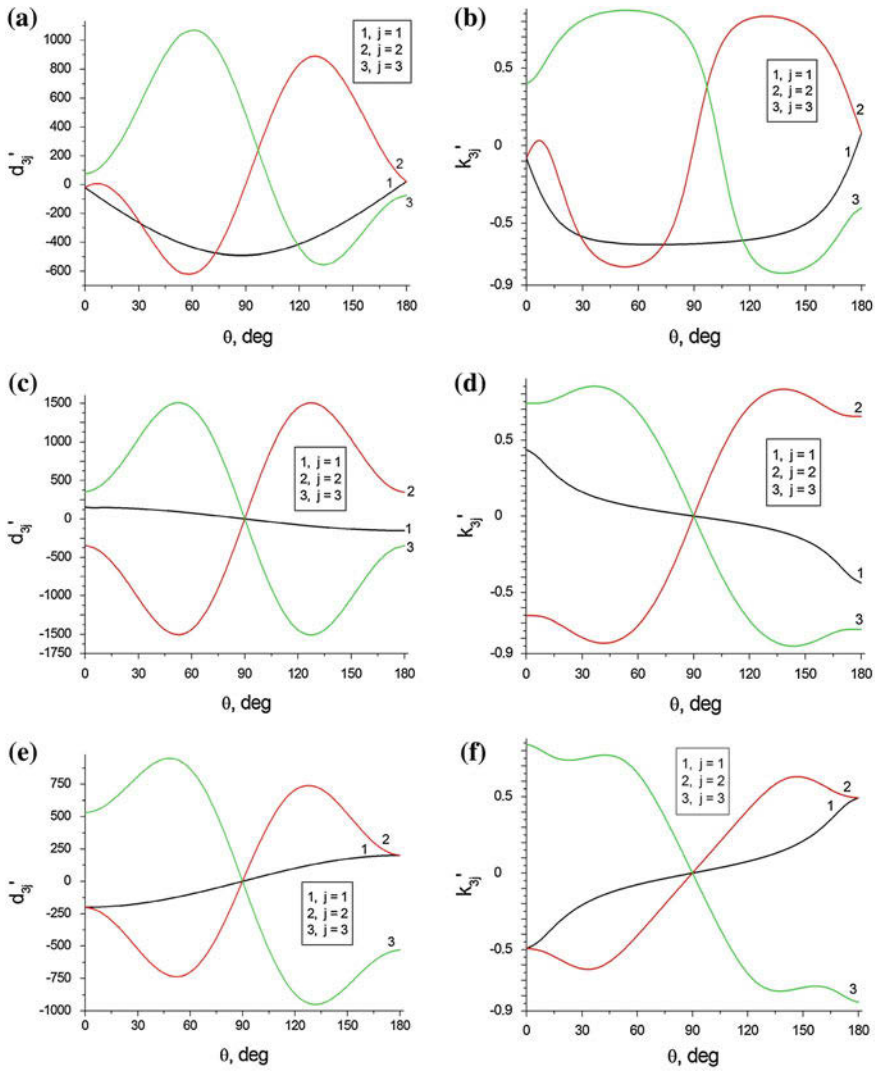

Fig. 2.7 Piezoelectric coefficients $d'_{3j}(\theta)$ (in pC/N, graphs **a, c** and **e**) and ECFs $k'_{3j}(\theta)$ (graphs **b, d** and **f**) of single-domain PIN–0.24–0.49 (**a** and **b**), PIN–0.27–0.40 (**c** and **d**) and PIN–*x*–*y* (**e** and **f**) SCs at $\varphi = \psi = 0°$. Calculations were performed using data from Table 2.3

Two examples of the effect of a 71° (109°) domain structure on the electromechanical properties are considered in the 3*m* phase of the PMN–0.33PT SC. This SC in the polydomain state (with either two or four domain types) is characterised by min $|d_{3j}*|$ and min $|k_{3j}*|$ in the "most symmetrical" cases of the domain arrangement, i.e., for equal volume fractions of the 71° (109°) domains separated by the planar $\{100\}_c$-type walls and the domain-wall displacement is neglected over the SC sample. In this context we deal with the so-called intrinsic contribution of the

non-180° domain structures on the effective electromechanical properties of SCs. Of course, the influence of an additional (extrinsic) contribution from the domain-wall and interphase-boundary displacements on the electromechanical properties would be needed and may be a subject of further studies.

Results shown in Figs. 2.2, 2.3, 2.6, and 2.7 suggest that the anisotropy of the piezoelectric coefficients d'_{3j} and ECFs k'_{3j} can be varied in a relatively wide range due to the orientation effect. This variation is achieved even by changing one of the Euler angles, for instance, θ (see the θ angle in Fig. 2.1b).

Undoubtedly, the role of symmetry is important in the interpretation of the orientation dependences of the electromechanical propertie and their anisotropy in relaxor-ferroelectric SCs. Irrespective of the symmetry class, the electromechanical properties represented by subscripts $i3$ and $3j$ are highly dependent on the Euler angle θ that directly links the spontaneous polarisation vector $\boldsymbol{P}_\mathbf{s}$ of the SC to the co-ordinate OX_3 axis (see Fig. 2.1). Taking into account features of the orientation behaviour of the piezoelectric coefficients d'_{3j}, one can analyse the remaining groups of the piezoelectric coefficients (e'_{3j}, g'_{3j} and h'_{3j}), ECFs k'_{3j} and related parameters which are of interest for sensor, actuator, transducer, and other applications.

References

1. Wada S, Park S-E, Cross LE, Shrout TR (1999) Engineered domain configuration in rhombohedral PZN-PT single crystals and their ferroelectric related properties. Ferroelectrics 221:147–155
2. Yin J, Cao W (2000) Domain configurations in domain engineered 0.955Pb($Zn_{1/3}Nb_{2/3}$)O_3-0.045$PbTiO_3$ single crystals. J Appl Phys 87:7438–7441
3. Yin J, Cao W (2002) Effective macroscopic symmetries and materials properties of multidomain 0.955Pb($Zn_{1/3}Nb_{2/3}$)O_3- 0.045$PbTiO_3$ single crystals. J Appl Phys 92:444–448
4. Zhang R, Jiang B, Cao W (2001) Elastic, piezoelectric, and dielectric properties of multidomain 0.67Pb($Mg_{1/3}Nb_{2/3}$)O_3- 0.33$PbTiO_3$ single crystals. J Appl Phys 90:3471–3475
5. Zhang R, Jiang W, Jiang B, Cao W (2002) Elastic, dielectric and piezoelectric coefficients of domain engineered 0.70Pb($Mg_{1/3}Nb_{2/3}$)O_3-0.30$PbTiO_3$ single crystal. In: Cohen RE (ed) Physics of ferroelectrics. American Institute of Physics, Melville, pp 188–197
6. Zhang R, Jiang B, Cao W, Amin A (2002) Complete set of material constants of 0.93Pb($Zn_{1/3}Nb_{2/3}$)O_3-0.07$PbTiO_3$ domain engineered single crystal. J Mater Sci Lett 21:1877–1879
7. Zhang R, Jiang B, Cao W (2003) Single-domain properties of 0.67Pb($Mg_{1/3}Nb_{2/3}$)O_3-0.33$PbTiO_3$ single crystals under electric field bias. Appl Phys Lett 82:787–789
8. Noheda B (2002) Structure and high-piezoelectricity in lead oxide solid solutions. Curr Opin Solid State Mater Sci 6:27–34
9. Zhang R, Jiang B, Cao W (2003) Orientation dependence of piezoelectric properties of single domain 0.67Pb($Mn_{1/3}Nb_{2/3}$)O_3-0.33$PbTiO_3$ crystals. Appl Phys Lett 82:3737–3739
10. Damjanovic D, Budimir M, Davis M, Setter N (2003) Monodomain versus polydomain piezoelectric response of 0.67Pb($Mg_{1/3}Nb_{2/3}$)O_3-0.33$PbTiO_3$ single crystals along nonpolar directions. Appl Phys Lett 83:527–529; Erratum ibid. 2490
11. Topolov VYu (2004) The remarkable orientation and concentration dependences of the electromechanical properties of 0.67Pb($Mg_{1/3}Nb_{2/3}$)O_3-0.33$PbTiO_3$ single crystals. J Phys: Condens Matter 16:2115–2128

12. Ikeda T (1990) Fundamentals of piezoelectricity. Oxford University Press, Oxford, New York, Toronto
13. Nakamura K, Kawamura Y (2000) Orientation dependence of electromechanical coupling factors in $KNbO_3$. IEEE Trans Ultrason Ferroelectr Freq Control 47:750–755
14. Topolov VYu, Bowen CR (2009) Electromechanical properties in composites based on ferroelectrics. Springer, London
15. Zheludev IS (1971) Physics of crystalline dielectrics, vol. 2. Electrical properties, Plenum, New York
16. Park S-E, Shrout TR (1997) Ultrahigh strain and piezoelectric behavior in relaxor based ferroelectric single crystals. J Appl Phys 82:1804–1811
17. Erhart J, Cao W (1999) Effective material properties in twinned ferroelectric crystals. J Appl Phys 86:1073–1081
18. Fousek J, Janovec V (1969) The orientation of domain walls in twinned ferroelectric crystals. J Appl Phys 40:135–142
19. Tagantsev AK, Cross LE, Fousek J (2010) Domains in ferroic crystals and thin films. Springer, New York
20. Akcakaya E, Farnell GW (1988) Effective elastic and piezoelectric constants of superlattices. J Appl Phys 64:4469–4473
21. Topolov VYu (1995) Anisotropy of electromechanical properties in $KNbO_3$ crystals with S-type domain boundaries. J Phys Condens Matter 7:7405–7408
22. Emelyanov AS, Raevskaya SI, Savenko FI, Topolov VYu, Raevski IP, Turik AV, Kholkin AL (2007) Dielectric and piezoelectric properties of (001)-oriented (1 - x)$Pb(Mg_{1/3}Nb_{2/3})O_3$ - x$PbTiO_3$ single crystals with $0.1 \leq x \leq 0.4$. Solid State Commun 143:188–192
23. Glushanin SV, Topolov VYu (2001) Features of electromechanical properties of piezoelectric composites with elements of connectivity 1–1. J Phys D Appl Phys 34:2518–2529
24. Topolov VYu, Turik AV (2002) An intermediate monoclinic phase and electromechanical interactions in x$PbTiO_3$- (1 - x)$Pb(Zn_{1/3}Nb_{2/3})O_3$crystals. Phys Solid State 44:1355–1362
25. Topolov VYu (2012) Heterogeneous ferroelectric solid solutions. Phases and domain states. Springer, Berlin
26. Dammak H, Renault A-É, Gaucher P, Thi MP, Calvarin G (2003) Origin of the giant piezoelectric properties in the [001] domain engineered relaxor single crystals. Jpn J Appl Phys, Pt 1 42:6477–6482
27. Topolov VYu, Turik AV (2001) Interphase boundaries and high piezoelectric activity of x$PbTiO_3$- (1 - x)$Pb(Zn_{1/3}Nb_{2/3})O_3$crystals. Phys Solid State 43:1117–1123
28. Fujishiro K, Vlokh R, Uesu Y, Yamada Y, Kiat J-M, Dkhil B, Yamashita Y (1998) Optical observation of heterophases and domain structure in relaxor ferroelectrics $Pb(Zn_{1/3}Nb_{2/3})O_3$ / 9% $PbTiO_3$. Jpn J Appl Phys Part 1 37:5246–5248
29. Ye Z-G, Dong M, Zhang L (1999) Domain structure and phase transitions in relaxor-based piezo-/ferroelectric (1 - x)$Pb(Zn_{1/3}Nb_{2/3})O_3$ - x$PbTiO_3$ single crystals. Ferroelectrics 229:223–232
30. Topolov VYu, Ye Z-G (2001) Elastic matching of morphotropic phases in polydomain (1 - x)$Pb(Zn_{1/3}Nb_{2/3})O_3$ - x$PbTiO_3$ single crystals. Ferroelectrics 253:71–78
31. Topolov VYu (2003) Heterophase states in 0.10$PbTiO_3$-0.90$Pb(Zn_{1/3}Nb_{2/3})O_3$ crystals. Phys Solid State 45:1295–1297
32. Ogawa T, Yamauchi Y, Numamoto Y, Matsushita M, Tachi Y (2002) Giant electromechanical coupling factor of k_{31} mode and piezoelectric d_{31} constant in $Pb[(Zn_{1/3}Nb_{2/3})_{0.91}Ti_{0.09}]O_3$ piezoelectric single crystal. Jpn J Appl Phys, Part 2 41:L55–L57
33. Guennou M, Dammak H, Thi MP (2008) 2 T domain-engineered piezoelectric single crystals: calculations and application to PZN-12%PT poled along [101]. J Appl Phys 104:074102 (6 pp.)
34. Guennou M (2007) Modifications des propriétés structurales et électromécaniques de monocristaux piézoélectriques $Pb(Zn_{1/3}Nb_{2/3})_{1-x}Ti_xO_3$: ingénierie des domaines et dopage au manganese. Dr Thesis, École Centrale Paris, Châtenay-Malabry

35. Delaunay T (2006) Caractérisation fonctionnelle et relations structure - proprieties de monocristaux piézoélectriques de type pérovskite. Ph.D Thesis, Université François Rabelais de Tours, Tours
36. Zhang S, Randall CA, Shrout TR (2004) Dielectric, piezoelectric and elastic properties of tetragonal $BiScO_3$-$PbTiO_3$ single crystal with single domain. Solid State Commun 131:41–45
37. He C, Jing W, Wang F, Zhu K, Qui J (2011) Full tensorial elastic, piezoelectric, and dielectric properties characterization of [011]-poled PZN-9%PT single crystal. IEEE Trans Ultrason Ferroelectr Freq Control 58:1127–1130
38. Topolov VYu (2005) Orientation relationships between electromechanical properties of monoclinic $0.91Pb(Zn_{1/3}Nb_{2/3})O_3$- $0.09PbTiO_3$ single crystals. Sens Actuat A 121:148–155
39. Wiesendanger E (1974) Dielectric, mechanical and optical properties of orthorhombic $KNbO_3$. Ferroelectrics 6:263–281
40. Uchino K (1997) Piezoelectric actuators and ultrasonic motors. Kluwer, Boston
41. Gorish AV, Dudkevich VP, Kupriyanov MF, Panich AE, Turik AV (1999) Piezoelectric device-making, vol. 1. Physics of ferroelectric ceramics. Radiotekhnika, Moscow (in Russian)
42. Haertling G (1999) Ferroelectric ceramics: history and technology. J Am Ceram Soc 82:797–818
43. Sun E, Cao W, Jiang W, Han P (2011) Complete set of material properties of single domain $0.24Pb(In_{1/2}Nb_{1/2})O_3$-$0.49Pb(Mg_{1/3}Nb_{2/3})O_3$-$0.27PbTiO_3$ single crystal and the orientation effects. Appl Phys Lett 99:032901 (3 pp.)
44. Zhang S, Liu G, Jiang W, Luo J, Cao W, Shrout TR (2011) Characterization of single domain $Pb(In_{0.5}Nb_{0.5})O_3$-$Pb(Mg_{1/3}Nb_{2/3})O_3$-$PbTiO_3$ crystals with monoclinic phase. J Appl Phys 110:064108 (5 pp.)
45. Li F, Zhang S, Xu Z, Wei X, Luo J, Shrout TR (2010) Electromechanical properties of tetragonal $Pb(In_{1/2}Nb_{1/2})O_3$-$Pb(Mg_{1/3}Nb_{2/3})O_3$-$PbTiO_3$ ferroelectric crystals. J Appl Phys 107:054107 (5 pp.)
46. Cao H, Schmidt VH, Zhang R, Cao W, Luo H (2004) Elastic, piezoelectric, and dielectric properties of $0.58Pb(Mg_{1/3}Nb_{2/3})O_3$- $0.42PbTiO_3$ single crystal. J Appl Phys 96:549–554

Chapter 3
Orientation Effects and Anisotropy of Properties in 2–2 and Related Composites

The 2–2 connectivity pattern of a composite [1–3] is a structure where there are two types of layers which are alternating in a certain direction. The 2–2 composite family is characterised by a laminar structure wherein two components are continuously distributed along two axes of a rectangular co-ordinate system $(X_1X_2X_3)$. Each component is present in the separate layer. The relative simplicity of the 2–2 composite structure and the possibility of varying the volume fractions of the components in a wide range allow the manufacture and design of the 2–2 composite with tailored (e.g., extreme) values of its effective parameters. Methods suitable for manufacturing these widespread 2–2 FC/polymer composites are discussed in a series of review papers (see, for instance, papers [3–5]).

The 2–2 FC/polymer composites are usually manufactured in two modifications (Fig. 3.1), namely, as composites with a series connection and a parallel connection of adjacent layers [1, 2]. In the series-connectied composite sample the C1 and C2 layers are alternating in the OX_3 direction (Fig. 3.1a) and interfaces are perpendicular to OX_3, and this co-ordinate axis is the poling axis. In the parallel-connected composite the poling axis OX_3 is parallel to the interfaces that separate the C1 and C2 layers (Fig. 3.1b). It is obvious that these two modifications are characterised by different electromechanical properties [2] and anisotropy with respect to the poling axis OX_3. In the series-connected composite the piezoelectric coefficients d^*_{3j} concerned with the poling axis obey the condition $d^*_{31} = d^*_{32} \neq d^*_{33}$, while the parallel-connected composite is characterised by an inequality $d^*_{31} \neq d^*_{32} \neq d^*_{33}$ [2].

The 2–2 composite architecture is of value due to a particular non-monotonic volume-fraction dependence of their effective parameters. For instance, the series-connected 2–2 composite based on the Pb(Zr, Ti)O_3-type FC is characterised by several types of the volume-fraction dependence [6, 7] of the thickness ECF $k^*_t = e^*_{33}/(c^{*D}_{33}\varepsilon^{*\xi}_{33})^{1/2}$ [see also Eq. (1.25)], maxima of the piezoelectric coefficient e^*_{31} and dielectric permittivity $\varepsilon^{*\sigma}_{11}$ and a strong dependence of k^*_t, e^*_{31}, $\varepsilon^{*\sigma}_{11}$, and other parameters on the ratio between the elastic moduli of the individual components [8]. Moreover, the piezoelectric coefficient e^*_{31} of the series-connected composite [9] can pass through a zero value and reach max $e^*_{31} > 0$, although both the

V. Yu. Topolov et al., *Piezo-Active Composites*,
Springer Series in Materials Science 185, DOI: 10.1007/978-3-642-38354-0_3,

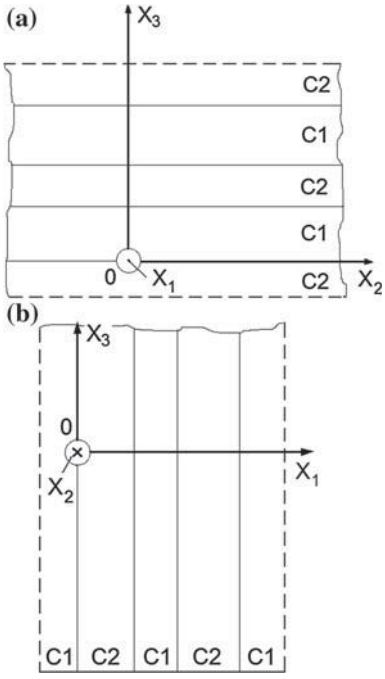

Fig. 3.1 Schematic of the 2–2 series-connected (**a**) and parallel-connected (**b**) composites with components denoted as C1 and C2. $(X_1X_2X_3)$ is the rectangular co-ordinate system

components ($n = 1$ and 2, i.e., C1 and C2 layers in Fig. 3.1a) have negative values of the piezoelectric coefficient $e_{31}^{(n)}$. A squared strain–voltage figure of merit

$$(Q_{33}^*)^2 = d_{33}^* g_{33}^* \tag{3.1}$$

exhibits a maxima [10] when varying the volume fraction of the FC component in a 2–2 series-connected composite. The parallel-connected 2–2 composite based on Pb(Zr, Ti)O_3-type FC exhibits a non-monotonic behaviour of the thickness ECF k_t^* and the hydrostatic (or hydrophone) piezoelectric coefficients [11, 12]

$$d_h^* = d_{33}^* + d_{32}^* + d_{31}^* \text{ and } g_h^* = g_{33}^* + g_{32}^* + g_{31}^*. \tag{3.2}$$

In this chapter we will discuss features of the performance of 2–2 and related composites based on either a FC or SC by taking into account the orientation effect and the anisotropy of the effective properties of these composites.

3.1 Ceramic/Polymer Composites: An Effect of the Orientation of the Remanent Polarisation Vector on the Piezoelectric Anisotropy

The first results on the performance of oriented 2–2 composites based on a "soft" PZT FC were published in work [3, 13]. The orientation angle of the remanent polarisation vector $\boldsymbol{P}_r^{(1)}$ in the FC layers with respect to the poling direction of the composite was varied from 0° to 75°. The maximum of the squared hydrostatic figure of merit

$$(Q_h^*)^2 = d_h^* g_h^* \tag{3.3}$$

in the oriented 2–2 composite [13] is achieved by varying the orientation angle and volume fraction of the FC component. Equation (3.3) comprises the hydrostatic piezoelectric coefficients d_h^* and g_h^* from (3.2). The sumations in (3.2) characterise the hydrostatic response of a piezo-active element with electrodes that are perpendicular to the OX_3 axis.

In this section we consider examples of the volume-fraction and orientation dependence of the piezoelectric properties and their anisotropy factors in 2–2 FC/polymer composites. Among the vast group of FCs (see Table 1.2) we choose two compositions. The first composition is a "soft" PCR-7M FC with high values of piezoelectric coefficients $|d_{3j}^{(1)}|$ and $|e_{3j}^{(1)}|$ and with the moderate anisotropy of $d_{3j}^{(1)}$ and $e_{3j}^{(1)}$. The second composition is a "hard" modified $PbTiO_3$ FC (I) with a large anisotropy of $d_{3j}^{(1)}$ and $e_{3j}^{(1)}$ at $e_{3j}^{(1)} > 0$. A piezo-passive polymer component can be chosen, for example, among compositions listed in Table 3.1.

It is assumed that the 2–2 composite represents a system of parallel-connected FC and polymer layers, and these layers form a regular laminar structure (Fig. 3.2). In the initial state (at the orientation angle $\alpha = 0°$ or $\beta = 0°$, see insets 1 and 2 in Fig. 3.2), the remanent polarisation vector in each FC layer is $\boldsymbol{P}_r^{(1)} || OX_3$. Hereafter we consider rotations of the $\boldsymbol{P}_r^{(1)}$ vector around one of the co-ordinate axes, OX_1 or OX_2, as shown in insets 1 and 2 in Fig. 3.2, and the FC layers in the composite sample have the same appointed orientation of $\boldsymbol{P}_r^{(1)}$. Subscripts "(1)" and "(2)" refer to the FC and polymer component, respectively. As mentioned earlier, the electrodes at the composite sample are perpendicular to the OX_3 axis.

Table 3.1 Elastic compliances $s_{ab}^{(n)}$ (in10^{-12}Pa^{-1}) and dielectric permittivity $\varepsilon_{pp}^{(n)}$ of piezo-passive polymers at room temperature

Polymer	$s_{11}^{(n)}$	$s_{12}^{(n)}$	$\varepsilon_{pp}^{(n)}/\varepsilon_0$
Araldite [14]	216	−78	4.0
Polyurethane [15]	405	−151	3.5
Elastomer [16]	3,300	−1, 480	5.0

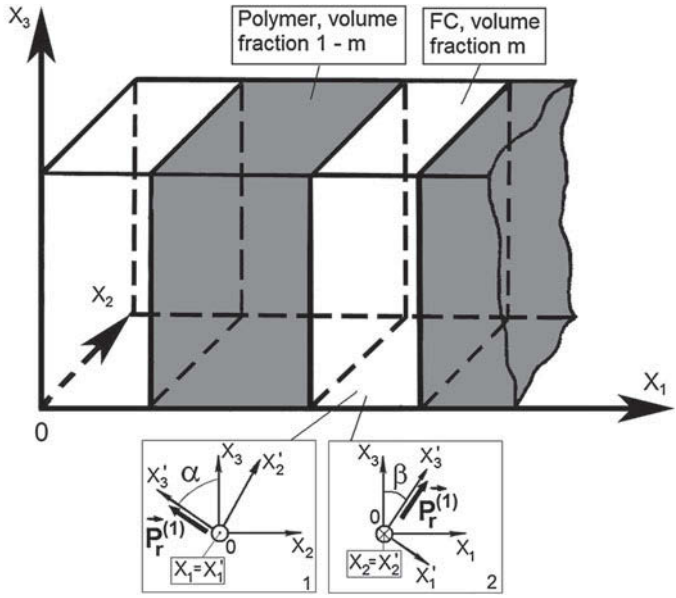

Fig. 3.2 Schematic of the 2–2 FC/polymer composite. $(X_1X_2X_3)$ is the rectangular co-ordinate system of the composite sample, α and β are angles of rotation of the remanent polarisation vector $\boldsymbol{P}_r^{(1)} || OX_3'$ of the FC layer around either the OX_1 axis (*inset 1*) or the OX_2 axis (*inset 2*)

The effective electromechanical properties of the composite studied are determined within the framework of the matrix approach [2] that is applied to piezoactive composite materials with planar microgeometry. The matrix of the effective properties of the composite in the co-ordinate system $(X_1X_2X_3)$

$$\| C^* \| = \begin{pmatrix} \| s^{*E} \| & \| d^* \|^t \\ \| d^* \| & \| \varepsilon^{*\sigma} \| \end{pmatrix} \tag{3.4}$$

is written in terms of $||s^{*E}||$ (6×6 matrix), $||d^*||$(3×6 matrix) and $||\varepsilon^{*\sigma}||$($3 \times 3$ matrix), and superscript "t" in (3.1) denotes the transposed matrix. The $||C^*||$ matrix from (3.4) is determined by averaging the electromechanical properties of the components on the volume fraction m and is given by

$$||C^*|| = [||C^{(1)}|| \cdot ||M||m + ||C^{(2)}||(1-m)] \cdot [||M||m + ||I||(1-m)]^{-1}, \tag{3.5}$$

where $||C^{(1)}||$ and $||C^{(2)}||$ are matrices of the electromechanical properties of the FC and polymer component, respectively, $||M||$ is concerned with the electric and mechanical boundary conditions [2] at interfaces $x_1 = \text{const}$ (Fig. 3.2), and $||I||$ is the identity 9×9 matrix. Elements of the $||C^{(1)}||$ matrix are written taking into account

the orientation of $\boldsymbol{P}_r{}^{(1)}$ in the FC layer [see Eq. (2.1)]. The boundary conditions at $x_1 = \text{const}$ (Fig. 3.2) imply a continuity of components of mechanical stress $\sigma_{11} = \sigma_1, \sigma_{12} = \sigma_6$ and $\sigma_{13} = \sigma_5$, strain $\xi_{22} = \xi_2, \xi_{23} = \xi_4/2$ and $\xi_{33} = \xi_3$, electric displacement D_1, and electric field E_2 and E_3. The $||M||$ matrix from (3.5) is written for $x_1 = \text{const}$ in the general form as $||M|| = ||m_1||^{-1}||m_2||$ where

$$\| m_n \| = \begin{pmatrix} 1 & 0 & 0 & 0 & 0 & 0 & 0 & 0 & 0 \\ s_{12}^{(n),E} & s_{22}^{(n),E} & s_{23}^{(n),E} & s_{24}^{(n),E} & s_{25}^{(n),E} & s_{26}^{(n),E} & d_{12}^{(n)} & d_{22}^{(n)} & d_{32}^{(n)} \\ s_{13}^{(n),E} & s_{23}^{(n),E} & s_{33}^{(n),E} & s_{34}^{(n),E} & s_{35}^{(n),E} & s_{36}^{(n),E} & d_{13}^{(n)} & d_{23}^{(n)} & d_{33}^{(n)} \\ s_{14}^{(n),E} & s_{24}^{(n),E} & s_{34}^{(n),E} & s_{44}^{(n),E} & s_{45}^{(n),E} & s_{46}^{(n),E} & d_{14}^{(n)} & d_{24}^{(n)} & d_{34}^{(n)} \\ 0 & 0 & 0 & 0 & 1 & 0 & 0 & 0 & 0 \\ 0 & 0 & 0 & 0 & 0 & 1 & 0 & 0 & 0 \\ d_{11}^{(n)} & d_{12}^{(n)} & d_{13}^{(n)} & d_{14}^{(n)} & d_{15}^{(n)} & d_{16}^{(n)} & \varepsilon_{11}^{(n),\sigma} & \varepsilon_{12}^{(n),\sigma} & \varepsilon_{13}^{(n),\sigma} \\ 0 & 0 & 0 & 0 & 0 & 0 & 0 & 1 & 0 \\ 0 & 0 & 0 & 0 & 0 & 0 & 0 & 0 & 1 \end{pmatrix}$$

is represented in terms of the electromechanical contants of the components ($n = 1$ or 2).

Rotation matrices related to the orientations of $\boldsymbol{P}_r^{(1)}$ (see insets 1 and 2 in Fig. 3.2) are given by

$$\| r(\alpha) \| = \begin{pmatrix} 1 & 0 & 0 \\ 0 & \cos\alpha & \sin\alpha \\ 0 & -\sin\alpha & \cos\alpha \end{pmatrix} \tag{3.6}$$

and

$$\| r(\beta) \| = \begin{pmatrix} \cos\beta & 0 & -\sin\beta \\ 0 & 1 & 0 \\ \sin\beta & 0 & \cos\beta \end{pmatrix}, \tag{3.7}$$

respectively. Thus, elements of $||C^*||$ from (3.2) depend either on m and α (rotation mode in inset 1 in Fig. 3.2) or on m and β (rotation mode in inset 2 in Fig. 3.2). We do not consider the case of a rotation of $\boldsymbol{P}_r{}^{(1)}$ around the OX_3 axis while the

piezoelectric coefficients of the FC component poled along OX_3 [9] obey an equality $d_{31}^{(1)} = d_{32}^{(1)}$.

Taking into account the $||d||$ matrix related to the FC component poled along the OX_3 axis (∞mm symmetry, see Sect. 1.1), Eq. (2.1) and rotation matrices from (3.6) and (3.7), we find the $||d||$ matrix at various angles α and β. At $0° < \alpha < 90°$ the $||d||$ matrix is written as

$$\| d \| = \begin{pmatrix} 0 & 0 & 0 & 0 & d_{15} & d_{16} \\ d_{21} & d_{22} & d_{23} & d_{24} & 0 & 0 \\ d_{31} & d_{32} & d_{33} & d_{34} & 0 & 0 \end{pmatrix},$$

however for $\alpha = 90°$ we have

$$\| d \| = \begin{pmatrix} 0 & 0 & 0 & 0 & 0 & d_{16} \\ d_{21} & d_{22} & d_{21} & 0 & 0 & 0 \\ 0 & 0 & 0 & d_{16} & 0 & 0 \end{pmatrix}.$$

We also examine that

$$\| d \| = \begin{pmatrix} d_{11} & d_{12} & d_{13} & 0 & d_{15} & 0 \\ 0 & 0 & 0 & d_{24} & 0 & d_{26} \\ d_{31} & d_{32} & d_{33} & 0 & d_{35} & 0 \end{pmatrix}$$

at $0° < \beta < 90°$ and

$$\| d \| = \begin{pmatrix} d_{11} & d_{12} & d_{12} & 0 & 0 & 0 \\ 0 & 0 & 0 & 0 & 0 & d_{26} \\ 0 & 0 & 0 & 0 & d_{26} & 0 \end{pmatrix}$$

at $\beta = 90°$ take place. The $||e||$ matrix has the form similar to that of $||d||$. Certainly, the orientation of the poled FC component influences the piezoelectric performance and anisotropy of the composite shown in Fig. 3.2.

To characterise the piezoelectric anisotropy of the studied 2–2 composite at $\alpha \neq 90°$ and $\beta \neq 90°$, we introduce anisotropy factors as follows:

$$\zeta_{d31} = d_{33}^*/d_{31}^* \text{ and } \zeta_{d32} = d_{33}^*/d_{32}^* \tag{3.8}$$

(for d^*_{3j} and $g^*_{3j} = d^*_{3j}/\varepsilon^{*\sigma}_{33}$), and

$$\zeta_{e31} = e^*_{33}/e^*_{31} \text{ and } \zeta_{e32} = e^*_{33}/e^*_{32} \tag{3.9}$$

(for e^*_{3j} and $h^*_{3j} = e^*_{3j}/\varepsilon^{*\xi}_{33}$). Equations (3.8) for the converse piezoelectric effect are represented as ratios of piezoelectric strains ξ_{33}/ξ_{11} and ξ_{33}/ξ_{22} as a result of the electric field $\boldsymbol{E_3}||OX_3$ in accordance with (1.6). Equations (3.9) enable us to evaluate ratios of piezoelectric polarisations, and therefore, ratios of surface charge densities, caused by external strains ξ_{jj} at the direct piezoelectric effect. According to (1.5), the piezoelectric polarisation P^*_3 of the composite (Fig. 3.2) equals $e^*_{33}\xi_3$ in the field of the longitudinal strain ξ_3, $e^*_{32}\xi_2$ in the field of the transverse strain ξ_2 or $e^*_{31}\xi_1$ in the field of the transverse strain ξ_1.

The anisotropy factors (3.8) and (3.9) are of value for high-anisotropic piezoactive elements that are used, for instance, in medical diagnostic devices with ultrasonic antennae based on pulse-echo principles and control of the preferred direction, in hydrophones, and other acoustic devices [17]. It should be added that various applications for high-anisotropic elements are attempting to effectively remove the interaction between the thickness and lateral vibration modes in the vicinity of the resonance of the thickness mode [17].

Examples of the volume-fraction and orientation behaviour of the anisotropy factors (3.8) and (3.9) are shown in Figs. 3.3 and 3.4. Graphs of the longitudinal piezoelectric coefficients e^*_{33} and d^*_{33} are represented in Fig. 3.5. Distinctions between the graphs in Figs. 3.3 and 3.4 are accounted for by the role of the elastic and piezoelectric properties in forming the piezoelectric anisotropy of the 2–2 composite. It is seen that the anisotropy factors ζ_{e3j} undergo considerably more changes than ζ_{d3j} irrespective of the FC component (cf. Figs. 3.3 and 3.4). Moreover, the longitudinal piezoelectric response concerned with e^*_{33} and d^*_{33} is similar, i.e., the anisotropy of the electromechanical properties of the FC component does not influence the configuration of curves in Fig. 3.5. The drastic changes in ζ_{e3j} may be a result of the presence of a system of interfaces $x_1 = \text{const}$ (Fig. 3.2) and the effect of the orientation of $\boldsymbol{P}_r{}^{(1)}$ of the FC on their elastic and piezoelectric properties and the effective properties of the composite as a whole. Taking into account the orientation effect and Eq. (1.12), one can write the anisotropy factors (3.8) in the general form as follows:

$$\zeta_{d31} = e^*_{3q}s^{*E}_{q3}/(e^*_{3q}s^{*E}_{q1}) = (e^*_{31}s^{*E}_{13} + e^*_{32}s^{*E}_{23} + \ldots + e^*_{36}s^{*E}_{63})/(e^*_{31}s^{*E}_{11} + e^*_{32}s^{*E}_{21} + \ldots + e^*_{36}s^{*E}_{61}) \text{ and } \zeta_{d32} = e^*_{3q}s^{*E}_{q3}/(e^*_{3q}s^{*E}_{q2}) = (e^*_{31}s^{*E}_{13} + e^*_{32}s^{*E}_{23} + \ldots + e^*_{36}s^{*E}_{63})/(e^*_{31}s^{*E}_{12} + e^*_{32}s^{*E}_{22} + \ldots + e^*_{36}s^{*E}_{62}). \tag{3.10}$$

The presence of the $e^*_{3q}\ s^{*E}_{q3}$-type terms in (3.10) leads to a simultaneous influence of the anisotropy of both e^*_{3j} and s^{*E}_{ab} on the anisotropy of d^*_{3j}, and we observe smooth

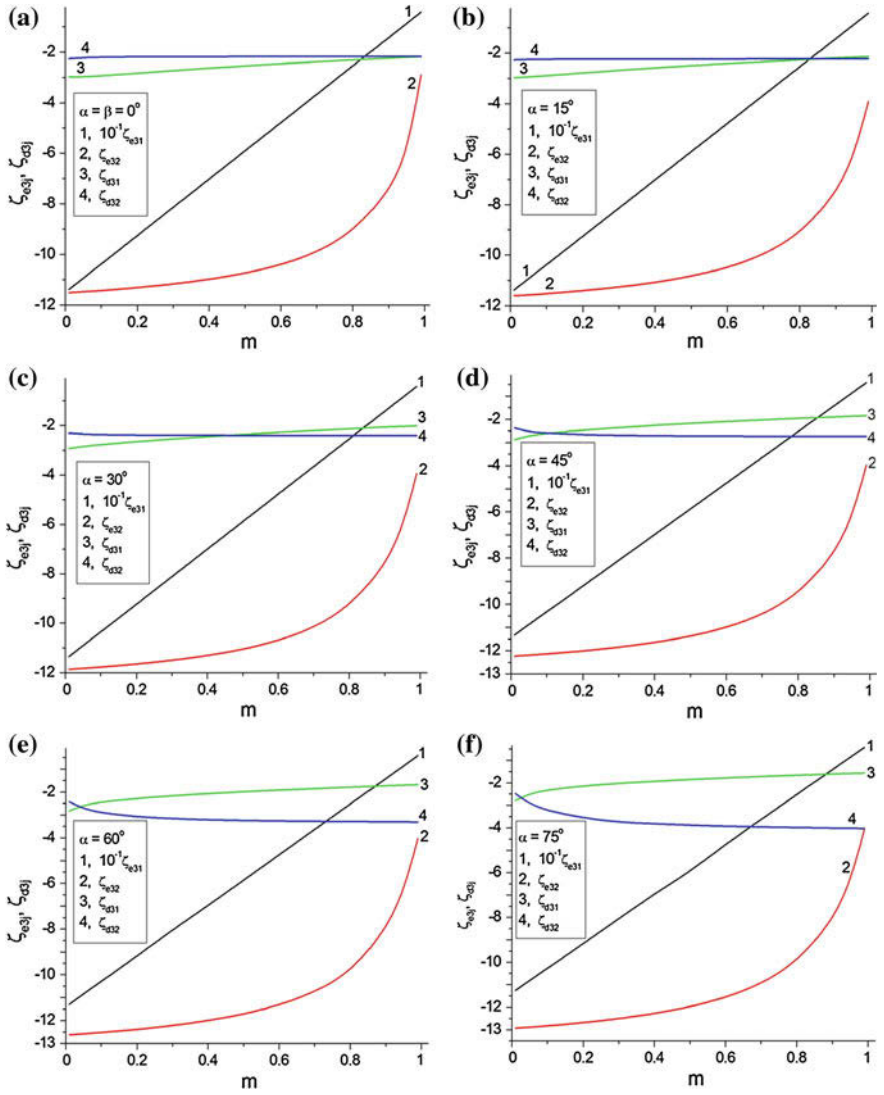

Fig. 3.3 Volume-fraction dependences of the anisotropy factors ζ_{e3j} and ζ_{d3j} of the 2–2 PCR-7M FC/polyurethane composite at $\alpha = \beta = 0°$ (**a**), $\alpha = \text{const} > 0°$ (**b–f**) and $\beta = \text{const} > 0°$ (**g–k**). Modes of rotation of the remanent polarisation vector $\boldsymbol{P}_r^{(1)}$ are shown in *insets* 1 and 2 in Fig. 3.2

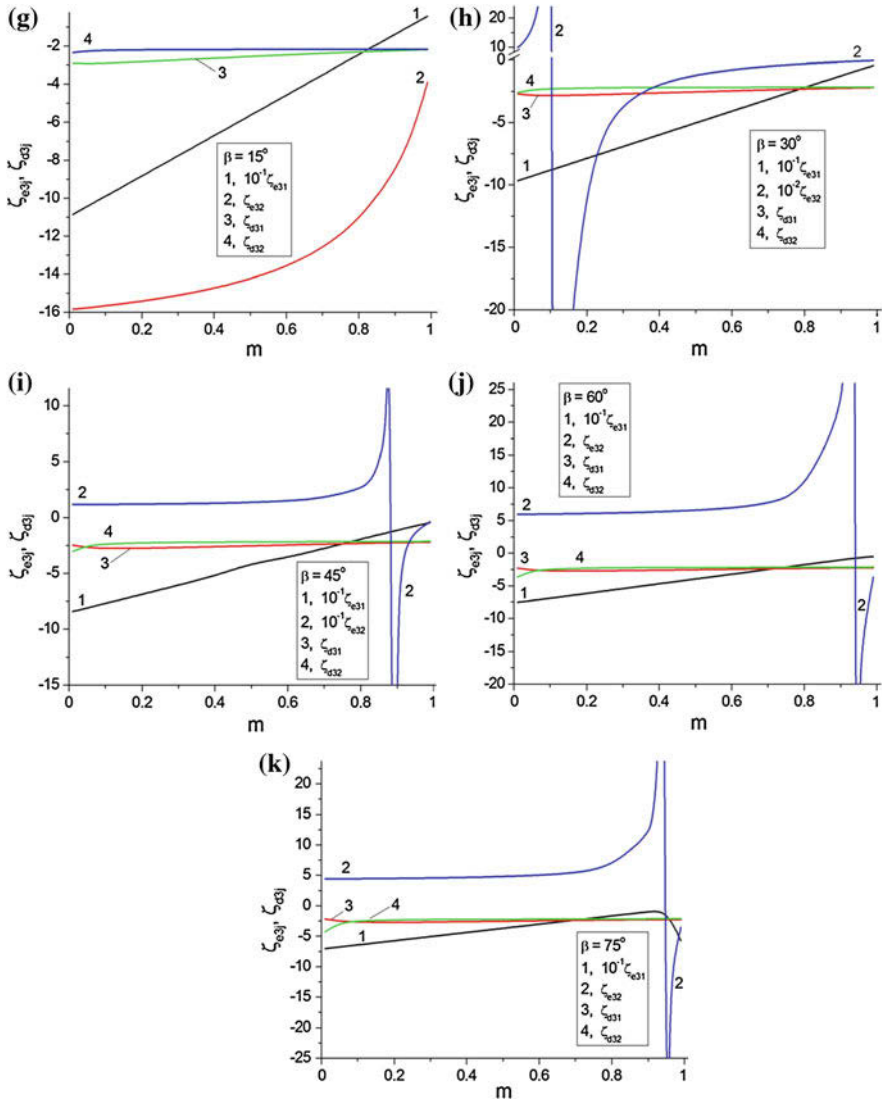

Fig. 3.3 (continued)

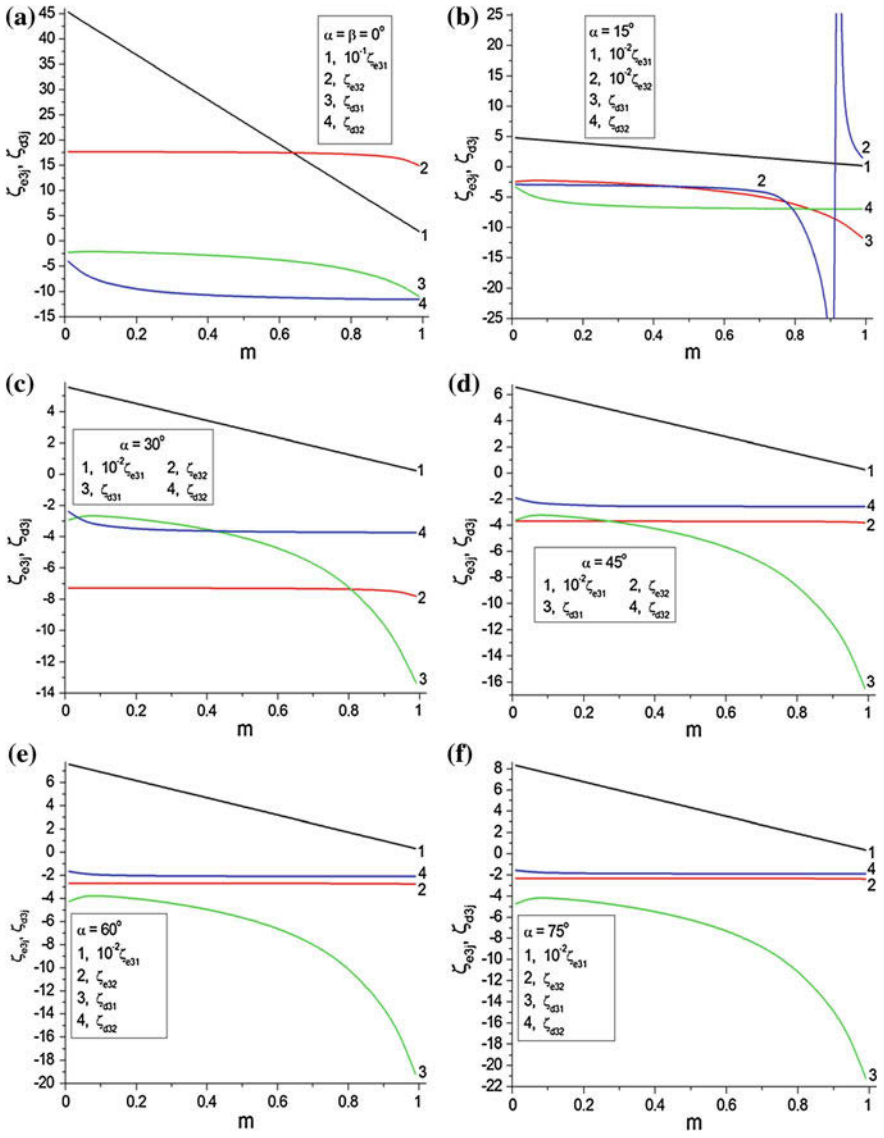

Fig. 3.4 Volume-fraction dependences of anisotropy factors ζ_{e3j} and ζ_{d3j} of the 2–2 modified $PbTiO_3$ FC/polyurethane composite at $\alpha = \beta = 0°$ (**a**), $\alpha = \text{const} > 0°$ (**b–f**) and $\beta = \text{const} > 0°$ (**g–k**). Modes of rotation of the remanent polarisation vector $\boldsymbol{P}_r^{(1)}$ are shown in insets 1 and 2 in Fig. 3.2

curves of ζ_{d3j} that change in restricted ranges (Figs. 3.3 and 3.4). It is also noteworthy that the anisotropy factors (3.9) obey conditions $\zeta_{e3j} \to \pm\infty$ (Figs. 3.3 and 3.4) in specific ranges of angles α and β. We see that the condition

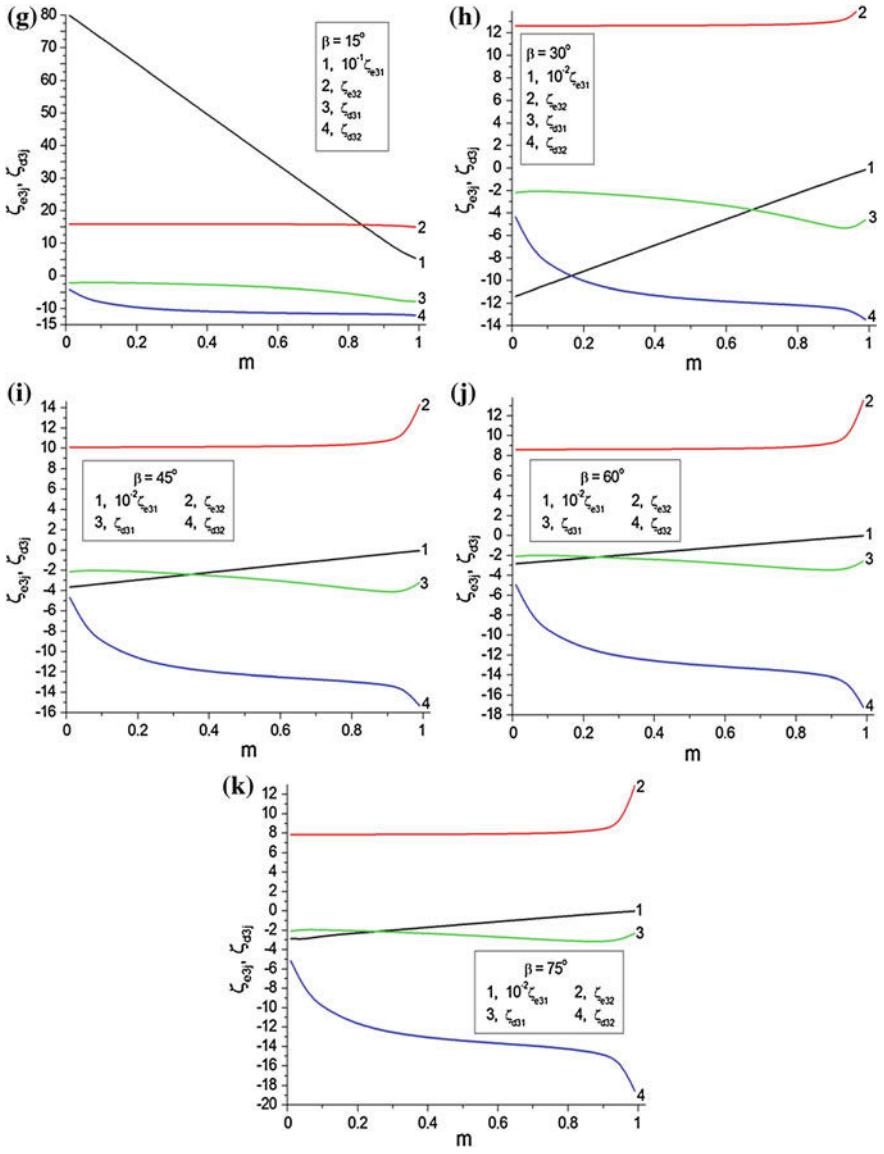

Fig. 3.4 (continued)

$$\zeta_{e32} \rightarrow \pm\infty \tag{3.11}$$

is achieved in the composite based on the modified $PbTiO_3$ FC (Fig. 3.4b), and this FC component is characterised by piezoelectric coefficients $e_{3j}^{(1)} > 0$ and $e_{15}^{(1)} > 0$. Such behaviour may be a result of the variable elastic anisotropy of the composite

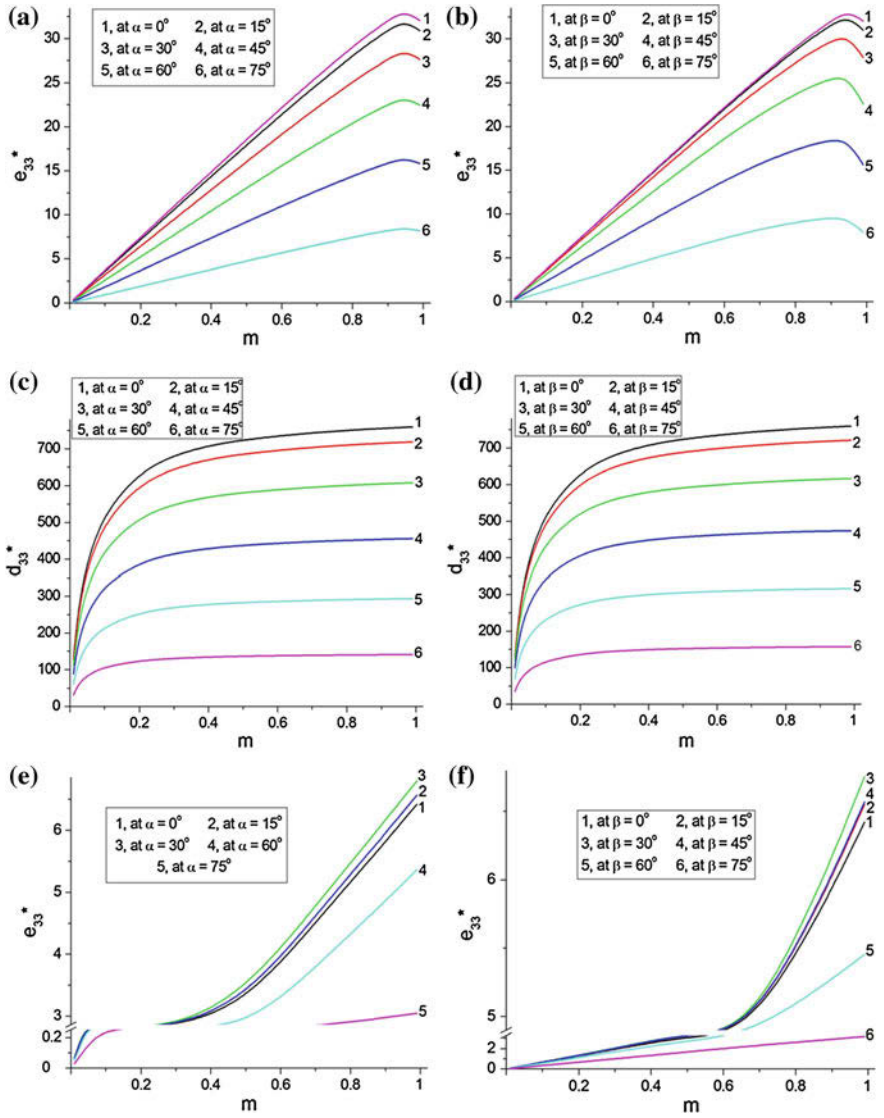

Fig. 3.5 Volume-fraction dependences of piezoelectric coefficients e_{33}^* (in C/m^2) and d_{33}^* (in pC/N) of the 2–2 PCR-7M FC/polyurethane composite (**a**–**d**) and a modified $PbTiO_3$ FC/polyurethane composite (**e**–**h**). Modes of rotation of the remanent polarisation vector $\boldsymbol{P}_r^{(1)}$ are shown in *insets* 1 and 2 in Fig.3.2

wherein the remanent polarisation vector $\boldsymbol{P}_r^{(1)}$ undergoes rotations in the plane of the interfaces (see inset 1 in Fig. 3.2). The same condition (3.11) is also valid in a relatively wide range of β in the composite based on the PCR-7M FC (Fig. 3.3h–k). In

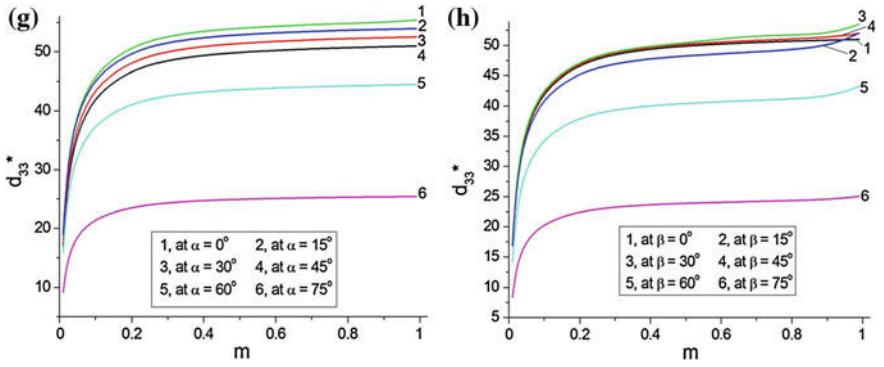

Fig. 3.5 (continued)

this composite the $\boldsymbol{P}_r^{(1)}$ vector undergoes rotations in the plane that is perpendicular to the interfaces (see inset 2 in Fig. 3.2), and the piezoelectric coefficients of the PCR-7M FC obey the condition [2]

$$\operatorname{sgn} e_{31}^{(1)} = -\operatorname{sgn} e_{33}^{(1)} = -\operatorname{sgn} e_{15}^{(1)} \tag{3.12}$$

In our opinion, such a rotation mode and the valid condition (3.12) favour the anisotropy of e_{3j}^* in the PCR-7M-based composite. In contrast to e_{3j}^*, the piezoelectric coefficients d_{3j}^* do not provide a large anisotropy at any variations of α and β (Fig. 3.3), and this performance may be due to the compensatory role of the aforementioned $e_{3q}^*\ s_{q3}^{*E}$-type terms in (3.10).

3.2 Single Crystal/Polymer Composites

3.2.1 Composites with Single-Domain Single-Crystal Components

3.2.1.1 PMN–*x*PT Single Crystals in 2–2 Composites

PMN–0.33PT has been the first perovskite-type relaxor-ferroelectric SC for which the full sets of the electromechanical constants were measured in both the single-domain and polydomain (domain-engineered) states at room temperature (see data in Tables 1.1 and 2.1). We highlight that the PMN–0.33PT SC is characterised by 3*m* or 4*mm* symmetry [18, 19] in the single-domain or polydomain state, respectively, and the molar concentration $x = 0.33$ indicates that this composition is located very close to the MPB [20]. In the single-domain state, the piezoelectric properties of the PMN–0.33PT SC have been analysed for various orientations of the main crystallographic axes [21], and some interconnections between the electromechanical

Table 3.2 Elastic compliances $s_{ab}^{(n),E}$ (in 10^{-12}Pa^{-1}), piezoelectric coefficients $d_{ij}^{(n)}$ (in pC/N) and dielectric permittivity $\varepsilon_{pp}^{(n),\sigma}$ of poled PMN–0.28PT SCs at room temperature [22]

Electromechanical constants	Single-domain $[111]_c$ -poled SC, $3m$ symmetry	Polydomain $[001]_c$ -poled SC, $4mm$ symmetry	Polydomain $[011]_c$-poled SC, $mm2$ symmetry
$s_{11}^{(n),E}$	8.78	44.57	13.40
$s_{12}^{(n),E}$	−4.90	−28.91	−21.18
$s_{13}^{(n),E}$	−0.93	−13.91	12.67
$s_{14}^{(n),E}$	16.87	0	0
$s_{22}^{(n),E}$	8.78	44.57	54.36
$s_{23}^{(n),E}$	−0.93	−13.91	−33.59
$s_{33}^{(n),E}$	6.32	34.38	28.02
$s_{44}^{(n),E}$	138.69	15.22	15.22
$s_{55}^{(n),E}$	138.69	15.22	147.06
$s_{66}^{(n),E}$	27.4	16.34	22.47
$d_{15}^{(n)}$	2,382	122	2,162
$d_{22}^{(n)}$	−312	0	0
$d_{24}^{(n)}$	2382	122	160
$d_{31}^{(n)}$	−43	−569	447
$d_{32}^{(n)}$	−43	−569	−1, 150
$d_{33}^{(n)}$	97	1,182	860
$\varepsilon_{11}^{(n),\sigma}/\ \varepsilon_0$	4,983	1,672	4,235
$\varepsilon_{22}^{(n),\sigma}/\ \varepsilon_0$	4,983	1,672	1,081
$\varepsilon_{33}^{(n),\sigma}/\ \varepsilon_0$	593	5,479	3,873

Data on the $[001]_c$- and $[011]_c$-poled polydomain SCs are related to their main crystallographic axes

properties of the single-domain and polydomain SCs were discussed in Chap. 2. To the best of our knowledge, PMN–0.28PT is the first relaxor-ferroelectric SC, for which self-consistent and full sets of electromechanical constants (Table 3.2) have been measured [22] along three poling directions, namely, along $[111]_c$, $[001]_c$ and $[011]_c$ in the perovskite unit cell. In the single-domain state at room temperature, the PMN–0.28PT SC is characterised by 3 m symmetry with a spontaneous polarisation vector $\boldsymbol{P}_s{}^{(1)} \parallel [111]_c$. The domain-engineered SC poled along $[001]_c$ exhibits $4mm$ symmetry and has an average spontaneous polarisation vector $\boldsymbol{P}_s{}^{(1)} \parallel [001]_c$. Poling along the $[011]_c$ axis leads to the domain-engineered state with $mm2$ symmetry and an average spontaneous polarisation vector $\boldsymbol{P}_s{}^{(1)} \parallel [011]_c$. As noted by Liu et al. [22], the full sets of electromechanical constants (Table 3.2) were determined from the same PMN–0.28PT crystal wafer, so that the composition and properties are uniform. Experimental data on PMN–xPT SCs (Tables 1.1, 2.1 and 3.2) enable a comparison of the effective electromechanical properties of the SC/polymer composites that comprise either the single-domain or polydomain SC component and are characterised by the same connectivity pattern.

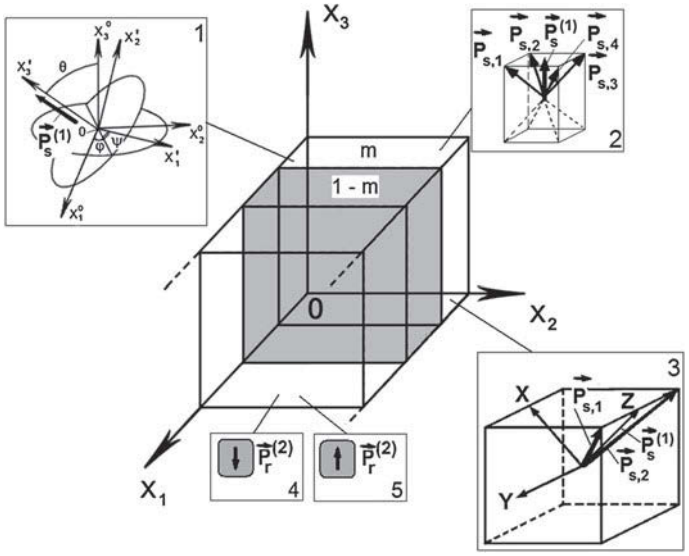

Fig. 3.6 Schematic of a 2–2 SC/polymer composite. ($X_1X_2X_3$) is the rectangular co-ordinate system, m and $1 - m$ are volume fractions of SC and polymer, respectively, $\boldsymbol{P}_s^{(1)}$ and $\boldsymbol{P}_r^{(2)}$ are the spontaneous polarisation vector of SC and the remanent polarisation vector of polymer, respectively. In *inset 1* φ, ψ and θ are Euler angles that characterise a rotation of the main crystallographic axes $(X_1^oX_2^oX_3^o) \rightarrow (X_1\prime X_2\prime X_3\prime)$ and the $\boldsymbol{P}_s^{(1)}$ vector in each single-domain SC layer. *Inset 2* comprises domain orientations in the $[001]_c$-poled SC with the effective spontaneous polarisation vector $\boldsymbol{P}_s^{(1)}$, *inset 3* comprises domain orientations in the $[011]_c$-poled SC with the effective spontaneous polarisation vector $\boldsymbol{P}_s^{(1)}$. $\boldsymbol{P}_{s,1}$, $\boldsymbol{P}_{s,2}$, $\boldsymbol{P}_{s,3}$, and $\boldsymbol{P}_{s,4}$ are spontaneous polarisation vectors of several domain types. x, y and z are the main crystallographic axes of the polydomain SC shown in *inset 3*. The remanent polarisation vector of polymer $\boldsymbol{P}_r^{(2)} \uparrow\downarrow OX_3$ can be oriented as shown in *insets 4* and *5*

The 2–2 SC/polymer composite (Fig. 3.6) is characterised by a regular distribution of alternating SC and polymer layers in the OX_1 direction, and the layers are assumed to be lengthy in the OX_2 and OX_3 directions. The layers of polyvinylidene fluoride ferroelectric polymer (PVDF, see data in Table 3.3) have a remanent polarisation vector oriented as shown in insets 4 and 5 in Fig. 3.6: either $\boldsymbol{P}_r^{(2)} \uparrow\downarrow OX_3$ (PVDF-1 in the composite sample) or $\boldsymbol{P}_r^{(2)} \uparrow\uparrow OX_3$ (PVDF-2 in the composite sample). The manufacture of 2–2 composites having components with various orientations of the $\boldsymbol{P}_s^{(1)}$ and $\boldsymbol{P}_r^{(2)}$ vectors can be achieved by individually poling the components. In respect of the studied SC/polymer composite, the coercive fields $E_c^{(n)}$ of the relaxor-ferroelectric SC ($n = 1$) and polymer ($n = 2$) obey an inequality [23, 24] $E_c^{(1)} << E_c^{(2)}$, that favours this type of the poling process. It is also assumed that the electrodes for the composite sample are perpendicular to the OX_3 axis (Fig. 3.6). A biased electric field can be also applied to the composite sample in order to maintain the single-domain state in the SC layers.

The procedure for averaging the electromechanical properties in the 2–2 SC/polymer composite is performed within the framework of the matrix method taking into consideration the boundary conditions for electric and mechanical fields in the adjacent layers of the composite sample (see Sect. 3.1).

3.2.1.2 2–2 Composite Based on PMN–0.33PT Single Crystal

Now we consider the effective piezoelectric coefficients $\Pi^*_{33}(m, \varphi, \psi, \theta)$ ($\Pi = d, e$ and g) of the PMN–0.33PT-based composite that contains PVDF-1 with the piezoelectric coefficients $d^{(2)}_{31} < 0, d^{(2)}_{33} > 0$ and $d^{(2)}_{15} > 0$. Such signs of the piezoelectric coefficients are typical of many perovskite-type FCs based on $BaTiO_3$, $Pb(Zr, Ti)O_3$ etc. (see Table 1.2). The piezoelectric coefficient d^*_{33} is directly determined from (3.5), while e^*_{33} and g^*_{33} are determined using Eqs. (1.12), (1.13) and (1.16). The orientation of the $\boldsymbol{P}^{(1)}_{\boldsymbol{s}}$ vector is characterised by a θ angle at $\varphi = \psi = 0°$ (see inset 1 in Fig. 3.6). It is worth noting, that even in the simplest case of the orientation of $\boldsymbol{P}^{(1)}_{\boldsymbol{s}}$, one can obtain a non-monotonic dependence of $\Pi^*_{33}(m, 0°, 0°, \theta)$ on θ (Fig. 3.7) or m (Fig. 3.7b, c). At volume fractions $m \to 1$ the polymer layers have a small influence on the piezoelectric performance of the composite. As a consequence, the orientation dependences of the piezoelectric coefficients d^*_{33} and e^*_{33} on m (Fig. 3.7a, b) are similar to those studied for the single-domain PMN–0.33PT SC (see Sect. 2.1). As observed in conventional 2–2 FC/polymer composites [2, 11], max $g^*_{33}(m, 0°, 0°, \theta)$ is observed at $m << 1$ and $\theta \leq 50°$(Fig. 3.7c).

Relatively small volume fractions of the SC component $0 < m < 0.1$ lead to a non-monotonic behaviour of g^*_{33} in the piezo-active composite [2] due to the effect of dielectric properties of polymer on piezoelectric sensitivity in accordance with (1.12) and (1.14). An increase in θ has a significant effect of the balance of the piezoelectric coefficients $d^{(1)}_{ij}$ and $g^{(1)}_{ij}$ of the single-domain PMN–0.33 PT SC, and these changes promote a non-monotonic behaviour of g^*_{33} at $m = \text{const}$ (Fig. 3.7c). We show the graph of $g^*_{33}(m, 0°, 0°, \theta)$ at volume fractions $0 \leq m \leq 0.2$ only (see Fig. 3.7c) due to the rapid decrease in $|g^*_{33}|$ at $m > 0.2$ and any θ values [26]. This decrease is caused by an intensive increase in dielectric permittivities $\varepsilon^{*\sigma}_{fh}$ of the composite in the same m range.

A presence of slight max $e^*_{33}(m, 0°, 0°, \theta)$ or min $e^*_{33}(m, 0°, 0°, \theta)$ at $0.9 < m < 1$ (Fig. 3.7b) is a result of the effect of elastic properties of the components on the piezoelectric response of the composite [see (1.13)] and with changes in the balance

Table 3.3 Elastic compliances $s^{(n),E}_{ab}$ (in 10^{-12} Pa^{-1}), piezoelectric coefficients $d^{(n)}_{ij}$ (in pC/N) and dielectric permittivity $\varepsilon^{(n),\sigma}_{pp}$ of poled PVDF at room temperature [25]

$s^{(n),E}_{11}$	$s^{(n),E}_{12}$	$s^{(n),E}_{13}$	$s^{(n),E}_{33}$	$s^{(n),E}_{44}$	$s^{(n)}_{66}$	$d^{(n)}_{15}$	$d^{(n)}_{31}$	$d^{(n)}_{33}$	$\frac{\varepsilon^{(n),\sigma}_{11}}{\varepsilon_0}$	$\frac{\varepsilon^{(n),\sigma}_{33}}{\varepsilon_0}$
333	−148	−87.5	299	1.90×10^4	943	38	−10.42	33.64	7.513	8.431

The orientation of the remanent polarisation vector is shown in inset 4 in Fig. 3.6

of the piezoelectric coefficients d_{ij}^* at relatively large volume fractions m. It should be mentioned that max e_{33}^* is also observed in the 2–2 FC/polymer composites (Fig. 3.5a, b) at various orientations of the remanent polarisation vector $\boldsymbol{P}_{\boldsymbol{r}}^{(1)}$ and sgn $e_{ij}^{(1)}$ in accordance with (3.12).

A comparison of graphs of $d_{33}^*(m, 0°, 0°, \theta)$, $e_{33}^*(m, 0°, 0°, \theta)$ and $g_{33}^*(m, 0°, 0°, \theta)$ (Fig. 3.7) enables us to discuss the effect of the combination of properties (in terms of work [2, 26, 27]) in the studied composite. As follows from (1.13) and (1.14), the piezoelectric coefficients e_{ij}^* are regarded as a combination of the piezoelectric and elastic properties, while the piezoelectric coefficients g_{ij}^* can be regarded as a combination of the piezoelectric and dielectric properties. When changing the θ angle, the elastic compliances $s_{ab}^{(1),E}$ of the single-domain PMN–0.33 PT SC vary to a

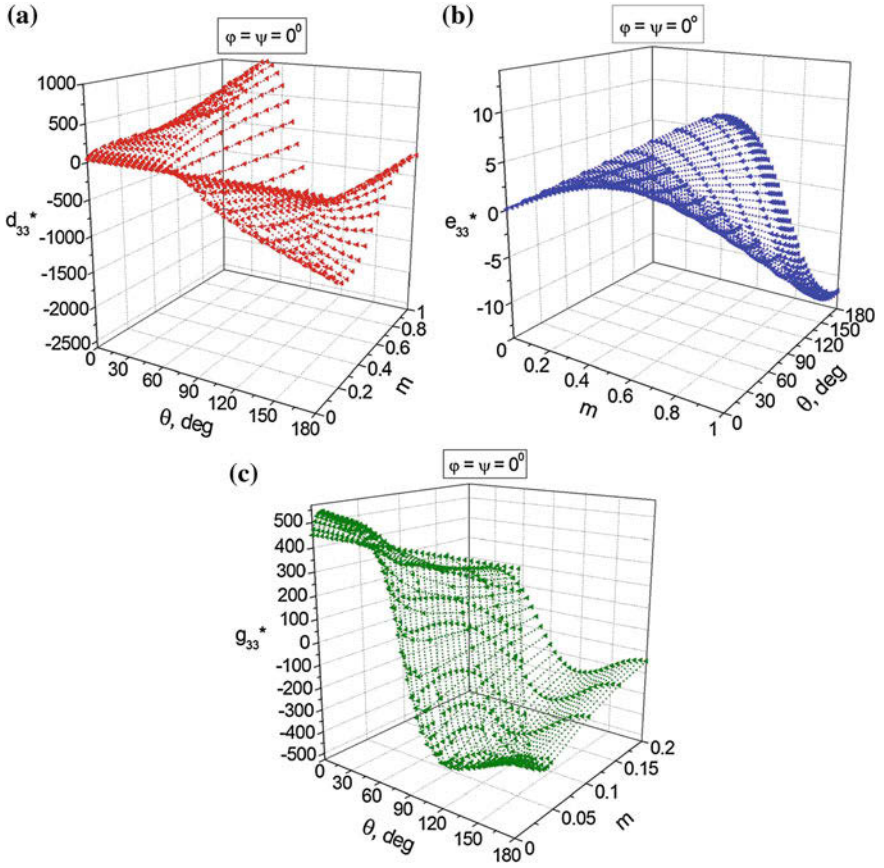

Fig. 3.7 Piezoelectric coefficients calculated for a 2–2 single-domain PMN–0.33PT SC/PVDF-1 composite: d_{33}^* (**a**, in pC/N), e_{33}^* (**b**, in C/m^2) and g_{33}^* (**c**, in mV·m/N) (reprinted from paper by Topolov and Krivoruchko [26], with permission from IOP Publishing)

lesser degree than the piezoelectric coefficients $d_{ij}^{(1)}$. We therefore see that the piezoelectric coefficient $e_{33}^*(m, 0°, 0°, \theta)$ varies in a fairly narrow range (Fig. 3.7b) owing to the dominating role of the elastic properties in forming this piezoelectric response. In contrast to $e_{33}^*(m, 0°, 0°, \theta)$, the piezoelectric coefficient $g_{33}^*(m, 0°, 0°, \theta)$ undergoes larger changes in the wide range (Fig. 3.7c), due to the considerable variations of both d_{ij}^* and $\varepsilon_{fh}^{*\sigma}$ in this composite.

3.2.1.3 Hydrostatic Parameters of the 2–2 Composite Based on PMN–xPT Single Crystal ($x = 0.28$ or 0.33)

In this section we compare the hydrostatic piezoelectric performance of 2–2 composites based on the single-domain PMN–xPT SCs. A prediction of the hydrostatic parameters and their extreme values is of importance for materials selection for hydroacoustic and other piezo-technical applications. Among these parameters, we study the hydrostatic piezoelectric coefficients d_h^* and g_h^* from (3.2), the hydrostatic piezoelectric coefficient

$$e_h^* = e_{33}^* + e_{32}^* + e_{31}^*, \tag{3.13}$$

the squared hydrostatic figure of merit $(Q_h^*)^2$ from (3.3), and the hydrostatic ECF

$$k_h^* = d_h^* / \sqrt{s_h^{*E} \varepsilon_{33}^{*\sigma}} \tag{3.14}$$

[see also (1.27)], where the hydrostatic compliance is given by $s_h^{*E} = \sum_{a=1}^{3} \sum_{b=1}^{3} s_{ab}^{*E}$ [15, 28]. The hydrostatic piezoelectric coefficients from (3.2) and (3.13) provide a measure of the activity and sensitivity of the composite under hydrostatic loading. $(Q_h^*)^2$ from (3.3) is introduced to evaluate the sensor signal-to-noise ratio of the composite and to characterise its piezoelectric sensitivity [2, 11, 16]. The ECF k_h^* from (3.14) enables one to characterise the transducer efficiency of the composite under hydrostatic loading. We add that the hydrostatic parameters Π_h^* from (3.2), (3.3), (3.13) and (3.14) are related to the composite sample (Fig. 3.6) with electrodes that are perpendicular to the OX_3 axis, and therefore, the piezoelectric coefficients with subscripts 31, 32 and 33 are taken into consideration.

Data on absolute maxima of the hydrostatic parameters Π_h^* are represented in Table 3.4. Based on these data and comparing them, it is possible to conclude that the PMN–0.28PT-based composite is of interest as a material with the largest hydrostatic piezoelectric coefficient e_h^*, and the PMN–0.33PT-based composite is of value as a piezo-active material with the large absolute values of the hydrostatic parameters, d_h^*, g_h^*, $(Q_h^*)^2$, and k_h^*. This good performance is due not only to the ansiotropy of the piezoelectric coefficients $d_{ij}^{(1)}$ etc. in the single-domain state, but also to the

Table 3.4 Absolute maxima (minima) of hydrostatic parameters $\Pi_h^*(m, \varphi, \psi, \theta)$ of the 2–2 single-domain PMN–xPT SC/PVDF-1 composite

Π_h^*	$x = 0.28$		$x = 0.33$	
	Value of absolute maxΠ_h^*	m, φ, ψ, and θ which correspond to the value of maxΠ_h^*	Value of absolute maxΠ_h^* (or absolute min Π_h^*)	m, φ, ψ, and θ which correspond to the value of maxΠ_h^* (or min Π_h^*)
d_h^*	133 pC/N	$m = 0.238$, $\varphi = 0°$, $\psi = 0°$, and $\theta = 74°$	–322 pC/N[a]	$m = 0.311$, $\varphi = 0°$, $\psi = 0°$, and $\theta = 86°$
g_h^*	242 mV· m/N	$m = 0.007$, $\varphi = 60°$, $\psi = 90°$, and $\theta = 57°$	–252 mV· m/N[a]	$m = 0.029$, $\varphi = 60°$, $\psi = 90°$, and $\theta = 127°$
e_h^*	45.1 C/m^2	$m = 0.868$, $\varphi = 60°$, $\psi = 90°$, and $\theta = 76°$	–22.3 C/m^{2a}	$m = 0.831$, $\varphi = 60°$, $\psi = 90°$, and $\theta = 117°$
$(Q_h^*)^2$	$12.3 \cdot 10^{-12}$ Pa^{-1}	$m = 0.021$,$\varphi = 60°$, $\psi = 90°$, and $\theta = 63°$	$21.5 \cdot 10^{-12}$ Pa^{-1}	$m = 0.067$, $\varphi = 60°$, $\psi = 90°$, and $\theta = 123°$
k_h^*	0.217	$m = 0.027$, $\varphi = 60°$, $\psi = 90°$, and $\theta = 63°$	0.294	$m = 0.085$,$\varphi = 60°$, $\psi = 90°$, and $\theta = 124°$

[a] Absolute minimum value

anisotropy of the electromechanical properties of the composite due to its laminar structure (Fig. 3.6).

Values of $e_h^* \approx$ (40–45) C/m^2 (Fig. 3.8) can be achieved in PMN–0.28PT-based composites near the absolute maximum point even with deviations of the Euler angles of approximately 5–10°, and deviations of the volume fraction of about 0.1 are also possible. It is noted for comparison that the single-domain $[111]_c$-poled PMN–0.28PT SC is characterised [22] by $e_h^{(1)} = -2.93$ C/m^2 at $\varphi = \psi = \theta = 0°$ and by $e_h^{(1)} = -0.708$ C/m^2 at $\varphi = 60°$,$\psi = 90°$ and $\theta = 76°$ (these Euler angles are related to absolute max e_h^*, see Table 3.4). The significant elastic anisotropy of the single-domain PMN–0.28PT SC (see elastic compliances $s_{ab}^{(n),E}$ in the second column of Table 3.2) leads to an effective re-distribution of mechanical fields in the composite sample and a favourable balance of the contributions from the piezoelectric coefficients e_{3j}^* (Fig. 3.8) into e_h^* [see (3.13)]. Data from Table 3.4 and Fig. 3.8 suggest that the Euler angle θ plays a key role in achieving the large hydrostatic piezoelectric coefficient e_h^* of this composite, and this circumstance is due to the orientation of the spontaneous polarisation vector $\boldsymbol{P}_s^{(1)}$ in the single-domain SC layer (see inset 1 in Fig. 3.6). The Euler angles $\varphi = 60°$ and $\psi = 90°$ are of interest to achieve absolute maxima of the four hydrostatic parameters (Table 3.4). Such orientations of the main crystallographic axes of the $[111]_c$-poled SC lead to an obvious simplification of the matrix of the piezoelectric properties of the composite $||p^*||$ where $p = d$, e and g. At $0 < m \leq 1$, $\varphi = 60°$, $\psi = 90°$, and various values of θ, this matrix is represented as

$$||p^*|| = \begin{pmatrix} p_{11}^* & p_{12}^* & p_{13}^* & 0 & p_{15}^* & 0 \\ 0 & 0 & 0 & p_{24}^* & 0 & p_{26}^* \\ p_{31}^* & p_{32}^* & p_{33}^* & 0 & p_{35}^* & 0 \end{pmatrix}, \tag{3.15}$$

and elements p_{31}^*, p_{32}^* and p_{33}^* from (3.15) promote large hydrostatic parameters of the composite. The large values of e_h^* (Table 3.4) are achieved at the most simple orientation of the electrodes, i.e., perprendicular to the OX_3 axis (Fig. 3.6). In comparison to this result, the absolute max $e_h^* = 42.6$ C/m^2 and absolute min $e_h^* = -44.4$ C/m^2 were predicted for the hydrostatic piezoelectric coefficient $e_h^* = e_{11}^* + e_{12}^* + e_{13}^* + e_{21}^* + e_{22}^* + e_{23}^* + e_{31}^* + e_{32}^* + e_{33}^*$ in a similar 2–2 PMN–0.33PT single-domain SC/PVDF-1 composite [26], but with electrodes having a more complex geometry, namely, a system of parallel-connected conducting layers oriented along the X_1OX_2, X_1OX_3 and X_2OX_3 planes. We note that the absolute max $e_h^* = 45.1$ C/m^2 (Table 3.4) evaluated in accordance with (3.13) is approximately 3–5 times larger than the hydrostatic piezoelectric coefficient e_h of the well-known PZT-type FCs [2, 28].

As for the PMN–0.33PT-based composite, its hydrostatic performance has some advantages over PMN–0.28PT-based composites due to large absolute values of min Π_h^* (Table 3.4). A reason for these values is concerned with the balance of the

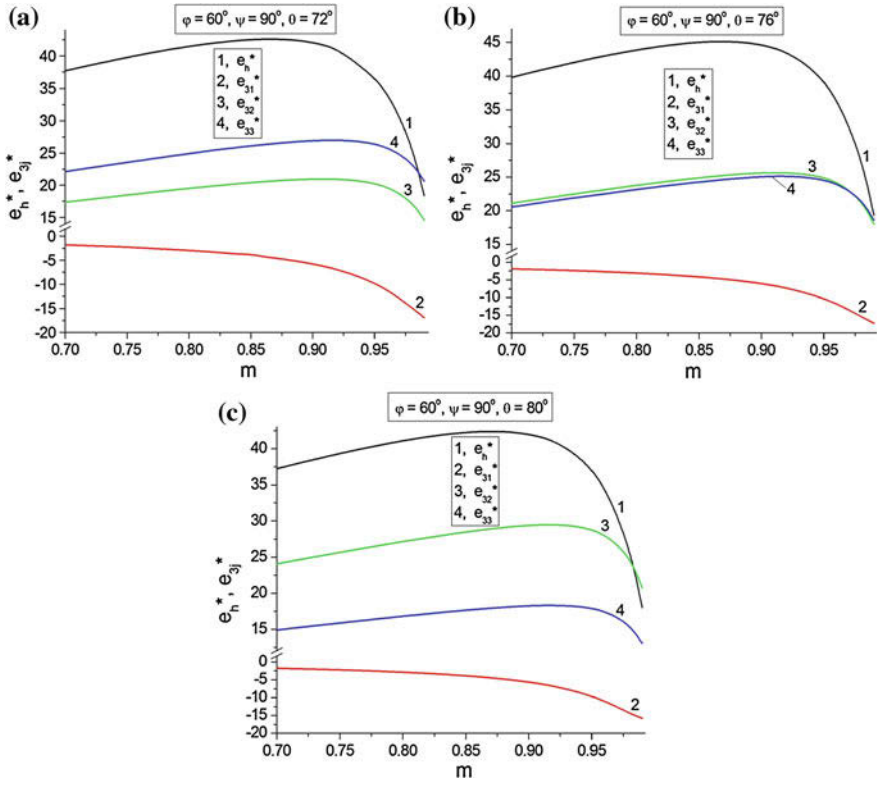

Fig. 3.8 Volume-fraction dependences of the piezoelectric coefficients e^*_{3j} and e^*_h (in $\mathrm{C/m^2}$) near absolute max $e^*_h(m, \varphi, \psi, \theta)$ in a 2–2 single-domain PMN–0.28PT SC/PVDF-1 composite at $\varphi = 60°, \psi = 90°$ and $\theta = 72°$ (**a**), $\varphi = 60°, \psi = 90°$ and $\theta = 76°$ (**b**), and $\varphi = 60°, \psi = 90°$ and $\theta = 80°$ (**c**)

piezoelectric coefficients $d^{(1)}_{ij}$ and with the anisotropy of elastic compliances $s^{(1),E}_{ab}$ of the single-domain PMN–0.33PT SC (see Table 2.1). A simple comparison of electromechanical constants from Tables 2.1 and 3.2 suggest that the single-domain PMN–0.33PT SC can be of value due to large positive values of both $d^{(1)}_{15}$ and $d^{(1)}_{22}$. The single-domain PMN–0.33PT SC is characterised by the large ratio $s^{(1),E}_{11}/s^{(1),E}_{33}$ (Table 2.1) that strongly influences the piezoelectric effect and its anisotropy in the composite. The absolute value of the hydrostatic piezoelectric coefficient $d^{(1)}_h$ of the single-domain PMN–0.33PT SC is also larger than that related to the single-domain PMN–0.28PT SC.

Thus, single-domain PMN–*x*PT SCs can be used to manufacture novel 2–2 composite with predictable hydrostatic parameters (Table 3.4). Criteria of the choice of the optimum SC component to achieve the largest $|\Pi^*_h|$ value may be formulated

in the future, after careful passing the molar-concentration range near the MPB and refining the full sets of electromechanical constants of SCs with related compositions.

3.2.2 Composites with Polydomain Single-Crystal Components: A Comparison of Hydrostatic Parameters

3.2.2.1 Composites Based on PMN–0.28PT Single Crystals

The next important step in the study of 2–2 SC/polymer composites is a comparison of the hydrostatic parameters that are achieved in the presence of a polydomain (domain-engineered) SC component with a specific domain arrangement. In Sect. 3.2.2 we will distinguish the following 2–2 composites:

(i) with polydomain $[001]_c$-poled SC layers (inset 2 in Fig. 3.6) and
(ii) with polydomain $[011]_c$-poled SC layers (inset 3 in Fig. 3.6).

We rotate the main crystallographic axes x, y and z of the polydomain SC layer in these composites around one of the co-ordinate axes–$OX_1||x$, $OX_2||y$ or $OX_3||$ z (see examples in Fig. 3.9). Such modes of rotation make it possible to maintain the polydomain state (insets 2 and 3 in Fig. 3.6) in the SC layer. It is assumed that at these rotations, the spontaneous polarisation vectors of domains $\boldsymbol{P_{s,1}}, \boldsymbol{P_{s,2}}$ etc. in the SC layer are situated either over or in the (X_1OX_2) plane (see Fig. 3.6). The rotation angles are varied in the following ranges [29–31]:

(i) for composites with $[001]_c$-poled layers, $-45° \leq \delta_x \leq 45°$ or $-45° \leq \delta_y \leq 45°$ (Fig. 3.9a), and
(ii) for composites with $[011]_c$-poled layers, $-\arcsin(1/\sqrt{3}) \leq \alpha \leq \arcsin(1/\sqrt{3})$, $-45° \leq \beta \leq 45°$ or $0° \leq \gamma \leq 360°$ (see Fig. 3.9b and inset 3 in Fig. 3.6).

Because of the 4*mm* symmetry of the $[001]_c$-poled PMN–0.28PT SC (see inset 2 in Fig. 3.6 and Table 3.2) and the equality of its piezoelectric coefficients $d_{31}^{(1)} = d_{32}^{(1)}$, we do not consider the mode of rotation of the main crystallographic axes x and y of this SC around $OX_3||$ z.

Values of absolute maxima of d_h^*, g_h^*, $(Q_h^*)^2$, and k_h^* of the composite with the $[001]_c$-poled layers are larger than those related to the composite with single-domain $[111]_c$-poled layers (cf. data in Tables 3.5 and 3.4). This is a result of the relatively high piezoelectric activity and the relatively small elastic anisotropy of the $[001]_c$-poled SC (see Table 3.2). As in the composite with single-domain $[111]_c$-poled layers, the absolute $\max g_h^*$ in the composite with $[001]_c$-poled layers is achieved at very low volume fraction of SC ($m < 1\,\%$), which could be problematic in terms of the manufacturing tolerance. The presence of $\max g_h^*$ at the small volume fractions m is due to the role of the dielectric properties of the polymer component [2, 26, 30, 31]: as is known, extreme points of piezoelectric coefficients g_{3j}^* in various two-component composites are observed in a volume-fraction range where the dielectric permittivity of the composite $\varepsilon_{33}^{*\sigma}$ obeys the condition $\varepsilon_{33}^{*\sigma} << \varepsilon_{33}^{(1),\sigma}$.

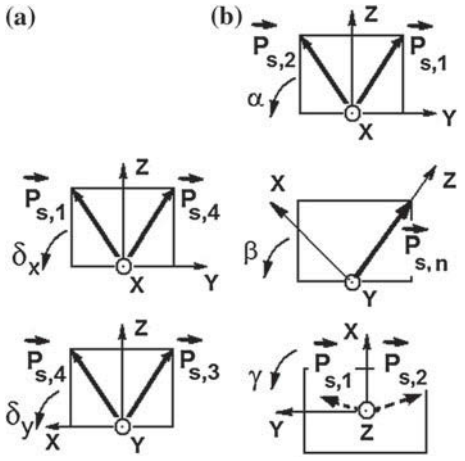

Fig. 3.9 Modes of rotation of the spontaneous polarisation vectors $\boldsymbol{P_{s,1}}$, $\boldsymbol{P_{s,2}}$, ... in the $[001]_c$-poled (**a**) and $[011]_c$-poled (**b**) SCs. x, y and z are the main crystallographic axes of the polydomain SC, δ_x and δ_y are rotation angles for the $[001]_c$-poled SC, and α, β and γ are rotation angles for the $[011]_c$-poled SC (reprinted from paper by Topolov et al. [29], with permission from Taylor and Francis)

The absolute maxima of d_h^*, g_h^*, $(Q_h^*)^2$, and k_h^* of the composite with $[011]_c$-poled layers (Table 3.5) are larger than those of the composites with single-domain (Table 3.4) and $[001]_c$-poled layers (Table 3.5). In our opinion, the high performance of the composite with $[011]_c$-poled layers is due to the unusual anisotropy of the electromechanical properties of the SC. For instance, in the $[011]_c$-poled PMN–0.28SC the elastic compliances $s_{ab}^{(n),E}$ are linked by the ratios

$$s_{11}^{(1),E} \approx s_{13}^{(1),E},\ |s_{23}^{(1),E}| \approx 2.7 s_{13}^{(1),E} \text{ and } s_{33}^{(1),E} \approx 2 s_{13}^{(1),E}, \tag{3.16}$$

while the piezoelectric coefficients $d_{3j}^{(n)}$ of the same SC obey the conditions

$$d_{33}^{(1)} \approx 1.9\, d_{31}^{(1)} \text{ and } |d_{32}^{(1)}| \approx 2.6\, d_{31}^{(1)} \tag{3.17}$$

(see Table 3.2). Variations of the rotation angles α and β lead to values of $\max \Pi_h^*$ which are lower than those in Table 3.5 for the composite with $[011]_c$-poled SC layers, and we omit results on $\Pi_h^*(m,\alpha)$ and $\Pi_h^*(m,\beta)$ for this composite.

The important advantage of composites with $[011]_c$-poled SC layers over the similar composites based on PMN–0.28PT is the optimal orientation of the main crystallographic axes of the $[011]_c$-poled state. In this case the five hydrostatic parameters $\Pi_h^*(m,\gamma)$ have absolute maxima at $\gamma = 90°$ and volume factions m from 0.012 to 0.876 (Table 3.5). It is worth noting that at $0 < m \leq 1$ and $\gamma = 90°$, the matrix $||d^*||$ of the piezoelectric coefficients of the composite with the $[011]_c$-poled SC layers has a form

Table 3.5 Absolute maxima of hydrostatic parameters Π_h^* of 2-2 polydomain PMN-0.28PT/ PVDF-1 composites

	Composite with $[001]_c$**-poled SC layers**		**Composite with** $[011]_c$**-poled SC layers**	
Π_h^*	Value of absolute maxΠ_h^*	Volume fraction m and angles at absolute maxΠ_h^*	Value of absolute maxΠ_h^*	Volume fraction m and angles at absolute maxΠ_h^*
d_h^*	228 pC/N	$m = 0.253$ and $\delta_x = 0°$, or $m = 0.253$ and $\delta_y = 0°$	372 pC/N	$m = 0.337$ and $\gamma = 90°$
g_h^*	230 mV· m/N	$m = 0.007$ and $\delta_x = 0°$, or $m = 0.007$ and $\delta_y = 0°$	284 mV· m/N	$m = 0.012$ and $\gamma = 90°$
e_h^*	24.3 C/m^2	$m = 0.811$ and $\delta_y = \pm 29°$	25.7 C/m^2	$m = 0.876$ and $\gamma = 90°$
$(Q_h^*)^2$	$15.3 \cdot 10^{-12}$ Pa^{-1}	$m = 0.038$ and $\delta_x = 0°$, or $m = 0.038$ and $\delta_y = 0°$	$33.8 \cdot 10^{-12}$ Pa^{-1}	$m = 0.068$ and $\gamma = 90°$
k_h^*	0.235	$m = 0.048$ and $\delta_x = 0°$, or $m = 0.048$ and $\delta_y = 0°$	0.361	$m = 0.095$ and $\gamma = 90°$

$$||d^*|| = \begin{pmatrix} 0 & 0 & 0 & 0 & d_{15}^* & 0 \\ 0 & 0 & 0 & d_{24}^* & 0 & 0 \\ d_{31}^* & d_{32}^* & d_{33}^* & 0 & 0 & 0 \end{pmatrix}. \tag{3.18}$$

A balance of d_{3j}^* in (3.18) promotes an increase of the hydrostatic piezoelectric coefficients d_h^*, g_h^*, and as a consequence, the squared hydrostatic figure of merit $(Q_h^*)^2$. In addition, the hydrostatic piezoelectric coefficient $d_h^{(1)}$ of the $[011]_c$-poled PMN–0.28PT SC at $\gamma = 0°$ is considerably more than $d_h^{(1)}$ in the $[111]_c$- and $[001]_c$-poled states.

3.2.2.2 Composites Based on PZN–0.07PT Single Crystals

The full set of electromechanical constants related to the $[011]_c$-poled relaxor-ferroelectric SC has first been measured [23] on PZN–0.07PT, a composition located near the MPB [20]. The PZN–0.07PT SC in the domain-engineered $[011]_c$-poled state (inset 3 in Fig. 3.6) is characterised [23] by *mm*2 symmetry and an unusual anisotropy of elastic and piezoelectric properties (cf. data from Tables 1.1 and 3.6). It is obvious that the symmetry and anisotropy of the properties differ from those particular to the $[001]_c$-poled PZN–*x*PT or PMN–*x*PT SCs. According to data from Table 3.6, the elastic compliances $s_{ab}^{(n),E}$ of the $[001]_c$-poled PZN–0.07PT SC are linked by ratios as follows:

$$s_{11}^{(n),E}/s_{12}^{(n),E} = -1.12, \quad s_{11}^{(n),E}/s_{13}^{(n),E} = 20.1 \text{ and } s_{11}^{(n),E}/s_{33}^{(n),E} = 1.09. \tag{3.19}$$

Ratios of the piezoelectric coefficients $d_{3j}^{(n)}$

$$d_{33}^{(n)}/d_{31}^{(n)} = 2.41 \text{ and } d_{33}^{(n)}/d_{32}^{(n)} = -0.788 \tag{3.20}$$

characterise the anisotropy of the piezoelectric effect in the same SC. We note that Eqs. (3.19) and (3.20) are related to the main crystallographic axes shown in inset 3 in Fig. 3.6. Ratios (3.19) and (3.20) differ from relations (3.16) and (3.17) which correspond to the $[011]_c$-poled PMN–0.28PT SC, and this circumstance is to be taken into account at the analysis of the effective parameters of the PZN–0.07PT-based composite.

It is assumed that the polydomain SC layers in the 2–2 composite (Fig. 3.10) represent crystal cuts with a clockwise rotation of the main crystallographic axes x and y around the co-ordinate axis $OX_3||$ z, where φ is the rotation angle. The composite sample is poled along the OX_3 axis. The macroscopic symmetry of the 2–2 composite based on the $[011]_c$-poled PZN–0.07PT SC enables us to consider a range of $0° \le \varphi \le 90°$ due to the condition $\Pi^*(m, \varphi) = \Pi^*(m, 180° - \varphi)$. The

Table 3.6 Elastic compliances $s_{ab}^{(n),E}$(in 10^{-12} Pa^{-1}), piezoelectric coefficients $d_{ij}^{(n)}$ (in pC/N) and dielectric permittivity $\varepsilon_{pp}^{(n),\sigma}$ of the domain-engineered $[011]_c$-poled PZN–0.07PT SC at room temperature [23]

$s_{11}^{(n),E}$	$s_{12}^{(n),E}$	$s_{13}^{(n),E}$	$s_{22}^{(n),E}$	$s_{23}^{(n),E}$	$s_{33}^{(n),E}$
67.52	–60.16	3.355	102.0	–54.47	62.02
$s_{44}^{(n),E}$	$s_{55}^{(n),E}$	$s_{66}^{(n),E}$	$d_{31}^{(n)}$	$d_{32}^{(n)}$	$d_{33}^{(n)}$
15.45	291.5	14.08	478	–1,460	1,150
$d_{15}^{(n)}$	$d_{24}^{(n)}$	$\varepsilon_{11}^{(n),\sigma}/\varepsilon_0$	$\varepsilon_{22}^{(n),\sigma}/\varepsilon_0$	$\varepsilon_{33}^{(n),\sigma}/\varepsilon_0$	
1,823	50	8,240	1,865	3,180	

Orientations of the spontaneous polarisation vectors in domains are shown in inset 3 in Fig. 3.6

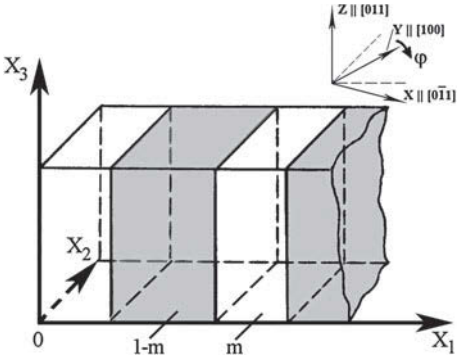

Fig. 3.10 Schematic of the 2–2 SC/polymer composite. $(X_1X_2X_3)$ is the rectangular co-ordinate system. m and $1 - m$ are volume fractions of the SC and polymer components, respectively, and φ is the angle of rotation of the main crystallographic axes x and y of the SC around the OX_3 axis (reprinted from paper by Krivoruchko and Topolov [30], with permission from IOP Publishing)

prediction of the effective properties and hydrostatic parameters of the composite is carried out using data from Tables 3.1 and 3.6. The matrix $||d^*||$ of the piezoelectric coefficients of the composite based on the $[011]_c$-poled PZN–0.07PT SC is given by (3.18).

Data on local maximum values $(\Pi^*)_m$ of the effective parameters at $\varphi = \text{const}$ (Table 3.7) characterise the piezoelectric response of the studied 2–2 composite. The piezoelectric anisotropy of the SC component [see, for instance, (3.19)] and its elastic anisotropy [see (3.20)] influence the orientation dependence of the effective parameters, such as g_{33}^*, g_h^*, $(Q_{33}^*)^2$, and $(Q_h^*)^2$. These parameters are concerned with the piezoelectric sensitivity of the composite and are increased by replacing araldite by a softer polymer. The presence of the very soft polymer (i.e., elastomer, see Table 3.1) in the composite leads to favourable changes in the piezoelectric coefficients d_{3j}^*, and these changes lead to an excellent hydrostatic piezoelectric activity of the composite (see Table 3.7 and curves 1–4 in Fig. 3.11a). Examples of the non-monotonic volume-fraction dependencies shown in Table 3.7 and Fig. 3.11 are closely connected with distinctions between the properties of the SC and polymer components as well as with a considerable redistribution of electric and mechanical fields in the 2–2 composite with interfaces $x_1 = \text{const}$ at the rotation mode shown in inset in Fig. 3.10.

We underline here the large changes in $(g_h^*)_m$ while there are relatively small changes in the related parameter $(g_{33}^*)_m$ (Table 3.7). Such behaviour is accounted for

Table 3.7 Local maximum values of the following effective parameters of the 2–2 $[011]_c$-poled PZN–0.07PT SC/polymer composite: piezoelectric coefficients $(g^*_{33})_m$ (in mV·m/N), $(h^*_{33})_m$ (in 10^8 V/m), $(e^*_{33})_m$ (in C/m^2), hydrostatic piezoelectric coefficients d^*_h (in pC/N), $(g^*_h)_m$ (in mV·m/N), and squared figures of merit $(Q^*_{33})^2_m$ (in 10^{-12} Pa^{-1}) and $(Q^*_h)^2_m$ (in 10^{-15} Pa^{-1})

Polymer	φ, deg	$(g^*_{33})_m$	$(h^*_{33})_m$	$(e^*_{33})_m$	$(d^*_h)_m$	$(g^*_h)_m$	$(Q^*_{33})^2_m$	$(Q^*_h)^2_m$
Araldite	0	499	34.4	7.88	–[a]	13.4	79.5	26.2
	15	493	33.0	7.67	–	−4.18	79.7	16.7
	30	457	26.5	7.42	–	8.08	81.2	152
	45	382	28.2	10.4	–	83.9	84.8	4,190
	60	426	38.2	13.1	–	187	84.5	1.28×10^4
	75	452	40.5	12.9	–	186	83.3	1.40×10^4
	90	458	41.0	12.8	–	184	83.0	1.39×10^4
Polyurethane	0	804	35.1	8.57	2.18	23.7	137	42.8
	15	795	33.6	8.30	0.318	5.34	137	42.2
	30	744	26.7	7.83	–	10.9	139	199
	45	640	28.3	11.5	–	136	143	6,970
	60	699	38.8	14.5	–	295	143	2.20×10^4
	75	737	41.1	14.1	–	297	141	2.48×10^4
	90	746	41.5	13.9	–	293	141	2.47×10^4
Elastomer	0	2,570	35.8	9.75	–	18.9	837	387
	15	2,560	34.2	9.38	–	5.97	864	153
	30	2,520	26.5	8.29	–	26.3	898	58.7
	45	2,410	27.1	14.5	–	235	917	9,510
	60	2,400	39.3	17.3	186	432	862	2.78×10^4
	75	2,430	41.8	16.1	224	445	825	3.30×10^4
	90	2,440	42.2	15.8	237	441	816	3.36×10^4

Reprinted from paper by Krivoruchko and Topolov [30], with permission from IOP Publishing
[a]The dash denotes monotonic increasing $d^*_h(m, \varphi)$ at $\varphi = \text{const}$

by changes in g^*_{31} and g^*_{32} as the main crystallographic axes x and y of SC undergo rotation (see inset in Fig. 3.10). The piezoelectric coefficients g^*_h and g^*_{33} demonstrate the possibilities of considerable increases in the sensitivity of the 2–2 composite at $\varphi \to 90°$ [30]: $(g^*_{33})_m/g^{(1)}_{33} \approx 63$ and $(g^*_h)_m/g^{(1)}_h \approx 75$ where $g^{(1)}_{33}$ and $g^{(1)}_h$ are related to the main crystallographic axes of the $[011]_c$-poled PZN–0.07PT SC. The difference between $(g^*_{33})_m$ and $(g^*_h)_m$ is associated with a change in a balance of the piezoelectric coefficients g^*_{3j} due to the piezoelectric coefficients $d^{(1)}_{3j}$ that obey conditions (3.20). In contrast to this result, the anisotropy of the elastic properties of the SC and the increase in softness of the polymer component lead to an increase in the piezoelectric coefficients h^*_{33} and e^*_{33}. In particular, the local maxima of $(h^*_{33})_m$ and $(e^*_{33})_m$ in a 2–2 $[011]_c$-poled PZN–0.07PT SC/elastomer composite become relatively large such that the ratios

$$(h^*_{33})_m/h^{(1)}_{33} = 2.9 \text{ and } (e^*_{33})_m/e^{(1)}_{33} = 4.7 \tag{3.21}$$

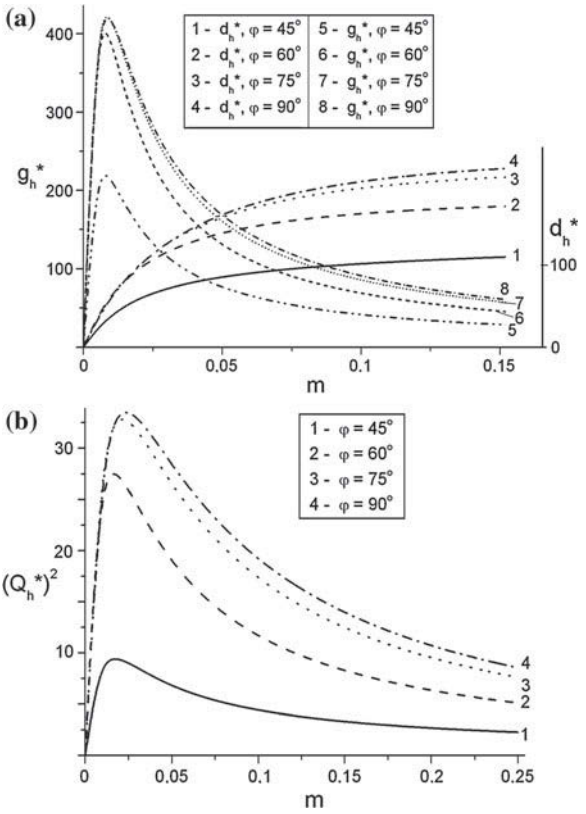

Fig. 3.11 Effective hydrostatic parameters of the 2–2 $[011]_c$-poled PZN–0.07PT SC/elastomer composite: piezoelectric coefficients d_h^* (**a**, in pC/N) and g_h^* (**a**, in mV· m/N) and squared figure of merit $(Q_h^*)^2$ (**b**, in 10^{-12} Pa^{-1}) (reprinted from paper by Krivoruchko and Topolov [30], with permission from IOP Publishing)

are valid [30], where $h_{33}^{(1)}$ and $e_{33}^{(1)}$ are related to the main crystallographic axes. A distinction between the volume-fraction dependences of h_{33}^* and e_{33}^* at φ = const is associated with dielectric permittivity $\varepsilon_{33}^{*\xi}$ that increases monotonously with increasing m. These large values of ratios (3.21) have first been mentioned [30] in research on the piezoelectric coefficients h_{33}^* and e_{33}^* of 2–2 relaxor-ferroelectric SC/polymer composites. We note for comparison that 1–β PZT-type FC/elastomer composites (β = 1, 2 or 3) are characterised by max $e_{33}^*/e_{33}^{(1)} \approx 1.1 - 1.2$ [2, 32] where e_{33}^* is a function of the volume fraction of FC, and $e_{33}^{(1)}$ is its piezoelectric coefficient.

The high piezoelectric activity of 2–2 composites based on $[011]_c$-poled PZN–0.07PT SC at small m values (see curves 1–4 in Fig. 3.11a) favours high piezoelectric sensitivity (see curves 5–8 in Fig. 3.11a and curves 1–4 in Fig. 3.11b). The hydrostatic parameters g_h^* and $(Q_h^*)^2$ at the ranges $0.01 < m < 0.10$ and $45° < \varphi < 90°$

(Fig. 3.11) are a few times larger than $\max g_h^*$ and $\max(Q_h^*)^2$ which are known [2, 11] for 2–2 parallel-connected FC/polymer composites.

The advantages of 2–2 composites based on $[011]_c$-poled PZN–0.07PT SC stem from the interconnection between the piezoelectric activity and sensitivity [30] and should be taken into consideration when manufacturing novel 2–2-type piezo-active composites.

3.2.3 Change in the Poling Orientation of Ferroelectric Polymer: An Additional Orientation Effect

Now we replace the PVDF-1 layers with the PVDF-2 layers over the 2–2 composite sample. The remanent polarisation vector $\boldsymbol{P}_r^{(2)}$ in the PVDF-2 layer is shown in inset 5 in Fig. 3.6: it is clear that this layer has been poled in the opposite direction (see inset 4 in Fig. 3.6) to the aforementioned PVDF-1 layer. The change in the poling direction of the ferroelectric polymer results in opposite signs of the piezoelectric coefficients of PVDF-2 in comparison to PVDF-1, and this effect can be taken into account in the subsequent consideration of the effective parameters of the composite. Negative values of $d_{33}^{(2)}$, $e_{33}^{(2)}$ and $g_{33}^{(2)}$ influence the volume-fraction dependence of g_{33}^*, g_h^* etc., however the change in the $\boldsymbol{P}_r^{(2)}$ direction does not give rise to considerable changes in the orientation dependence of the effective parameters of the 2–2 composite. Data on the 2–2 composite based on the single-domain PMN–0.33PT SC (Table 3.8) show that maximum (or minimum) values of the effective parameters related to small volume fractions of the SC component ($m \ll 1$) undergo considerable changes due to the influence of the piezoelectric and dielectric properties of the polymer component. It should be remembered that the piezoelectric coefficient $d_{33}^{(2)}$ of PVDF is about four times less than $d_{33}^{(1)}$ of the single-domain PMN–0.33PT SC (cf. data from Tables 2.1 and 3.3) and may play an important role in determining the electromechanical properties of the composite even at $m \approx 1/4$. Changes in the value of $(Q_h^*)^2$ (Table 3.8) are caused not only by the changes in signs of $d_{3j}^{(2)}$ and $g_{3j}^{(2)}$, but also by a shift of the volume fraction m, at which absolute $\max(Q_h^*)^2$ is achieved, to lower values. This means that the hydrostatic piezoelectric coefficient g_h^* plays the dominant role in forming the volume-fraction dependence of $(Q_h^*)^2$.

The value of absolute min e_h^* undergoes very minor changes at the transition from the composite with the PVDF-1 layers to the composite with the PVDF-2 layers (Table 3.8). The volume faction $m \approx 0.83$ at which absolute min e_h^* is achieved in both the composites demonstrates the key role of the SC component in forming the piezoelectric performance of the composites. Similar changes in max e_{33}^* are observed at $m \approx 0.97$ (Table 3.8) and, therefore, a weak influence of the polymer component on the longitudinal piezoelectric response of the composite is expected.

An important example of changes in the composite performance is concerned with three orientations of the remanent polarisation vector $\boldsymbol{P}_r^{(2)}$ in the polymer layers. It

Table 3.8 Absolute maxima (minima) of longitudinal and hydrostatic parameters of the 2–2 single-domain PMN–0.33PT SC/PVDF-2 composite in comparison to the 2–2 single-domain PMN–0.33PT SC/PVDF-1 composite

	Composite with PVDF-2 layers[a]		Composite with PVDF-1 layers[b]
Π^*	Value of absolute max Π^* (or min Π^*)	m, φ, ψ, and θ which correspond to the value of absolute max Π^* (or min Π^*)	Value of absolute max Π^* (or min Π^*)
g_{33}^*	-605 mV·m/N[c]	$m = 0.020$, $\varphi = 0°$, $\psi = 0°$, and $\theta = 106°$	539 mV· m/N
e_{33}^*	12.4 C/m^2	$m = 0.969$, $\varphi = 0°$, $\psi = 0°$, and $\theta = 0°$	12.4 C/m^2
d_h^*	-327 pC/N[c]	$m = 0.303$, $\varphi = 0°$, $\psi = 0°$, and $\theta = 86°$	-322 pC/N[c]
g_h^*	-305 mV·m/N[c]	$m = 0.015$, $\varphi = 60°$, $\psi = 90°$, and $\theta = 127°$	-252 mV·m/N[c]
e_h^*	-22.4 C/m^2[c]	$m = 0.831$, $\varphi = 60°$, $\psi = 90°$, and $\theta = 117°$	-22.3 C/m^2[c]
$(Q_h^*)^2$	$23.8 \cdot 10^{-12}$ Pa^{-1}	$m = 0.055$, $\varphi = 60°$, $\psi = 90°$, and $\theta = 124°$	$21.5 \cdot 10^{-12}$Pa^{-1}
k_h^*	-0.304[c]	$m = 0.071$, $\varphi = 60°$, $\psi = 90°$, and $\theta = 124°$	0.294

[a] Orientations of $\mathbf{P}_r^{(2)}$ and $\mathbf{P}_s^{(1)}$ are shown in Fig. 3.6, see insets 1 and 5, respectively

[b] Orientations of $\mathbf{P}_r^{(2)}$ and $\mathbf{P}_s^{(1)}$ are shown in Fig. 3.6, see insets 1 and 4, respectively

[c] Absolute minimum value

is assumed that the 2–2 composite contains layers of the $[011]_c$-poled PZN–0.07PT SC and PVDF, and the remanent polarisation vector $\boldsymbol{P}_r^{(2)}$ in PVDF is oriented as follows:

(i) $\boldsymbol{P}_r^{(2)}$ $\uparrow\downarrow OX_3$ (PVDF-1),
(ii) $\boldsymbol{P}_r^{(2)}$ $\uparrow\uparrow OX_3$ (PVDF-2) or
(iii) $\boldsymbol{P}_r^{(2)}$ $\uparrow\uparrow OX_2$ (PVDF-p).

The main crystallographic axes in each SC layer rotate as shown in the inset in Fig. 3.10.

The PZN–0.07PT-based composite shows high hydrostatic piezoelectric activity (Fig.3.12a–c): values of max $d_h^* = 2.26 d_h^{(1)}$, max $d_h^* = 2.06 d_h^{(1)}$ and max $d_h^* = 2.28 d_h^{(1)}$ are achieved in the presence of the PVDF-2, PVDF-p and PVDF-1 layers, respectively. The minor changes in max d_h^* values are also accounted for by a slight influence of the polymer component (and, therefore, the orientation of the poling axis therein) on the piezoelectric coefficients d_{3j}^* at $m \approx 0.4$–0.5. The max d_h^* values found for the PZN–0.07PT-based composite [31] are about 5–6 times more than max d_h^* of the 2–2 PZT-type FC/polymer composites [11]. The max g_h^* values related to the PZN–0.07PT-based composite are about 1.5–2 times more than max g_h^* of the 2–2 PZT-type FC/polymer composites [11], and as in the 2–2 SC/polymer composites, max g_h^* is achieved at relatively small volume fractions ($m \ll 1$) of the SC component. Changes in graphs of g_h^* and $(Q_h^*)^2$ become distinct at $0 < m < 0.1$ (Fig.3.12d–i), since the piezoelectric and dielectric properties of the PVDF layers have a strong influence on the performance of the 2–2 composite, irrespective of the $\boldsymbol{P}_r^{(2)}$ orientation in these layers.

Thus, the above-described orientation effect concerned with the orientation of the remanent polarisation vector $\boldsymbol{P}_r^{(2)}$ in ferroelectric polymer layers (see insets 4 and 5 in Fig. 3.6) may be regarded as an additional effect that would lead to major changes in the effective parameters of the 2–2 composite at volume fractions of SC $0 < m < 0.1$ only.

3.2.4 Composites with Auxetic Polymer Components

In this section we discuss an effect of the elastic properties of the polymer layers on the piezoelectric anisotropy and hydrostatic parameters of the composite. Among the polymer components of interest, we choose for comparison a monolithic polyurethane (a conventional isotropic polymer with a Poisson's ratio $\nu^{(n)} = -s_{12}^{(n)}/s_{11}^{(n)} = 0.37$, see constants in Table 3.1) and an auxetic polyethylene (PE) with the negative Poisson's ratio $\nu^{(n)} = -0.83$.[1] The presence of an auxetic polymer component enables us

[1] According to experimental data [33], this piezo-passive auxetic polymer is characterised by elastic compliances $s_{11}^{(n)} = 5,260$ and $s_{12}^{(n)} = 4,360$ (in 10^{-12} Pa^{-1}) and dielectric permittivity $\varepsilon_{pp}^{(n)}/\varepsilon_0 = 2.3$ at room temperature. We add that an effect of the auxetic polymer on the perfor-

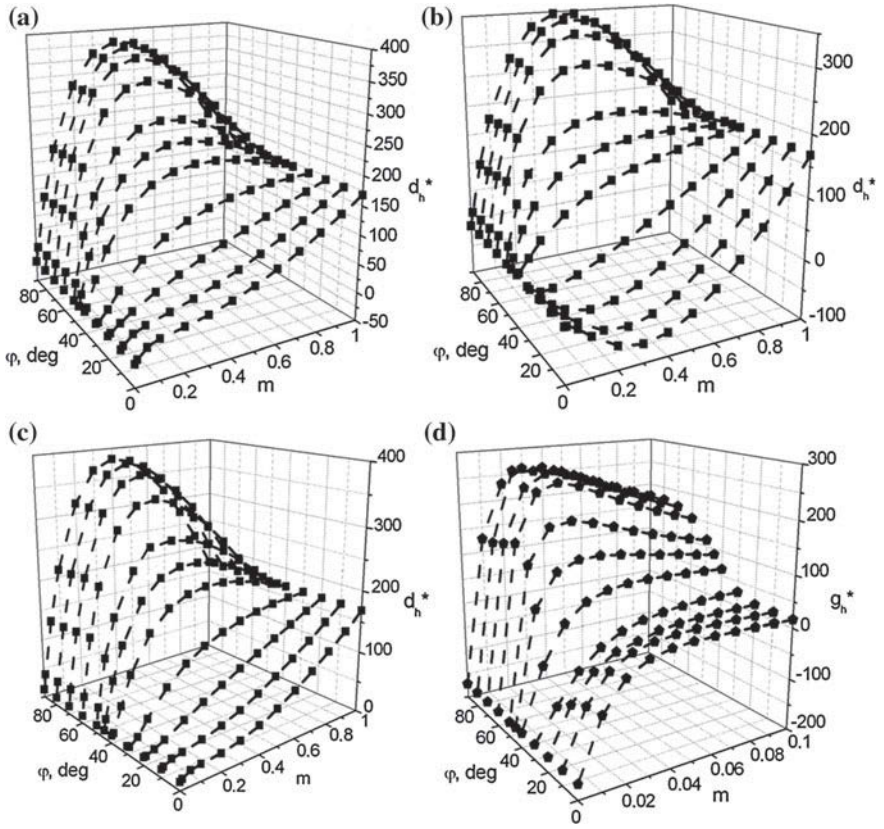

Fig. 3.12 Effective hydrostatic parameters of a 2–2 $[011]_c$-poled PZN–0.07PT SC/PVDF composite with layers of PVDF-2 (**a**, **d**, **g**), PVDF-p (**b**, **e**, **h**), or PVDF-1 (**c**, **f**, **i**): d_h^* (**a**–**c**, in pC/N), g_h^* (**d**–**f**, in mV·m/N) and $(Q_h^*)^2$ (**g**–**i**, in 10^{-12} Pa^{-1}) (reprinted from paper by and Topolov and Krivoruchko [31] with permission from the American Institute of Physics)

to characterise the laminar composite as a simple 2–2 type composite, without details in connectivity of the polymer layers. In Sect. 2.4 we considered the performance of the single-domain relaxor-ferroelectric PIN–*x*–*y* SCs, and the following compositions are now considered as components of the studied composite: PIN–0.24–0.49 (3*m* symmetry) and PIN–0.27–0.40 (*mm*2 symmetry) [34, 35]. It is assumed that the SC/polymer composite has a regular laminar structure with interfaces $x_1 = \text{const}$, and the orientation of the crystallographic axes and the spontaneous polarisation vector $\boldsymbol{P}_s^{(1)}$ in each SC layer is shown in inset 1 in Fig. 3.6. As earlier, we assume that the electrodes are perpendicular to the OX_3 axis.

mance of the 1–3-type piezo-active composites is discussed in Sect. 4.3.4 where variations of the elastic properties of the auxetic polymer component are taken into account.

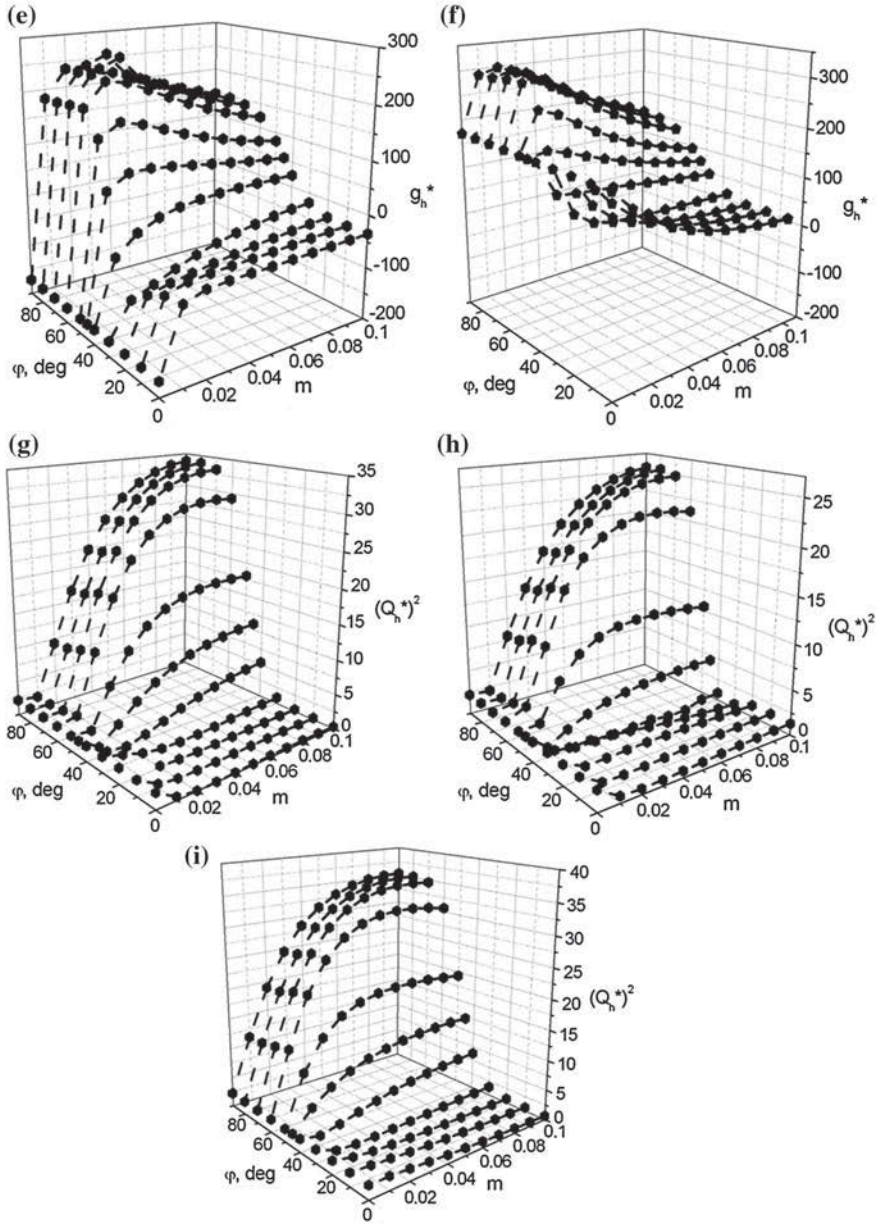

Fig. 3.12 (continued)

3.2.4.1 Anisotropy Factors

As follows from a comparison of the sets of electromechanical constants of single-domain PIN–*x*–*y* SCs (Table 2.3), the PIN–0.24–0.49 SC exhibits a larger anisotropy of piezoelectric coefficients $d_{3j}^{(1)}$ and ECFs $k_{3j}^{(1)}$ so that the ratios $d_{33}^{(1)}/d_{31}^{(1)} = -3.6$ and $k_{33}^{(1)}/k_{31}^{(1)} = -4.9$ hold. By analogy with these ratios we consider the anisotropy factors ζ_{d3j} from (3.8) and

$$\zeta_{k31} = k_{33}^{*}/k_{31}^{*} \text{ and } \zeta_{k32} = k_{33}^{*}/k_{32}^{*} \tag{3.22}$$

where the ECFs k_{3j}^{*} of the composite are determined with relations similar to (1.21) and (1.22):

$$k_{3j}^{*} = d_{3j}^{*}/(\varepsilon_{33}^{*\sigma} s_{jj}^{*E})^{1/2} \tag{3.23}$$

where $j = 1$, 2 and 3. Taking into account (3.8) and (3.23), we represent ζ_{k3j} from (3.22) as

$$\zeta_{k31} = \zeta_{d31}(s_{11}^{*E}/s_{33}^{*E})^{1/2} \text{ and } \zeta_{k32} = \zeta_{d32}(s_{22}^{*E}/s_{33}^{*E})^{1/2}. \tag{3.24}$$

Hereafter we consider the conditions for a large anisotropy of d_{3j}^{*} and k_{3j}^{*} of the composite in the following form:

$$|\zeta_{d31}| \geq 10 \text{ and } |\zeta_{d32}| \geq 10 \tag{3.25}$$

and

$$|\zeta_{k31}| \geq 10 \text{ and } |\zeta_{k32}| \geq 10, \tag{3.26}$$

respectively.

From our analysis of the volume-fraction and orientation dependences of the piezoelectric coefficients d_{3j}^{*} and ECFs k_{3j}^{*}, we observe that both conditions (3.25) and (3.26) are not valid in polyurethane-containing composites. Replacing the polyurethane layers with an auxetic PE enables us to find regions of validity of conditions (3.25) and (3.26) (Fig.3.13). For the PIN–0.24–0.49-based composite with a larger anisotropy of $d_{3j}^{(1)}$ and $k_{3j}^{(1)}$, conditions (3.25) and (3.26) are valid (Fig.3.13a) even when only varying the Euler angle θ (see inset in Fig. 3.1). Changes in the orientation of the main crystallographic axes of the single- domain SC with $3m$ symmetry are related to the rotation of the spontaneous polarisation vector $\boldsymbol{P}_s^{(1)}$ with respect to the OX_3 axis (see inset 1 in Fig. 3.6). We note that the smaller regions of the simultaneous fulfilment of conditions (3.25) and (3.26) are achieved in the PIN–0.27–0.40-based composite (Fig. 3.13c, d). Such a response can be accounted for by the smaller anisotropy of $d_{3j}^{(1)}$, $s_{ab}^{(1),E}$ and $k_{3j}^{(1)}$ in the single-domain PIN–0.27–0.40

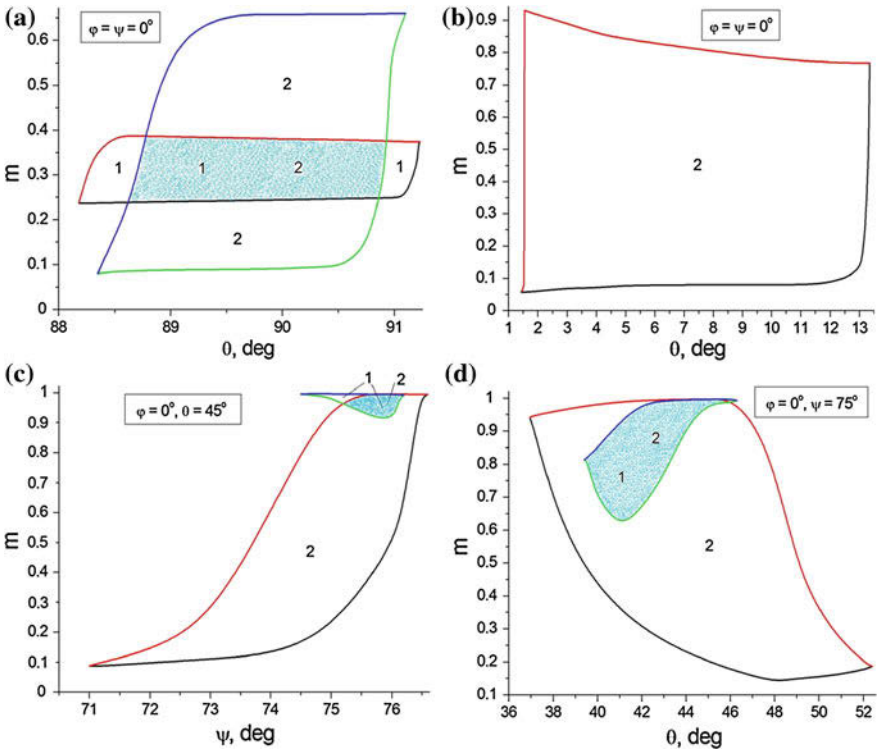

Fig. 3.13 Regions of the large anisotropy of d^*_{3j} and k^*_{3j} in a 2–2 single-domain PIN–0.24–0.49 SC/auxetic PE composite (**a**, **b**) and in a 2–2 single-domain PIN–0.27–0.40 SC/auxetic PE composite (**c**, **d**) at variations of the Euler angle θ (see inset 1 in Fig. 3.5). Conditions (3.25) are valid in region 1, and conditions (3.26) are valid in region 2. Filled areas in graphs (**a**), (**c**), (**d**) are related to the simultaneous fulfilment of conditions (3.25) and (3.26) (reprinted from paper by Topolov et al. [36], with permission from Wiley-VCH Verlag)

SC with *mm*2 symmetry. Irrespective of the SC component, the use of an auxetic polymer component promotes a larger piezoelectric anisotropy due to the unusual strain and the re-distribution of internal elastic and electric fields in the composite.

It is important to highlight that conditions (3.25) and (3.26) are valid at volume fractions m, for which the piezoelectric coefficient $d^*_{33}\ (m, \varphi, \psi, \theta) \approx d^{(1)}_{33}$ and ECF $k^*_{33}\ (m, \varphi, \psi, \theta) \approx 0.6$ [36]. The orientation dependence of the electromechanical properties of the SC component plays an important role in achieving a large piezoelectric anisotropy. According to results [36], the piezoelectric coefficient $d^{(1)}_{33}$, elastic compliance $s^{(1),E}_{33}$ and ECF $k^{(1)}_{33}$ of single-domain PIN–0.24–0.49 SC undergo large changes upon varying the angle θ. The 2–2 single-domain PIN–0.24–0.49 SC/auxetic PE composite shows some advantages over well-known FCs based on $PbTiO_3$ [17] due to larger values of d^*_{33} and k^*_{33} in regions where the conditions (3.25) and (3.26)

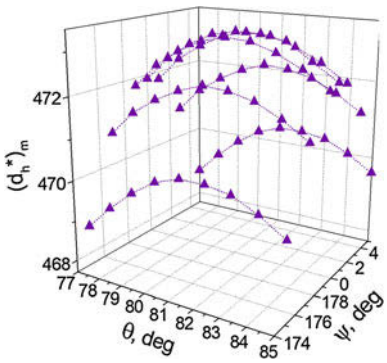

Fig. 3.14 Local maxima of the hydrostatic piezoelectric coefficient $(d_h^*)_m$ (in pC/N) in the 2–2 single-domain PIN–0.24–0.49 SC/auxetic PE composite near absolute max d_h^*. This graph was built at $\varphi = 0°$ (reprinted from paper by Topolov et al. [36], with permission from Wiley-VCH Verlag)

are valid, and this performance is important in piezo-technical applications such as actuators, transducers, acoustic antennae based on pulse-echo principles.

3.2.4.2 Hydrostatic Parameters

The hydrostatic parameters (3.2) and (3.3) are highly dependent on the anisotropy factors ζ_{d3j} from (3.8) and vary in a wide range when changing m, φ, ψ, and θ [36]. An increase in the hydrostatic parameters of the composite is observed by replacing the conventional polymer layers with an auxetic polymer. Figure 3.14 shows, that even in the presence of a single-domain PIN–0.24–0.49 SC with $d_h^{(1)}$ = 33 pC/N [34], a considerable increase in the effective hydrostatic piezoelectric coefficient d_h^* of the composite is expected. A value of absolute max d_h^* $(m, \varphi, \psi, \theta)$ = 473 pC/N $\approx 14.3\, d_h^{(1)}$ [36] is found at $m = 0.188$, $\varphi = \psi = 0°$ and $\theta = 81°$. The 2–2 single-domain PIN–0.24–0.49 SC/auxetic PE composite is characterised by large values of absolute maxima of g_h^* and $(Q_h^*)^2$, however these maxima are observed at very low volume fractions of SC. According to work [36], absolute max$g_h^*(m, \varphi, \psi, \theta)$ = 3,860 mV· m/N can be achieved at $m_{gh} = 0.0008$, and absolute max$[Q_h^*(m, \varphi, \psi, \theta)]^2 = 1.71 \cdot 10^{-9}$ Pa^{-1} is achieved at $m_{Qh} = 0.0014$. This is due to the large elastic compliances of the auxetic component [33] as compared to the SC and by the influence of the dielectric properties of the polymer component [2] on the non-monotonic behaviour of g_h^* and $(Q_h^*)^2$ at $m \ll 1$. It is obvious that the aforementioned volume fractions $0 < m_{gh} < 0.01$ and $0 < m_{Qh} < 0.01$ make it difficult to manufacture a composite sample with extremely high values of g_h^* and $(Q_h^*)^2$. To avoid this weak spot in the performance of the novel 2–2-type composite, we consider local maxima of its hydrostatic parameters (3.2) and (3.3) at larger volume fractions of SC, namely, at $m = 0.05$ (Fig. 3.15) and $m = 0.10$ (Fig. 3.16).

The large decrease of g_h^* (Figs. 3.15a and 3.16a) and $(Q_h^*)^2$(Figs. 3.15b and 3.16b) in comparison to the aforementioned values of absolute max g_h^* $(m, \varphi, \psi, \theta)$ and max$[Q_h^*(m, \varphi, \psi, \theta)]^2$, respectively, is due to the increasing dielectric permittivity

$\varepsilon_{33}^{*\sigma}$. At $0.05 \leq m \leq 0.10$ the inequality $\varepsilon_{33}^{*\sigma} \ll \varepsilon_{33}^{(1),\sigma}$ holds, and this feature favours relatively large values of $g_h^* \sim 10^2$ mV·m/N (Figs.3.15a, d, and 3.16a, d) and $(Q_h^*)^2 \sim 10^{-11} - 10^{-10}$ Pa^{-1} (Figs. 3.15b and 3.16b) which are of interest for hydroacoustic applications. It should be added that the relatively large absolute value of the hydrostatic piezoelectric coefficient $|d_h^*| \sim 10^2$ pC/N (Figs. 3.15c and 3.16c) is due to the rapid increase of $|d_{3j}^*|$ in the presence of the soft auxetic polymer layers, and this increase also favours large values of $(Q_h^*)^2$ in accordance with (3.2) and (3.3). Values of $d_h^* < 0$ and $g_h^* < 0$ (Figs. 3.15c, d and 3.16c, d) are accounted for by the dependence of the hydrostatic response of the composite on the Euler angle $90° < \theta < 180°$: at such orientations a negative projection of the spontaneous polarisation vector $\boldsymbol{P}_s^{(1)}$ onto the OX_3 axis (see inset 1 in Fig. 3.6) promotes $d_{33}^* < 0$ that has a strong influence on the balance of d_{3j}^* in (3.2) and therefore sgn d_h^* respect to the poling direction [3].

Thus, the 2–2 relaxor-ferroelectic SC/auxetic polymer composites demonstrate important advantages over the conventional 2–2 FC/polymer composites due to the large piezoelectric anisotropy, hydrostatic parameters etc. The dominating effect, that causes these advantages, is the elastic properties of the SC and auxetic polymer components at the strong influence of the rotation of the crystallographic axes of the single-domain SC component on the elastic and piezoelectric anisotropy. The composite performance discussed in Sects. 3.2.4.1 and 3.2.4.2 is of value for transducer, sensor, hydroacoustic, and other applications.

It should be noted that values of $(Q_h^*)^2$ of the 2–2 single-domain PIN–0.24–0.49 SC/auxetic PE composite at $m = 0.05$ (Fig. 3.15b) and 0.10 (Fig. 3.16b) remain much more than absolute $\max[Q_h^*(m, \varphi, \psi, \theta)]^2$ of the composites with polyurethane layers [36]. The PIN–0.24–0.49 SC/polyurethane and PIN–0.27–0.40/polyurethane composites are characterised by max d_h^* [36] that are comparable to local max d_h^* of the PIN–0.24–0.49/auxetic PE composite at $m = 0.05$ (Fig. 3.15c) and 0.10 (Fig. 3.16c), however these volume fractions of SC are much less than $m \approx 0.3$ related to max d_h^* in the aforementioned polyurethane-containing composites. This clear difference in the volume fractions m is also one of the advantages of the 2–2 single-domain PIN–0.24–0.49 SC/auxetic PE composite over the related SC/polyurethane composites [36].

Evaluating the performance of the PIN–0.24–0.49-based composite, one can underline that the presence of an auxetic polymer leads to obvious advantages of this composite over the PZT-type FC/conventional polymer composites with typical values of max$d_h^* \approx$ (50–80) pC/N and max$g_h^* \approx$ (100–300) mV·m/N [2, 11]. We add for comparison that an experimental value of $\max(Q_h^*)^2 \approx 5 \cdot 10^{-11}$ Pa^{-1} (i.e., about 3 times lower than the $(Q_h^*)^2$ values in Fig. 3.15b) can be achieved in a 2–2 PZT-type FC/polymer composite with a specific orientation of the FC layers.

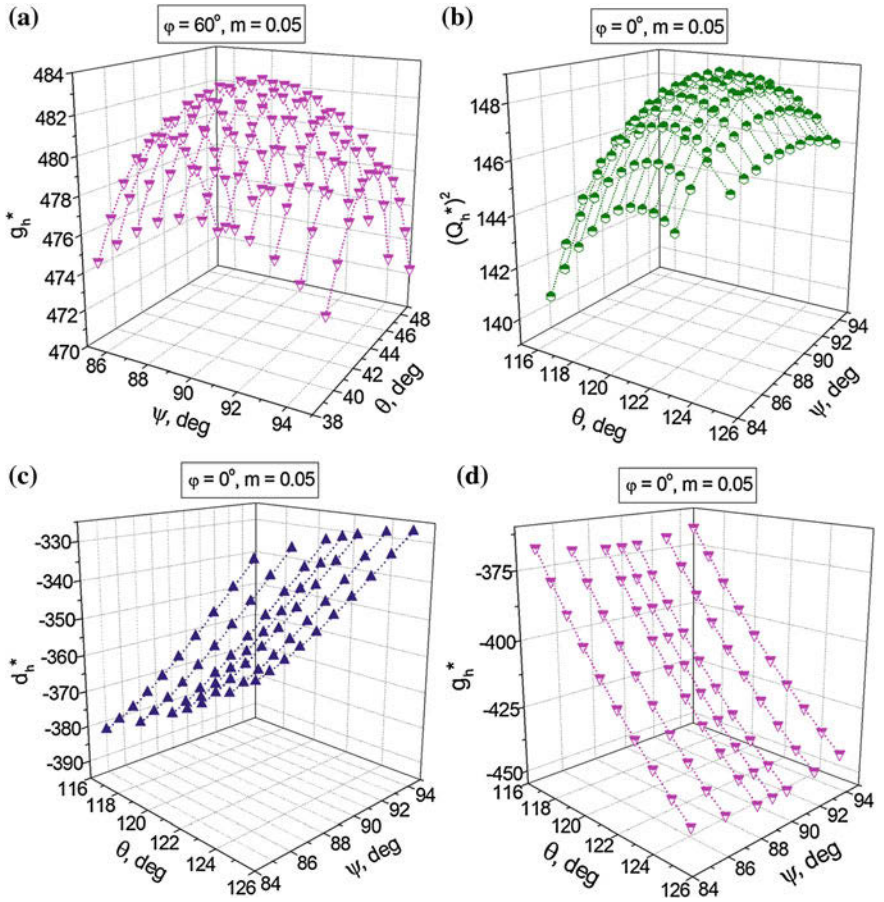

Fig. 3.15 Hydrostatic parameters of the 2–2 single-domain PIN–0.24–0.49 SC/auxetic PE composite in the vicinity of local max g_h^* (**a**) and max$[(Q_h^*)^2]$ (**b**–**d**) at $m = 0.05$: g_h^*(in mV·m/N, **a**, **d**), $(Q_h^*)^2$ (in 10^{-12} Pa^{-1}, **b**) and d_h^* (in pC/N, **c**) (reprinted from paper by Topolov et al. [36], with permission from Wiley-VCH Verlag)

3.3 2–2–0 Composites with Porous Polymer Matrices

In this section we consider a porous structure within the polymer layers and the influence of porosity on the effective parameters of the 2–2-type composite. It is now assumed that the composite sample (Fig. 3.17) contains a system of parallel layers which are made from relaxor-ferroelectric SC and porous polymer and are alternating in the OX_1 direction. These layers are assumed to be continuous along the OX_2 and OX_3 axes of the rectangular co-ordinate system $(X_1X_2X_3)$. The main crystallographic axes x, y and z in each SC layer are oriented as shown in inset 1 in Fig. 3.17.

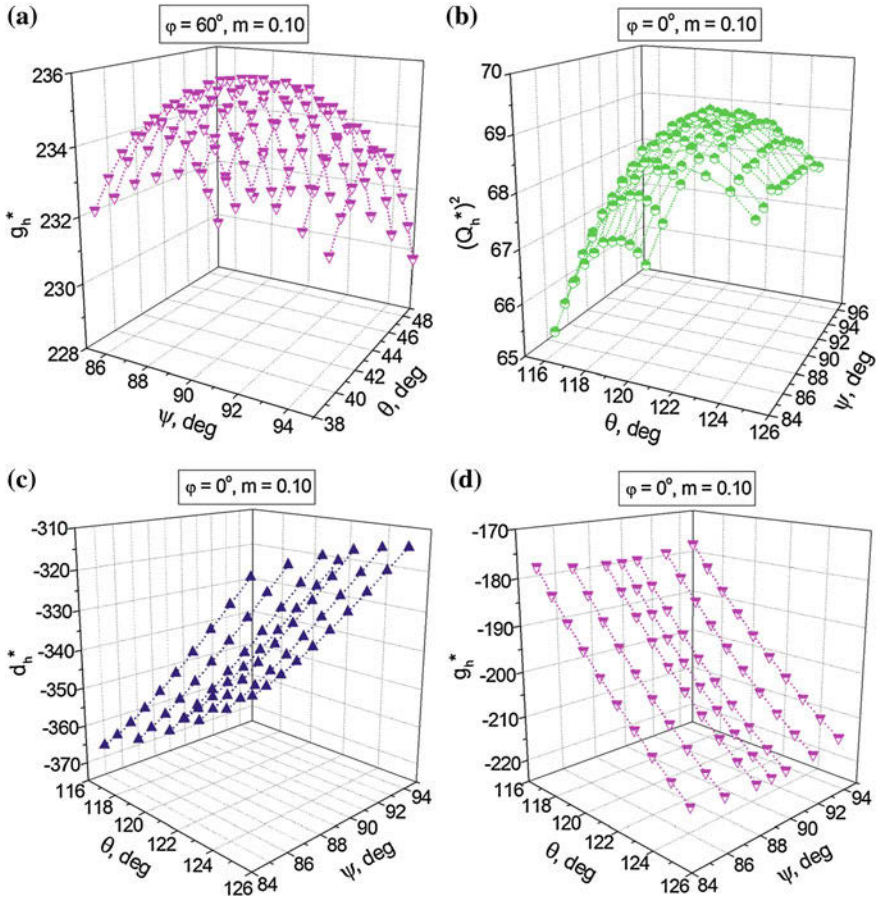

Fig. 3.16 Hydrostatic parameters of the 2–2 single-domain PIN–0.24–0.49 SC/auxetic PE composite in the vicinity of local maxg_h^* (**a**) and max$[(Q_h^*)^2]$ (**b**–**d**) at $m = 0.10$: g_h^* (in mV·m/N, **a** and **d**), $(Q_h^*)^2$(in 10^{-12} Pa^{-1}, **b**) and d_h^* (in pC/N, **c**) (reprinted from paper by Topolov et al. [36], with permission from Wiley-VCH Verlag)

Each polymer layer contains a systems of isolated air pores and can be regarded as a porous material P-*k* with 3–0 connectivity. Hereafter we consider the following porous structures:

(i) spherical pores distributed randomly in the matrix (P-1, see inset 2 in Fig. 3.17),
(ii) oblate spheroidal air pores that are regularly distributed and described by an equation

$$(x_1/a_1)^2 + (x_2/a_2)^2 + (x_3/a_3)^2 = 1 \tag{3.27}$$

in the $(X_1X_2X_3)$ system. Semi-axes a_i in (3.27) are linked by one of the aspect ratios – either $\rho_1 = a_3/a_1 = a_3/a_2 < 1$ (P-2, see inset 3 in Fig. 3.17) or $\rho_2 = a_1/a_2 = a_1/a_3 < 1$ (P-3, see inset 4 in Fig. 3.17). The corresponding composite with any porous matrix P-*k* (insets 2–4 in Fig. 3.17) represents examples of 2–2–0 connectivity. The air pores in the polymer layers are characterised by the volume fraction (porosity) m_p, and the sizes of these pores are considerably less than the thickness of the polymer layer in the OX_1 direction. This assumption on the sizes enables us to determine the effective electromechanical properties in the 2–2–0 composite in two stages. At the first stage calculating the effective constants of the porous polymer P-*k* at various m_p and ρ_i $(i = 1\,or\,2)$ is performed using formulae [37, 38]. At the second stage the effective electromechanical properties of the composite are determined by means of the matrix method applied to the 2–2 composite [see (3.4) and (3.5)]. The effective properties and related parameters of the 2–2–0 composite are represented in the general form as $\Pi^*(m, \varphi, m_p, \rho_i)$. For a composite with the P-1 layers (see inset 2 in Fig. 3.17), a condition $\rho_1 = \rho_2 = 1$ holds.

Forming the porous structure in the polymer matrix leads to a large increase of the hydrostatic piezoelectric coefficient g_h^*, squared figures of merit $(Q_{33}^*)^2$ and $(Q_h^*)^2$ etc. It is seen that local maxima of $(g_h^*)_m$(curves 2, 4 and 6 in Fig. 3.18a), $(Q_{33}^*)_m^2$ and $(Q_h^*)_m^2$ (Fig. 3.18b) in the 2–2–0 composite become larger than similar parameters of the related 2–2 composite (see Fig. 3.11 and Table 3.7). The increase in $(d_h^*)_m$(curves 1, 3 and 5 in Fig. 3.18a) is less pronounced. This feature of the composite is a result of a decrease of the elastic moduli $c_{ab}^{(2)}$ of the porous polymer and with a change in ratios of diagonal $(a = b)$ and off-diagonal $(a \neq b)$ elastic moduli $c_{ab}^{(2)}$, however

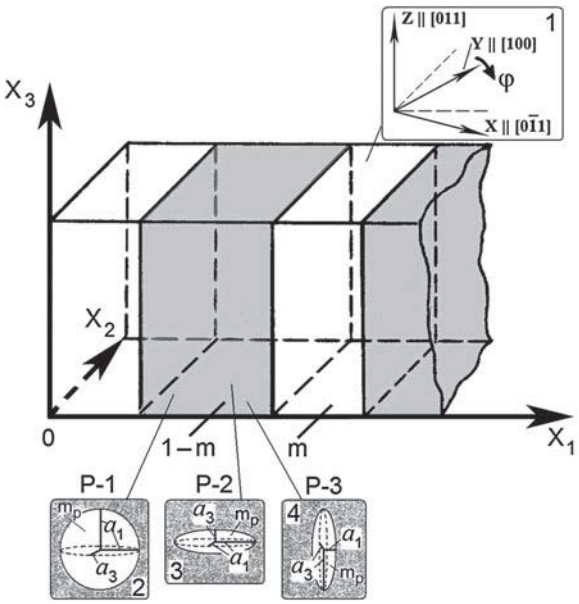

Fig. 3.17 Schematic of the 2–2–0 SC/porous polymer composite. $(X_1X_2X_3)$ is the rectangular co-ordinate system. m and $1 - m$ are volume fractions of the SC and porous polymer components, respectively. In *inset* 1 φ is the angle of rotation of the main crystallographic axes x and y of the SC layer around the OX_3 axis. In *insets* 2–4 a_i are semi-axes of the spheroidal air pore, and m_p is porosity in the polymer layer

in the porous polymers P-k their elastic moduli remains much smaller than those of the SC component. The porous structure of the polymer layer influences the balance of the piezoelectric coefficients d^*_{3j} that lead to a change in the relations between $(Q^*_{33})^2_m$ and $(Q^*_h)^2_m$ (compare curves 1, 3 and 5 with curves 2, 4 and 6, respectively, in Fig. 3.18b). Fig. 3.18a and curves 2, 4 and 6 in Fig. 3.18b suggest that the largest values of the three hydrostatic parameters, d^*_h, g^*_h and $(Q^*_h)^2$, are attained in the 2–2–0 composite in the vicinity of $\varphi = 90°$ irrespective of the porous material P-k. Such an orientation of the main crystallographic axes of the SC layer (see inset 1 in Fig. 3.17) weakens the influence of the negative piezoelectric coefficient $d^{(1)}_{32}$ of the $[011]_c$-poled PZN–0.07PT SC and strengthens an influence of the positive piezoelectric coefficient $d^{(1)}_{31}$ on the hydrostatic response of the 2–2–0 composite. In particular, the 2–2–0 composite with P-2 is characterised by the largest $(Q^*_{33})^2$ values (see Fig. 3.18c and curve 3 in Fig. 3.18b). The presence of oblate spheroidal pores with $\rho_1 < 1$ and an equality of the piezoelectric coefficients $d^{(1)}_{31} = d^{(1)}_{32}$ in the SC layer at $\varphi = 45°$ are regarded as the main factors that favour an appreciable increase of the piezoelectric sensitivity of the 2–2–0 composite along the OX_3 axis.

The increase of $(Q^*_h)^2$ at $45° < \varphi < 90°$ (see Fig. 3.18d) is due to the influence of the piezoelectric coefficients $d^{(1)}_{31}$ and $d^{(1)}_{32}$ of the SC layer on the hydrostatic response of the 2–2–0 composite. Such an increase has obvious advantages: even when increasing the volume fraction m by 0.05 (see curve 4 in Fig. 3.18d) the $(Q^*_h)^2$ value at $\varphi = 90°$ is about five times more than $\max[(Q^*_h)^2]$ of the oriented 2–2 FC/polymer composite [3]. A relatively slow decrease of $(Q^*_h)^2$ with increasing m (as $\max[(Q^*_h)^2]$ is passed, see curves 2–4 in Fig. 3.18d) and at $\varphi > 45°$ is associated with the favourable balance of the piezoelectric coefficients $d^{(1)}_{3j}$ of the $[011]_c$-poled PZN–0.07PT SC (see Table 3.6) and with the smaller differences $c^{(1),E}_{ab} - c^{(2)}_{ab}$ related to the 2–2–0 composite with P-2.

Thus, as with an auxetic polymer layer, the use of a porous polymer layer (expecially P-2) promotes a high piezoelectric sensitivity and an increase of the hydrostatic parameters (3.1)–(3.3) of the 2–2–0 composite (Fig. 3.17) at the appropriate orientation of the main crystallographic axes of the SC component. The values of $(Q^*_{33})^2$ and $(Q^*_h)^2$ remain fairly large after passing the maxima points and increasing the volume fraction m by 5 % (Fig. 3.18c, d). Such a performance is of value for sensor, hydrophone and other potential applications of the 2–2–0 SC/porous polymer composite. The aspect ratios ρ_i of the air pores also influence the effective parameters of the composite [30], and replacing the P-2 layer with the P-3 layer at $m_p = \text{const}$ means an orientation effect is to be taken into account for the prediction of the optimum performance of these novel piezo-active composites.

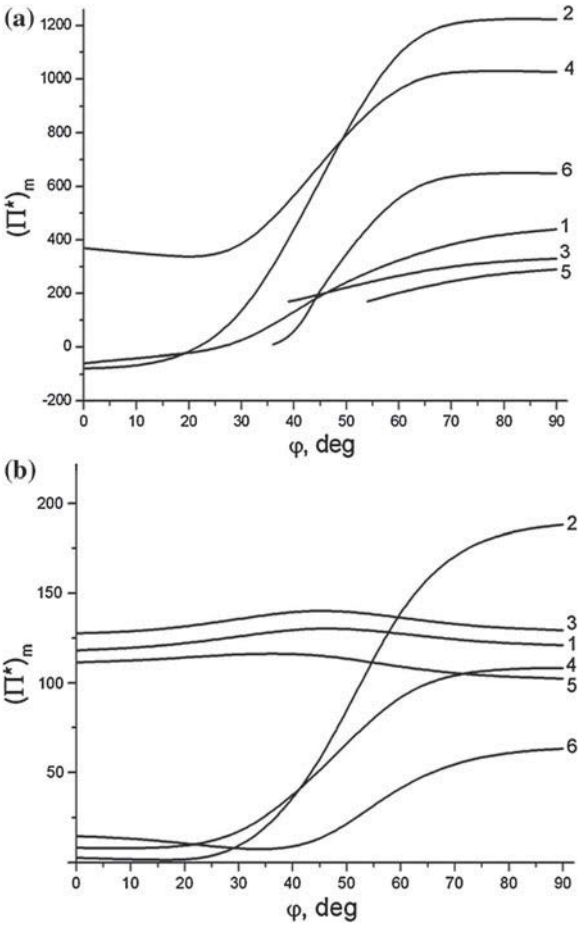

Fig. 3.18 Effective parameters of the 2–2–0 PZN–0.07PT SC / porous elastomer composites with porous P-*k* layers at poroisty $m_p = 0.2$ therein: **a** Local maxima of hydrostatic piezoelectric coefficients $(d_h^*)_m$ (in pC/N, *curves 1*, *3* and *5*) and $(g_h^*)_m$ (in mV·m/N, *curves 2*, *4* and *6*), **b** Local maxima of squared figures of merit $(Q_{33}^*)_m^2$ (in 10^{-11}Pa^{-1}, *curves 1*, *3* and *5*) and $(Q_h^*)_m^2$ (in 10^{-12} Pa^{-1}, *curves 2*, *4* and *6*), **c** Squared figure of merit $(Q_{33}^*)^2$ (in 10^{-11}Pa^{-1}) of the composite with the P-2 layers, and **d** Squared hydrostatic figure of merit $(Q_h^*)^2$ (in 10^{-12}Pa^{-1}) of the composite with the P-2 layers. In graphs *curves 1* and *2* are related to the composite with the P-1 layers, *curves 3* and *4* are related to the composite with the P-2 layers, and *curves 5* and *6* are related to the composite with P-3. In graphs *curves 1*, *2*, *3*, and *4* are related to rotation angles $\varphi = 45°$, 60°, 75°, and 90°, respectively. The rotation mode is shown in inset in Fig. 3.11, and P-*k* layers are schematically represented in insets 2–4 of Fig. 3.17 (reprinted from paper by Krivoruchko and Topolov [30], with permission from IOP Publishing)

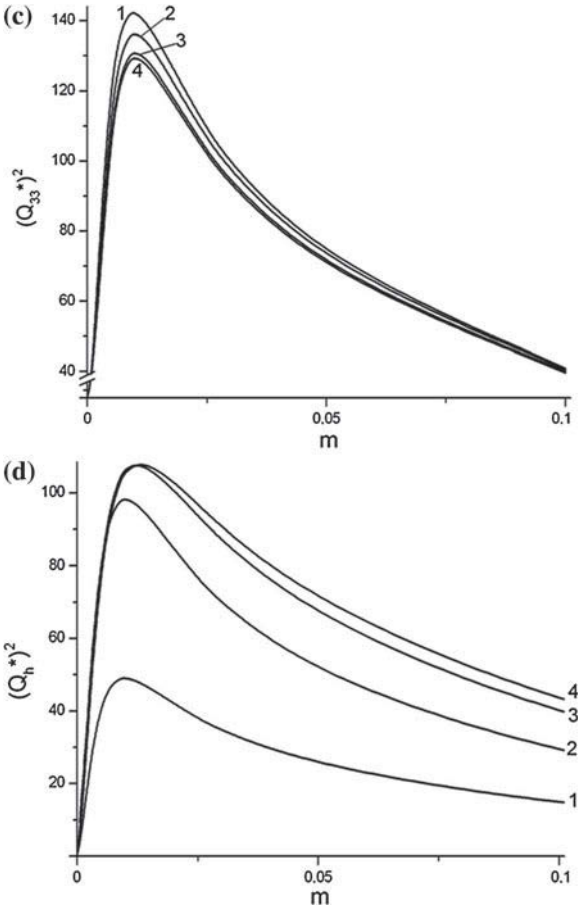

Fig. 3.18 (continued)

3.4 Conclusion

In this Chapter we have discussed the performance of the 2–2-type (laminar) composites based on either FCs or relaxor-ferroelectric SCs. A systematic study of the orientation effects and anisotropic properties has been carried out for the 2–2 and related composites with the following types of the polymer layers: monolithic, auxetic and porous with 3–0 connectivity. The piezoelectric activity and remanent polarisation of ferroelectric polymers has been taken into account. Various orientations of the main crystallographic axes in SCs (single-domain SC poled along $[111]_c$ of the perovskite unit cell and polydomain SC poled along either $[011]_c$ or $[001]_c$ of the perovskite unit cell) have been analysed to study the polarisation orientation effect on the piezoelectric anisotropy and hydrostatic response of the composites.

The anisotropy factors (3.8), (3.9) and (3.22) have been introduced to characterise the piezoelectric response and electromechanical coupling of the 2–2-type composites along the co-ordinate axes. As follows from the results systematised in this chapter, the anisotropy of the piezoelectric coefficients e^*_{3j} and d^*_{3j} and ECFs k^*_{3j} considerably depends on the FC (SC) component and the orientation of the main crystallographic axes in the SC component. In both cases changes in the piezoelectric anisotropy of the FC (SC) component due to the polarisation orientation effect influence the anisotropy factors (3.8), (3.9) and (3.22) in the composite. An additional influence is observed in the presence of the porous or auxetic polymer components with specific ratios of elastic moduli $c^{(2)}_{ab}$. The anisotropy of the piezoelectric coefficients d^*_{3j} is to be taken into consideration at the prediction of the hydrostatic piezoelectric response of the the 2–2-type composites.

The comparative study of the effects of the crystallographic orientation on the performance of the 2–2 SC/polymer composites based on PMN–0.28PT has been carried out for the following poling directions of the SC layers: $[111]_c$ (single-domain state), $[001]_c$ and $[011]_c$ (polydomain states). The effect of the orientation of the main crystallographic axes in the SC component on the hydrostatic parameters (3.2), (3.3), (3.13), and (3.14) has been studied to find maximum values of these parameters for further applications. Of particular interest are large values of the hydrostatic piezoelectric coefficient $e^*_h \approx$(40–45) C/m^2 (Fig. 3.8) in the composite based on the $[111]_c$-poled PMN–0.28PT SC. To a large degree, an increase of e^*_h in comparison to e^*_h of related piezo-active 2–2 composites based on either $[001]_c$- or $[011]_c$-poled SCs is caused by the appreciable elastic anisotropy of the $[111]_c$-poled PMN–0.28PT SC (see Table 3.2).

Conditions (3.25) and (3.26) for the large anisotropy of d^*_{3j} and k^*_{3j} are valid in the SC/auxetic polymer composite, however the simultaneous validity of (3.25) and (3.26) is observed in restricted ranges of the Euler angles and volume fractions of SC (Fig. 3.13). The use of an auxetic polymer as a soft component with the negative Poisson's ratio $\nu^{(n)}$ leads to a considerable hydrostatic piezoelectric response of the composite (Fig. 3.16) even at volume fractions m that are by 5–10 % more than those related to the absolute maximum (minimum) values of the hydrostatic parameters, and this feature is also important for hydrostatic and transducer applications.

In general, data from this chapter enable us to conclude that the performance of the 2–2-type piezo-active composites is highly dependent on the orientation of the main crystallographic axes in SCs effects, and the anisotropy factors change in relatively wide ranges due to the orientation effects.

References

1. Newnham RE, Skinner DP, Cross LE (1978) Connectivity and piezoelectric-pyroelectric composites. Mater Res Bull 13:525–536
2. Topolov VYu, Bowen CR (2009) Electromechanical properties in composites based on ferroelectrics. Springer, London

3. Safari A, Akdogan EK (2006) Rapid prototyping of novel piezoelectric composites. Ferroelectrics 331:153–179
4. Janas VF, Safari A (1995) Overview of fine-scale piezoelectric ceramic/polymer composite processing. J Am Ceram Soc 78:2945–2955
5. Akdogan EK, Allahverdi M, Safari A (2005) Piezoelectric composites for sensor and actuator applications. IEEE Trans Ultrason Ferroelectr Freq Control 52:746–775
6. Huebner W, Reidmeyer MR, Stevenson JW, Busse L (1995) Fabrication of 2–2 connectivity PZT / thermoplastic composites for high efficiency linear arrays. In: Pandey RK, Liu M, Safari A (eds) ISAF'94: Proceedings of the 9th IEEE International symposium on applications of ferroelectrics, University Park, Pennsylvania, 7–10 Aug 1994. IEEE, Piscataway, pp 206–209
7. Zhang QM, Geng X (1994) Dynamic modeling of piezoceramic polymer composite with 2–2 connectivity. J Appl Phys 76:6014–6016
8. Getman IP, Ryabov AP, Ustinov YuA (1987) On possibilities of the averaging method in a task on propagation of waves in an electroelastic layer with a periodic thickness inhomogeneity. Izvestiya Akademii Nauk SSSR. Mekhanika Tverdogo Tela 3:118–124 (in Russian)
9. Khoroshun LP, Maslov BP, Leshchenko PV (1989) Prediction of effective properties of piezoactive composite materials. Naukova Dumka, Kiev (in Russian)
10. Cao W, Zhang QM, Cross LE (1993) Theoretical study on the static performance of piezoelectric ceramic-polymer composites with 2–2 connectivity. IEEE Trans Ultrason Ferroelectr Freq Control 40:103–109
11. Grekov AA, Kramarov SO, Kuprienko AA (1987) Anomalous behavior of the two-phase lamellar piezoelectric texture. Ferroelectrics 76:43–48
12. Hashimoto KY, Yamaguchi M (1986) Elastic, piezoelectric and dielectric properties of composite materials. In: Proceedings of IEEE Ultrasonic Symposium, 17–19 Nov 1986. Williamsburg, New York, pp 697–702
13. Turcu S, Jadidian B, Danforth SC, Safari A (2002) Piezoelectric properties of novel oriented ceramic-polymer composites with 2–2 and 3–3 connectivity. J Electroceram 9:165–171
14. Levassort F, Lethiecq M, Millar C, Pourcelot L (1998) Modeling of highly loaded 0–3 piezoelectric composites using a matrix method. IEEE Trans Ultrason Ferroelectr Freq Control 45:1497–1505
15. Gibiansky LV, Torquato S (1997) On the use of homogenization theory to design optimal piezocomposites for hydrophone applications. J Mech Phys Solids 45:689–708
16. Grekov AA, Kramarov SO, Kuprienko AA (1989) Effective properties of a transversely isotropic piezoelectric composite with cylindrical inclusions. Mech Compos Mater Struct 25:54–61
17. Turik AV, Topolov VYu (1997) Ferroelectric ceramics with a large piezoelectric anisotropy. J Phys D Appl Phys 30:1541–1549
18. Zhang R, Jiang B, Cao W (2003) Single-domain properties of $0.67Pb(Mg_{1/3}Nb_{2/3})O_3 - 0.33PbTiO_3$ single crystals under electric field bias. Appl Phys Lett 82:787–789
19. Zhang R, Jiang B, Cao W (2003) Orientation dependence of piezoelectric properties of single domain $0.67Pb(Mn_{1/3}Nb_{2/3})O_3 - 0.33PbTiO_3$ crystals. Appl Phys Lett 82:3737–3739
20. Noheda B (2002) Structure and high-piezoelectricity in lead oxide solid solutions. Curr Opin Solid State Mater Sci 6:27–34
21. Topolov VYu (2004) The remarkable orientation and concentration dependences of the electromechanical properties of $0.67Pb(Mg_{1/3}Nb_{2/3})O_3 - 0.33PbTiO_3$ single crystals. J Phys Condens Matter 16:2115–2128
22. Liu G, Jiang W, Zhu J, Cao W (2011) Electromechanical properties and anisotropy of single- and multi-domain $0.72Pb(Mg_{1/3}Nb_{2/3})O_3 - 0.33PbTiO_3$ single crystals. Appl Phys Lett 99:162901–3P
23. Zhang R, Jiang B, Jiang W, Cao W (2006) Complete set of elastic, dielectric, and piezoelectric coefficents of $0.93Pb(Zn_{1/3}Nb_{2/3})O_3 - 0.33PbTiO_3$ single crystal poled along [011]. Appl Phys Lett 89:242908 (3 pp.)
24. Sessler GM (1981) Piezoelectricity in polyvinylidenefluoride. J Acoust Soc Am 70:1596–1608

25. Kar-Gupta R, Venkatesh TA (2007) Electromechanical response of 1–3 piezoelectric composites: an analytical model. Acta Mater 55:1093–1108
26. Topolov VYu, Krivoruchko AV (2009) Polarization orientation effect and combination of electromechanical properties in advanced $0.67Pb(Mg_{1/3}Nb_{2/3})O_3 - 0.33PbTiO_3$ single crystal/polymer composites with 2–2 connectivity. Smart Mater Struct 18:065011 (11 pp.)
27. Newnham RE (1994) Nonmechanical properties of composites. In: Kelly A, Cahn RW, Bever MB (eds) Concise encyclopedia of composite materials. Elsevier, Oxford, pp 214–220
28. Berlincourt DA, Cerran DR, Jaffe H (1964) Piezoelectric and piezomagnetic materials and their function in transducers. In: Mason W (ed) Physical acoustics. Principles and methods. Methods and devices, vol 1. Pt A. Academic Press, New York, London, pp 169–270
29. Topolov VYu, Krivoruchko AV, Bowen CR, Panich AA (2010) Hydrostatic piezoelectric coefficients of the 2–2 composite based on [011]-poled $0.71Pb(Mg_{1/3}Nb_{2/3})O_3 - 0.33PbTiO_3$single crystals. Ferroelectrics 400:410–416
30. Krivoruchko AV, Topolov VYu (2007) On the remarkable performance of novel 2–2-type composites based on [011] poled $0.93Pb(Zn_{1/3}Nb_{2/3})O_3 - 0.33PbTiO_3$ single crystals. J Phys D Appl Phys 40:7113–7120
31. Topolov VYu, Krivoruchko AV (2009) Orientation effects in 2–2 piezocomposites based on $(1-x)Pb(A_{1/3}Nb_{2/3})O_3 - xPbTiO_3$ single crystals (A = Mg or Zn). J Appl Phys 105:074105 (7 pp.)
32. Topolov VYu, Glushanin SV (2002) Evolution of connectivity patterns and links between interfaces and piezoelectric properties of two-component composites. J Phys D Appl Phys 35:2008–2014
33. Evans KE, Alderson KL (1992) The static and dynamic moduli of auxetic microporous polyethylene. J Mater Sci Lett 11:1721–1724
34. Sun E, Cao W, Jiang W, Han P (2011) Complete set of material properties of single domain $0.24Pb(In_{1/2}Nb_{1/2})O_3$-$0.49Pb(Mg_{1/3}Nb_{2/3})O_3 - 0.33PbTiO_3$ single crystal and the orientation effects. Appl Phys Lett 99:032901 (3 pp.)
35. Zhang S, Liu G, Jiang W, Luo J, Cao W, Shrout TR (2011) Characterization of single domain $Pb(In_{0.5}Nb_{0.5})O_3$-$Pb(Mg_{1/3}Nb_{2/3})O_3 - 0.33PbTiO_3$ crystals with monoclinic phase. J Appl Phys 110:064108 (5 pp.)
36. Topolov VYu, Krivoruchko AV, Bowen CR (2012) Anisotropy of electromechanical properties and hydrostatic response of advanced 2–2-type composites. Phys Status Solidi A 209:1334–1342
37. Dunn M (1995) Effects of grain shape anisotropy, porosity, and microcracks on the elastic and dielectric constants of polycrystalline piezoelectric ceramics. J Appl Phys 78:1533–1541
38. Dunn ML, Taya M (1993) Electromechanical properties of porous piezoelectric ceramics. J Am Ceram Soc 76:1697–1706

Chapter 4
Orientation Effects and Anisotropy of Properties in 1–3 and Related Composites

In a 1–3 composite, the first component is piezo-active (poled FC, ferroelectric SC etc.) and self-connected in one dimension, and the second component, either piezo-passive or exhibiting a low piezoelectric activity, is self-connected in three dimensions [1–3]. A typical example of such a composite consists of a system of parallel thin piezo-active rods which are regularly distributed in a large matrix [4–6], and the poling direction is parallel to each rod. The 1–3 connectivity is wide-spread due to favourable poling conditions and a variety of advantages over the piezo-active FC and SC components [2, 4–7].

The combination of the relatively low dielectric permittivity and the high piezoelectric activity of the composite, even at volume fractions of the piezo-active component of less than 10 % [4–6], leads to high piezoelectric sensitivity for the 1–3 composite [2, 6, 7], and this performance is of value for sensor and other piezo-technical applications. Changes in the cross section of the FC rod and in the orientation of the main crystallographic axes in the SC rod give rise to the orientation effect and the variable anisotropy of the piezoelectric properties, hydrostatic parameters, ECFs and their anisotropy. An additional stimulus in improving the performance of the 1–3 composite is concerned with a modification of properties in the polymer matrix, for instance, by forming a porous structure [7, 8] that leads to a 1–3–0 connectivity of the composite and has a strong influence on the elastic anisotropy of the matrix.

In Chap. 4 we consider many examples of the piezoelectric performance of the 1–3-type composites in the context of the orientation effects associated with the presence of specific components and tailored microgeometry. The anisotropy of the electromechanical properties of these modern piezo-active composites with various components (FCs, relaxor-ferroelectric SCs and polymers) is also the focus of discussions in Chap. 4.

V. Yu. Topolov et al., *Piezo-Active Composites*,
Springer Series in Materials Science 185, DOI: 10.1007/978-3-642-38354-0_4,

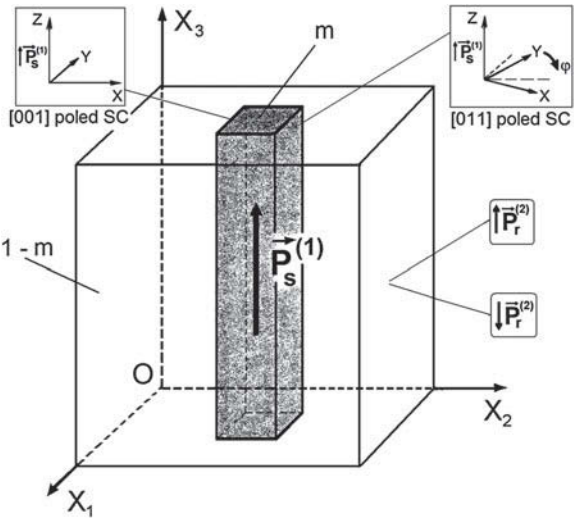

Fig. 4.1 Schematic of the 1–3 SC/polymer composite. $(X_1X_2X_3)$ is the rectangular co-ordinate system. m and $1-m$ are volume fractions of SC and polymer, respectively, x, y and z are main crystallographic axes of SC, φ is the rotation angle. $\boldsymbol{P}_s^{(1)}$ and $\boldsymbol{P}_r^{(2)}$ are the spontaneous polarisation vector of SC and the remanent polarisation vector of polymer, respectively (reprinted from paper by Topolov et al. [11], with permission from Taylor and Francis)

4.1 Single Crystal/Polymer Composites with Square Cross Section Rods

4.1.1 Model Concepts and Averaging Procedures

The 1–3 composite (Fig. 4.1) contains a system of relaxor-ferroelectric SC rods in the form of rectangular parallelepipeds which are continuous in the OX_3 direction, having a square base and characterised by a square arrangement in the (X_1OX_2) plane. It is assumed that the rods are regularly distributed in a continuous polymer matrix and poled along either the [011] or [001] direction in the cubic (perovskite) unit cell. [1] The domain-engineered PZN–0.07PT SCs, poled along the aforementioned directions, and their electromechanical properties have been studied in papers [9, 10]. In the [001]-poled PZN–0.07PT SC the main crystallographic axes x, y and z are parallel to the following perovskite unit-cell directions: x|| [001], y|| [010] and z|| [001]. In the [011]-poled PZN–0.07PT SC these axes are oriented as follows: x || $[0\bar{1}1]$, y || [100] and z || [011]. The orientation of the main crystallographic axes in the rods made from the [011]-poled SC is given by a rotation angle φ (right upper inset in Fig. 4.1). The angle $\varphi = 0°$ is related to x || OX_1, y || OX_2 and z || OX_3, and $\varphi = 90°$ means that the orientation of the main crystallographic axes obeys the conditions x || OX_2, y || OX_1 and z || OX_3 [11]. Each SC rod is characterised by the spontaneous polarisation vector $\boldsymbol{P}_s^{(1)} \uparrow\uparrow OX_3$, and this orientation is valid for both the [001]- and [011]-poled SC rods at any values of the rotation angle φ.

[1] In Chap. 4 we omit subscript "*c*" after square brackets in the unit-cell direction notation. It is assumed that any poling direction [*hkl*] of the SC component is related to the cubic (perovskite) unit-cell axes.

It is assumed that the poled ferroelectric polymer matrix surrounds the SC rods in the composite examined here. For example, a matrix made of PVDF can be poled so that its remanent polarisation vector $\boldsymbol{P}_r^{(2)}$ would be $\boldsymbol{P}_r^{(2)} \uparrow\uparrow OX_3$ or $\boldsymbol{P}_r^{(2)} \uparrow\downarrow OX_3$ (Fig. 4.1). These different orientations of $\boldsymbol{P}_r^{(2)}$ can be achieved on poling the composite sample in an electric field $\boldsymbol{E}||OX_3$ due to the large difference between the coercive fields $E_c^{(n)}$ of the relaxor-ferroelectric SC component ($n = 1$) and the ferroelectric polymer component ($n = 2$). As is known from experimental studies [10, 12], the condition $E_c^{(2)} \gg E_c^{(1)}$ is valid at room temperature.

The prediction of the effective electromechanical properties of the 1–3 composite (Fig. 4.1) with planar interfaces is carried out using the matrix approach applied to 2–2 composites (Chap. 3). The averaging procedure [11] implies averaging of the electromechanical constants of the SC rods and the polymer matrix in the OX_1 and OX_2 directions, in which the periodical structure of the composite (Fig. 4.1) is observed. In this procedure full sets of elastic compliances $s_{ij}^{(n),E}$ (measured at $E = \text{const}$), piezoelectric coefficients $d_{kl}^{(n)}$ and dielectric permittivities $\varepsilon_{ff}^{(n),\sigma}$ (measured at mechanical stress $\sigma = \text{const}$) of the components are used. The effective electromechanical properties of the 1–3 composite (the full set of s_{ij}^{*E}, d_{kl}^{*} and $\varepsilon_{ff}^{*\sigma}$) determined in this way are regarded as homogenised properties in the long-wave approximation [3, 11]. We note that s_{ij}^{*E}, d_{kl}^{*} and $\varepsilon_{ff}^{*\sigma}$ are represented as functions of the volume fraction m and the rotation angle φ.

The effective electromechanical properties are also calculated using the FEM for comparison. In the last decades, the FEM has been applied to 1–3 ceramic/polymer and 1–3 SC/polymer composites with a periodic arrangement of rods [14–19]. To perform FEM calculations, a unit-cell model of the 1–3 composite with a square arrangement of the rods (Fig. 4.1) is generated, and appropriate boundary conditions for the representative unit cell are considered. The COMSOL package [20] is used to obtain a volume-fraction dependence of the effective electromechanical properties. The square representative unit cell, containing a SC parallelepiped-shaped rod with a square sided base adjusted to yield the appropriate volume fraction, is discretised using triangular elements. The unknown displacement field is interpolated using second-order Lagrange shape functions, leading to a problem with approximately 120,000 degrees of freedom. The full sets of elastic moduli $c_{ij}^{(n),E}$ (measured at $E = \text{const}$), piezoelectric coefficients $e_{kl}^{(n)}$ and dielectric permittivities $\varepsilon_{ff}^{(n),\xi}$ (measured at mechanical strain ξ=const) of both components are involved in the FEM calculation procedure.

Periodic boundary conditions are enforced on interfaces (Fig. 4.1) which are orthogonal to the OX_a axes ($a = 1$ and 2), and the matrix of the effective electromechanical properties of the composite

$$\left\| C^* \right\| = \begin{pmatrix} ||c^{*E}|| & ||e^*||^t \\ ||e^*|| & -||\varepsilon^{*\xi}|| \end{pmatrix}, \tag{4.1}$$

that contains effective electromechanical constants, is computed column-wise, performing calculations for diverse average strain and electric fields imposed to the 1–3 structure. In (4.1) superscript "t" is related to the transposed matrix. We note that $||C^*||$ from (4.1) differs from $||C^*||$ in (3.4) because of the use of different pairs of piezoelectric equations of the electroelastic medium (see Sect. 1.1). Matrix $||C^*||$ from (4.1) stems from Eqs. (1.4) and (1.5), while $||C^*||$ from (3.4) is related to Eqs. (1.6) and (1.7).

After solving the equilibrium problem, the full set of the effective elastic moduli c_{ij}^{*E}, piezoelectric coefficients e_{kl}^* and dielectric permittivities $\varepsilon_{ff}^{*\xi}$ of the studied 1–3 composite (Fig. 4.1) is computed by means of averaging the resulting local stress and electric-displacement fields over the representative unit cell.

4.1.2 Orientation Effect and Hydrostatic Piezoelectric Response

Calculations of the effective electromechanical constants and related parameters of the 1–3 SC/polymer composite are carried out using the full sets of room-temperature electromechanical constants of PZN–0.07PT SC ([001] and [011] poling directions) [9, 10] and PVDF [21] (see Tables 1.1, 3.3 and 3.6). The piezoelectric coefficients $d_{3j}^{(2)}$ of PVDF [21] with $\boldsymbol{P_r^{(2)}} \uparrow\uparrow OX_3$ obey the condition

$$\operatorname{sgn} d_{31}^{(2)} = -\operatorname{sgn} d_{33}^{(2)} = -\operatorname{sgn} d_{15}^{(2)} > 0, \tag{4.2}$$

and the [001]-poled PZN–0.07PT SC [9, 10] is characterised by the following relationship of the piezoelectric coefficients:

$$\operatorname{sgn} d_{31}^{(1)} = -\operatorname{sgn} d_{33}^{(1)} = -\operatorname{sgn} d_{15}^{(1)} < 0. \tag{4.3}$$

Of particular interest are examples of the volume-fraction dependence of the effective piezoelectric coefficients d_{3k}^*, g_{33}^*, e_{3k}^*, and h_{33}^* ($k = 1$ and 3), squared figure of merit $(Q_{33}^*)^2$ from (3.1) and the similar hydrostatic parameters d_h^* and g_h^* from (3.2) and $(Q_h^*)^2$ from (3.3) at a fixed rotation angle φ (see for instance, Fig. 4.2 and Table 4.1). The hydrostatic parameters from (3.2) are related to a composite sample with electrodes that are parallel to the (X_1OX_2) plane. Table 4.1 contains data on local maxima of the effective parameters that characterise the piezoelectric activity, sensitivity and hydrostatic piezoelectric response of the composite based on PZN–0.07PT. Features of the volume-fraction dependence of the effective parameters of the 1–3 composite are represented as follows.

1. The antiparallel orientation of the polarisation vectors of the components (i.e., the case of $\boldsymbol{P_r^{(2)}} \uparrow\downarrow \boldsymbol{P_s^{(1)}}$ in Fig. 4.1) favours an increase in all effective parameters (Table 4.1), especially at volume fractions $m \leq 0.2$ (Fig. 4.2). This increase is

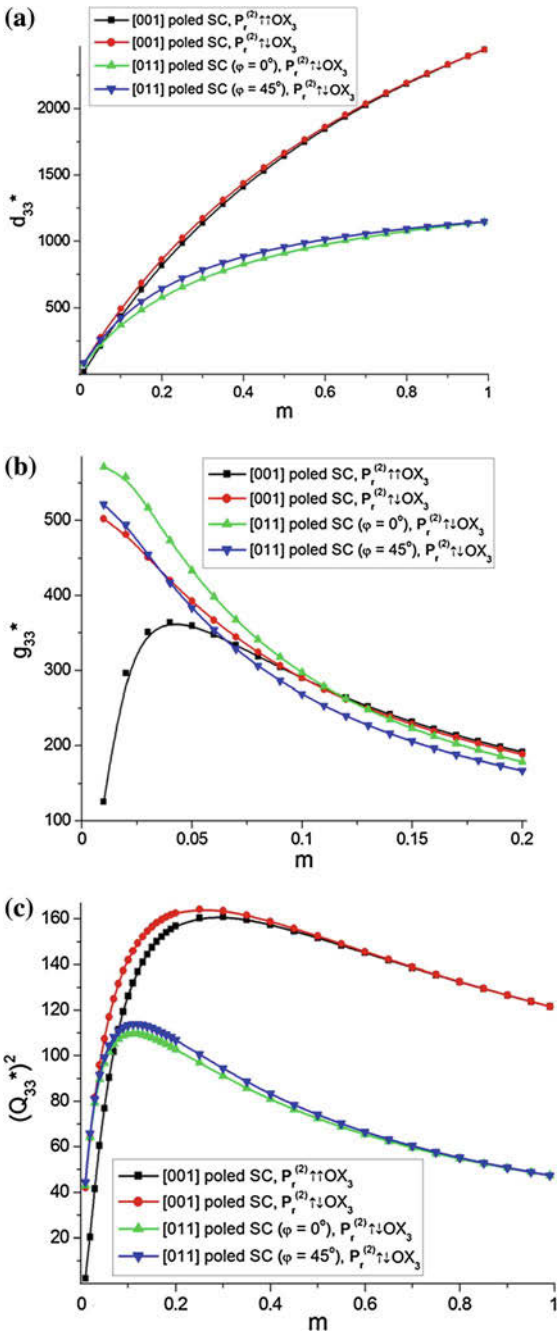

Fig. 4.2 Volume-fraction dependences of effective parameters calculated for the 1–3 PZN–0.07PT SC/PVDF composite at different orientations of the main crystallographic axes of SC and different poling directions of polymer: d_{33}^* (**a**, in pC/N), g_{33}^* (**b**, in mV· m/N), $(Q_{33}^*)^2$ (**c**, in 10^{-12} Pa^{-1}), d_h^* (**d**, in pC/N), g_h^* (**e**, in mV· m/N), and $(Q_h^*)^2$ (**f**, in 10^{-12} Pa^{-1}) (reprinted from paper by Topolov et al. [11], with permission from Taylor and Francis)

Fig. 4.2 (continued)

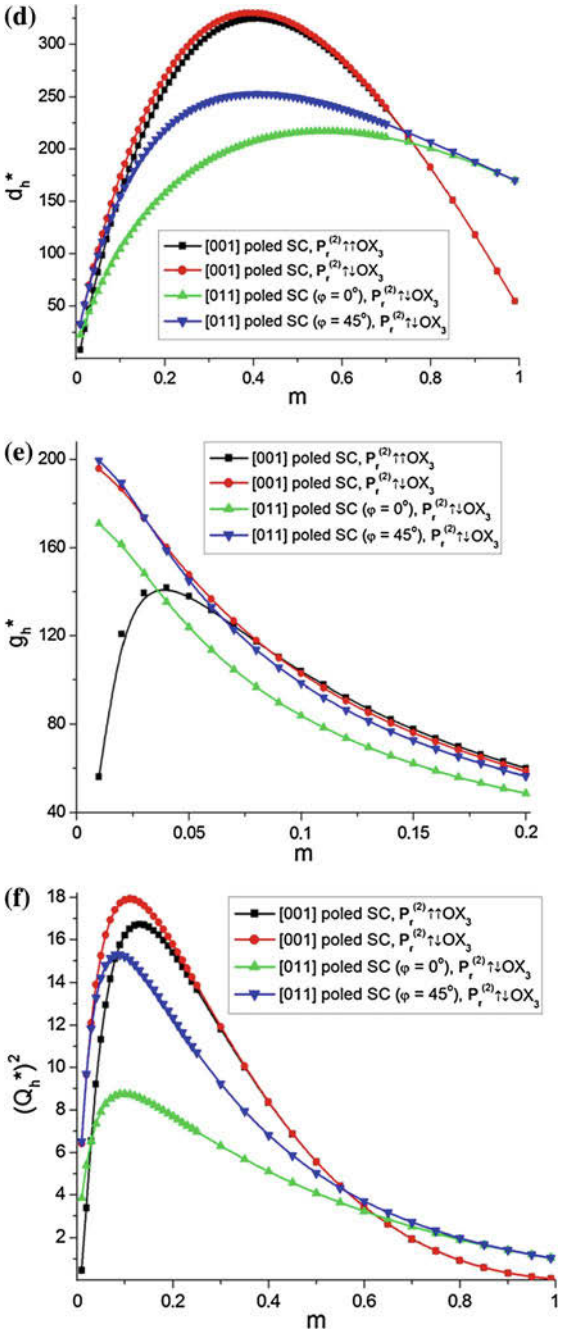

Table 4.1 Maximum values of effective parameters g_{33}^*, $(Q_{33}^*)^2$, d_h^*, g_h^*, and $(Q_h^*)^2$ which have been calculated for the 1–3 PZN–0.07PT SC/PVDF composite by means of the matrix approach (reprinted from paper by Topolov et al. [11], with permission from Taylor and Francis)

Polymer component with $\boldsymbol{P}_r^{(2)}$	SC component with $\boldsymbol{P}_s^{(1)} \uparrow\uparrow OX_3$	max g_{33}^*, mV m/N	max$[(Q_{33}^*)^2]$, 10^{-12} Pa^{-1}	max d_h^*, pC/N	max g_h^*, mV m/N	max$[(Q_h^*)^2]$, 10^{-12} Pa^{-1}
$\uparrow\uparrow OX_3$	[001]-poled	365	161	324	142	16.7
		(0.041)[a]	(0.283)	(0.405)	(0.037)	(0.130)
	[011]-poled,	409	101	216	110	7.94
	$\varphi = 0°$	(0.039)	(0.147)	(0.571)	(0.044)	(0.134)
	[011]-poled,	371	107	249	143	13.9
	$\varphi = 45°$	(0.036)	(0.145)	(0.425)	(0.034)	(0.109)
$\uparrow\downarrow OX_3$	[001]-poled	502	164	330	196	17.9
		(0.009)	(0.256)	(0.396)	(0.009)	(0.110)
	[011]-poled,	574	110	217	172	8.74
	$\varphi = 0°$	(0.012)	(0.112)	(0.562)	(0.006)	(0.097)
	[011]-poled,	522	114	253	200	15.3
	$\varphi = 45°$	(0.009)	(0.115)	(0.409)	(0.009)	(0.086)

[a] Values of optimal volume fractions m_{opt} of the SC component which correspond to the maximum values (i.e., max $\Pi^* = \Pi^*(m_{opt})$ in our notations) are in parentheses

caused by signs of the piezoelectric coefficients of PVDF

$$\operatorname{sgn} d_{31}^{(2)} = -\operatorname{sgn} d_{33}^{(2)} = -\operatorname{sgn} d_{15}^{(2)} < 0 \tag{4.4}$$

at $\boldsymbol{P}_r^{(2)} \uparrow\downarrow OX_3$ so that conditions (4.2) and (4.4) have the similar form and both components demonstrate the piezoelectric effect of the same sign. Moreover, this increase is pronounced in a low volume-fraction range, wherein the piezoelectric and dielectric properties of PVDF strongly influence parameters such as g_{33}^*, g_h^*, $(Q_{33}^*)^2$, and $(Q_h^*)^2$ (Fig. 4.2b, c, e, f). Hereafter in Sect. 4.1 we consider combinations of components with favourable poling directions $\boldsymbol{P}_s^{(1)} \uparrow\uparrow OX_3$ and $\boldsymbol{P}_r^{(2)} \uparrow\downarrow OX_3$.

2. Lack of the correlation between the $d_{33}^*(m)$ and $g_{33}^*(m)$ curves (cf. Figs. 4.2a, b) is a result of the dielectric properties of the SC component. For example, the dielectric permittivity $\varepsilon_{33}^{(1),\sigma}$ of a [001]-poled SC is about 1.8 times more than $\varepsilon_{33}^{(1),\sigma}$ of the [011]-poled SC [9, 10], and this distinction results in a higher piezoelectric sensitivity for the composite based on [011]-poled SC (see Fig. 4.2b and max $g_{33}^*(m)$ values in Table 4.1). The larger piezoelectric coefficient $d_{33}^{(1)}$ of the [001]-poled SC has a key role in forming the piezoelectric response and large $(Q_{33}^*)^2$ values of the composite (cf. Figs. 4.2a, c) in a wide volume-fraction range. The max$g_{33}^*(m)$ values listed in Table 4.1 are comparable with max $g_{33}^*(m)$ found [6] for a similar 1–3 PMN–0.30PT SC/epoxy composite. The latter composite contains one piezo-active component, i.e., the SC rods with $d_{33}^{(1)} = 1{,}500$ pC/N,

and this $d_{33}^{(1)}$ value is intermediate between those measured [9, 10] on the [001]- and [011]-poled PZN–0.07PT SC samples.

3. Higher hydrostatic piezoelectric activity is related to the composite based on the [001]-poled SC (see Fig. 4.2d and max $d_h^*(m)$ values in Table 4.1) while this SC is characterised by a lower hydrostatic piezoelectric coefficient $d_h^{(1)}$. Such a discrepancy is due to a balance of d_{3l}^* of the composite [see items in (4.3)] and with the larger absolute values of the elastic compliances $s_{i3}^{(1),E}$ of the [001]-poled SC, where $i = 1$ and 2 and $l = 1$, 2 and 3. The ratio max $d_h^*(m)/d_h^{(1)} = 6.91$ related to the composite with the [001]-poled SC is larger than the max $d_h^*(m)/d_h^{(1)}$ ratios [3] known for 1–3 [001]-poled SC/araldite composites based on relaxor-ferroelectric solid solutions with $d_{3l}^{(1)} \sim 10^3$ pC/N(PZN–xPT or PMN–yPT). According to data [3], in the aforementioned 1–3 composites comprising a SC with $d_h^{(1)} > 0$ and piezo-passive araldite, ratios max $d_h^*(m)/d_h^{(1)} \approx 1.7$–4.1 can be achieved.
4. A transition from $g_{33}^*(m)$ to $g_h^*(m)$ (Figs. 4.2b, e) results in a transposition of curves. This change is a result of the important role of the effective piezoelectric coefficients $g_{3w}^*(w = 1$ and 2) and by a balance of the piezoelectric coefficients $d_{3l}^{(1)}$ of the SC component ($l = 1$, 2 and 3). Larger g_h^* values (Fig. 4.2e) are predicted for composites with SC rods poled along either [001] or [011] (with the rotation angle $\varphi = 45°$, see inset in Fig. 4.1). The piezoelectric coefficients related to these orientations of the main crystallographic axes obey the conditions

$$d_{31}^{(1)} = d_{32}^{(1)} < 0 \quad \text{and} \quad d_{33}^{(1)} > 0. \tag{4.5}$$

   The volume-fraction dependence of the hydrostatic piezoelectric coefficient g_h^* (Fig. 4.2e) and data from Table 4.1 suggest that the largest ratio max $g_h^*(m)/g_h^{(1)} = 207$ is expected in the composite based on [001]-poled SC, however it takes place at $m < 0.01$. It is clear that composites with the relatively low volume fraction m must be manufactured for hydrophone and related applications to achieve large values of g_h^*.
5. As follows from the sequence of curves in graphs of $(Q_{33}^*)^2$ and $(Q_h^*)^2$(*cf.* Figs. 4.2c, f), larger $(Q_h^*)^2$ values are achieved in the presence of a SC component with piezoelectric coefficients that obey conditions (4.5). A breach of conditions (4.5) leads to a decrease of $(Q_h^*)^2$: an example of this behaviour is shown in Fig. 4.2f for the composite based on [011]-poled SC at $\varphi = 0°$. The maximum values of $(Q_{33}^*)^2$ and $(Q_h^*)^2$ (Table 4.1) take place at volume fractions $m_{opt} > 0.08$. It is important to note for comparison, that Choy et al. [22] manufactured a 1–3 FC/polymer composite with low volume fractions of FC rods (about 0.033, 0.066 etc.). Therefore it is possible that the technological challenges of forming low volume fractions of SC can be met in the case of the 1–3 SC/polymer composite. The max$[Q_h^*(m)]^2$ values determined for the 1–3 PZN–0.07PT SC/PVDF composites (Table 4.1) are considerably more than those which

are typical of the 1–3 FC/polymer composites [2, 3], and this advantage is due to the large $|d_{3l}^{(1)}|$ values of PZN–0.07PT SC [9, 10].

The full set of electromechanical constants c_{ij}^{*E}, e_{kl}^{*} and $\varepsilon_{ff}^{*\xi}$ from (4.1) has been calculated [11] for a 1–3 composite that comprises [001]-poled PZN–0.07PT SC rods with $\boldsymbol{P_s^{(1)}} \uparrow\uparrow OX_3$ (their volume fraction obeys condition $0.01 \leq m \leq 0.99$) and a PVDF matrix with $\boldsymbol{P_r^{(2)}} \uparrow\uparrow OX_3$. A transition from the c_{ij}^{*E}, e_{kl}^{*} and $\varepsilon_{ff}^{*\xi}$ constants to the s_{ij}^{*E}, d_{kl}^{*} and $\varepsilon_{ff}^{*\sigma}$ constants of the same composite is performed using conventional formulae [23] for the piezoelectric medium. Good agreement between the matrix-method and FEM data is attained for $d_{3l}^{*}(m)$, $g_{3l}^{*}(m)$, $e_{33}^{*}(m)$, and $h_{33}^{*}(m)$ in the whole m range. The difference between the similar parameters calculated using the matrix approach and FEM can be 20 % for $e_{31}^{*}(m)$ or $h_{31}^{*}(m)$ at $0.01 \leq m < 0.05$. In the same volume-fraction range, the difference between the $[Q_h^{*}(m)]^2$ values calculated by the aforementioned methods does not exceed 4 %. Values of maxima of $g_{33}^{*}(m)$, $h_{33}^{*}(m)$ and $[Q_h^{*}(m)]^2$ and the corresponding m_{opt} values, which are calculated by means of the FEM, are in good agreement with those listed in Table 4.1. The difference between the $e_{31}^{*}(m)$ values calculated by means of the matrix method and FEM, as well as the similar difference between the $h_{31}^{*}(m)$ values are accounted for by features of the electromechanical interaction between the components. The studied composite based on the [001]-poled PZN–0.07PT SC contains the components whose piezoelectric coefficients obey conditions [11] $|d_{31}^{(1)}/d_{31}^{(2)}| = 115$, $|d_{33}^{(1)}/d_{33}^{(2)}| = 72.7$, $|e_{31}^{(1)}/e_{31}^{(2)}| = 535$, and $|e_{33}^{(1)}/e_{33}^{(2)}| = 137$. It is obvious that the large difference between absolute values of the two last ratios is due to the elastic anisotropy of the SC and polymer components. This anisotropy influences the piezoelectric response of the composite in a wide volume-fraction range. As a consequence, a moderate difference $|d_{31}^{(1)}/d_{31}^{(2)}| - |d_{33}^{(1)}/d_{33}^{(2)}|$ does not lead to the considerable difference between $d_{31}^{*}(m)$, however the considerable difference $|e_{31}^{(1)}/e_{31}^{(2)}| - |e_{33}^{(1)}/e_{33}^{(2)}|$ promotes some difference between $e_{31}^{*}(m)$. An increase in the volume fraction m leads to the influence of the piezo-active polymer component being less pronounced so that relatively small differences between the effective parameters calculated by different methods are observed.

4.1.3 Effect of the Porous Polymer Component on the Piezoelectric Anisotropy and the Anisotropy of Electromechanical Coupling Factors

In Sect. 4.1.3 we consider a similar composite that contains a system of single-domain SC rods in a porous polymer matrix. The SC rods have a square base and are characterised by a periodical square arrangement in the $(X_1 O X_2)$ plane. The main crystallographic axes x, y and z of each SC rod are parallel to the co-ordinate axes as shown in Fig. 4.1: x$||OX_1$, y$||OX_2$ and z$||OX_3$. Each SC rod is characterised by

a spontaneous polarisation vector $\boldsymbol{P}_s^{(1)} \uparrow\uparrow OX_3$. It is assumed that a single-domain state in each SC rod is stabilised by the bias field $\boldsymbol{E} \uparrow\uparrow OX_3$.

The polymer matrix of the studied composite contains a system of spheroidal air inclusions (pores) that are described by the equation

$$(x_1/a_1)^2 + (x_2/a_1)^2 + (x_3/a_3)^2 = 1 \tag{4.6}$$

relative to the axes of the rectangular co-ordinate system $(X_1X_2X_3)$, and semi-axes of the spheroid from (4.6) are $a_1, a_2 = a_1$ and a_3. The porous matrix is characterised by 3–0 connectivity, and the connectivity of the composite sample is 1–3–0. The pores are regularly distributed in the polymer matrix and occupy sites of a simple tetragonal lattice. The shape of each pore is characterised by an aspect ratio $\rho_p = a_1/a_3$ that is assumed to be fixed over the composite sample. The radius or the largest semi-axis of each pore (e.g., $a_1 = a_2$ for the oblate pore) is considered much smaller than the length of the side of the square being intersected the rod in the (X_1OX_2) plane. It should be added that methods for manufacturing such porous polymer materials with a regular arrangement of pores having the appointed shape are known from patents [24, 25], and these porous materials are also termed "patterned porous polymers".

The effective electromechanical properties of the 1–3–0 composite studied here are determined in two stages. At the first stage, the effective properties of the polymer matrix with aligned spheroidal pores are determined as a function of the volume fraction of the pores (i.e., porosity of the polymer matrix) m_p and the aspect ratio ρ_p. The corresponding calculation is based on Eshelby's concept of spheroidal inclusions in heterogeneous solids [26]. The effective properties of the 3–0 porous polymer medium are represented in the matrix form [27] as follows:

$$||C^{(3)}|| = ||C^{(2)}||\cdot[||I|| - m_p(||I|| - (1 - m_p)||S||)^{-1}]. \tag{4.7}$$

In (4.7) $||C^{(2)}||$ is the 9×9 matrix of the electromechanical properties of monolithic polymer, $||I||$ is a 9×9 identity matrix, and $||S||$ is the 9×9 matrix that comprises components of the electroelastic Eshelby tensor. Matrices $||C^{(2)}||$ and $||C^{(3)}||$ have the structure shown in (4.1). In this section we use superscripts "(1)" and "(2)" to denote the properties of SC and polymer, respectively. Superscript "(3)" refers to the porous polymer medium, and superscript "*" refers to the composite. Components of $||S||$ from (4.7) depend on the aspect ratio ρ_p of the pores, their volume fraction in the polymer matrix (i.e., porosity) m_p and on the properties of polymer.

At the second stage, the effective electromechanical properties of the composite are calculated out using either the matrix method or FEM (see Sect. 4.1.1). The study of the anisotropy of the piezoelectric coefficients and ECFs of the composite is carried out using experimental electromechanical constants single-domain PMN–0.42PT SC ($4mm$ symmetry) [28] and polyurethane (isotropic material) [29]. To characterise the performance of the studied composite, we introduce a system of anisotropy factors. The first anisotropy factor

$$\zeta_d = d_{33}^*/|d_{31}^*| \tag{4.8}$$

characterises the piezoelectric anisotropy (in absolute values), the second anisotropy factor

$$\zeta_{3j} = k_{33}^*/|k_{31}^*| \tag{4.9}$$

is used to describe the anisotropy of ECFs

$$k_{3j}^* = d_{3j}^*/(\varepsilon_{33}^{*\sigma} s_{jj}^{*E})^{1/2} \tag{4.10}$$

(in absolute values). The third anisotropy factor

$$\zeta_{t-p} = k_t^*/|k_p^*| \tag{4.11}$$

characterises the anisotropy of ECFs (in absolute values) at the thickness and planar oscillation modes, where

$$k_t^* = [(c_{33}^{*D} - c_{33}^{*E})/c_{33}^{*D}]^{1/2} \quad \text{and} \quad k_p^* = k_{31}^*[2s_{11}^{*E}/(s_{11}^{*E} + s_{12}^{*E})]^{1/2} \tag{4.12}$$

are thickness ECF and planar ECF [23], respectively, c_{33}^{*D} and c_{33}^{*E} are longitudinal elastic moduli at electric displacement $D = \text{const}$ and electric field $E = \text{const}$, respectively.

Data on the 1–3–0 PMN–0.42PT SC/porous polyurethane composite (Fig. 4.3) suggest that both the aspect ratio ρ_p and porosity m_p influence thenisotropy factors (4.8), (4.9) and (4.11) in the wide m range. A transition from highly prolate pores ($\rho_p \ll 1$) to the highly oblate pores ($\rho_p \gg 1$) in the polymer matrix leads to an increase of the anisotropy factors and gives rise to sharper maxima of ζ_{3j} and ζ_{t-p} (Fig. 4.3b, c). Increasing the porosity m_p also favours an increase in the anisotropy factors (cf. Figs. 4.3a, 4.4).

Changes in ρ_p and m_p lead to changes in the elastic anisotropy of the porous matrix and its effect on the anisotropy factors of the composite. This effect becomes pronounced at larger values of m_p and mainly at $\rho_p > 1$ (see, e.g., Fig. 4.4). The small anisotropy of elastic compliances of the porous matrix (i.e., $s_{11}^{(3)}/s_{33}^{(3)} \approx 1$) is observed at $\rho_p < 1$ and partially at $\rho_p > 1$ (as a rule, at porosity $m_p < 0.2$). The formation of highly oblate pores and an increase of the porosity of the matrix lead to $s_{11}^{(3)}/s_{33}^{(3)} \gg 1$, and finally, to a larger anisotropy of EFCs and piezoelectric coefficients. It is seen that even at small porosity ($m_p = 0.1$), inequalities $\zeta_{3j} > 10$ and $\zeta_d > 10$ hold (see Fig. 4.3a, b) in the presence of the oblate pores with $\rho_p > 10$. However the anisotropy factor ζ_{t-p} at $m_p = 0.1$ remains less than 8 even at $\rho_p = 100$ (Fig. 4.3a). The dielectric properties of the porous matrix at various values of ρ_p and m_p vary in a relatively narrow range [8], and condition $\varepsilon_{pp}^{(3)}/\varepsilon_{pp}^{(1),\sigma} \ll 1$ is valid. Thus, the elastic anisotropy of the porous matrix strongly influences behaviour of the anisotropy factors (4.8), (4.9) and (4.11) in the studied 1–3–0 composite.

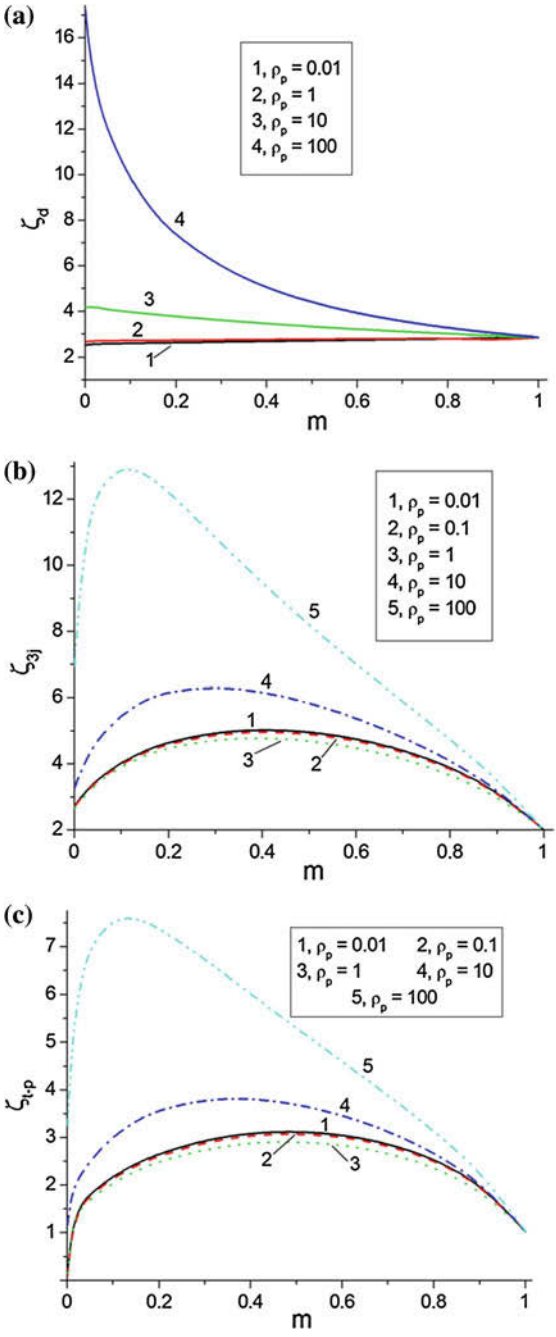

Fig. 4.3 Volume-fraction dependence of anisotropy factors ζ_d **(a)**, ζ_{3j} **(b)** and ζ_{t-p} **(c)** of a 1–3–0 PMN–0.42PT SC/ porous polyurethane composite at $m_p = 0.1$. Calculations were made using (4.7) at the first stage and the matrix method at the second stage (reprinted from paper by Topolov et al. [8], with permission from Elsevier)

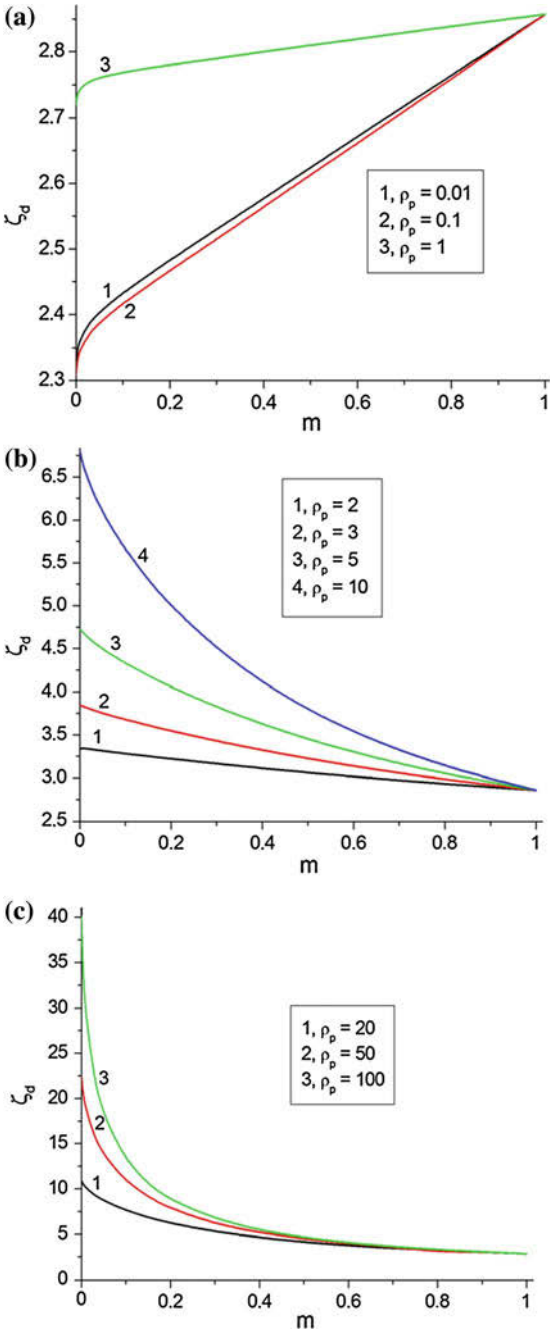

Fig. 4.4 Volume-fraction dependence of the anisotropy factor ζ_d of a 1–3–0 PMN–0.42PT SC/porous polyurethane composite at $m_p = 0.3$. Calculations were made using (4.7) at the first stage and the matrix method at the second stage (reprinted from paper by Topolov et al. [8], with permission from Elsevier)

To show the important role of the elastic anisotropy of the composite, we consider interconnections between the anisotropy factors that involve ECFs from (4.10) and (4.12). Taking into account (4.8)–(4.10), we derive that

$$\zeta_{3j} = \zeta_d (s_{11}^{*E}/s_{33}^{*E})^{1/2}. \tag{4.13}$$

Taking into account equality $k_t^* \approx k_{33}^*$ (that is valid for various 1–3 composites at various volume fractions of the piezo-active rod component [4, 5, 8]), we represent the anisotropy factor ζ_{t-p} from (4.11) as

$$\zeta_{t-p} \approx (k_{33}^*/|k_{31}^*|)[(s_{11}^{*E} + s_{12}^{*E})/(2s_{11}^{*E})]^{1/2} \approx \zeta_{3j}[(s_{11}^{*E} + s_{12}^{*E})/(2s_{33}^{*E})]^{1/2}. \tag{4.14}$$

Thus, as follows from (4.13) and (4.14), the anisotropy factors ζ_{3j} and ζ_{t-p} strongly depend on ζ_d and elastic compliances s_{ab}^{*E} of the 1–3–0 composite.

Results on the anisotropy factor ζ_d at $m_p = 0.1$ (Fig. 4.3a) and $m_p = 0.3$ (Fig. 4.4) show that a relatively small porosity m_p in the matrix has a slight influence on the balance of the piezoelectric coefficients d_{3j}^* of the composite, especially at $0 < \rho_p \leq 10$, and increasing the porosity m_p leads to the larger ζ_d values. At $m_p = 0.3$, we single out three variants of behaviour of ζ_d (Fig. 4.4), and these variants are mainly concerned with considerable changes in the ratio $s_{11}^{(3)}/s_{33}^{(3)}$.

In general, good agreement between the parameters calculated using the matrix method and FEM [8] is observed in wide m and ρ_p ranges. The piezoelectric coefficient d_{33}^* and ECFs k_{33}^* and k_t^* show very small differences (<2 %) as the corresponding values calculated using the aforementioned methods are compared. Some difference between the matrix-method and FEM data at volume fractions $0 < m \ll 1$ [8] is accounted for by an approximation in the matrix method [3, 8, 11]: the boundary conditions at the rod-matrix interfaces $x_a = \text{const}$ ($a = 1$ and 2, see Fig. 4.1) are considered without taking into account a possible stress concentration near the edge of the SC rod. Such an additional stress field could influence the piezoelectric coefficient d_{31}^*, ECF k_{31}^* and other effective parameters linked with d_{31}^*. The volume fractions m, for which this field is important, are from the region, where elastic compliances $s_{ab}^{*E} \sim s_{ab}^{(3)}$. Moreover, FEM results [15, 17] on the 1–3 FC/polymer composites with the parallelepiped-shaped rods also show that the stress concentration near the edge of the ceramic rod takes place in only a restricted region and is important at small volume fractions of FC. In the current study of the 1–3–0 composite, we show that the similar effect is appreciable at small volume fractions of SC in the presence of a porous polymer matrix with a variable elastic anisotropy.

Data from Table 4.2 also highlight the good consistency of results obtained using the matrix method and FEM. One of advantages of the studied 1–3–0 composite over conventional $PbTiO_3$-type FCs [30] with a large anisotropy of the piezoelectric coefficients d_{3j} consists in the fact, that even at volume fractions of SC ($m \approx 0.05$), the piezoelectric coefficient of the composite d_{33}^* is about 3–4 times more [8] than d_{33} of the $PbTiO_3$-type FCs [30]. The stronger electromechanical coupling in the studied 1–3–0 composite in comparison to the $PbTiO_3$-type FCs is achieved due to

Table 4.2 Volume-fraction dependence of anisotropy factors of the 1–3–0 PMN–0.42PT SC/porous polyurethane composite ($m_p = 0.3$ and $\rho_p = 0.01$, 10 or 100)

m	ζ_d, matrix method	ζ_d, FEM	ζ_{3j}, matrix method	ζ_{3j}, FEM	ζ_{t-p}, matrix method	ζ_{t-p}, FEM
$\rho_p = 0.01$						
0.01	2.68	2.69	3.58	3.69	1.91	1.91
0.03	2.69	2.70	4.13	4.32	2.27	2.09
0.05	2.70	2.70	4.58	4.83	2.57	2,59
0.10	2.71	2.71	5.41	5.77	3.12	3.14
0.30	2.75	2.75	6.85	7.22	4.24	4.22
0.50	2.78	2.79	6.88	7.03	4.46	4.41
0.70	2.82	2.82	6.01	6.04	4.01	3.98
0.90	2.86	2.84	4.05	4.05	2.70	2.69
$\rho_p = 10$						
0.01	5.98	6.14	4.60	4.84	2.32	2.49
0.03	5.78	5.95	5.90	6.36	3.14	3.31
0.05	5.61	5.78	6.75	7.35	3.66	3.84
0.10	5.28	5.38	7.99	8.75	4.47	4.63
0.30	4.33	4.32	8.70	9.24	5.29	5.28
0.50	3.71	3.69	7.53	7.72	4.82	4.76
0.70	3.29	3.28	5.85	5.88	3.86	3.82
0.90	2.98	2.97	3.67	3.66	2.40	2.39
$\rho_p = 100$						
0.01	27.7	34.4	16.0	20.1	8.95	11.2
0.03	20.9	25.9	19.1	24.5	10.9	13.6
0.05	17.5	20.8	19.8	24.7	11.4	13.8
0.10	12.9	14.1	19.2	22.3	11.3	12.6
0.30	6.62	6.59	13.8	14.4	8.62	8.58
0.50	4.61	4.56	9.78	9.88	6.38	6.26
0.70	3.63	3.62	6.78	6.78	4.52	4.65
0.90	3.06	3.06	3.92	3.92	2.59	2.58

Calculations were made using (4.7) at the first stage and by means of either the matrix method or FEM at the second stage

the presence of the relaxor-based SC component with higher piezoelectric activity. Moreover, the porous polymer component with a high elastic anisotropy strongly influences the anisotropy factors ζ_{3j} and ζ_{t-p} and the hydrostatic electromechanical coupling in the composite [8]. The aforementioned advantages are important for transducer, sensor, hydrophone, and other applications of the 1–3–0 composite based on the single-domain PMN–0.42PT SC.

4.2 Effect of the Orientation of Pores in the Polymer Matrix on the Performance of Composites Based on Ferroelectric Ceramics

Now we consider the 1–3–0 composite (Fig. 4.5) that contains FC rods in the form of a rectangular parallelepiped with a square base. These rods are continuous in the OX_3 direction and characterised by a square arrangement in the (X_1OX_2) plane and by the remanent polarisation vector $\boldsymbol{P}_r^{(1)} \uparrow\uparrow OX_3$. The polymer matrix surrounding the FC rods contains a system of spheroidal pores that are described by the equation

$$(x_1^0/a_1)^2 + (x_2^0/a_1)^2 + (x_3^0/a_3)^2 = 1 \tag{4.15}$$

in axes of the rectangular co-ordinate system $(X_1^0X_2^0X_3^0)$ related to the separate pore (Fig. 4.5, inset). The pores are oriented uniformly with respect to the co-ordinate system $(X_1X_2X_3)$ related to the composite sample, i.e., the condition $\theta = \text{const}$ is valid over the composite matrix (Fig.4.5). The pores are regularly distributed in the polymer medium and occupy the sites of a simple tetragonal lattice. The aspect ratio of each pore $\rho_p = a_1/a_3$ is fixed over the composite sample, and the semi-axes a_i of the pore from (4.15) obey the condition $a_1 = a_2 \neq a_3$. The radius or the largest semi-axis of each pore is considerably less than the length of the side of the square being intersected by the rod in the (X_1OX_2) plane. The effective properties of the porous matrix depend on porosity m_p, the aspect ratio of pores ρ_p and the rotation angle of pores θ. As a consequence, the effective electromechanical properties and related parameters of the composite are represented in the general form as $X^* = X^*(m, m_p, \rho_p, \theta)$.

In Sect. 4.2 we show examples of the effective parameters of the 1–3–0 composite based on the "soft" PCR–7M FC (FC of the PZT type, see electromechanical constants in Table 1.2) with high piezoelectric and dielectric properties [3, 32]. The matrix of the effective piezoelectric coefficients $d_{kl}^* = d_{kl}^*(m, m_p, \rho_p, \theta)$ of the composite with a system of aligned spheroidal pores (Fig. 4.5) is given by

$$||d^*|| = \begin{pmatrix} 0 & 0 & 0 & 0 & d_{15}^* & d_{16}^* \\ d_{21}^* & d_{22}^* & d_{23}^* & d_{24}^* & 0 & 0 \\ d_{31}^* & d_{32}^* & d_{33}^* & d_{34}^* & 0 & 0 \end{pmatrix}, \tag{4.16}$$

and the piezoelectric coefficients g_{kl}^* of the same composite are represented by the matrix that has the form shown in (4.16). At $\theta = 90°b$ $(b = 0, 1, 2, \ldots)$, the form of $||d^*||$ from (4.16) becomes simpler due to $d_{kl}^* = 0$ and $g_{kl}^* = 0$ with $kl = 16, 21, 22, 23,$ and 34. Due to the presence of $d_{2l}^* \neq 0$ and $g_{2l}^* \neq 0$ in (4.16), we now consider the hydrostatic piezoelectric coefficients of the composite as $d_h^* = d_{33}^* + d_{32}^* + d_{31}^* + d_{23}^* + d_{22}^* + d_{21}^*$ and $g_h^* = g_{33}^* + g_{32}^* + g_{31}^* + g_{23}^* + g_{22}^* + g_{21}^*$.

Of particular interest is an effect of the orientation of pores (Fig. 4.5, inset) on the piezoelectric sensitivity of the composite. To analyse this effect, we vary the

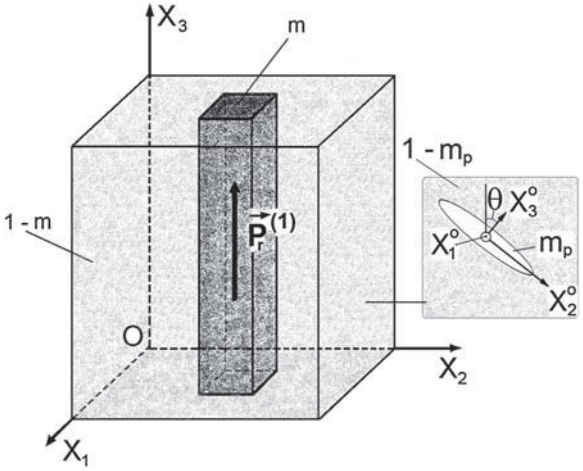

Fig. 4.5 Schematic diagram of the 1–3–0 FC/porous polymer composite. $(X_1X_2X_3)$ is the rectangular co-ordinate system concerned with the composite sample, $(X_1^0X_2^0X_3^0)$ is the rectangular co-ordinate system concerned with the orientation of the spheroidal pore in the polymer matrix. m and $1-m$ are volume fractions of FC and porous polymer, respectively, m_p is the volume fraction of air in the porous matrix, θ is the rotation angle, and $\boldsymbol{P}_r^{(1)}$ is the remanent polarisation vector of FC (reprinted from paper by Topolov and Panich [7], with permission from Taylor and Francis)

orientation angle θ and the volume fraction m at $m_p = \text{const}$ and $\rho_p = \text{const}$. Elastic compliances $s_{ij}^{(2)}$ of the porous matrix (Fig. 4.5) at $\theta \neq 90°b$ are represented as

$$||s^{(2)}|| = \begin{pmatrix} s_{11}^{(2)} & s_{12}^{(2)} & s_{13}^{(2)} & s_{14}^{(2)} & 0 & 0 \\ s_{12}^{(2)} & s_{22}^{(2)} & s_{23}^{(2)} & s_{24}^{(2)} & 0 & 0 \\ s_{13}^{(2)} & s_{23}^{(2)} & s_{33}^{(2)} & s_{34}^{(2)} & 0 & 0 \\ s_{14}^{(2)} & s_{24}^{(2)} & s_{34}^{(2)} & s_{44}^{(2)} & 0 & 0 \\ 0 & 0 & 0 & 0 & s_{55}^{(2)} & s_{56}^{(2)} \\ 0 & 0 & 0 & 0 & s_{56}^{(2)} & s_{66}^{(2)} \end{pmatrix}. \tag{4.17}$$

At $\theta = 90°b$, elastic compliances $s_{ij}^{(2)}$ from (4.17) obey conditions

$$s_{i4}^{(2)} = 0, s_{56}^{(2)} = 0, s_{13}^{(2)} = s_{23}^{(2)}, s_{11}^{(2)} = s_{22}^{(2)}, \text{ and } s_{44}^{(2)} = s_{55}^{(2)} (i = 1, 2 \text{ and } 3). \tag{4.18}$$

Examples of the dependence of the effective parameters of the 1–3–0 composite on m and θ_p are shown in Fig. 4.6. The graphs in Fig. 4.6 have been built for volume fractions $m \leq 0.2$ because of the lack of extreme points of the effective parameters

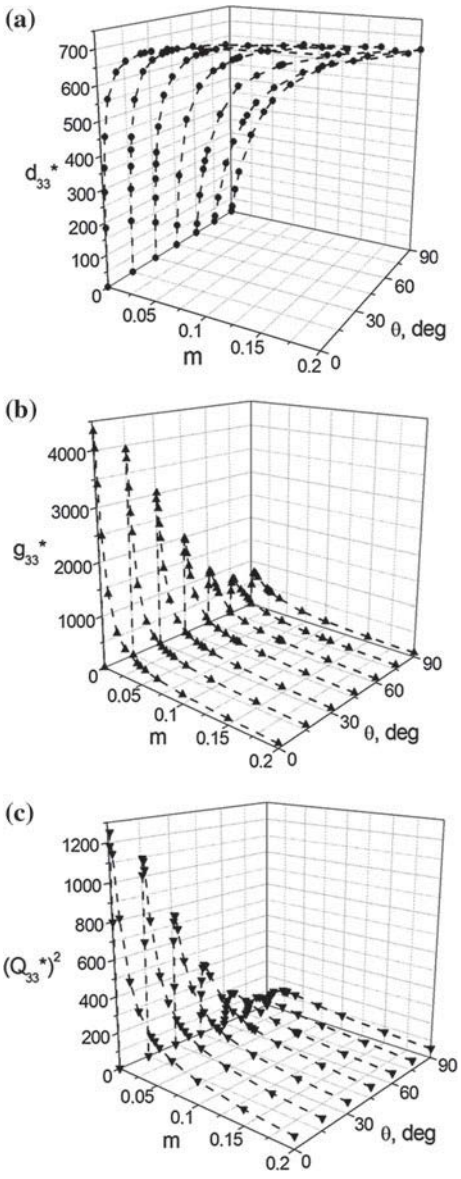

Fig. 4.6 Effective piezoelectric coefficients d_{33}^* (**a**, in pC/N), g_{33}^* (**b**, in mV· m/N), squared figure of merit $(Q_{33}^*)^2$ (**c**, in $10^{-12}\,\mathrm{Pa}^{-1}$, graph **a**) and related hydrostatic parameters d_h^* (**d**, in pC/N), g_h^* (**e**, in mV· m/N) and $(Q_h^*)^2$ (**f**, in $10^{-12}\,\mathrm{Pa}^{-1}$) which have been calculated for the 1–3–0 PCR-7M/porous poluyrethane composite with $m_p = 0.2$ and $\rho_p = 100$ (reprinted from paper by Topolov and Panich [7], with permission from Taylor and Francis)

Fig. 4.6 (continued)

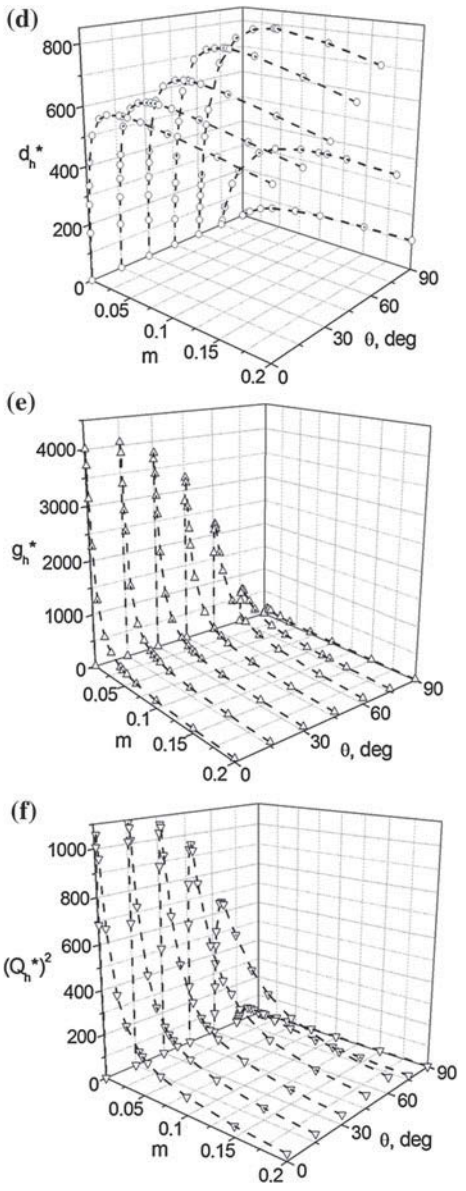

at $m > 0.2$. The configuration of curves related to the longitudinal parameters at $\theta = \text{const}$ (Fig. 4.6a–c) is the same, as in the conventional FC/polymer composite [3]. A rapid decrease of the local maximum values of g_{33}^* and $(Q_{33}^*)^2$ in the range $0° \le \theta \le 90°$ (Fig. 4.6b, c) is a result of the strong influence of elastic properties of the porous matrix on the piezoelectric sensitivity of the composite. Such an influence is concerned with the considerable effect of the orientation of the pore on the elastic anisotropy of the porous matrix. By varying the rotation angle θ, we vary elastic compliances $s_{ij}^{(2)}$ and their anisotropy [see matrix (4.17) and conditions (4.18)]. Non-monotonic behaviour of the hydrostatic parameters d_h^*, g_h^* and $(Q_h^*)^2$ (Fig. 4.6d–f) is observed with an increase of the rotation angle θ at $m = \text{const}$.

A violation of equalities (4.18) and the appreciable elastic anisotropy of the porous matrix with elastic compliances $s_{ij}^{(2)}$ from (4.17) promote a significant re-distribution of internal electric and mechanical fields in the composite sample. This re-distribution leads to an increase of the hydrostatic parameters d_h^*, g_h^* and $(Q_h^*)^2$ due to an improved balance of the piezoelectric coefficients d_{ij}^* and g_{ij}^*. As follows from our analysis [7], the piezoelectric coefficients $d_{3j}^* > 0$ at $m < 0.10$ provide the main contribution to d_h^* from Eq. (4.5) and lead to high values of d_h^* as compared to those at $\theta = 0°$ or 90°. The piezoelectric coefficients $g_{3j}^* > 0$ play a similar role in forming the high hydrostatic piezoelectric sensitivity of the composite.

To show the role of the orientation effect in the studied composite, we provide two sets of its effective parameters for comparison. According to data [7], the composite with $m_p = 0.2$, $\rho_p = 100$ and $\theta = 0°$ is characterised by $\max d_h^* \approx 10 d_h^{(1)}$ that corresponds to the volume fraction of FC $m = 0.049$ (Fig. 4.6d). At this volume fraction, the effective parameters of the same composite are given by

$$g_{33}^* \approx 26 g_{33}^{(1)},\ g_h^* \approx 210 g_h^{(1)},\ (Q_{33}^*)^2 \approx 18 (Q_{33}^{(1)})^2,\ \text{and}\ (Q_h^*)^2 \approx 2,120 (Q_h^{(1)})^2. \tag{4.19}$$

In the composite with pores at $\theta = 60°$, the condition $\max d_h^* \approx 14 d_h^{(1)}$ is attained at $m = 0.093$ (Fig. 4.6d). At the same m_p, ρ_p, θ, and m values, the composite is characterised by the following parameters: $g_{33}^* \approx 9.9 g_{33}^{(1)}$, $g_h^* \approx 185 g_h^{(1)}$, $(Q_{33}^*)^2 \approx 8.0 (Q_{33}^{(1)})^2$, and $(Q_h^*)^2 \approx 2,560 (Q_h^{(1)})^2$. At the volume fraction $m = 0.049$ (as in the above-considered case of $\theta = 0°$) and $\theta = 60°$, we have the following effective parameters of the composite:

$$g_{33}^* \approx 17 g_{33}^{(1)},\ g_h^* \approx 360 g_h^{(1)},\ (Q_{33}^*)^2 \approx 12 (Q_{33}^{(1)})^2,\ \text{and}\ (Q_h^*)^2 \approx 4,900 (Q_h^{(1)})^2. \tag{4.20}$$

A comparison of data from (4.19) and (4.20) enables us to conclude the important role of the orientation of pores in forming the large piezoelectric coefficient g_{33}^*, squared figure of merit $(Q_{33}^*)^2$ and their hydrostatic analogues. It should be added that the presence of the porous matrix at $\theta = 90°$ leads to an appreciable decrease in the piezoelectric coefficient d_h^* and other effective parameters of the composite (Fig. 4.6) mainly due to a change in the balance of elastic compliances $s_{ij}^{(2)}$ from (4.17). Spheroidal pores at $\theta = 90°$ do not provide high ratios of elastic moduli

$c_{11}^{(2)}/c_{13}^{(2)}$ and $c_{11}^{(2)}/c_{33}^{(2)}$ in the porous polymer matrix and, as a consequence, lead to a lower piezoelectric sensitivity for the corresponding composite. The studied orientation effect is to be taken into consideration in future applications of composite materials with high piezoelectric sensitivity and large figures of merit.

The related 1–3 PCR-7M/polyurethane composite is characterised by maximum values of the effective parameters [32] as follows: $\max g_{33}^* \approx 34 g_{33}^{(1)}$, $\max g_h^* \approx 91 g_h^{(1)}$, $\max[(Q_{33}^*)^2] \approx 8.3(Q_{33}^{(1)})^2$, and $\max[(Q_h^*)^2] \approx 54(Q_h^{(1)})^2$. However, these maximum values are attained at different volume fractions m of FC, and this circumstance highlights the lower performance of the 1–3 composite in comparison to its 1–3–0 analogue. According to experimental data [33], the 1–3-type PZT/porous epoxy composite with the volume fraction of FC $m = 0.06$ is characterised by hydrostatic parameters $d_h^* = 220\,\text{pC/N}$, $g_h^* = 228\,\text{mV}\cdot\text{m/N}$ and $(Q_h^*)^2 = 50.2 \times 10^{-12}\,\text{Pa}^{-1}$ at porosity of the matrix $m_p = 0.20$ and $d_h^* = 284\,\text{pC/N}$, $g_h^* = 294\,\text{mV}\cdot\text{m/N}$ and $(Q_h^*)^2 = 83.5 \times 10^{-12}\,\text{Pa}^{-1}$ at $m_p = 0.40$. Data from Fig. 4.6d–f testify to higher piezoelectric sensitivity of the studied PCR-7M-based composite at the volume fraction $m = 0.06$ and various angles θ.

4.3 Ceramic/Polymer Composites with Elliptical Cross Section Rods

4.3.1 Modelling of Effective Electromechanical Properties

In the last decades, piezo-active 1–3 composites with various cross sections have been studied to show the role of the pillar effect [13, 15, 17, 18] on the effective properties and their anisotropy. Below we consider an example of a 1–3 FC/polymer composite with elliptical cross sections of rods in the plane perpendicular to the poling axis (Fig. 4.7). It is assumed that the composite has a cellular structure and

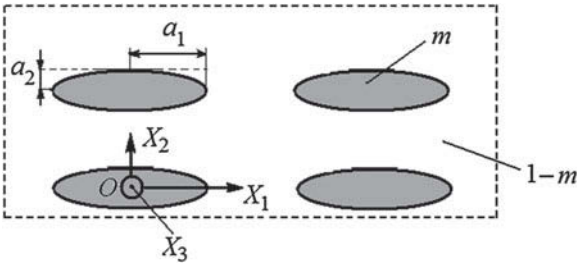

Fig. 4.7 Cross section of the 1–3 FC/polymer composite by the X_1OX_2 plane. $(X_1X_2X_3)$ is the rectangular co-ordinate system, a_1 and a_2 are semi-axes of the ellipse, m is the volume fraction of FC, and $1 - m$ is the volume fraction of polymer (reprinted from paper by Topolov and Bisegna [34], with permission from Springer)

a regular distribution of the FC rods in the large polymer matrix. Cross sections of these rods by the (X_1OX_2) plane of the rectangular co-ordinate system $(X_1X_2X_3)$ (Fig. 4.7) are described by the equation

$$(x_1/a_1)^2 + (x_2/a_2)^2 = 1 \tag{4.21}$$

relative to the axes of the co-ordinate system $(X_1X_2X_3)$. Semi-axes of the ellipse a_f ($f = 1$ and 2) from (4.21) are constant in the whole composite sample. Centres of symmetry of these ellipses are arranged periodically on the OX_1 and OX_2 directions. It is assumed that the FC rods are aligned along the OX_3 axis and the height of each rod obeys the condition $h \gg a_f$.

The remanent polarisation vector of the FC rod is $\boldsymbol{P}_r^{(1)} \uparrow\uparrow OX_3$. The polymer matrix can be either ferroelectric (piezo-active in the poled state) with a remanent polarisation vector $\boldsymbol{P}_r^{(2)}$ or simply dielectric (piezo-passive) with $\boldsymbol{P}_r^{(2)} = \boldsymbol{0}$. Taking into account the considerable difference between coercive fields of the FC and ferroelectric polymer components [12, 35, 36], one can manufacture composites with $\boldsymbol{P}_r^{(2)} \uparrow\uparrow OX_3$, $\boldsymbol{P}_r^{(2)} \uparrow\downarrow OX_3$ or other $\boldsymbol{P}_r^{(2)}$ orientations in the polymer matrix.

The effective electromechanical properties of the studied 1–3 composite are determined in the long-wave approximation [3]. Calculations of the effective electromechanical properties are carried out within the framework of either the EFM or FEM. In these methods, the following electromechanical constants of components are used for calculations: elastic moduli $c_{ab}^{(n),E}$, piezoelectric coefficients $e_{ij}^{(n)}$ and dielectric permittivities $\varepsilon_{pq}^{(n),\xi}$, where $n = 1$ is related to the FC component, and $n = 2$ is related to the polymer component.

Based on the EFM concepts [3, 19, 27], one can describe an electromechanical interaction in the system of "rods–matrix" using a local electric field that acts on each rod. This effective field is determined by taking into account a system of interacting piezo-active rods and boundary conditions concerned with the rod shape. The boundary conditions involve components of electric and mechanical fields at the rod - matrix interface. The 9×9 matrix characterising the electromechanical properties of each component ($n = 1$ or 2) is written by analogy with (4.1). In the EFM, the effective electromechanical properties of the 1–3 composite are described by the 9×9 matrix [3, 19]

$$||C^*|| = ||C^{(2)}|| + m(||C^{(1)}|| - ||C^{(2)}||)[||I|| + (1-m)||S||||C^{(2)}||^{-1}(||C^{(1)}|| - ||C^{(2)}||)]^{-1}. \tag{4.22}$$

In (4.22) matrices of electromechanical constants of components $||C^{(1)}||$ and $||C^{(2)}||$ have the form shown in (4.1), m is the volume fraction of FC, $||I||$ is the identity matrix, and $||S||$ is the matrix that contains the Eshelby tensor components [26] depending on the elements of $||C^{(2)}||$ and the rod shape. Hereafter the ratio of semi-axes $\eta = a_2/a_1$ in the rod cross section [see Fig. 4.7 and Eq. (4.21)] and the volume fraction m of FC are regarded as two independent parameters to be varied [34] in ranges $0 < \eta \leq 1$ and $0 < m < \pi/4$, respectively. The limiting case of $\eta = 0$ corresponds to the 2–2 parallel-connected composite, and the limiting case of $\eta = 1$ is relevant to a circular rod cross section and the 1–3 connectivity pattern.

For comparison, the prediction of the electromechanical properties of the 1–3 composite is also carried out using the FEM via the COMSOL package (see Sect. 4.1.1). The rectangular representative unit cell, containing the FC rod in the form of an elliptical cylinder with semi-axes a_f adjusted to yield the appropriate volume fraction of FC (Fig. 4.7), is discretised using triangular elements. The unknown displacement field is interpolated using second-order Lagrange shape functions, leading to a problem with approximately 120,000 to 200,000 degrees of freedom. The number of the degrees of freedom depends on the ratio of semi-axes η. Periodicity is enforced at the boundary of the rectangular representative unit cell of the composite. After solving the equilibrium problem, the effective elastic moduli $c^{*E}_{ab}(m, \eta)$, piezoelectric coefficients $e^*_{ij}(m, \eta)$ and dielectric permittivities $\varepsilon^{*\xi}_{pq}(m, \eta)$ of the composite are computed [34] by means of averaging the resulting local stress and electric-displacement fields over the representative unit cell.

4.3.2 Anisotropy of Piezoelectric Coefficients

Calculations are carried out using experimental room-temperature electromechanical constants of the FC and polymer components. To predict the effective properties of the composite, we have chosen the "soft" PCR-7M[Pb(Zr, Ti)O_3-based] FC composition with high piezoelectric and dielectric properties [31] and the "hard" modified $PbTiO_3$ FC composition with a large piezoelectric anisotropy and moderate piezoelectric and dielectric properties [30]. Ferroelectric 75/25 mol.% copolymer of vinylidene fluoride and trifluoroethylene (VDF-TrFE) with a high piezoelectric anisotropy [5] and araldite (piezo-passive material) [37] have been chosen as matrix components.[2]

The effective properties of the 1–3 composite are characterised by *mm*2 symmetry, as follows from the analysis of the matrix $||C^*|| = ||C^*(m, \eta)||$ from (4.22). In this case the piezoelectric properties of the composite are represented as

$$||y^*|| = \begin{pmatrix} 0 & 0 & 0 & 0 & y^*_{15} & 0 \\ 0 & 0 & 0 & y^*_{24} & 0 & 0 \\ y^*_{31} & y^*_{32} & y^*_{33} & 0 & 0 & 0 \end{pmatrix},$$

where $y = d$, e, g, or h. Below we consider some examples of the piezoelectric coefficients $y^*_{3j}(m, \eta)$ in the context of the anisotropy of the properties of the studied composite.

Due to the system of FC rods parallel to the OX_3 axis, the piezoelectric coefficients e^*_{3j} and h^*_{3j} of the composite are characterised by a large anisotropy in wide ranges of m and η. This means that inequalities $e^*_{33}/|e^*_{31}| \gg 1$, $e^*_{33}/|e^*_{32}| \gg 1$, $h^*_{33}/|h^*_{31}| \gg 1$, and $h^*_{33}/|h^*_{32}| \gg 1$ hold for different combinations of the aforemen-

[2] Their electromechanical constants are given in Table 5.2 (see Sect. 5.2.1).

tioned components and often irrespective of the signs of the piezoelectric coefficients $e_{ij}^{(n)}$ of these components.

A comparison of the EFM results with those obtained using the FEM is carried out for the piezoelectric coefficients d_{3j}^* of a series of composites with $0.01 \leq \eta \leq 1$ [34]. Values of d_{3j}^* calculated by these two methods are in good agreement in wide ranges of m and η. Some deviations of results for d_{31}^* and d_{32}^*, especially at small η values [34], may be explained by an approximate character of the averaging procedure in the EFM. The effective field acting along the OX_1 and OX_2 axes (Fig. 4.7) at $\eta \ll 1$ is affected by curvature of rods more considerably than that accounted in (4.22). At the same time, values of the hydrostatic piezoelectric coefficient d_h^* from (4.3) agree in wide ranges of m and η very well. Approaching $\eta \to 1$ makes the deviations between the results of the EFM and FEM smaller. In the limiting case of $\eta = 1$, the results of both EFM and FEM calculations agree with data obtained using formulae [38] for the 1–3 composite with rods in the form of the circular cylinder. In a limiting case of $\eta = 0$ (i.e., $a_2 = 0$, see Fig. 4.7), this composite becomes laminar with 2–2 connectivity and interfaces $x_2 = \text{const}$. The effective electromechanical properties of the 2–2 composite are determined using the matrix method [3] that allows for the electromechanical interaction between the piezo-active layers distributed regularly. Dependences of d_{31}^*, d_{32}^*, e_{31}^*, and e_{32}^* on η at $m = \text{const}$ [34] suggest that only slight differences between the similar parameters take place at $\eta \leq 10^{-3}$. The piezoelectric coefficients d_{33}^* and e_{33}^* which characterise the longitudinal piezoelectric properties remain almost constant at $0 \leq \eta \leq 1$ because the interfaces in the composite are parallel to the OX_3 axis irrespective of the curvature of the rod base. This constancy is in agreement with data [17] on the 1–3 composite poled along the OX_3 axis.

Analysing various combinations of the FC and polymer components in the 1–3 composite, one can find four typical examples of dependences of the piezoelectric properties on m at $\eta = \text{const}$ [34]. These dependences are observed in the following composites:

(i) PCR-7M FC/araldite (composite I), monotonic d_{3j}^* and non-monotonic g_{3j}^* ($j = 1$ and 2),

(ii) modified $PbTiO_3$FC/araldite (composite II), non-monotonic d_{3j}^* and non-monotonic g_{3j}^* ($j = 1$ and 2),

(iii) PCR-7M FC/VDF–TrFE with $\boldsymbol{P}_r^{(2)} \uparrow\downarrow OX_3$ (composite III), monotonic d_{3j}^* and monotonic g_{3j}^* ($j = 1$ and 2), and

(iv) modified $PbTiO_3$FC/VDF–TrFE with $\boldsymbol{P}_r^{(2)} \uparrow\downarrow OX_3$ (composite IV), non-monotonic d_{3j}^* and monotonic g_{3j}^* ($j = 1$ and 2).

The FC rods and the polymer matrix in composites III and IV are poled antiparallel, and this mutual orientation is achieved due to the large difference [12, 35, 36] between the coercive fields of the FC and polymer components.

Examples of the non-monotonic dependence of d_{3j}^* and g_{3j}^* are shown in the volume-fraction range $0 \leq m \leq 0.2$ (Fig. 4.8). Furthermore, increasing the volume fraction of FC m at $\eta = \text{const}$ leads to monotonically decreasing $|g_{3j}^*|$ only. As long

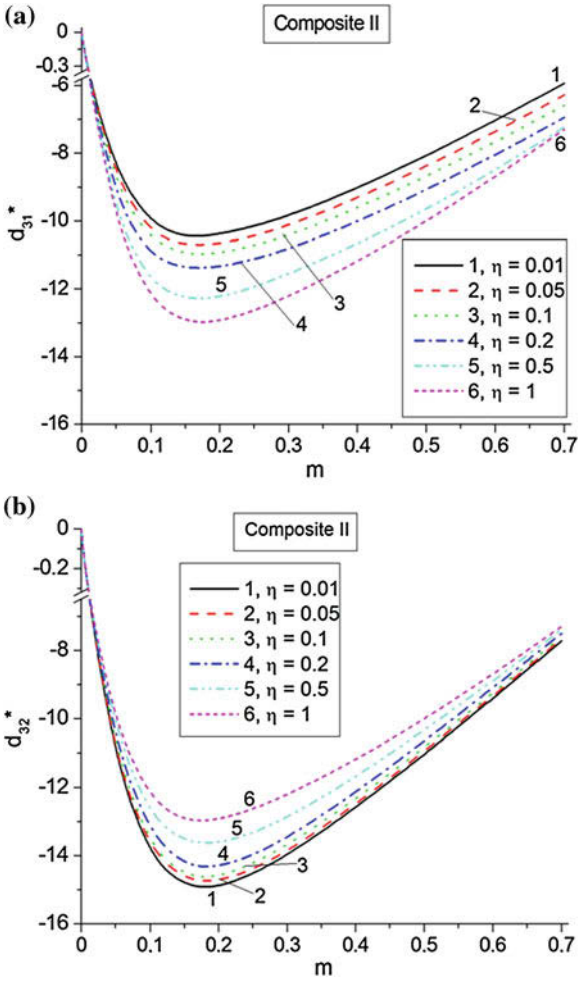

Fig. 4.8 Effective piezoelectric coefficients $d^*_{3j}(m, \eta)$ (**a** and **b**, in pC/N) and $g^*_{3j}(m, \eta)$ (**c** and **d**, in mV· m/N) of a 1–3 modified $PbTiO_3$ FC/araldite composite, FEM calculations (reprinted from paper by Topolov and Bisegna [34], with permission from Springer)

as the $g^{(2)}_{3j}$ values of the FC components are many times less than $\max|g^*_{3j}|$, it is possible to avoid the "tails" of the volume-fraction dependence of g^*_{3j} at $m > 0.2$ [34].

The non-monotonic volume-fraction dependence of d^*_{31} and d^*_{32} is observed in 1–3 composites based on $PbTiO_3$-type FCs irrespective of the polymer matrix [34]. This peculiarity is due to the elastic anisotropy of the FC component. For instance, ratios of elastic moduli $c^{(1),E}_{11}/c^{(1),E}_{12} = 4.4$ and $c^{(1),E}_{11}/c^{(1),E}_{13} = 5.9$, which hold for the modified $PbTiO_3$ FC [30] considerably differ from those in VDF-TrFE, araldite, polyurethane, and other polymers [5, 39, 38]. The anisotropy of $c^{(1),E}_{ab}$ and positive

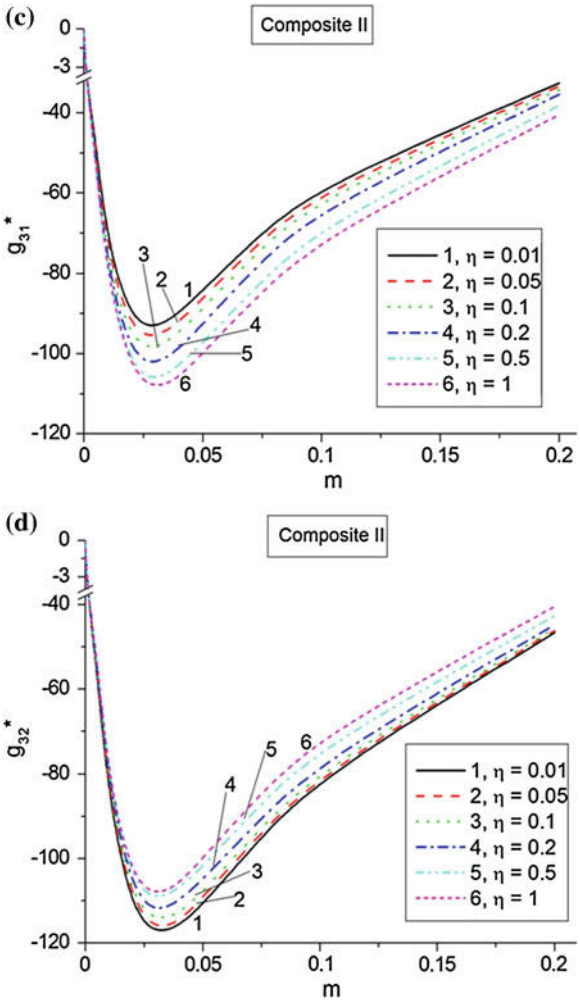

Fig. 4.8 (continued)

signs of $e_{3j}^{(1)}$ of the modified $PbTiO_3$ FC have a strong influence on the balance of items in relations [23]

$$d_{31}^* = e_{31}^* s_{11}^{*E} + e_{32}^* s_{12}^{*E} + e_{33}^* s_{13}^{*E}, d_{32}^* = e_{31}^* s_{12}^{*E} + e_{32}^* s_{22}^{*E} + e_{33}^* s_{23}^{*E}$$
$$\text{and} \quad d_{33}^* = e_{31}^* s_{13}^{*E} + e_{32}^* s_{23}^{*E} + e_{33}^* s_{33}^{*E} \tag{4.23}$$

which link the piezoelectric coefficients of the composite [see also (1.12)]. Contrary to d_{31}^* and d_{32}^* from (4.23), the piezoelectric coefficient d_{33}^* is characterised by a monotonic volume-fraction dependence in composites I–IV [34]. This means that

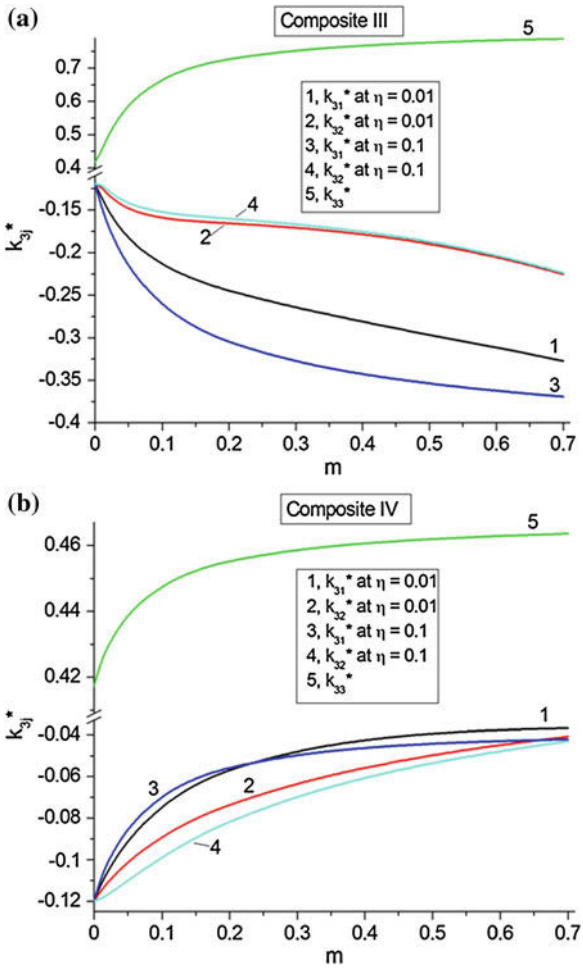

Fig. 4.9 ECFs $k^*_{3j}(m)$ of the 1–3 PCR-7M FC/VDF–TrFE (**a**) and modified $PbTiO_3$FC/VDF–TrFE (**b**) composites with $\boldsymbol{P}_r^{(2)} \uparrow\downarrow OX_3$ at $\eta = 0.01$ and $\eta = 0.1$, FEM calculations (reprinted from paper by Topolov and Bisegna [34], with permission from Springer)

the anisotropy of elastic compliances s^{*E}_{j3} involved in (4.23) cannot strongly influence the piezoelectric effect and its anisotropy in the 1–3 composites studied here.

4.3.3 Anisotropy of Electromechanical Coupling Factors

In Sect. 4.3.3 we consider an important example of the volume-fraction dependence and anisotropy of ECFs k^*_{3j} from (4.10) at $\eta = \text{const}$. The monotonic behaviour

of ECFs in composites III and IV (Fig. 4.9) with the piezo-active polymer matrix is observed irrespective of peculiarities of d_{3j}^{*} (m, η) and changes in η. Dielectric permittivity $\varepsilon_{33}^{*\sigma}$ of composites III and IV increases monotonically with increasing m at various values of η. It seems reasonable to assume that changes in elastic compliances s_{jj}^{*E} strongly influence the balance of electromechanical constants in (4.9) and the monotonic volume-fraction dependence of ECFs k_{3j}^{*}. In composite IV the conditions $5 < k_{33}^{*}/|k_{31}^{*}| < 12$ and $5 < k_{33}^{*}/|k_{32}^{*}| < 12$ are valid in wide volume-fraction ranges (Fig. 4.9b) due to the presence of the FC and polymer components with a large anisotropy of the piezoelectric coefficients $d_{3j}^{(n)}$. In composite III the anisotropy of ECFs k_{3j}^{*} is not very large and varies in a restricted range (Fig. 4.9a) mainly due to the presence of a FC component with a moderate piezoelectric anisotropy (according to experimental data [31] on PCR-7M, $d_{33}^{(1)}/|\mathrm{d}_{31}^{(1)}| \approx 2.2$).

4.3.4 *Effect of the Auxetic Polymer Component on the Piezoelectric Properties and Their Anisotropy*

An important opportunity for improving the performance of 1–3-type composites based on FCs consists in use of the auxetic matrix, i.e., the matrix with a negative Poisson's ratio $\nu^{(2)}$ [39–44]. The auxetic polymer component provides a considerable re-distribution of internal electric and mechanical fields in the composite sample and influences the effective electromechanical properties and their anisotropy. An effect of the auxetic polymer matrix on the performance of the 1–3-type piezo-active composites was discussed in earlier studies [29, 43, 45]. Even a piezo-passive auxetic polymer matrix leads to an increase of the hydrostatic piezoelectric coefficient d_h^{*} of the 1–3-type composite, and inequalities $d_h^{*} > d_{33}^{*}$ and $d_{31}^{*} > 0$ [29, 45] hold in certain ranges of the volume fraction of FC. At the same time, no study on the anisotropy of the piezoelectric and other properties of the piezo-active composites was carried out in the context of the auxetic polymer component with variable properties. Changes in elastic properties of PE–from a conventional high-density specimen with $\nu^{(2)} > 0$ to a series of microporous auxetic specimens with $\nu^{(2)} < 0$ – were studied in work [42]. Experimental results [42] suggest that $\nu^{(2)}$ of auxetic PE can be varied from -0.20 to -0.83, and in comparison to these data, conventional PE is characterised by $\nu^{(2)} = 0.20$.

In Sect. 4.3.4 we analyse the role of variations of $\nu^{(2)}$ in forming the piezoelectric properties and their anisotropy in the 1–3-type composite. It is assumed that the composite consists of a system of extended cylindrical FC rods aligned parallel to the poling axis OX_3. These rods are surrounded by a continuous polymer matrix and regularly distributed over the composite sample. In the case of a circular cross section of each rod in the (X_1OX_2) plane (i.e., $\eta = 1$), a square arrangement of the rods in the (X_1OX_2) plane is observed. In the case of an elliptical cross section (see Fig. 4.7), semi-axes a_i of each ellipse obey condition (4.21), and a rectangular arrangement of the rods in the (X_1OX_2) plane takes place.

The effective electromechanical properties of the studied composite are determined in the long-wave approximation as a function of the volume fraction m of FC by means of the EFM (for the circular cross section of the rod) and the FEM (for the elliptical cross section of the rod), see also Sect. 4.3.1. Among the components of interest for comparison and potential applications, we choose PCR-7M FC [31] and PE specimens [42] with variable elastic properties. It is assumed that the dielectric permittivity of PE is $\varepsilon_{pp}^{(2)}/\varepsilon_0 = 2.3$ (as is known for monolithic PE [46]) and $\varepsilon_{pp}^{(2)} << \varepsilon_{pp}^{(1)}$ at $p = 1$ and 3.

An important feature of the studied composites with auxetic polymer components is the non-monotonic volume-fraction dependence of anisotropy factors

$$\zeta_d^* = d_{33}^*/d_{31}^* \quad \text{and} \quad \zeta_k^* = k_{33}^*/k_{31}^* = \zeta_d^*(s_{11}^{*E}/s_{33}^{*E})^{1/2}. \tag{4.24}$$

Values of $\zeta_d^* \to \pm\infty$ and $\zeta_k^* \to \pm\infty$ (Fig. 4.10a) are achieved at a critical volume fraction m^* as condition $d_{31}^*\,(m^*) = 0$ holds. To show features of the volume-fraction dependence of the anisotropy factors in the presence of the auxetic polymer component, we introduced direct ratios in (4.24) instead of those concerned with $|d_{31}^*|$ and $|k_{31}^*|$ (see (4.8) and (4.9) for comparison). It should be noted that ζ_d^* and ζ_k^* of the related composite with a monolithic PE matrix (Fig. 4.10b) vary without any breaks because of the piezoelectric coefficient $d_{31}^* < 0$ in the composite at any m values. It is clear that changes in the Poisson's ratio of the polymer matrix ($\nu^{(2)} = -0.20$ in data from Fig. 4.10a and $\nu^{(2)} = 0.20$ in data from Fig. 4.10b) lead to drastic changes in the anisotropy factors (4.24). At the same time, volume-fraction dependences $d_{33}^*(m)$ and $k_{33}^*(m)$ (see, e.g., Fig.4.10c) undergo relatively small changes (less than 5 %) at replacing the PE matrix and changing its $\nu^{(2)}$ value, even if we choose the conventional PE component with $\nu^{(2)} > 0$ instead of its auxetic analogue with $\nu^{(2)} < 0$. In our opinion, the ratio of elastic moduli of components $c_{33}^{(1),E}/c_{33}^{(2)} = c_{33}^{(1),E}/c_{11}^{(2)} \gg 1$ plays an important role in forming the longitudinal piezoelectric effect in the 1–3-type composite, including $d_{33}^*(m)$ and $k_{33}^*(m)$.

Data on the anisotropy factors ζ_d^* and ζ_k^* of the 1–3-type composites with auxetic PE matrices at $0.05 \le m < m^*$ (Table 4.3) suggest that

(i) $\zeta_k^* > \zeta_d^*$ (this inequality is accounted for by the ratio $s_{11}^{*E}/s_{33}^{*E} > 1$ in (4.24), and such behaviour of elastic compliances s_{aa}^{*E} of the composite is caused by the presence of the FC rods oriented along the OX_3 axis) and
(ii) decreasing the critical volume fraction m^* is achieved by increasing the ratio $c_{11}^{(2)}/|c_{12}^{(2)}|$ of the auxetic component.

As a consequence, auxetic PE-4 with the largest value of $c_{11}^{(2)}/|c_{12}^{(2)}|$ provides the largest anisotropy factors ($\zeta_d^* > 10$ and $\zeta_k^* > 10$) at $m \approx 0.15$. It should be added that the composite at this volume fraction of ceramic is characterised by relatively large values of $d_{33}^*(m)$ and $k_{33}^*(m)$ (see, e.g., Fig. 4.10c) and, therefore, has obvious advantages over high-anisotropic FCs of the $PbTiO_3$ type [30]. The studied composite based on the PZT-type FC has no analogues among the known piezo-active materials

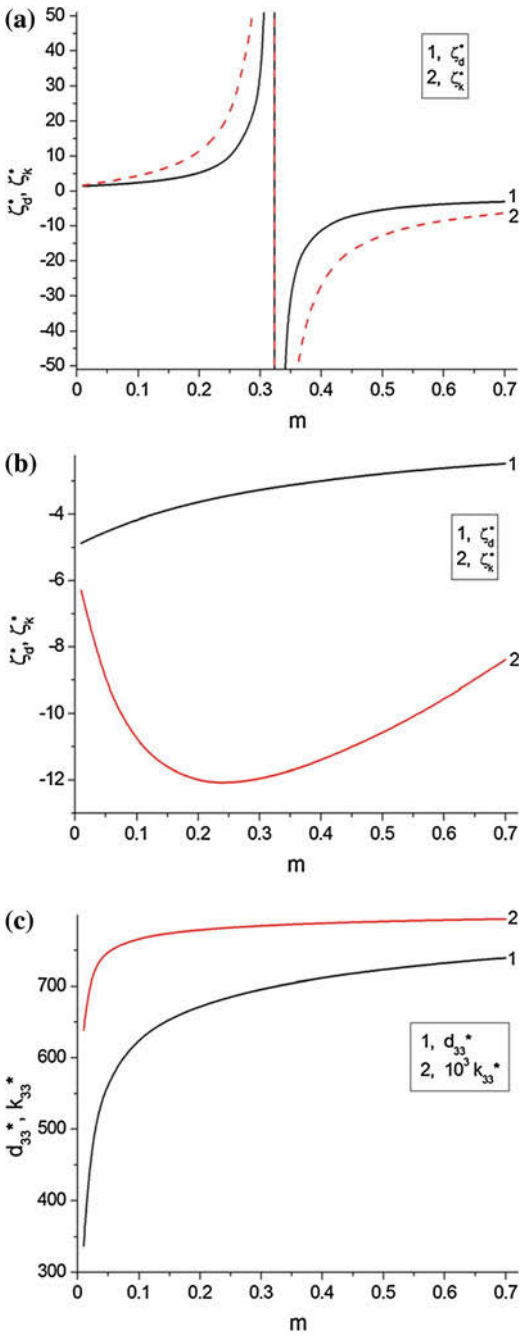

Fig. 4.10 Volume-fraction dependences of anisotropy factors ζ_d^* and ζ_k^* (**a** and **b**), piezoelectric coefficient d_{33}^* (in pC/N) and ECF k_{33}^*, which have been calculated by means of EFM for the following 1–3-type composites with circular cross sections of rods: PCR-7M FC/auxetic PE-1 (**a** and **c**) and PCR-7M FC/PE (**b**)

Table 4.3 Anisotropy factors ζ_d^* and ζ_k^* and critical volume fractions m^*, which are related to 1–3-type PCR-7M/auxetic PE composites with circular cross sections of rods (EFM data, fixed values of the volume fraction of FC m are given in parentheses), and ratios of elastic moduli $c_{11}^{(2)}/|c_{12}^{(2)}|$ of auxetic PE

Polymer component	ζ_d^*	ζ_k^*	m^*	$c_{11}^{(2)}/\lvert c_{12}^{(2)}\rvert$
	1.71 (0.05)	2.63 (0.05)		
Auxetic PE-1	2.32 (0.10)	4.30 (0.10)	0.324	2.28
	3.30 (0.15)	6.77 (0.15)		
	4.02 (0.05)	11.5 (0.05)		
Auxetic PE-4	6.15 (0.10)	22.9 (0.10)	0.220	3.86
	11.3 (0.15)	48.6 (0.15)		
	3.04 (0.05)	9.62 (0.05)		
Auxetic PE-6	4.39 (0.10)	18.2 (0.10)	0.252	3.22
	7.06 (0.15)	33.7 (0.15)		
	2.32 (0.05)	5.72 (0.05)		
Auxetic PE-8	3.24 (0.10)	10.2 (0.10)	0.285	2.73
	4.83 (0.15)	17.4 (0.15)		
	1.61 (0.05)	3.42 (0.05)		
Auxetic PE-9	2.19 (0.10)	5.85 (0.10)	0.330	2.21
	3.09 (0.15)	9.33 (0.15)		

and can be used as a material with large values of d_{33}^*, k_{33}^*, ζ_d^*, and ζ_k^* in relatively wide ranges of m.

4.3.5 *Effect of the Auxetic Polymer Component on the Hydrostatic Piezoelectric Response*

A change in the aspect ratio η of the elliptical cross section of the FC rods (see Fig. 4.7) influences both the piezoelectric anisotropy and hydrostatic response of the composite (Fig. 4.11). The largest maximum values of $d_{3j}^*(m) > 0$ ($j = 1$ and 2) are achieved at $\eta = 1$, i.e., in the presence of the circular cylindrical FC rods, and this composite microgeometry promotes a larger hydrostatic piezoelectric coefficient d_h^* (curve 6 in Fig. 4.11d) evaluated according to (4.3). We add that the auxetic PE-9 component leads to the largest value of $\max d_h^*$ in the studied composites with a circular cross section of rods and with an auxetic PE matrix. Changes in the aspect ratio η give rise to insignificant changes in $d_{33}^*(m)$ (Fig. 4.11c) due to the weak effect of the cross section of the rod on the lateral piezoelectric activity of the composite. It is also seen that approaching $\eta \to 1$ leads to an increase in the value of $\max d_h^*$ by about 10-15% in comparison to the case of the composite at $\eta \to 0$ (Fig. 4.11d).

Data from Fig. 4.11c, d suggest that large values of $d_h^* \approx (1000 - 1500)$ pC/N and $d_h^* \approx 2d_{33}^*$ are achieved in a relatively wide volume-fraction range due to the strong

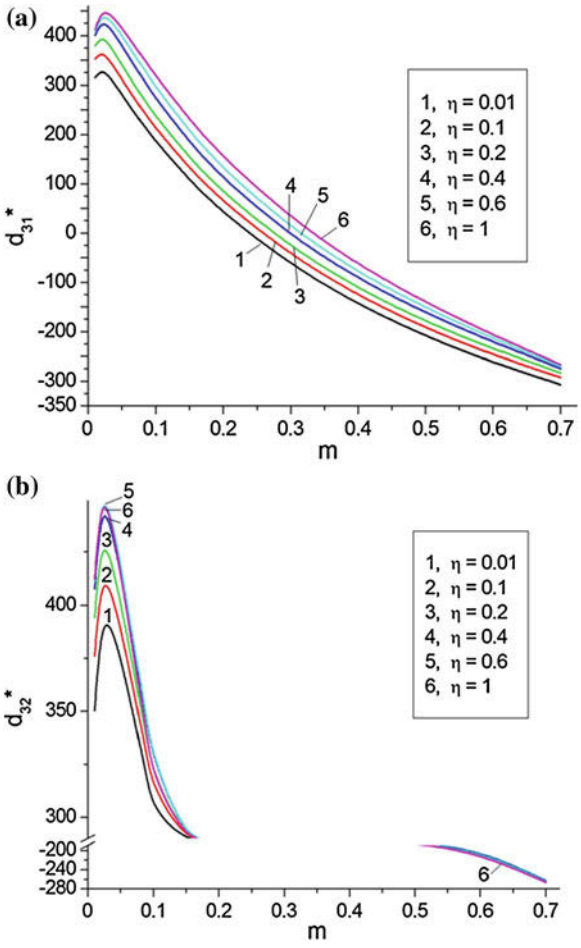

Fig. 4.11 Volume-fraction dependences of piezoelectric coefficients d_{3j}^* (**a–c**, in pC/N) and d_h^* (**d**, in pC/N) of a 1–3-type PCR-7M FC/ auxetic PE-9 composite with elliptical cross sections of rods, FEM calculations

influence of the lateral piezoelectric coefficients $d_{3j}^* > 0$ [see (3.2)]. Undoubtedly, the high performance of the 1–3-type composite with an auxetic polymer component (Table 4.4) is of value for hydroacoustic, sensor and actuator applications. Effective parameters are given in Table 4.4 for fixed volume fractions m of the FC component. It is clear that even after passing the extreme values of these parameters at $m < 0.05$, the performance of the composite remains high and can be regarded as a particular advantage.

A comparison of the data calculated for the 1–3-type composite with an auxetic polymer component at $\eta = 1$ shows that the effective electromechanical properties (c_{ab}^{*E}, e_{ij}^* and $\varepsilon_{pp}^{*\xi}$) determined by means of the EFM agree with the similar FEM evaluations in the volume-fraction range $0 < m \leq 0.7$. Differences between the

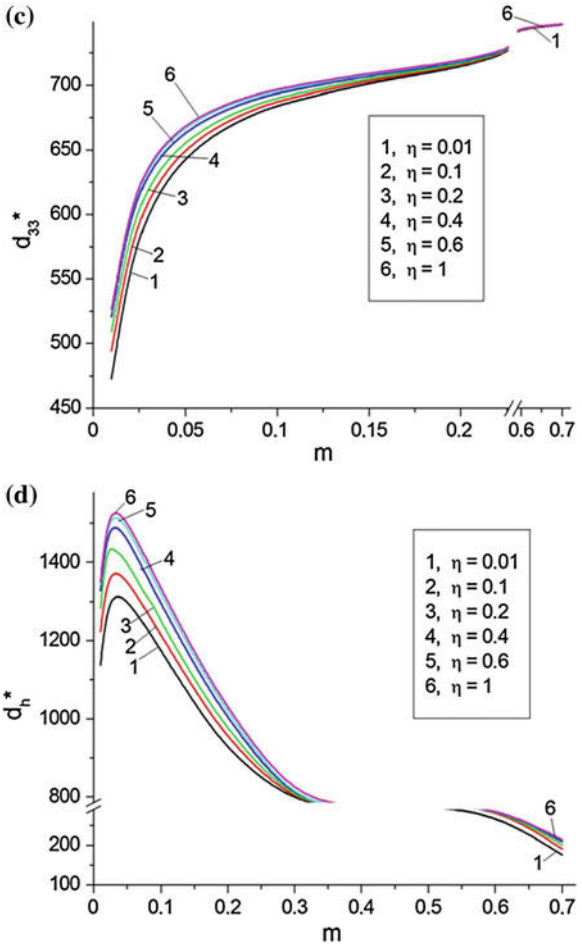

Fig. 4.11 (continued)

electromechanical constants calculated using the aforementioned methods for various combinations of FCs and auxetic polymers are $< 5\,\%$. It should be added that the largest values of hydrostatic parameters predicted for the related 1–3–0 PZT FC/auxetic polyurethane composite [29] are $d_h^* = 1,458\,\text{pC/N}$ and $(Q_h^*)^2 = 5.655 \times 10^{-9}\,\text{Pa}^{-1}$.

Table 4.4 Effective parameters of 1–3-type PCR-7M/PE composites with circular cross sections of rods at volume fractions of FC m = const (EFM data). g_{33}^* and g_h^* in mV· m / N, $(Q_{33}^*)^2$ and $(Q_h^*)^2$ in 10^{-15} Pa^{-1}, d_h^* in pC/N, and values of the volume fraction m are given in parentheses

Polymer component	g_{33}^*	$(Q_{33}^*)^2$	d_h^*	g_h^*	$(Q_h^*)^2$
Auxetic PE-1	290 (0.05)	1.64×10^5 (0.05)	1,230 (0.05)	629 (0.05)	7.72×10^5 (0.05)
	152 (0.10)	9.50×10^4 (0.10)	1,160 (0.10)	283 (0.10)	3.29×10^5 (0.10)
	103 (0.15)	6.75×10^4 (0.15)	1,050 (0.15)	166 (0.15)	1.08×10^5 (0.15)
Auxetic PE-4	312 (0.05)	2.12×10^5 (0.05)	1,020 (0.05)	467 (0.05)	4.74×10^5 (0.05)
	152 (0.10)	1.14×10^5 (0.10)	946 (0.10)	212 (0.10)	2.00×10^5 (0.10)
	103 (0.15)	7.81×10^4 (0.15)	855 (0.15)	126 (0.15)	1.08×10^5 (0.15)
Auxetic PE-6	315 (0.05)	2.20×10^5 (0.05)	1,160 (0.05)	523 (0.05)	6.03×10^5 (0.05)
	161 (0.10)	1.16×10^5 (0.10)	1,050 (0.10)	234 (0.10)	2.46×10^5 (0.10)
	108 (0.15)	7.90×10^4 (0.15)	941 (0.15)	138 (0.15)	1.30×10^5 (0.15)
Auxetic PE-8	310 (0.05)	2.07×10^5 (0.05)	1,240 (0.05)	577 (0.05)	7.17×10^5 (0.05)
	159 (0.10)	1.12×10^5 (0.10)	1,140 (0.10)	257 (0.10)	2.93×10^5 (0.10)
	107 (0.15)	7.69×10^4 (0.15)	1,020 (0.15)	151 (0.15)	1.54×10^5 (0.15)
Auxetic PE-9	311 (0.05)	2.08×10^5 (0.05)	1,500 (0.05)	696 (0.05)	1.04×10^6 (0.05)
	159 (0.10)	1.10×10^5 (0.10)	1,330 (0.10)	303 (0.10)	4.05×10^5 (0.10)
	107 (0.15)	7.57×10^4 (0.15)	1,170 (0.15)	1,76 (0.15)	2.05×10^5 (0.15)
Conventional high-density PE	296 (0.05)	1.78×10^5 (0.05)	334 (0.05)	165 (0.05)	5.51×10^4 (0.05)
	156 (0.10)	1.05×10^5 (0.10)	349 (0.10)	81.0 (0.10)	2.83×10^4 (0.10)
	106 (0.15)	7.41×10^4 (0.15)	338 (0.15)	51.2 (0.15)	1.73×10^4 (0.15)

4.4 Conclusion

In Chap. 4 we have systematised results on 1–3 and related composites wherein their orientation effects influence the electromechanical properties and hydrostatic response. The presence of the aligned piezo-active rods and the matrix with specific ratios of elastic constants influence the anisotropy of the piezoelectric coefficients, ECFs etc. Based on the results of Chap. 4, we conclude as follows.

1. The results on the orientation effect (Sect. 4.1.2) indicate the potential advantages of the 1–3 composites examined based on PZN–0.07SCs. For instance, the composite based on [001]–poled SC is more suitable for actuator applications requiring a large d_{33}^* value. For sensor applications demanding a large g_{33}^* value, the composite comprising [011]-poled rods ($\varphi = 0°$) and the matrix with the remanent polarisation $\boldsymbol{P}_r^{(2)} \uparrow\downarrow \boldsymbol{P}_s^{(1)}$ is suitable. The largest values of the hydrostatic piezoelectric coefficient d_h^* and squared figures of merit $(Q_{33}^*)^2$and $(Q_h^*)^2$ are achieved in the composite that contains [001]-poled rods and a matrix with $\boldsymbol{P}_r^{(2)} \uparrow\downarrow \boldsymbol{P}_s^{(1)}$.
2. Changes in porosity m_p and aspect ratio of the pore ρ_p in the polymer matrix open up possibilities for creating novel 1–3–0 SC/porous polymer composites (Sect. 4.1.3) with large anisotropy factors ζ_{3j}, ζ_{t-p} and ζ_d and piezoelectric activity that certainly exceeds the piezoelectric activity of the anisotropic ferroelectric $PbTiO_3$-type FCs. It is important to note that the anisotropy factors ζ_{3j}, ζ_{t-p} are expressed in terms of ζ_d and elastic compliances s_{ab}^{*E} of the composite [see (4.13) and (4.14)]. Among s_{ab}^{*E} one can single out s_{11}^{*E} and s_{33}^{*E} as parameters that promote a significant re-distribution of internal fields and influence the anisotropy of ECFs in a wide volume-fraction range.
3. The increase in the hydrostatic piezoelectric coefficients d_h^* and g_h^* and squared figure of merit $(Q_h^*)^2$ of the 1–3–0 FC/porous polymer composite is attained in a variety of ways (Sect. 4.2) due to variations of volume fractions of FC and pores, changes in the aspect ratio and /or orientation of pores, the elastic anisotropy of the porous matrix, and other factors. The orientation of the spheroidal pores in the polymer matrix can improve piezoelectric sensitivity and hydrostatic parameters of the composite due to a more favourable balance of the piezoelectric coefficients d_{3j}^* and g_{3j}^*. This balance is mainly achieved due to the elastic anisotropy of the porous polymer matrix.
4. The 1–3 FC/polymer composites with rods in the form of elliptical cylinders are characterised by *mm*2 symmetry and a specific anisotropy of the effective electromechanical properties and ECFs (Sects. 4.3.2 and 4.3.3). The aspect ratio η of the ellipse in the rod base is an important factor that influences the anisotropy of the piezoelectric coefficients of the composites examined.
5. An auxetic PE matrix with a negative Poisson's ratio promotes relatively large values of maxima of effective hydrostatic parameters d_h^*, g_h^* and $(Q_h^*)^2$ and piezoelectric coefficient g_{33}^* for the 1–3-type composite based on the PZT-type FC (Sects. 4.3.4 and 4.3.5). While the FC component shows the piezoelectric

anisotropy $d_{33}^{(1)}/|d_{31}^{(1)}| \approx 2.2$ at $d_{33}^{(1)} \approx 750$ pC / N [3, 31], the auxetic component promotes $d_h^* \sim 10^3$ pC/N, $g_h^* \sim 10^2$ mV· m /N and $(Q_h^*)^2 \sim (10^{-10}-10^{-9})$ Pa^{-1} (Table 4.4) due to the piezoelectric coefficients $d_{3j}^* > 0$. Such behaviour opens up new possibilities of use of the composites with the high piezoelectric activity at $\zeta_d^* \gg 1$ and $\zeta_k^* \gg 1$.

References

1. Newnham RE, Skinner DP, Cross LE (1978) Connectivity and piezoelectric-pyroelectric composites. Mater Res Bull 13:525–536
2. Akdogan EK, Allahverdi M, Safari A (2005) Piezoelectric composites for sensor and actuator applications. IEEE Trans Ultrason Ferroelectr Freq Control 52:746–775
3. Topolov VYu, Bowen CR (2009) Electromechanical properties in composites based on ferroelectrics. Springer, London
4. Chan HLW, Unsworth J (1989) Simple model for piezoelectric ceramic/polymer 1–3 composites used in ultrasonic transducer applications. IEEE Trans Ultra Ferroelectr Freq Control 36:434–441
5. Taunaumang H, Guy IL, Chan HLW (1994) Electromechanical properties of 1–3 piezoelectric ceramic/piezoelectric polymer composites. J Appl Phys 76:484–489
6. Wang F, He C, Tang Y (2007) Single crystal 0.7Pb($Mg_{1/3}Nb_{2/3}$)O_3–0.3$PbTiO_3$ epoxy 1–3 piezoelectric composites prepared by the lamination technique. Mater Chem Phys 105:273–277
7. Topolov VYu, Panich AE (2009) Problem of piezoelectric sensitivity of 1–3-type composites based on ferroelectric ceramics. Ferroelectrics 392:107–119
8. Topolov VYu, Krivoruchko AV, Bisegna P (2011) Electromechanical coupling and its anisotropy in a novel 1–3–0 composite based on single-domain 0.58Pb($Mg_{1/3}Nb_{2/3}$)O_3–0.42$PbTiO_3$ crystal. Compos Sci Tech 71:1082–1088
9. Zhang R, Jiang B, Cao W, Amin A (2002) Complete set of material constants of 0.93Pb($Zn_{1/3}Nb_{2/3}$)O_3–0.07$PbTiO_3$ domain engineered single crystal. J Mater Sci Lett 21:1877–1879
10. Zhang R, Jiang B, Jiang W, Cao W (2002) Complete set of elastic, dielectric, and piezoelectric coefficients of 0.93Pb($Zn_{1/3}Nb_{2/3}$)O_3–0.07$PbTiO_3$ single crystal poled along [011]. Appl Phys Lett 89:242908 (3 pp.)
11. Topolov VYu, Krivoruchko AV, Bisegna P, Bowen CR (2008) Orientation effects in 1–3 composites based on 0.93Pb($Zn_{1/3}Nb_{2/3}$)O_3–0.07$PbTiO_3$ single crystals. Ferroelectrics 376:140–152
12. Sessler GM (1981) Piezoelectricity in polyvinylidenefluoride. J Acoust Soc Am 70:1596–1608
13. Bennett J, Hayward G (1997) Design of 1–3 piezocomposite hydrophones using finite element analysis. IEEE Trans Ultrason Ferroelectr Freq Control 44:565–574
14. Poizat C, Sester M (1997) Effective properties of composites with embedded piezoelectric fibres. Comput Mater Sci 16:89–97
15. Pettermann HE, Suresh S (2000) A comprehensive unit cell model: a study of coupled effects in piezoelectric 1–3 composites. Int J Solids Struct 37:5447–5464
16. Kar-Gupta R, Venkatesh TA (2005) Electromechanical response of 1–3 piezoelectric composites: effect of poling characteristics. J Appl Phys 98:054102 (14 pp.)
17. Kar-Gupta R, Marcheselli C, Venkatesh TA (2008) Electromechanical response of 1–3 piezoelectric composites: effect of fiber shape. J Appl Phys 104:024105 (17 pp.)
18. Kar-Gupta R, Venkatesh TA (2008) Electromechanical response of piezoelectric composites: effects of geometric connectivity and grain size. Acta Mater 56:3810–3823
19. Topolov VYu, Bisegna P, Krivoruchko AV (2008) Features of electromechanical properties of 1–3 composites based on $PbTiO_3$–type ceramics. J Phys D Appl Phys 41:035406 (8 pp.)

20. COMSOL, Inc. 2007, COMSOL Multiphysics™User's Guide (version 3.4). http://www.comsol.com/
21. Kar-Gupta R, Venkatesh TA (2007) Electromechanical response of 1–3 piezoelectric composites: an analytical model. Acta Mater 55:1093–1108
22. Choy SH, Chan HLW, Ng MW, Liu PCK (2004) Study of 1–3 PZT fibre/epoxy composites with low volume fraction of ceramics. Integr Ferroelectr 63:109–115
23. Ikeda T (1990) Fundamentals of piezoelectricity. Oxford University Press, Oxford, New York, Toronto
24. Asakawa K, Hiraoka T, Akasaka Y, Hotta Y, (2004) Method for manufacturing porous structure and method for forming pattern. US Patent 6,565,763
25. Clark P, Moya W (2003) Three dimensional patterned porous structures. US Patent 6,627,291
26. Huang JH, Yu S (1994) Electroelastic Eshelby tensors for an ellipsoidal piezoelectric inclusion. Compos Eng 4:1169–1182
27. Dunn ML, Taya M (1993) Electromechanical properties of porous piezoelectric ceramics. J Am Ceram Soc 76:1697–1706
28. Cao H, Hugo Schmidt V (2004) Elastic, piezoelectric, and dielectric properties of $0.58Pb(Mg_{1/3}Nb_{2/3})O_3$–$0.42PbTiO_3$ single crystal. J Appl Phys 96:549–554
29. Gibiansky LV, Torquato S (1997) On the use of homogenization theory to design optimal piezocomposites for hydrophone applications. J Mech Phys Solids 45:689–708
30. Ikegami S, Ueda I, Nagata T (1971) Electromechanical properties of $PbTiO_3$ ceramics containing La and Mn. J Acoust Soc Am 50:1060–1066
31. Dantsiger AYa, Razumovskaya ON, Reznitchenko LA, Grineva LD, Devlikanova RU, Dudkina SI, Gavrilyatchenko SV, Dergunova NV, Klevtsov AN, (1994) Highly effective piezoceramic materials (Handbook). Kniga, Rostov-on-Don (in Russian)
32. Topolov VYu, Turik AV (2001) Porous piezoelectric composites with extremely high reception parameters. Tech Phys 46:1093–1100
33. Haun MJ, Newnham RE (1986) An experimental and theoretical study of 1–3 and 1–3–0 piezoelectric PZT-polymer composites for hydrophone applications. Ferroelectrics 68:123–139
34. Topolov VYu, Bisegna P (2010) Anisotropic piezoelectric properties of 1–3 ceramic/polymer composites comprising rods with elliptic cross section. J Electroceram 25:26–37
35. Ng KL, Chan HLW, Choy CL (2000) Piezoelectric and pyroelectric properties of PZT/P(VDF-TrFE) composites with constituent phases poled in parallel or antiparallel directions. IEEE Trans Ultrason Ferroelectr Freq Control 47:1308–1315
36. Sessler GM (1994) Poling and properties of polarization of ferroelectric polymers and composites. Key Eng Mater 92–93:249–274
37. Levassort F, Lethiecq M, Certon D, Patat F (1997) A matrix method for modeling electroelastic moduli of 0–3 piezo-composites. IEEE Trans Ultrason Ferroelectr Freq Control 44:445–452
38. Grekov AA, Kramarov SO, Kuprienko AA (1989) Effective properties of a transversely isotropic piezoelectric composite with cylindrical inclusions. Mech Compos Mater 25:54–61
39. Lakes R (1987) Foam structures with a negative Poisson's ratio. Science 235:1038–1040
40. Friis EA, Lakes RS, Park JB (1988) Negative Poisson's ratio polymeric and metallic foams. J Mater Sci 23:4406–4414
41. Choi JB, Lakes R (1992) Nonlinear properties of polymer cellular materials with a negative Poisson's ratio. J Mater Sci 27:4678–4684
42. Evans KE, Alderson KL (1992) The static and dynamic moduli of auxetic microporous polyethylene. J Mater Sci Lett 11:1721–1724
43. Smith WA, (1991) Optimizing electromechanical coupling in piezocomposites using polymers with negative Poisson's ratio. In: Proceedings of the IEEE ultrasonics symposium, December 8–11, 1991, Lake Buena Vista, FL, USA. V. 1. IEEE, New York, pp 661–666
44. Liu Y, Hu H (2010) A review on auxetic structures and polymeric materials. Sci Res Essays 5:1052–1063

45. Topolov VYu, Bowen CR (2008) Characteristics of 1–3-type ferroelectric ceramic/auxetic polymer composites. Modell Simul Mater Sci Eng 16:015007 (12 pp.)
46. Groznov IN, (1983) Dielectric permittivity. In: Physics encyclopaedia. Sovetskaya Entsiklopediya, Moscow, pp 178–179 (in Russian)

Chapter 5
Orientation Effects and Anisotropy of Properties in 0–3 Composites

A piezo-active composite with 0–3 connectivity represents a system of isolated inclusions (either FC or ferroelectric SC) in a large matrix that may be either a polymer or FC. As follows from the analysis of papers on 0–3 ferroelectric based composites, in the last decades the FC/polymer composites have attracted widespread interest as they are attractive for piezo-technical applications [1–3]. Of an independent interest are the SC/polymer [3] and SC/FC [3–5] composites with various 0–3 connectivity patterns. The effective electromechanical properties of 0–3 composites comprising one or two ferroelectric components have been studied using experimental [6–12] and theoretical [3, 13–19] methods. In these studies the microgeometry of the composite, electromechanical properties of its components, poling conditions of the composite sample, etc. have been discussed to show specific advantages of the 0–3 composite materials. The role of the microgeometrical factor in forming the electromechanical properties at a transition from the 0–3 connectivity pattern to related patterns [3, 18] is also of interest in the context of the prediction of the performance of the composite materials.

Chapter 5 is concerned with the study of the effective properties, their anisotropy and orientation effects in piezo-active 0–3 composites. We discuss results on the 0–3 composites and show routes for improving some parameters of these materials to make them more suitable for a variety of piezo-technical applications.

5.1 Composites Based on Ferroelectric Ceramics

5.1.1 Role of Microgeometry in Forming the Large Anisotropy of Properties

The 0–3 $PbTiO_3$-type FC/epoxy resin composite is an example of a modern piezo-active material prepared by electric-field structuring [12]. The microstructure and electromechanical properties of this composite are attained due to use of

V. Yu. Topolov et al., *Piezo-Active Composites*,
Springer Series in Materials Science 185, DOI: 10.1007/978-3-642-38354-0_5,

dielectrophoresis for the structural modification. When using this process, a dispersion of FC particles embedded in a liquid polymer or pre-polymer is exposed to a moderate electric field, that leads to the formation of chain-like structures in a polymer matrix. After a solidification of the polymer medium, these structures remain stable in the composite sample [12]. An analysis of the composite microstructure suggests that this material is characterised by 0–3 connectivity, and the shape of the FC inclusions therein approaches a spheroidal shape.

The effective electromechanical properties of the 0–3 FC/polymer composite with spheroidal inclusions can be predicted on the basis of different averaging methods and procedures (see, e.g., papers [3, 13–15, 17, 19]) where full sets of electromechanical constants were predicted. We follow a model [19] that has first been applied to 0–3 composites based on the $(Pb_{1-x}Ca_x)TiO_3$ FC [3] with a large piezoelectric anisotropy. In this model the shape of each inclusion (Fig. 5.1, component 1) is spheroidal and obeys Eq. (3.27) relative to the axes of the rectangular co-ordinate system $(X_1X_2X_3)$. The semi-axes of each spheroidal inclusion are $a_1 = a_2$ and a_3, and the aspect ratio is $\rho = a_1/a_3$. A remanent polarisation vector of each inclusion is $\boldsymbol{P}_r^{(1)} \uparrow\uparrow OX_3$, and the OX_3 axis is the poling axis of the composite sample as a whole. A regular distribution of spheroidal inclusions is considered so that these inclusions would occupy sites of a simple tetragonal lattice with unit-cell vectors parallel to the OX_j axes. Electrical conductivities $\gamma^{(1)}$ of the FC and $\gamma^{(2)}$ of the polymer are linked with an inequality $\gamma^{(2)} \geq \gamma^{(1)}$, and surface charges caused by the ferroelectric polarisation are fully screened by free carriers coming to the interfaces in the composite sample.

The components of the composite are characterised by sets of elastic moduli $c_{ab}^{(n),E}$, piezoelectric coefficients $e_{ij}^{(n)}$ and dielectric permittivities $\varepsilon_{pp}^{(n),\xi}$, where $n = 1$ is related to FC (inclusions), and $n = 2$ is related to polymer (the surrounding matrix). The effective electromechanical properties determined in the long-wavelength limit [3] depend on the volume fraction m of FC and the aspect ratio ρ.

The calculation procedure is based on the EFM and Eshelby's concept of spheroidal inclusions [3, 17, 19, 20], and this concept is regarded [3, 17] as a variant of the self-consistent scheme for the calculation of effective constants of the piezoactive composite. A matrix of the effective electromechanical properties of the 0–3 composite is determined as $||C^*|| = ||C^*(m, \rho)||$ in accordance with (4.22) and is

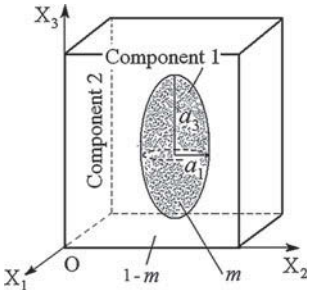

Fig. 5.1 Schematic of the 0–3 composite with spheroidal inclusions. $(X_1X_2X_3)$ is the rectangular co-ordinate system, a_i are semi-axes of the spheroid, m is the volume fraction of component 1, and $1 - m$ is the volume fraction of component 2

represented in the general form (4.1). The electromechanical properties are characterised by $||C^{(1)}||$ (FC) and $||C^{(2)}||$ (polymer), and these matrices have the form similar to that shown in (4.1).

As is known from experimental data [3, 19], important features of the $PbTiO_3$-type FCs are three positive piezoelectric coefficients $e_{ij}^{(1)}$ (Table 5.1) and a large anisotropy of the piezoelectric coefficients $d_{3j}^{(1)}$ at room temperature, i.e., an inequality $d_{33}^{(1)}/|d_{31}^{(1)}| \gg 1$ holds, and signs of $d_{3j}^{(1)}$ obey (4.3). Examples of the calculated volume-fraction dependence of effective parameters of the 0–3 composite based on the modified $PbTiO_3$ FC are shown in Fig. 5.2. To avoid some distinctions between the properties of the $PbTiO_3$-type FC from experimental work [12] and the modified $PbTiO_3$ FC [3] involved in our calculations, we introduce normalised dielectric permittivity $\beta_\varepsilon = \varepsilon_{33}^{*\sigma}/\varepsilon_{33}^{(1),\sigma}$ and normalised piezoelectric coefficients $\beta_d = d_{33}^*/d_{33}^{(1)}$ and $\beta_g = g_{33}^*/g_{33}^{(1)}$. Good agreement between the experimental and calculated volume-fraction dependences of β_ε is observed at aspect ratios $\rho = 0.13 - 0.19$ (Fig. 5.2a). The structured 0–3 FC/polymer composite can be represented as an aggregate of prolate inclusions in a matrix, with the aforementioned aspect ratios of these inclusions. A similar microstructure of the 0–3 composite is observed in experimental work [12]. The volume-fraction dependence of β_ε for an unstructured 0–3 composite with the same components may be approximated by pieces of curves at $\rho \approx 0.32 - 0.50$ (Fig. 5.2b). It is obvious that a transition from the prolate FC inclusion (oriented along the poling direction) to the spherical (or oblate) FC inclusion leads to the creation of obstacles for poling the composite sample and leads to poor piezoelectric properties.

Among the piezoelectric coefficients d_{3j}^*, e_{3j}^*, g_{3j}^*, and h_{3j}^* of the studied 0–3 composite, g_{31}^* and g_{33}^* are the most sensitive [19, 21] to changes in the volume fraction m and the aspect ratio ρ of the SC inclusions. For example, at $\rho = 0.01-0.20$, ratios $\max \beta_g \approx 3 - 10$ and $\min g_{31}^*/g_{31}^{(1)} \approx 9 - 40$ are attained. A difference between the aforementioned ratios is related to the key role of the system of the prolate FC inclusions in forming the anisotropic piezoelectric response of the 0–3 composite (Fig. 5.1). Due to this system, the volume-fraction dependence of β_d and β_g (Fig. 5.2c, d) resembles the volume-fraction dependence of the piezoelectric coefficients d_{33}^* and g_{33}^*, respectively, in the 1–3$PbTiO_3$-type FC/polymer composite [3, 18]. An advantage of the studied 0–3 composite is the relatively large $\max \beta_g$ values near the volume fraction $m = 0.1$ at various aspect ratios ρ (Fig. 5.2d), and this performance is concerned with a favourable balance of elastic moduli $c_{ab}^{(n),E}$ of components and with a relatively low dielectric permittivity $\varepsilon_{33}^{*\sigma}$ of the composite at $0 < m \leq 0.1$. As follows from (1.12), $\varepsilon_{33}^{*\sigma}$ strongly influences both g_{33}^* and β_g of the composite. Examples of behaviour of two anisotropy factors, ζ_d^* from (4.24) and

$$\zeta_e^* = e_{33}^*/e_{31}^* = (2d_{31}^* c_{13}^{*E} + d_{33}^* c_{33}^{*E})/[d_{31}^*(c_{11}^{*E} + c_{12}^{*E}) + d_{33}^* c_{13}^{*E}], \tag{5.1}$$

are shown in Fig. 5.2e, f, respectively. It is seen that ζ_e^* is varied in a wider range, and this variation is due to the influence of elastic properties of the FC and polymer

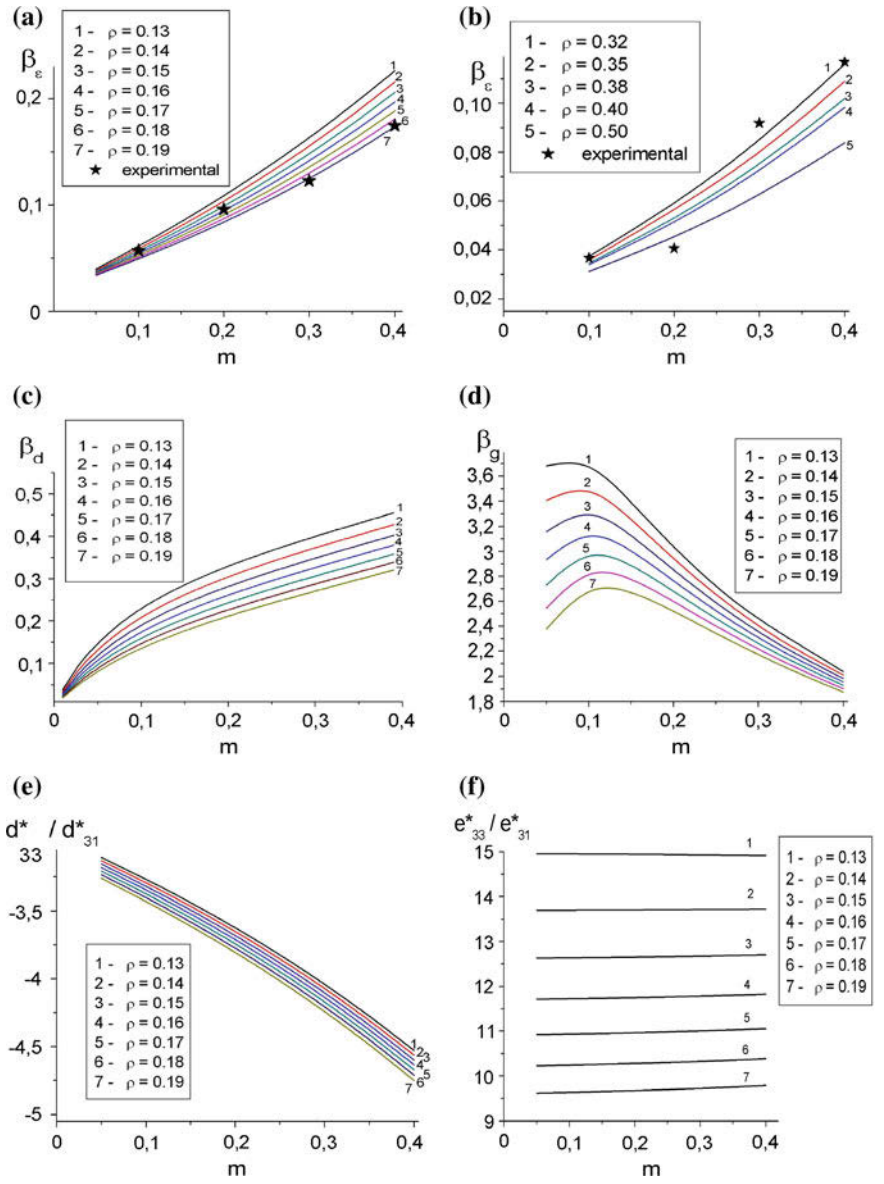

Fig. 5.2 Volume-fraction dependence of normalised dielectric permittivity β_ε (**a**), (**b**) normalised piezoelectric coefficients β_d (**c**) and β_d (**d**), and factors of the piezoelectric anisotropy ζ_d^* (**e**) and ζ_e^* (**f**) of the 0–3 $PbTiO_3$-based FC/epoxy composite. Graphs **a** and **b** correspond to the structured composite and unstructured composite, respectively. Experimental points are from dielectric measurements [12] (reprinted from paper by Topolov and Krivoruchko [22], with permission from Nova Science Publishers)

Table 5.1 Room-temperature values of elastic moduli c^E_{pq} (in 10^{10} Pa),[a] piezoelectric coefficients e_{fp} (in C / m^2) and dielectric permittivities ε^{ξ}_{ff} of FCs of the $PbTiO_3$ and PZT types

	$(Pb_{0.9625}La_{0.025})\cdot(Ti_{0.99}Mn_{0.01})O_3$ (modified $PbTiO_3$)[b] [21]	$(Pb_{0.80}Ca_{0.20})\cdot TiO_3^c$ [19]	$(Pb_{0.75}Ca_{0.25})\cdot TiO_3^c$ [19]	ZTS-19 [13][b]
c^E_{11}	14.33	18.5	18.9	10.9
c^E_{12}	3.220	4.76	5.19	6.1
c^E_{13}	2.413	4.68	5.06	5.4
c^E_{33}	13.16	18.0	18.3	9.3
c^E_{44}	5.587	6.79	6.76	2.4
e_{31}	0.4584	0.844	1.33	–4.9
e_{33}	6.499	4.31	5.09	14.9
e_{15}	5.923	1.77	1.95	10.6
$\varepsilon^{\xi}_{11}/\varepsilon_0$	210	126	152	820
$\varepsilon^{\xi}_{33}/\varepsilon_0$	140	123	147	840

[a] FCs poled along the OX_3 axis are characterised [3, 13–15] by ∞mm symmetry and a relation $c_{66} = (c^E_{11} - c^E_{12})/2$

[b] Experimental values of the PZT-type FC

[c] Electromechanical constants have been calculated using the EMM. Spherical grains of the FC sample are assumed to be split into 90° lamellar domains of two types with equal volume fractions, and these domains are separated by planar 90° domain walls. These domain walls are assumed to be almost motionless so that a contribution from their displacements under external electric or mechanical fields into the electromechanical constants of the ceramic approaches zero [19]

components on the piezoelectric coefficients e^*_{3j} in the presence of the prolate FC inclusions (Fig. 5.1). Changes in the anisotropy factor ζ^*_d are observed in a narrow range, while the system of the isolated FC inclusions is surrounded by the piezo-passive polymer matrix, that impedes an electromechanical interaction between the inclusions. On increasing the volume fraction m, $|\zeta^*_d|$ increases (Fig. 5.2e) due to the large anisotropy factor $d^{(1)}_{33}/d^{(1)}_{31}$ of the modified $PbTiO_3$ FC, and in this case the aspect ratio ρ cannot strongly influence $\zeta^*_d(m)$.

5.1.2 Variations of the Anisotropy Factors

In Sect. 5.1.2 we discuss examples of changes in the anisotropy factors $\zeta^*_d(m)$ and $\zeta^*_k(m)$ in the 0–3 FC-based composites and choose FC compositions with different ratios $d^{(1)}_{33}/|d^{(1)}_{31}|$ and $e^{(1)}_{33}/e^{(1)}_{31}$. For example, the $(Pb_{1-x}Ca_x)O_3$ FC is characterised by ratios $d^{(1)}_{33}/|d^{(1)}_{31}| > 10$ and $e^{(1)}_{33}/e^{(1)}_{31} \approx 4$–5 at $e^{(1)}_{ij} > 0$ [19], while the ZTS-19 FC based on $Pb(Zr_{1-x}Ti_x)O_3$ is characterised by moderate ratios $d^{(1)}_{33}/|d^{(1)}_{31}|$ and $e^{(1)}_{33}/|e^{(1)}_{31}|$ [13] (see full sets of electromechanical constants in Table 5.1).

To compare results, we use two methods for averaging the electromechanical properties, namely, the EFM [see Eq. (4.22)] and FEM. The COMSOL package [23] is applied to obtain the volume-fraction dependence of the effective electromechanical properties of the 0–3 composite within the framework of the FEM. A representative unit cell, containing the spheroidal inclusion (Fig. 5.3a) with a radius adjusted to yield the appropriate volume fraction m, is discretised using tetrahedral elements [24]. Their number, depending on the aspect ratio ρ of the spheroidal inclusion, varies from 320,000 to 760,000. The unknown displacement and electric-potential fields are interpolated using linear Lagrangian shape functions. The corresponding number of degrees of freedom varies from 200,000 to 500,000. Periodic boundary conditions are enforced on the boundary of the representative unit cell. The matrix of effective constants of the composite is computed column-wise, performing calculations for diverse average strain and electric fields imposed to the structure. The Geometric Multigrid [25] iterative solver (V-cycle, successive over-relaxation pre- and post-smoother, direct coarse solver) is employed. After solving the electroelastic equilibrium problem, the effective electromechanical constants of the 0–3-composite are computed, by averaging the resulting local stress and electric-displacement fields over the unit cell shown in Fig. 5.3a. In both the EFM [3] and FEM [24] the matrix of the effective electromechanical properties $\| C^* \|$ is represented in the form (4.1) and regarded as a function of m and ρ.

Graphs in Fig. 5.3b–d suggest that the EFM and FEM data on the anisotropy factors from (4.24) are consistent for the $(Pb_{1-x}Ca_x)O_3$-based composite. Some discrepancies, especially at $m > 0.2$, are due to the electromechanical interaction between the FC inclusions being taken into account in the FEM averaging procedure. In the composite with the softer polymer matrix (data in Fig. 5.3d) differences between the curves calculated using the EFM and FEM become more pronounced. This means that the so-called effective field would have a stronger influence on the effective properties in the case of the stiffer matrix, however this peculiarity of the electromechanical interaction is not emphasised in the EFM averaging procedure and Eq. (4.22). Data from Fig. 5.3b–d are of interest for sensor and antenna applications of the composite while conditions $|\zeta_d^*| > 5$ and $|\zeta_k^*| > 5$ hold simultaneously.

The next example is concerned with the anisotropy factors $\zeta_d^*(m)$ and $\zeta_k^*(m)$ of a 0–3 ZTS-19 FC / clay composite with spheroidal inclusions. Clay is an isotropic material with Young modulus 300 MPa, Poisson's ratio 0.30 and dielectric permittivity 8.0 [26, 27]. The EFM prediction of the effective properties of the 0–3 composite was carried out using Eq. (4.22), and the FEM modelling was performed using the COMSOL package [23] as described above.

The anisotropy factor $\zeta_d^*(m)$ is represented by either an increasing or decreasing dependence, and some differences between values of $\zeta_k^*(m)$ calculated using the EFM and FEM are observed (Fig. 5.4). These discrepancies are accounted for by an approximate character of the EFM and by not taking into account the internal electroelastic fields when considering the FC component exhibiting considerable piezoelectric activity (for instance, in ZTS-19 $d_{3j}^{(1)} \sim 10^2$ pC / N [28]). A comparison of graphs in Fig. 5.4 enables us to conclude that the prolate shape of the spheroidal

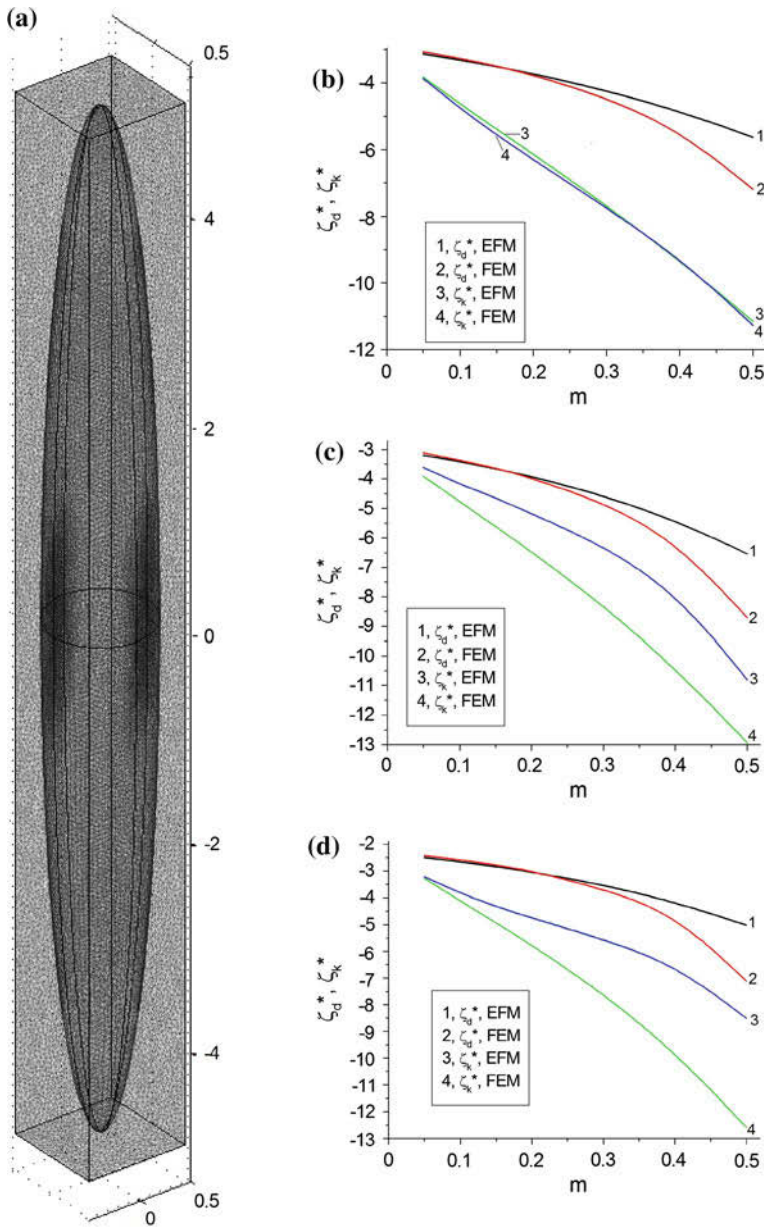

Fig. 5.3 Representative unit cell of the 0–3 composite (**a**) with spheroidal inclusions at FEM modelling and anisotropy factors ζ_d^* and ζ_k^* which have been calculated for the following 0–3 composites at $\rho = 0.1$: $(Pb_{0.80}Ca_{0.20})O_3$ FC/araldite (**b**) $(Pb_{0.75}Ca_{0.25})O_3$ FC/araldite (**c**) and $(Pb_{0.75}Ca_{0.25})O_3$ FC/elastomer (**d**)

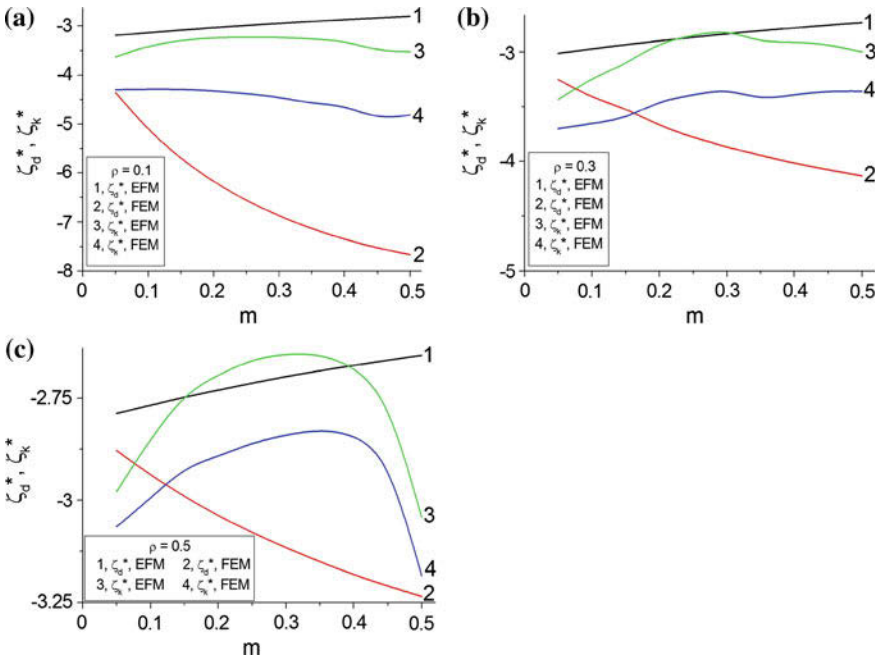

Fig. 5.4 Anisotropy factors ζ_d^* and ζ_k^* which have been calculated for the 0–3 ZTS-19 FC/clay composite with spheroidal inclusions at $\rho = 0.1$ (**a**), 0.3 (**b**), 0.5 (**c**)

inclusions (Fig. 5.1) in the composite sample promotes and increasing $|\zeta_d^*|$, but in a restricted range only. Variations of ζ_k^* are observed in the restricted ranges irrespective of the aspect ratio ρ (see curves 3 and 4 in Fig. 5.4). We remind the reader that ζ_d^* and ζ_k^* are linked in accordance with (4.24), and therefore, the elastic anisotropy of the studied composite does not promote a large increase of $|\zeta_k^*|$ with changes in m and ρ. It should be added that the piezoelectric activity of the ZTS-19 FC / clay composite rapidly decreases as the aspect ratio ρ increases at m = const.

Thus, the above-given examples show that high values of $|\zeta_d^*|$ and $|\zeta_k^*|$ can be simultaneously reached in $(Pb_{1-x}Ca_x)O_3$-based composites (Fig. 5.3b–d). This composite contains the highly anisotropic piezo-active component [$(Pb_{1-x}Ca_x)O_3$ FC, $x = 0.20$ or 0.25] distributed as a system of the aligned prolate spheroidal inclusions, and this circumstance plays the dominating role in forming the anisotropic 0–3 composite.

5.2 Relaxor-Ferroelectric Single Crystal/Polymer Composites

In Sect. 5.2 we consider examples of the performance of 0–3 composites with spheroidal SC inclusions (Fig. 5.1) that are uniformly aligned in the matrix and form a

periodic structure. It is assumed, that the main crystallographic axes x, y and z in each inclusion obey conditions x $\parallel OX_1$, y $\parallel OX_2$ and z $\parallel OX_3$, and centres of symmetry of the inclusions occupy sites of a simple lattice with unit-cell vectors parallel to the OX_j axes. The SC inclusions have a spontaneous polarisation $\boldsymbol{P}_s^{(1)} \parallel$ z $\parallel OX_3$, and the composite sample as a whole is poled along the OX_3 axis.

To determine the effective electromechanical properties of the 0–3 SC/polymer composite, we apply averaging procedures [3, 24] that allow for an electromechanical interaction between the piezo-active SC inclusions in the surrounding medium. This medium can be either piezo-passive or piezo-active, but the piezoelectric activity of the SC incluison remains higher than that of the surrounding medium. The first procedure is based on the EFM, the second procedure is based on the EMM, and the third procedure is concerned with the FEM modelling by means of the COMSOL package (details are in Sect. 5.1.2). In the EFM approach the full set of electromechanical constants of the composite is determined from (4.22). In the EMM approach a single inclusion is considered to be surrounded by a homogenised (effective) medium, and this medium is regarded as a matrix with the similar inclusions. The effective electromechanical properties of the 0–3 composite are found according to the EMM [3, 24] from the matrix

$$\parallel C^* \parallel = \parallel C^{(2)} \parallel + m(\parallel C^{(1)} \parallel - \parallel C^{(2)} \parallel) \parallel A \parallel . \tag{5.2}$$

The matrix $\parallel A \parallel$ from (5.2) is related to the boundary conditions in the "inclusion—surrounding medium" region (see Fig. 5.1) and represented [3, 19, 22, 24] as

$$\parallel A \parallel = [\parallel I \parallel + \parallel S \parallel \parallel C^* \parallel^{-1} (\parallel C^{(1)} \parallel - \parallel C^* \parallel)]^{-1}, \tag{5.3}$$

where $\parallel I \parallel$ is the 9×9 identity matrix, $\parallel S \parallel$ is the 9×9 matrix containing components of the Eshelby electroelastic tensor [20], and $\parallel C^* \parallel$ is the 9×9 matrix from (5.2). It should be noted that elements of $\parallel S \parallel$ from (5.3) depend on electromechanical constants of the matrix of the 0–3 composite and on the aspect ratio $\rho = a_1/a_3$ of the spheroidal inclusion (Fig. 5.1). In the EMM [24] the effective electromechanical properties of the composite (i.e., elements of $\parallel C^* \parallel = \parallel C^*(m, \rho) \parallel$) are evaluated as a result of a series of iterations involving (5.2) and (5.3). In the three aforementioned methods, i.e., within the framework of the EFM, EMM and FEM approaches, the effective properties of the composite are determined in the long-wave approximation [3]. This approximation is appropriate in a case when the wavelength of an external acoustic field is much longer than the semi-axes a_1 and a_3 of the separate inclusion (see Fig. 5.1).

5.2.1 Electromechanical Properties

To predict the performance of the 0–3 composite, we use full sets of experimental values of elastic moduli $c_{ab}^{(n),E}$, piezoelectric coefficients $e_{ij}^{(n)}$ and dielectric permittivities $\varepsilon_{pq}^{(n),\xi}$ [3, 19, 24]. These constants are involved in $\| C^{(n)} \|$ from (5.2) and (5.3). Among the relaxor-ferroelectric SC components, of particular interest is the PMN–0.33PT composition [29] chosen near the MPB. As is known, at room temperature the single-domain PMN–0.33PT SC is characterised by a rhombohedral distortion of the perovskite unit cell (3*m* symmetry, see Sect. 2.1). However, the domain-engineered PMN–0.33PT SC [29] poled along the perovskite unit-cell axis z ∥ [001] is characterised by macroscopic 4*mm* symmetry and four domain types (Fig. 2.4) that provide the effective spontaneous polarisation $\boldsymbol{P}_s^{(1)} \parallel OX_3$ of the SC sample. Electromechanical constants of the domain-engineered PMN–0.33PT SC are given in Table 5.2[1]. It should be added that this domain-engineered SC shows a high piezoelectric activity ($d_{3j}^{(1)} \sim 10^3$ pC / N) [29] and a considerable anisotropy of the piezoelectric coefficients $e_{3j}^{(1)}$: as follows from Table 5.2, $e_{33}^{(1)}/|e_{31}^{(1)}| = 5.6$.

Now we compare results on the effective properties and related parameters in a 0–3 PMN–0.33PT SC/araldite composite. In an attempt to attain large absolute values of the longitudinal piezoelectric coefficients $\Phi_{33}^*(\Phi = e, d, g,$ and $h)$ in the composite and to weaken the depolarising electric field therein in the presence of the SC inclusions, we consider a case of the prolate inclusions ($0 < \rho < 1$). Graphs in Fig. 5.4 suggest that the prolate shape of the SC inclusion with the lower ρ value leads to a higher composite piezoelectric activity at m = const. This prolate geometry also helps attain high piezoelectric sensitivity (i.e., large values of the piezoelectric coefficient $g_{33}^* = d_{33}^*/\varepsilon_{33}^{*\sigma}$) due to the large piezoelectric coefficient d_{33}^* combined [3] with a relatively low dielectric permittivity $\varepsilon_{33}^{*\sigma}$ of the studied composite at $0 < m < 0.1$.

The reason for the difference between the values of the piezoelectric coefficients Φ_{33}^* calculated using different methods (see Fig. 5.5a–d) is possibly due to the relatively small ratio of the elastic moduli of the PMN–0.33PT SC and araldite (see Table 5.2). At the same time we have large ratios of dielectric permittivities of the SC and polymer components. This may also explain the difference between values of dielectric permittivity $\varepsilon_{33}^{*\xi}$ (Fig. 5.5e). The matrix of effective constants $\| C^* \|$ from (4.22) and (5.2) contains the piezoelectric coefficients e_{ij}^*, elastic moduli c_{ab}^{*E} and dielectric permittivities $\varepsilon_{pp}^{*\xi}$, and these constants are calculated directly following the EFM, EMM or FEM. According to our evaluations involving the electromechanical constants of the PMN–0.33PT SC (component 1) and araldite (component 2), the ratios $c_{11}^{(1),E}/c_{11}^{(2)} = 14.7$ and $c_{33}^{(1),E}/c_{11}^{(2)} = 13.2$ are an order-of-magnitude less than $\varepsilon_{33}^{(1),\xi}/\varepsilon_{33}^{(2)} = 170$. This distinction leads to a significant re-distribution of internal

[1] Hereafter in Chap. 5 we use the notation "PMN–0.33PT SC" that is related to the domain-engineered SC sample with 4*mm* symmetry [29] and electromechanical constants listed in Table 5.2

electric and mechanical fields in the 0–3 PMN–0.33PT SC / araldite composite and enables us to believe that the EFM could be applied with some restrictions for 0–3 connectivity. We note that a similar mutual arrangement of curves $e_{33}^{*}(m)$ and $d_{33}^{*}(m)$ from EFM, FEM and EMM data [24] takes place in case of the 0–3 FC / polymer composite.

The ratios $c_{11}^{(1),E}/c_{11}^{(2)} \approx 19$, $c_{33}^{(1),E}/c_{11}^{(2)} \approx 16$ and $\varepsilon_{33}^{(1),\xi}/\varepsilon_{33}^{(2)} \approx 110$ hold, and an order-of-magnitude difference between dielectric constants is again attained. However, it should be added for comparison, that in work [35] on the 1–3 $PbTiO_3$-type FC/polymer composite with circular cylindrical inclusions (i.e., in case of $\rho = 0$), good agreement between the parameters calculated using both EFM and FEM is observed in a wide volume-fraction range. The 1–3 composite based on the $PbTiO_3$-type FC consists of components, for which ratios $c_{11}^{(1),E}/c_{11}^{(2)} \approx 24$, $c_{33}^{(1),E}/c_{11}^{(2)} \approx 23$ and $\varepsilon_{33}^{(1),\xi}/\varepsilon_{33}^{(2)} \approx 31 - 37$ [35] are true and no aforementioned order-of-magnitude difference is observed.

The striking difference between values of $\varepsilon_{33}^{*\sigma}$ evaluated at volume fractions $m > 0.2$ (see, for example, curves 1, 3 and 5 in Fig. 5.4f) is related to the difference between values of $\varepsilon_{33}^{*\xi}$ (Fig. 5.4e) and to the considerable piezoelectric effect in the composite with the PMN–0.33PT SC inclusions. On increasing the volume fraction of the SC, m, absolute values of the piezoelectric coefficients $|e_{3j}^{*}|$ and $|d_{3j}^{*}|$ increase

Table 5.2 Room-temperature values of elastic moduli c_{pq}^{E} (in 10^{10} Pa), piezoelectric coefficients e_{fp} (in C/m^2) and dielectric permittivities ε_{ff}^{ξ} of some components of composites

	PMN–0.33PT SC[a] [29]	$(Pb_{0.76}Ca_{0.24})TiO_3$ SC[b] [30]	PMN–0.35PT FC[c] [31]	VDF–TrFE[d] [32]	Araldite[e] [33]
c_{11}^{E}	11.5	26.6	14.67	0.85	0.78
c_{12}^{E}	10.3	15.1	8.84	0.36	0.44
c_{13}^{E}	10.2	9.42	9.68	0.36	0.44
c_{33}^{E}	10.3	7.53	14.78	0.98	0.78
c_{44}^{E}	6.9	7.81	2.99	–	0.17
c_{66}^{E}	6.6	13.2	2.92	0.25	0.17
e_{31}	–3.9	0.653	–5.0	0.007	0
e_{33}	20.3	6.48	28.0	–0.222	0
e_{15}	10.1	5.36	14.3	–	0
$\varepsilon_{11}^{\xi}/\varepsilon_0$	1,434	171	1,650	–	4.0
$\varepsilon_{33}^{\xi}/\varepsilon_0$	680	66.4	2,650	6.0	4.0

[a] Domain-engineered SC, $4mm$ symmetry, experimental data
[b] Single-domain SC, $4mm$ symmetry, calculated data
[c] Poled textured FC, ∞mm symmetry, experimental data
[d] Elastic moduli c_{pq}^{E} and piezoelectric coefficients e_{fp} of 75 / 25 mol.% copolymer of vinylidene fluoride and trifluoroethylene (VDF–TrFE, ∞mm symmetry) were calculated using experimental values of elastic compliances s_{ab}^{E} and piezoelectric coefficients d_{ij} from work [32]. In our calculations, equalities $c_{44}^{E} \approx c_{66}^{E}$, $\varepsilon_{11}^{\xi} \approx \varepsilon_{33}^{\xi}$ and $e_{15} \approx -e_{33}$ are assumed [34] to be correct for VDF–TrFE
[e] Piezo-passive polymer, experimental data

monotonically (see, for example Fig. 5.4a, b) and, therefore, the difference $\varepsilon_{33}^{*\sigma} - \varepsilon_{33}^{*\xi}$ caused by the piezoelectric effect [see Eq. (1.16)] increases.

The difference between values of k_{33}^* calculated using different methods (Fig. 5.5g) is primarily due to values of $\varepsilon_{33}^{*\sigma}$ (Fig. 5.5f) and d_{33}^* (Fig. 5.5b), which have also been calculated using different methods. Of specific interest are curves of $g_{33}^*(m)$ shown in Fig. 5.5c. The volume-fraction dependence of the piezoelectric coefficient $g_{33}^*(m) = d_{33}^*(m)/\varepsilon_{33}^{*\sigma}(m)$ is non-monotonic and is due to the combination of the piezoelectric $[d_{33}^*(m)]$ and dielectric $[\varepsilon_{33}^{*\sigma}(m)]$ properties, see graphs in Fig. 5.5b, f. The location of $\max g_{33}^*(m)$ strongly depends on the aspect ratio ρ of the inclusions: at $\rho = 0.1$, when the highly prolate SC inclusions in the polymer matrix give rise to a slight depolarising effect, $\max g_{33}^*(m)$ is found at small volume fractions $(0 < m < 0.05)$, and on increasing ρ, when the depolarising effect becomes stronger and dielectric permittivity $\varepsilon_{33}^{*\sigma}(m)$ increases slower, $\max g_{33}^*(m)$ shifts towards the larger values of m. A significant piezoelectric sensitivity for the composite ($g_{33}^* > 200$ mV· m / N, i.e., about 6 times more than $g_{33}^{(1)}$ of PMN–0.33PT SC [29]) is predicted in the presence of inclusions with $\rho = 0.1$ at volume fractions $m \leq 0.1$ (Fig. 5.5c).

5.2.2 *Role of the Longitudinal Piezoelectric Effect*

The PMN–0.33PT-based composite is also of interest due to the leading role of the longitudinal piezoelectric effect in forming the interconnections between the elastic, piezoelectric and dielectric properties [see formulae (1.12–1.19)]. The presence of the highly piezo-active prolate SC inclusions, irrespective of the piezoelectric properties of the matrix surrounding them, enables one to simplify links between the piezoelectric coefficients from (1.12–1.15) and interconnections between effective constants in (1.16–1.19) with taking into account symmetry of the composite. To show the role of the longitudinal piezoelectric coefficients Φ_{33}^*, we introduce ratios

$$R_1 = d_{33}^* e_{33}^* / (\varepsilon_{33}^{*\sigma} - \varepsilon_{33}^{*\xi}),\ R_2 = e_{33}^* s_{33}^{*E} / d_{33}^*,\ R_3 = h_{33}^* s_{33}^{*D} / g_{33}^*, \text{ and}$$
$$R_4 = k_t^* / k_{33}^* \tag{5.4}$$

and an anisotropy factor

$$\zeta_e^* = e_{33}^* / e_{31}^*. \tag{5.5}$$

Examples of the volume-fraction dependence of R_i and ζ_e^* from (5.4) and (5.5) are shown in Fig. 5.6. It should be mentioned that ratios R_i from (5.4) mainly comprise electromechanical constants that are determined indirectly while the matrix of the effective properties of the composite $\| C^* \|$ [see (4.22) and (5.2)] comprises e_{ij}^*, c_{ab}^{*E} and $\varepsilon_{pp}^{*\xi}$ only.

Due to $R_1 > 0.9$ (Fig. 5.6a), the piezoelectric contribution from the longitudinal piezoelectric effect (i.e., $d_{33}^* e_{33}^*$) into the difference between dielectric permittivities

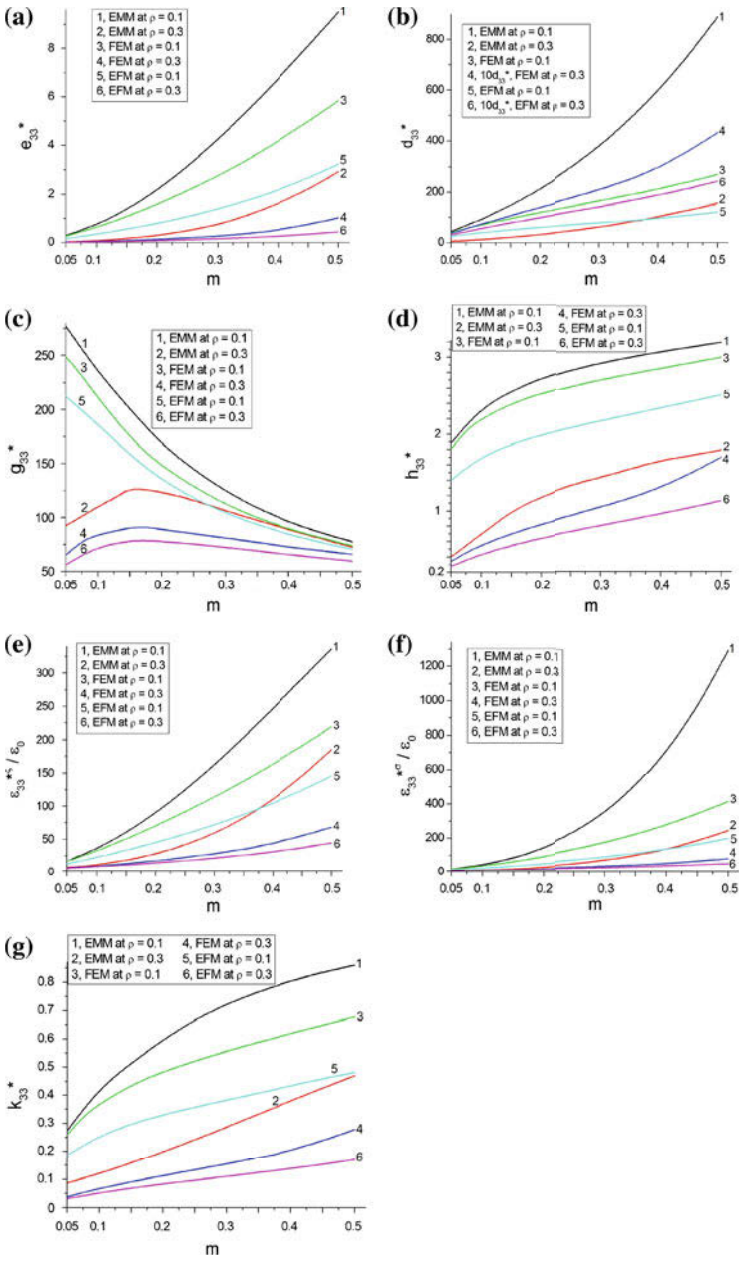

Fig. 5.5 Effective parameters calculated for the 0–3 PMN–0.33PT SC/araldite composite by means of the EMM, FEM and EFM: piezoelectric coefficients e_{33}^* (**a**, in C/m^2), d_{33}^* (**b**, in pC / N), g_{33}^* (**c**, in mV· m/N), and h_{33}^* (**d**, in GV/m), relative dielectric permittivities $\varepsilon_{33}^{*\xi}/\varepsilon_0$ (**e**) and $\varepsilon_{33}^{*\sigma}/\varepsilon_0$ (**f**), and ECF k_{33}^* (**g**) (reprinted from paper by Topolov et al. [24], with permission from Taylor and Francis)

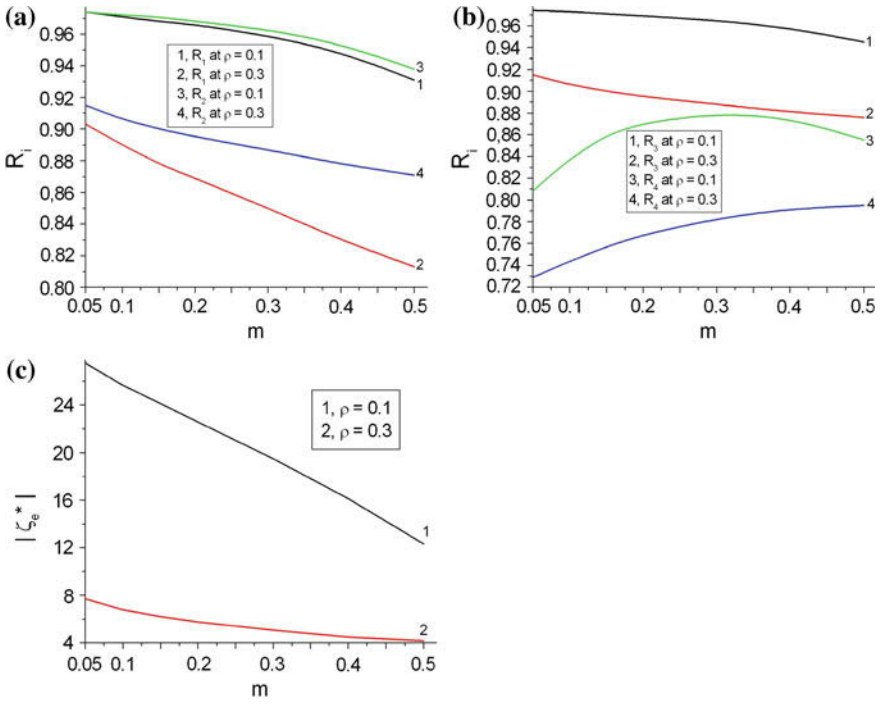

Fig. 5.6 Ratios R_i and anisotropy factor ζ_e^* which have been calculated for the 0–3 PMN–0.33PT SC/araldite composite by means of FEM

$\varepsilon_{33}^{*\sigma} - \varepsilon_{33}^{*\xi} = d_{33}^* e_{33}^* + 2d_{31}^* e_{31}^*$ [see (1.16)] can exceed 90 %. It is seen that at $\rho = 0.1$, the equality $R_1 = R_2$ holds with an accuracy to 1 % (cf. curves 1 and 3 in Fig. 5.6a), and the inequality $R_3 > R_1$ is valid in a wide volume-fraction range (Fig. 5.6a). As a result, the piezoelectric coefficient g_{33}^* that describes a longitudinal sensitivity of the composite has a negligible contribution from the transverse electromechanical interaction between the SC inclusion and the polymer matrix.

To understand the volume-fraction behaviour of R_4 at $\rho = \text{const}$ (see curves 3 and 4 in Fig. 5.6b), we remind the reader, that, in accordance with formulae [3, 36],

$$(k_t^*/k_{33}^*)^2 = [(e_{33}^*)^2/(c_{33}^{*D}\varepsilon_{33}^{*\xi})]/[(d_{33}^*)^2/(s_{33}^{*E}\varepsilon_{33}^{*\sigma})]. \tag{5.6}$$

Equation (5.6) can be simplified if to take into consideration equalities as follows: $c_{33}^{*D} = c_{33}^{*E}/[1 - (k_t^*)^2]$, $\varepsilon_{33}^{*\xi} = \varepsilon_{33}^{*\sigma}[1 - (k_t^*)^2]$ [36] and $d_{33}^* \approx e_{33}^* s_{33}^{*E}$ (that holds at $R_2 \approx 1$, see, for instance, Fig. 5.6a). Thus, the relation $R_4 \approx (c_{33}^{*E} s_{33}^{*E})^{-1/2}$ is valid. The largest values of $R_4 \approx 0.9$ (see curve 3 in Fig. 5.6b) and the equality

$$k_t^* \approx k_{33}^* \tag{5.7}$$

are achieved at $\rho = 0.1$. We note for comparison that relation (5.7) holds in the conventional 1–3 FC / polymer composite [32], and the aspect ratio $\rho = 0.1$ enables us to surmise that a distinction between the electromechanical properties of the studied 0–3 composite with prolate inclusions and the related 1–3 composite becomes minor.

As follows from Fig. 5.6c, $|\zeta_e^*(m)|$ decreases monotonically at ρ = const, and a similar monotonic decrease is also peculiar to $R_1(m)$ and $R_2(m)$ (see Fig. 5.6a). The reason for this correlation is the transverse piezoelectric response of the composite.

On increasing the volume fraction m the electromechanical interaction between the SC inclusions in the composite becomes more significant and therefore, the role of the piezoelectric coefficient $e_{31}^*(m)$ in forming the effective electromechanical properties increases.

5.2.3 *Effect of the Poling Direction on the Piezoelectric Properties and Their Anisotropy*

An important possibility is the ability to vary the electromechanical properties of the 0–3 composite using a change in the poling direction of the ferroelectric polymer component [9, 10]. A similar effect of the poling direction on the electromechanical properties was discussed in earlier studies [37] for 2–2 SC/polymer composites and may be important for piezo-technical applications. Below we show how the change in the poling direction of polymer influences the piezoelectric performance of the 0–3 composite based on PMN–0.33PT SC.

The effective electromechanical properties of the SC/polymer composite are determined within the framework of the model of the composite with spheroidal inclusions (Fig. 5.1) distributed regularly in a large matrix, and the FEM approach is used for our further calculations. The polymer matrix is characterised by a remanent polarisation vector that has one of the following directions: either $\boldsymbol{P}_r^{(2)} \uparrow\uparrow OX_3$ or $\boldsymbol{P}_r^{(2)} \uparrow\downarrow OX_3$. We remind that such modes of poling can be attained due to a large difference between coercive fields $E_c^{(n)}$ [38, 39] of the ferroelectric polymer and SC components. Among the ferroelectric polymer components of interest we choose VDF–TrFE (see electromechanical constants in Table 5.2) with $E_c^{(2)} \gg E_c^{(1)}$ at room temperature.

Data in Table 5.3 show the effect of the poling direction of the polymer component (i.e., the $\boldsymbol{P}_r^{(2)}$ orientation) on the piezoelectric coefficients and ECFs. To describe the anisotropy of these parameters, we use ζ_d^* and ζ_e^* from (4.24) and (5.1), respectively. Numerous changes in $\mathrm{sgn}d_{3j}^*$ and $\mathrm{sgn}e_{3j}^*$ take place in the presence of the polymer component with $\boldsymbol{P}_r^{(2)} \uparrow\uparrow OX_3$ (see Table 5.3). Such a poling direction of the polymer leads to the piezoelectric coefficients $d_{3j}^{(2)}$ and $e_{3j}^{(2)}$ whose signs differ from signs of $d_{3j}^{(1)}$ and $e_{3j}^{(1)}$ in PMN–0.33PT SC [29]. As a consequence, equations $d_{3j}^*(m) = 0$ and

Table 5.3 Piezoelectric coefficients d^*_{3j} (in pC / N) and e^*_{3j} (in C / m^2) and anisotropy factors ζ^*_d and ζ^*_e of the 0–3 PMN–0.33PT SC / VDF–TrFE composite (FEM caluclations)

ρ	m	d^*_{31}	d^*_{33}	$10^2 e^*_{31}$	e^*_{33}	ζ^*_d	ζ^*_e
	Polymer component with $\boldsymbol{P}_r^{(2)} \uparrow\uparrow OX_3$						
0.1	0.01	10.6	–34.0	0.488	–0.282	–3.21	–173
	0.03	9.17	–30.1	$-8.1 \cdot 10^{-3}$	–0.291	–3.28	$3.59 \cdot 10^3$
	0.05	8.19	–29.0	–0.471	–0.304	–3.54	64.5
	0.10	6.24	–25.8	–1.05	–0.333	–4.13	20.2
	0.20	2.87	–20.8	–4.63	–0.379	–7.25	7.54
	0.30	–0.070	–15.2	–9.30	–0.386	217	4.15
	0.40	–5.65	–6.19	–17.9	–0.270	1.10	1.51
	0.50	–16.8	–19.6	–38.0	0.499	11.7	–1.31
0.3	0.01	11.7	–37.7	0.521	–0.302	–3.22	–58.0
	0.03	11.0	–36.8	0.059	–0.322	–3.35	–546
	0.05	10.3	–35.8	–0.367	–0.339	–3.48	92.4
	0.10	8.67	–33.4	–1.45	–0.380	–3.85	26.2
	0.20	5.66	–29.5	–4.11	–0.457	–5.21	11.1
	0.30	2.71	–26.0	–8.13	–0.534	–9.59	6.57
	0.40	–0.80	–21.0	–15.0	–0.585	–26.3	3.90
	0.50	–7.57	–6.37	–30.4	–0.365	0.841	1.20
	Polymer component with $\boldsymbol{P}_r^{(2)} \uparrow\downarrow OX_3$						
0.1	0.01	–13.0	41.5	–0.780	0.332	–3.19	–42.6
	0.03	–13.5	43.4	–0.747	0.383	–3.21	–51.3
	0.05	–13.6	44.3	–0.719	0.423	–3.26	–58.8
	0.10	–13.7	45.7	–0.654	0.516	–3.34	–78.9
	0.20	–13.7	48.7	–0.536	0.719	–3.55	–134
	0.30	–14.5	53.9	–0.468	0.999	–3.72	–213
	0.40	–17.0	64.0	–0.624	1.46	–3.76	–234
	0.50	–25.1	90.9	–2.54	2.47	–3.62	–97.2
0.3	0.01	–12.3	39.5	–0.672	0.312	–3.21	–46.4
	0.03	–12.7	41.3	–0.501	0.349	–3.25	–69.7
	0.05	–12.9	42.4	–0.375	0.382	–3.29	–102
	0.10	–12.9	44.0	–0.124	0.458	–3.41	–369
	0.20	–12.6	46.1	0.338	0.615	–3.66	182
	0.30	–12.6	48.8	0.856	0.812	–3.87	94.9
	0.40	–13.1	53.2	1.36	1.10	–4.06	80.9
	0.50	–16.9	66.4	0.396	1.75	–3.93	442

$e^*_{3j}(m) = 0$ are achieved in a wide volume-fraction range and strongly influence the piezoelectric anisotropy of the 0–3 PMN–0.33PT SC / VDF–TrFE composite.

5.2.4 *Effect of the Arrangement of Inclusions on the Piezoelectric Properties and Their Anisotropy*

An additional effect needs to be considered when taking into account microgeometric features, i.e., a particular spatial distribution of the inclusions within the composite matrix. Poizat and Sester [40] analysed an effect of the arrangement of FC inclusions on the piezoelectric properties in 0–3 FC/polymer composites, however the similar effect was not considered in earlier studies on the SC/polymer composites, especially in the presence of relaxor-ferroelectric components with high piezoelectric activity. In Sect. 5.2.4 we consider 0–3 SC/polymer composites with a regular distribution of spheroidal inclusions in a matrix. In the first case the centres of symmetry of these inclusions occupy corners of a simple cubic lattice, and in the second case we assume that the same centres of symmetry form a body-centered cubic lattice. These distinctions in the arrangement influence both the longitudinal and transverse piezoelectric responses of the composite. It is assumed in both the cases that the spontaneous polarisation of each SC inclusion obeys a condition $\boldsymbol{P}_s^{(1)} \uparrow\uparrow OX_3$.

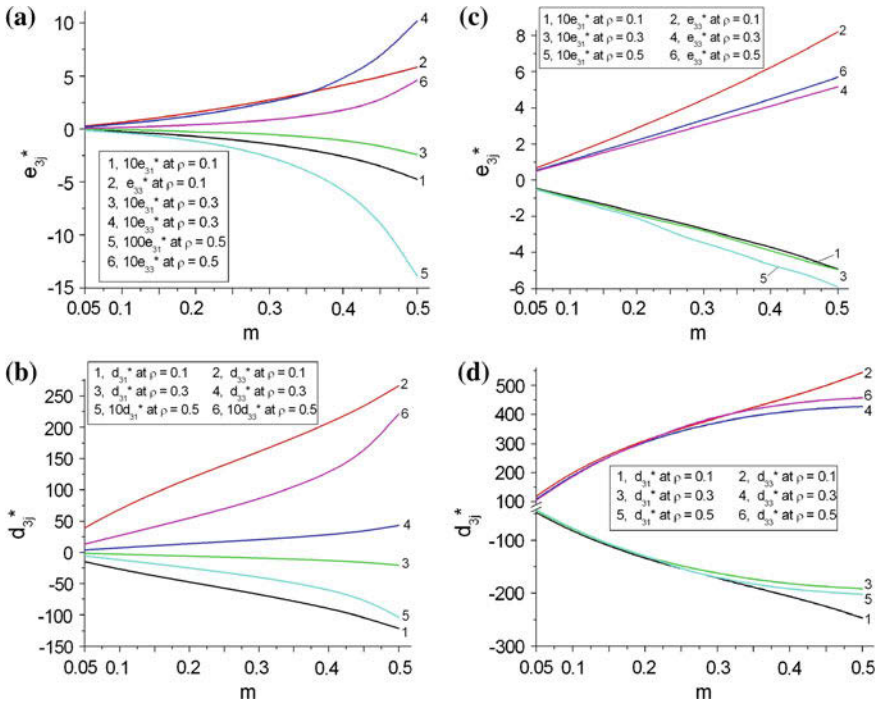

Fig. 5.7 Piezoelectric coefficients e_{3j}^* (**a** and **c**, in C/m^2) and d_{3j}^* (**b** and **d**, in pC/N) which have been calculated for the 0–3 PMN–0.33PT SC/araldite composite by means of FEM. Graphs a and b are related to the simple-cubic arrangement of the spheroidal SC inclusions in the polymer matrix, graphs c and d are related to the body-centered cubic arrangement of the spheroidal SC inclusions in the polymer matrix

Table 5.4 ECFs k^*_{3j}, k^*_t and k^*_p and anisotropy factos ζ^*_k and ζ^*_{t-p} of the 0–3 PMN–0.33PT SC/araldite composite (FEM calculations)

ρ	m	k^*_{33}	k^*_{31}	k^*_t	k^*_p	ζ^*_k	ζ^*_{t-p}
Composite with the simple-cubic arrangement of inclusions							
0.1	0.1	0.369	–0.112	0.370	–0.212	–3.29	–1.75
	0.3	0.559	–0.155	0.560	–0.308	–3.61	–1.82
	0.5	0.677	–0.206	0.680	–0.436	–3.29	–1.56
0.3	0.1	0.0664	–0.0244	0.0668	–0.0320	–2.72	–2.09
	0.3	0.153	–0.0505	0.156	–0.101	–3.03	–1.54
	0.5	0.278	–0.0836	0.287	–0.188	–3.33	–1.53
0.5	0.1	0.0275	–0.0113	0.0259	–0.0207	–2.43	–1.25
	0.3	0.0791	–0.0298	0.0823	–0.0589	–2.65	–1.40
	0.5	0.182	–0.0572	0.190	–0.129	–3.18	–1.47
Composite with the body-centered cubic arrangement of inclusions							
0.1	0.1	0.628	–0.232	0.629	–0.434	–2.71	–1.45
	0.3	0.756	–0.268	0.757	–0.533	–2.82	–1.42
	0.5	0.811	–0.291	0.812	–0.593	–2.79	–1.37
0.3	0.1	0.619	–0.248	0.621	–0.455	–2.50	–1.36
	0.3	0.749	–0.266	0.753	–0.512	–2.82	–1.47
	0.5	0.773	–0.289	0.778	–0.584	–2.67	–1.33
0.5	0.1	0.607	–0.247	0.609	–0.448	–2.46	–1.36
	0.3	0.748	–0.310	0.751	–0.589	–2.41	–1.28
	0.5	0.771	–0.309	0.773	–0.612	–2.50	–1.26

Examples of the volume-fraction dependence of the piezoelectric coefficients, ECFs and anisotropy factors, which are related to the aforementioned arrangements, are given in Fig. 5.7 and Table 5.4. To describe the anisotropy of ECFs (Table 5.4), we use two factors, ζ^*_k from (4.24) and

$$\zeta^*_{t-p} = k^*_t / k^*_p \tag{5.8}$$

where the thickness ECF k^*_t and the planar ECF k^*_p are given by (4.12).

The transition from the simple-cubic arrangement of inclusions to the body-centered cubic arrangement leads to an increase of $|e^*_{3j}|$, $|d^*_{3j}|$, $|k^*_{3j}|$, k^*_t, and k^*_p at fixed values of m and ρ. A more dense packing of the highly piezo-active inclusions in the 0–3 composite (i.e., the case of the body-centered cubic arrangement) leads to a more intensive electromechanical interaction between them even when they are embedded in the piezo-passive matrix. As a consequence, a higher piezoelectric performance is obtained (see Fig. 5.7c, d and Table 5.4) and a more pronounced transverse piezoelectric effect. The last circumstance gives rise to a decreasing $|\zeta^*_k|$ and $|\zeta^*_{t-p}|$ in a wide volume-fraction range. At the same time, the condition $|\zeta^*_e| \gg 1$ is valid (see, e.g., data in Fig. 5.7a, c), and the composite with a body-centered cubic arrangement of inclusions at $0.1 \leq \rho \leq 0.5$ remains similar to a 1–3 composite with the same components. An additional and essential argument for this analogy is that

the condition (5.7) related to 1–3 composites [32] is valid at various m and ρ values (see Table 5.4).

5.3 Single Crystal/Ceramic Composites

In the last decades, novel ferroelectric SC/FC ceramic composites have attracted the attention of researchers for several reasons. First, features of the synthesis and microstructure of such composites based on perovskite-type FCs have been studied [4, 5] to optimise the conditions for obtaining monolithic bulk samples with predictable properties. Second, in contrast to the well-known FC/polymer and SC/polymer composites, the SC/FC composite system contains components with comparable electromechanical properties. Third, there are restricted experimental data (see, for instance, work [5]) on the performance of the SC/FC composites that could be of importance for piezo-technical applications.

In Sect. 5.3 we discuss some examples of the electromechanical properties and anisotropy factors of the 0–3 SC / FC composites with spheroidal inclusions. Following the model of the 0–3 composite (Fig. 5.1), we regard component 1 as a SC and component 2 as a poled FC medium surrounding the SC inclusions. It is assumed that a body-centered cubic arrangement of the SC inclusions takes place therein, and the SC and FC components have the spontaneous polarisation vector $\boldsymbol{P}_s^{(1)} \uparrow\uparrow OX_3$ and the remanent polarisation vector $\boldsymbol{P}_r^{(2)} \uparrow\uparrow OX_3$, respectively. Hereafter we follow the FEM approach to calculate a full set of effective electromechanical constants and a series of effective parameters of the composite when varying the volume fraction m and aspect ratio ρ. The electromechanical constants of the components of the 0–3 composites to be considered are shown in Tables 5.1 and 5.2. Combining the properties of the components with equal or opposite signs of the piezoelectric coefficients $e_{3j}^{(n)}$ and with various anisotropy factors $e_{33}^{(n)}/e_{31}^{(n)}$, we obtain a series of important volume-fraction dependences of the effective piezoelectric properties, which are now discussed.

5.3.1 Two Components with a Large Anisotropy of Piezoelectric Coefficients $e_{3j}^{(n)} > 0$

We consider here a composite that consists of two components with related chemical compositions. Single-domain $(Pb_{0.76}Ca_{0.24})TiO_3$ SC and modified $PbTiO_3$ FC are characterised by a large anisotropy of the piezoelectric coefficients $e_{3j}^{(n)}$ and $\operatorname{sgn} e_{3j}^{(n)} > 0$ (see Tables 5.1, 5.2) and by moderate piezoelectric activity [21, 30]. Moreover, the anisotropy of the elastic moduli of the modified $PbTiO_3$ FC $c_{ab}^{(2),E}$ strongly differs from the elastic anisotropy of the conventional PZT-type FCs [3, 13, 28]. Such

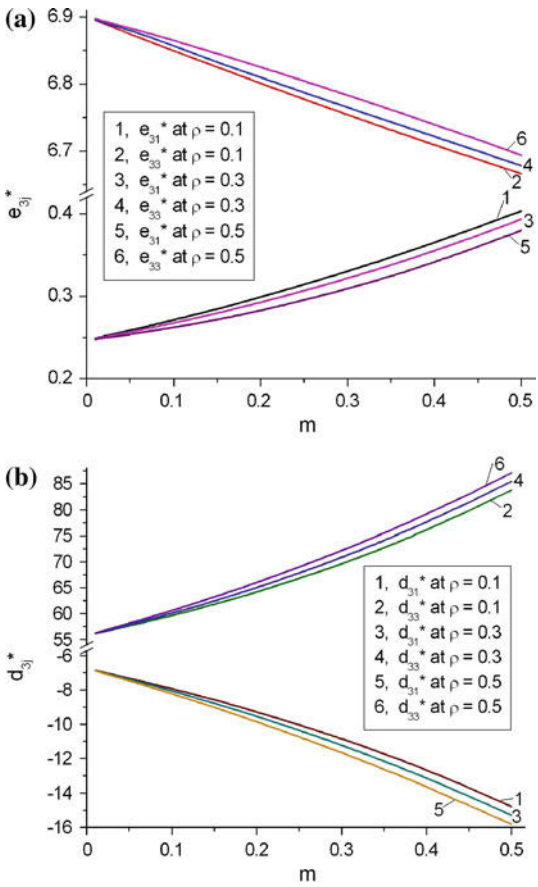

Fig. 5.8 Piezoelectric coefficients e^*_{3j} (**a**, in C/m^2) and d^*_{3j} (**b**, in pC/N) which have been calculated for the 0–3 $(Pb_{0.76}Ca_{0.24})TiO_3$ SC/modified $PbTiO_3$ FC composite by means of FEM

a combination of piezo-active components enables us to obtain a unique volume-fraction dependence in terms of the piezoelectric properties (Fig. 5.8) of the 0–3 SC/FC composite. These properties are characterised by the following features:

(i) inequalities $\zeta^*_e > 10$ and $5 < |\zeta^*_d| < 10$ hold in the wide volume-fraction range,

(ii) a combination of components leads to the conditions $\operatorname{sgn} e^*_{31} = \operatorname{sgn} e^*_{33} > 0$ and $\operatorname{sgn} d^*_{31} = -\operatorname{sgn} d^*_{33} < 0$, and these signs coincide with those of the piezoelectric coefficients of the interacting components, and

(iii) minor changes in the volume-fraction dependences $e^*_{3j}(m)$ and $d^*_{3j}(m)$ are observed at variations of the aspect ratio ρ of the prolate SC inclusion, i.e., the shape of the inclusion does not play a key role in forming the piezoelectric properties of the composite.

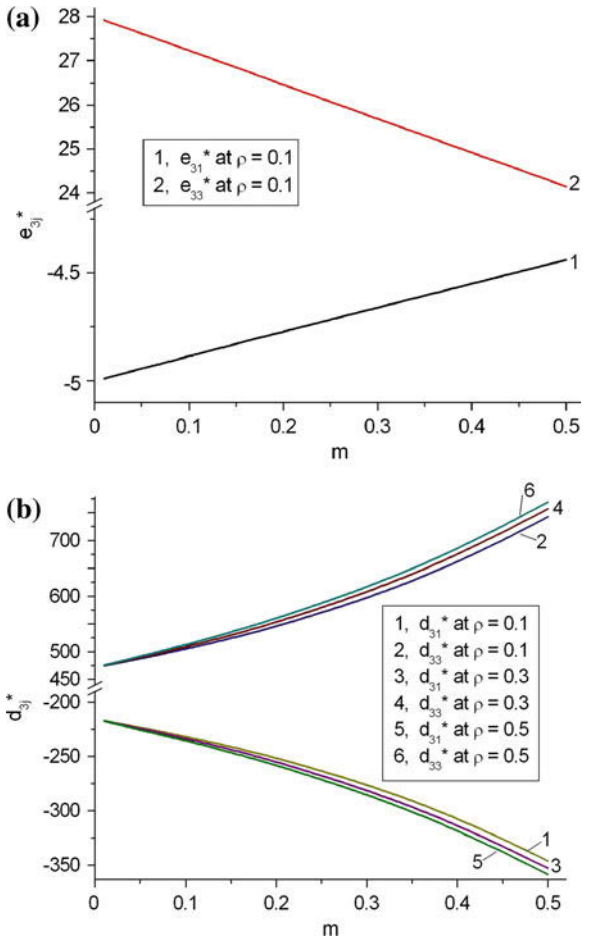

Fig. 5.9 Piezoelectric coefficients e^*_{3j} (**a**, in C/m^2) and d^*_{3j} (**b**, in pC/N) which have been calculated for the 0–3 PMN–0.33PT SC/PMN–0.35PT FC composite by means of FEM

5.3.2 Two Components with Piezoelectric Coefficients Obeying Conditions $sgn\, e_{33}^{(n)} = -sgn\, e_{31}^{(n)} > 0$

It is now assumed that the 0–3 composite consists of a system of PMN–0.33PT SC inclusions and a PMN–0.35PT FC matrix. The relative chemical compositions and high piezoelectric activity of the chosen SC and FC components along with the moderate ratios of the piezoelectric coefficients $d_{33}^{(n)}/d_{31}^{(n)}$ of the components [29, 31] predetermine the volume-fraction dependence of the effective properties in the composite. Examples of the piezoelectric properties of the studied SC / FC composite at variations of m and ρ are shown in Fig. 5.9.

Because of very minor changes in the volume-fraction dependence of $e^*_{3j}(m)$ at aspect ratios of ρ from 0.1 to 0.5, we have omitted the e^*_{3j} curves related to $0.1 < \rho \leq 0.5$ (see Fig. 5.9a). The reason for such behaviour of $e^*_{3j}(m)$ is due to the electromechanical interaction of the components with the piezoelectric coefficients $e^{(n)}_{3j}$ that obey a condition $e^{(1)}_{33}/e^{(1)}_{31} \approx e^{(2)}_{33}/e^{(2)}_{31}$. As an important consequence, a relation $\zeta^*_e \approx e^{(2)}_{33}/e^{(2)}_{31}$ is valid in a wide range of both m and ρ. The relatively minor changes in $d^*_{3j}(m)$ at $0.1 \leq \rho \leq 0.5$ (Fig. 5.9b) are mainly accounted for by a difference between the elastic anisotropy of the SC and FC components (compare data on elastic moduli c^E_{ab} in Tables 5.1 and 5.2). As in the case considered in Sect. 5.3.1, we state that the shape of the SC inclusion plays no major role in forming the piezoelectric properties of the composite studied.

5.3.3 *Components with Piezoelectric Coefficients Obeying Conditions* $\mathbf{sgn\, e^{(1)}_{33} = -sgn\, e^{(1)}_{31} > 0}$ *and* $\mathbf{sgn\, e^{(2)}_{33} = sgn\, e^{(2)}_{31} > 0}$

A combination of a highly piezo-active PMN–0.33PT SC [29] and a highly anisotropic FC of modified $PbTiO_3$ with moderate piezoelectric activity [21] provides us with a new example of the effective properties of 0–3 composites. The different signs of the piezoelectric coefficients $e^{(n)}_{31}$ for the SC and FC components (see Tables 5.1, 5.2) lead to validity of the condition $e^*_{31}(m) = 0$ and to very large values of $|\zeta^*_e|$ in a specific m range. At the same time, the anisotropy factor ζ^*_d affected by the piezoelectric properties of the SC and FC components with $\mathrm{sgn}d^{(n)}_{33} = -\mathrm{sgn}d^{(n)}_{31} > 0$ changes in a restricted range. Some results of FEM modelling of the piezoelectric response of the 0–3 composites are shown in Fig. 5.10. As in Sect. 5.2.4, for comparison we consider two versions of the arrangement of the SC inclusions in the FC matrix, namely, a simple-cubic and body-centered cubic arrangements.

The graphs in Fig. 5.10 suggest that the piezoelectric performance of the composite does not undergo large changes at the transition from a simple-cubic arrangement of the SC inclusions to a body-centered cubic arrangement. It is seen that $e^*_{3j}(m)$ (Fig. 5.10a, c) and $d^*_{3j}(m)$ (Fig. 5.10b, d) vary in ranges that are weakly dependent on the aspect ratio ρ and features of the arrangement of the inclusions. The difference between the curves becomes negligible (see Fig. 5.10c, d) at the body-centered cubic arrangement, i.e., at the denser packing of the inclusions in the composite sample.

The relatively small values of $|\zeta^*_d|$ of the composite (in comparison to $d^{(2)}_{33}/|d^{(2)}_{31}| \approx 11.6$ in the $PbTiO_3$-type FC component [21]) over a wide m range implies that the highly piezo-active SC component plays a key role in forming the piezoelectric properties for this 0–3 SC/FC composite. It should be added that a similar situation, however with other values of $|\zeta^*_d|$, has been observed in ferroelectric SC/polymer

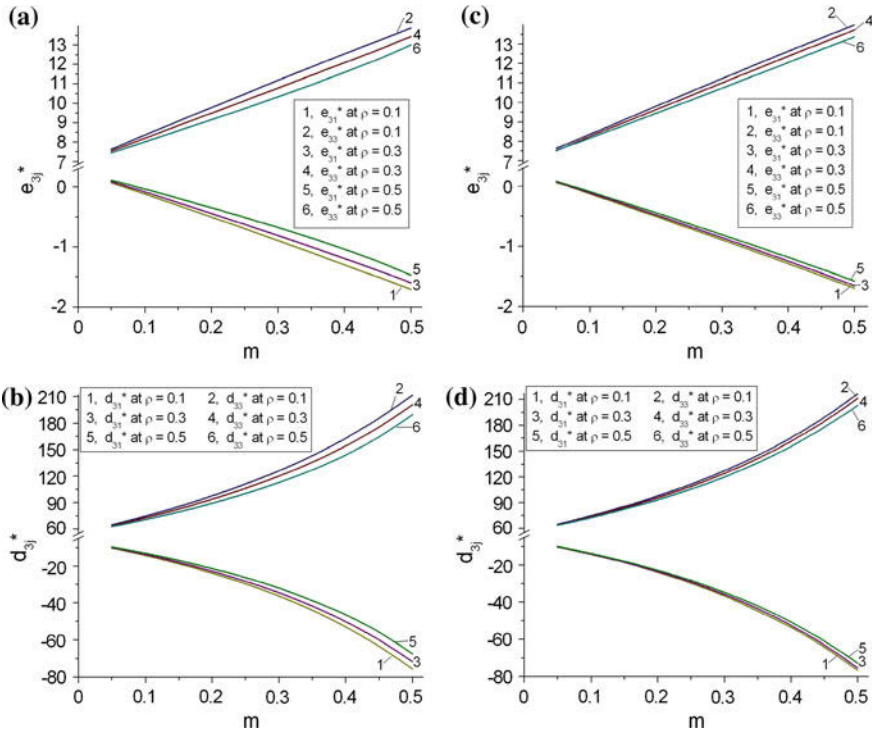

Fig. 5.10 Piezoelectric coefficients e^*_{3j} (**a** and **c**, in C / m^2) and d^*_{3j} (**b** and **d**, in pC / N) which have been calculated for the 0–3 PMN–0.33PT SC/modified $PbTiO_3$ FC composite by means of FEM. Graphs a and b are related to the simple-cubic arrangement of the spheroidal SC inclusions in the FC matrix, graphs c and d are related to the body-centered cubic arrangement of the spheroidal SC inclusions in the FC matrix

and FC / polymer composites (see Sects. 5.1 and 5.2). The key role of the SC component is also shown in Table 5.5: minor differences between the similar ECFs, related to the simple-cubic and body-centered cubic arrangement of the prolate inclusions, are achieved in a wide volume-fraction range. Otherwise, the FC matrix could not strongly affect the volume-fraction dependence of ECFs and anisotropy factors, and values of $|\zeta^*_k|$ and $|\zeta^*_{t-p}|$ rapidly decrease on increasing m at any type of the SC-inclusion arrangement. It is seen that the inequality $|\zeta^*_k| > 5$ holds at $m < 0.15$, i.e., at small volume fractions of the highly piezo-active SC component. Moreover, Eq. (5.7) holds in almost the whole volume-fraction range (see Table 5.5), and this circumstance resembles the relation between ECFs in the conventional 1–3 FC/polymer composite [32].

Table 5.5 ECFs k^*_{3j}, k^*_t and k^*_p and anisotropy factors ζ^*_k and ζ^*_{t-p} of the 0–3 PMN–0.33PT SC/modified $PbTiO_3$ FC composite at $\rho = 0.1$ (FEM calculations)

m	k^*_{33}	k^*_{31}	k^*_t	k^*_p	ζ^*_k	ζ^*_{t-p}
Composite with the simple-cubic arrangement of inclusions						
0.05	0.470	–0.0795	0.493	–0.131	–5.91	–3.76
0.10	0.511	–0.0988	0.512	–0.165	–5.17	–3.10
0.15	0.531	–0.118	0.531	–0.200	–4.50	–2.66
0.20	0.550	–0.136	0.551	–0.243	–4.04	–2.27
0.25	0.571	–0.154	0.572	–0.271	–3.71	–2.11
0.30	0.592	–0.171	0.593	–0.307	–3.46	–1.93
0.35	0.613	–0.189	0.615	–0.343	–3.24	–1.79
0.40	0.635	–0.207	0.637	–0.381	–3.07	–1.67
0.45	0.657	–0.225	0,660	–0.420	–2.92	–1.57
0.50	0.680	–0.243	0.683	–0.443	–2.80	–1.54
Composite with the body-centered cubic arrangement of inclusions						
0.05	0.492	–0.0799	0.492	–0.131	–6.16	–3.76
0.10	0.511	–0.0992	0.511	–0.166	–5.15	–3.08
0.15	0.530	–0.118	0.630	–0.200	–4.49	–3.15
0.20	0.550	–0.135	0.551	–0.235	–4.07	–2.34
0.25	0.571	–0.153	0.574	–0.271	–3.73	–2.12
0.30	0.593	–0.169	0.595	–0.307	–3.51	–1.94
0.35	0.615	–0.186	0.617	–0.344	–3.31	–1.78
0.40	0.638	–0.202	0.640	–0.382	–3.16	–1.68
0.45	0.661	–0.219	0.664	–0.421	–3.02	–1.58
0.50	0.685	–0.235	0.688	–0.462	–2.91	–1.49

5.4 Conclusion

Chapter 5 has been devoted to the piezoelectric performance and anisotropy of various matrix composites with 0–3 connectivity. Our modelling and property predictions have been carried out within the framework of the model of a 0–3 piezo-active composite with spheroidal inclusions distributed regularly in a large matrix (see a fragment in Fig. 5.1). The model concepts and methods for averaging the electromechanical properties (EMM, EFM and FEM) have been applied to 0–3 composites based on either FE or relaxor-ferroelectric SCs. The following combinations of components have been analysed in the context of the effective properties:

(i) $PbTiO_3$-type FC with a large ratio $d^{(1)}_{33}/|d^{(1)}_{31}|$/piezo-passive polymer,
(ii) PZT-type FC with a moderate ratio $d^{(1)}_{33}/|d^{(1)}_{31}|$/clay (piezo-passive component),
(iii) relaxor-ferroelectric SC with high piezoelectric activity/piezo-passive polymer,
(iv) relaxor-ferroelectric SC with high piezoelectric activity/piezo-active polymer,
(v) relaxor-ferroelectric SC with high piezoelectric activity/$PbTiO_3$-type FC with a large ratio $d^{(2)}_{33}/|d^{(2)}_{31}|$,

(vi) relaxor-ferroelectric SC with high piezoelectric activity/PZT-type FC with a moderate ratio $d_{33}^{(2)}/|d_{31}^{(2)}|$, and

(vii) ferroelectric SC with a large ratio $e_{33}^{(1)}/|e_{31}^{(1)}|$/$PbTiO_3$-type FC with a large ratio $d_{33}^{(2)}/|d_{31}^{(2)}|$.

For the combinations (i)–(vii) examples of the volume-fraction dependence of the piezoelectric coefficients, ECFs and anisotropy factors have been considered under the condition that the composite contains prolate spheroidal inclusions with a fixed aspect ratio ρ from a range $0.1 \leq \rho \leq 0.5$. Orientation effects caused by the poling direction of the ferroelectric polymer matrix and the arrangement of the SC inclusions in the polymer (or FC) matrix have been considered, and the role of these effects in forming the piezoelectric properties and their anisotropy in the 0–3 composites has been analysed. Examples of behaviour of ECFs and their anisotropy at different arrangements of the SC inclusions in the matrix (Tables 5.4, 5.5) have been discussed. It has been shown that the highly piezo-active SC inclusion influences the electromechanical properties and ECFs of the composite in different ways, depending on the piezoelectric properties and their anisotropy in the matrix of the 0–3 composite.

The four ratios (5.4) describing the interconnections between the effective electromechanical properties in 0–3 composites have been introduced to interpret features of the longitudinal dielectric and piezoelectric response of composite structures with prolate SC inclusions that exhibit high piezoelectric activity. Hereby the important role of piezoelectric anisotropy and activity of the composite components in the longitudinal piezoelectric effect has been analysed for 0–3 composites with a variety of combinations of components [see items (i)–(vii)].

Results of the study on the piezoelectric performance, anisotropy and orientation effects can be of value for piezo-technical, acoustic and other applications of modern piezo-active 0–3 composites as materials whose piezoelectric properties and anisotropy factors vary in wide ranges.

References

1. Akdogan EK, Allahverdi M, Safari A (2005) Piezoelectric composites for sensor and actuator applications. IEEE Trans Ultrason Ferroelectr Freq Control 52:746–775
2. Safari A, Akdogan EK (2006) Rapid prototyping of novel piezoelectric composites. Ferroelectrics 331:153–179
3. Topolov VYu, Bowen CR (2009) Electromechanical properties in composites based on ferroelectrics. Springer, London
4. Smotrakov VG, Eremkin VV, Alyoshin VA, Tsikhotsky ES (2000) Preparation and study of single-crystal-ceramic composite. Izv Akad Nauk Ser Fiz 64:1220–1223 (in Russian)
5. Takahashi H, Tukamoto S, Qiu J, Tani J, Sukigara T (2003) Property of composite ceramics composed of single crystals and ceramic matrix using hybrid sintering. Jpn J Appl Phys Pt 1(42):6055–6058
6. Chan HLW, Cheung MC, Choy CL (1999) Study on $BaTiO_3$/ P(VDF-TrFE) 0–3 composites. Ferroelectrics 224:113–120

7. Lam KH, Chan HLW, Luo HS, Yin QR, Yin ZW, Choy CL (2003) Dielectric properties of 65PMN-35PT / P(VDF-TrFE) 0–3 composites. Microelectron Eng 66:792–797
8. Ngoma JB, Cavaille JY, Paletto J (1990) Dielectric and piezoelectric properties of copolymer-ferroelectric composite. Ferroelectrics 109:205–210
9. Chan HLW, Ng PKL, Choy CL (1999) Effect of poling procedure on the properties of lead zirconate titanate / vinylidene fluoride-trifluoroethylene composites. Appl Phys Lett 74:3029–3031
10. Ng KL, Chan HLW, Choy CL (2000) Piezoelectric and pyroelectric properties of PZT/P(VDF-TrFE) composites with constituent phases poled in parallel or antiparallel directions. IEEE Trans Ultrason Ferroelectr Freq Control 47:1308–1315
11. Fang D-N, Soh AK, Li C-Q, Jiang B (2001) Nonlinear behavior of 0–3 type ferroelectric composites with polymer matrices. J Mater Sci 36:5281–5288
12. Wilson SA, Maistros GM, Whatmore RW (2005) Structure modification of 0–3 piezoelectric ceramic / polymer composites through dielectrophoresis. J Phys D: Appl Phys 38:175–182
13. Khoroshun LP, Maslov BP, Leshchenko PV (1989) Prediction of effective properties of piezo-active composite materials. Naukova Dumka, Kiev (in Russian)
14. Luchaninov AG (2002) Piezoelectric effect in non-polar heterogeneous ferroelectric materials. Volgograd State Academy of Architecture and Construction, Volgograd (in Russian)
15. Sokolkin YuV, Pan'kov AA (2003) Electroelasticity of piezo-composites with irregular structures. Fizmatlit, Moscow (in Russian)
16. Poon YM, Ho CH, Wong YW, Shin FG (2007) Theoretical predictions on the effective piezoelectric coefficients of 0–3 PZT / polymer composites. J Mater Sci 42:6011–6017
17. Levin VM, Rakovskaja MI, Kreher WS (1999) The effective thermoelectroelastic properties of microinhomogeneous materials. Int J Solids Struct 36:2683–2705
18. Levassort F, Topolov VYu, Lethiecq M (2000) A comparative study of different methods of evaluating effective electromechanical properties of 0–3 and 1–3 ceramic / polymer composites. J Phys D: Appl Phys 33:2064–2068
19. Glushanin SV, Topolov VYu, Krivoruchko AV (2006) Features of piezoelectric properties of 0–3-type ceramic / polymer composites. Mater Chem Phys 97:357–364
20. Huang JH, Yu S (1994) Electroelastic Eshelby tensors for an ellipsoidal piezoelectric inclusion. Compos Eng 4:1169–1182
21. Ikegami S, Ueda I, Nagata T (1971) Electromechanical properties of $PbTiO_3$ ceramics containing La and Mn. J Acoust Soc Am 50:1060–1066
22. Topolov VYu, Krivoruchko AV (2010) Ferroelectric $PbTiO_3$: from a single-domain state to composite components. In: Borowski M (ed) Perovskites: Structure, properties and uses. Nova Science Publishers, Hauppage, pp 481–499
23. COMSOL, Inc. COMSOLMultiphysics^{TM} user's guide (version 3.5a, 2008), http://www.comsol.com
24. Topolov VYu, Bisegna P, Bowen CR (2011) Analysis of the piezoelectric performance of modern 0–3-type composites based on relaxor-ferroelectric single crystals. Ferroelectrics 413:176–191
25. Hacksbusch W (1985) Multi-grid methods and applications. Springer, Berlin
26. Bowles JE (1996) Foundation analysis and design. McGraw-Hill, New York
27. Balkevich VL (1984) Technical ceramics. Stroyizdat, Moscow
28. Gorish AV, Dudkevich VP, Kupriyanov MF, Panich AE, Turik AV (1999) Piezoelectric device-making. Physics of ferroelectric ceramics, vol. 1. Radiotekhnika, Moscow (in Russian)
29. Zhang R, Jiang B, Cao W (2001) Elastic, piezoelectric, and dielectric properties of multidomain $0.67Pb(Mg_{1/3}Nb_{2/3})O_3$- $0.33PbTiO_3$ single crystals. J Appl Phys 90:3471–3475
30. Topolov VYu, Glushanin SV (2002) Effective electromechanical properties of ferroelectric piezoactive composites of the crystal-ceramic type based on $(Pb_{1-x}Ca_x)TiO_3$. Tech Phys Lett 28:279–282
31. Levassort F, Thi MP, Hemery H, Marechal P, Tran-Huu-Hue L-P, Lethiecq M (2006) Piezoelectric textured ceramics: effective properties and application to ultrasonic transducers. Ultrasonics 44:621–626

32. Taunaumang H, Guy IL, Chan HLW (1994) Electromechanical properties of 1–3 piezoelectric ceramic / piezoelectric polymer composites. J Appl Phys 76:484–489
33. Levassort F, Lethiecq M, Millar C, Pourcelot L (1998) Modeling of highly loaded 0–3 piezoelectric composites using a matrix method. IEEE Trans Ultrason Ferroelectr Freq Control 45:1497–1505
34. Topolov VYu, Glushanin SV, Panich AE (2004) Features of the piezoelectric response for a novel four-component composite structure. Ferroelectrics 308:53–65
35. Topolov VYu, Krivoruchko AV, Bisegna P (2008) Features of electromechanical properties of 1–3 composites based on $PbTiO_3$-type ceramics. J Phys D: Appl Phys 41:035406–035408
36. Ikeda T (1990) Fundamentals of piezoelectricity. Oxford University Press, Oxford, New York, Toronto
37. Topolov VYu, Krivoruchko AV (2009) Orientation effects in 2–2 piezocomposites based on $(1-x)Pb(A_{1/3}Nb_{2/3})O_3-xPbTiO_3$ single crystals (A = Mg or Zn). J Appl Phys 105:074105–074107
38. Sessler GM (1981) Piezoelectricity in polyvinylidenefluoride. J Acoust Soc Am 70:1596–1608
39. Zhang R, Jiang B, Cao W (2003) Single-domain properties of $0.67Pb(Mg_{1/3}Nb_{2/3})O_3 - 0.33PbTiO_3$ single crystals under electric field bias. Appl Phys Lett 82:787–789
40. Poizat C, Sester M (2001) Homogénéisation périodique de composites piézoélectriques 0–3: influence de la distribution. Rev Compos Matér Av 11:65–74

Chapter 6
Conclusions

Science is an edged tool, with which men play like children, and cut their own fingers.

A. Eddington

As niche applications become more prevalent in the future, composites and displacement-amplifying techniques and materials will proliferate in a continuing effort to widen the force–displacement envelope of performance. These devices, too, will become smarter and smarter as the applications demand.

G. H. Haertling

6.1 From Orientation Effects to a Large Anisotropy of Properties

Current challenges in the research field of composite materials are associated with the extension of the field of these materials from structural composites to functional and multifunctional composites [1] with the effective properties that depend on a large number of factors. The development of the composites for piezoelectric, pyroelectric and other functional applications can stimulate the manufacture of highly effective composites with tailored and predictable performance. In this context the orientation effects discussed in the present monograph broaden our outlook when studying the well-known *composition—structure—properties* relations [2, 3] in the piezo-active composites. Examination of the orientation effects has to lead to an improvement of the performance of the piezo-active composites, the anisotropy of their piezoelectric coefficients and ECFs, the hydrostatic piezoelectric response, etc. It is obvious that fundamental links between the domain orientations and electromechanical properties in modern relaxor-ferroelectric SCs with high piezoelectric activity rep-

V. Yu. Topolov et al., *Piezo-Active Composites*,
Springer Series in Materials Science 185, DOI: 10.1007/978-3-642-38354-0_6,

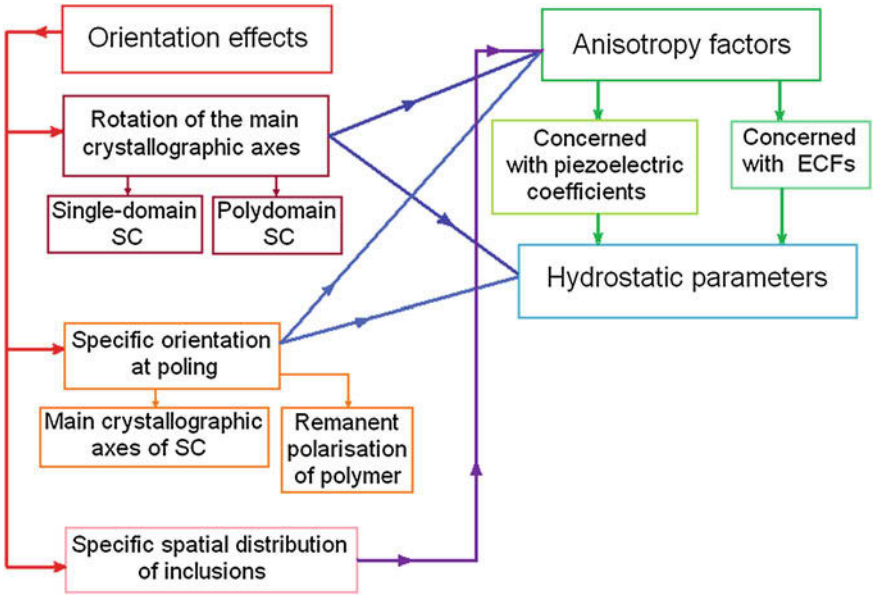

Fig. 6.1 Interconnections between the orientation effects, anisotropy factors and hydrostatic parameters in composites based on ferroelectric SCs

resent a considerable opportunity for improving the performance of the SC/polymer and SC/porous polymer composites. We have obtained new "freedom degrees" that enable us to have control over the piezoelectric performance and anisotropy of the novel composites. The orientation effects in the FC-based composites studied in the monograph are less pronounced, but are also important and should be taken into account when predicting performance and for future applications.

In Chap. 3–5 we have considered three main examples of the connectivity patterns, namely, 2–2, 1–3 and 0–3, and on their basis we have additionally analysed some modified composite architectures, for instance, 1–3–0 with a porous polymer matrix. As follows from our results, in the composites with porous polymers there are more opportunities to vary the piezoelectric coefficients, anisotropy factors and hydrostatic parameters in wide ranges. The additional "freedom degrees" associated with the porous structure (features of microgeometry, volume fraction, spatial distribution of pores, etc.) in the composite systems studied are of value for a variety of piezotechnical, hydroacoustic and other applications.

We represent the main trends in the current study by means of two diagrams (Figs. 6.1 and 6.2). These diagrams enable us to emphasise the role of various factors and interconnections which are concerned with the orientation effects, microgeometric and anisotropic characteristics of the composites discussed. It is clear that the issue of the large piezoelectric anisotropy, discussed mainly in papers on the $PbTiO_3$-type FCs [4–6] in the 1980–1990s, can be solved in different ways, for

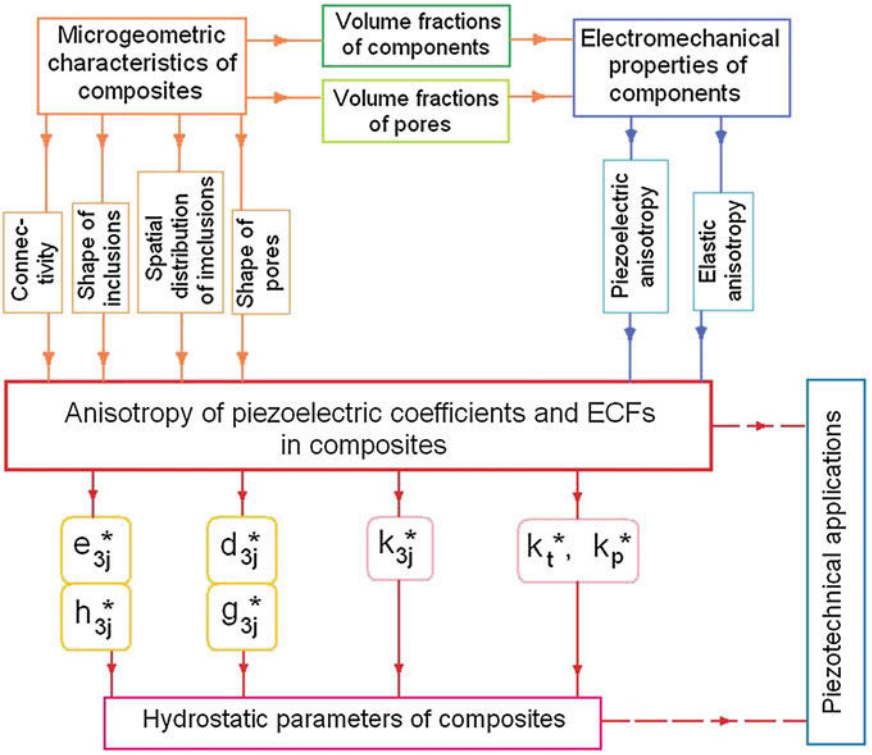

Fig. 6.2 *Microgeometry—properties—anisotropy* relations in piezo-active composites

instance, by creating highly anisotropic composites containing a SC component with considerable piezoelectric activity and a porous polymer matrix; along with taking into account features of the orientation dependence of the electromechanical properties of the SC component and forming a specific porous structure in the polymer medium. Solving this problem in the composite (not FC) field, we find new important relations between microgeometry and electromechanical properties of the composite (Fig. 6.2), and these findings are to be taken into consideration in manufacturing new composites and further applications.

Knowledge of the aforementioned interconnections (see Figs. 6.1 and 6.2) can lead to an improvement of the piezoelectric performance and anisotropy factors of the composites based on ferroelectrics. Undoubtedly, the diagrams shown in Figs. 6.1 and 6.2 may be reinforced in future studies devoted to the advanced composites based on ferroelectrics or related materials. It is clear, that due to many additional microgeometric, technological and other factors, it is impossible to draw a universal picture of methods of improving the performance of the piezo-active composite or controlling its anisotropy factors even in a restricted range. In this case we would like

to finish with the following words by P. Valéry: “Science means simply the aggregate of all the recipes that are always successful. The rest is literature”.

References

1. Chung DDL (2010) Composite materials: science and applications. Springer, London
2. Newnham RE (2005) Properties of materials: anisotropy, symmetry, structure. Oxford University Press, New York
3. Topolov VYu, Bowen CR (2009) Electromechanical properties in composites based on ferroelectrics. Springer, London
4. Gururaja TR, Jang SJ, Cross LE (1986) Electromechanical anisotropy in modified lead titanate ceramics. In: ISAF’86: Proceedings of the 6^{th} IEEE International symposium on applications of ferroelectrics, Bethlehem, PA, 8–10 June, 1986 (New York), pp 344–347.
5. Ichinose N, Fuse Y, Yamada Y, Sato R (1989) Piezoelectric anisotropy in the modified $PbTiO_3$ ceramics. Jpn J Appl Phys 28(Suppl. 28–2):87–90
6. Turik AV, Topolov VYu (1997) Ferroelectric ceramics with a large piezoelectric anisotropy. J Phys D 30:1541–1549

Appendix A
Abbreviations

ECF	Electromechanical coupling factor
EFM	Effective field method
EMM	Effective medium method
FC	Ferroelectric ceramic
FEM	Finite element method
MPB	Morphotropic phase boundary
PCR	Piezoelectric ceramic from Rostov-on-Don (Russia)
PE	Polyethylene
PIN–*x*–*y*	Relaxor-ferroelectric solid solutions of $x\mathrm{Pb}(\mathrm{In}_{1/2}\mathrm{Nb}_{1/2})\mathrm{O}_3 - y\mathrm{Pb}(\mathrm{Mg}_{1/3}\mathrm{Nb}_{2/3})\mathrm{O}_3 - (1-x-y)\mathrm{PbTiO}_3$
PMN–*x*PT	Relaxor-ferroelectric solid solutions of $(1-x)\mathrm{Pb}(\mathrm{Mg}_{1/3}\mathrm{Nb}_{2/3})\mathrm{O}_3 - x\mathrm{PbTiO}_3$
PVDF	Polyvinylidene fluoride
PZN–*x*PT	Relaxor-ferroelectric solid solutions of $(1-x)\mathrm{Pb}(\mathrm{Zn}_{1/3}\mathrm{Nb}_{2/3})\mathrm{O}_3 - x\mathrm{PbTiO}_3$
PZT	Piezoelectric ceramic of the $\mathrm{Pb(Zr, Ti)O_3}$ type
SC	Single crystal
VDF-TrFE	75/25 mol.% copolymer of vinylidene fluoride and trifluoroethylene

V. Yu. Topolov et al., *Piezo-Active Composites*,
Springer Series in Materials Science 185, DOI: 10.1007/978-3-642-38354-0,

Appendix B
Electromechanical Constants of Components

To predict the effective properties and related parameters of a piezo-active composite, we have used full sets of electromechanical constants of components such as ferroelectric and relaxor-ferroelectric SCs (either single-domain or domain-engineered), FCs and polymers. The constants involved in (1.4)–(1.7) were measured at room temperature. A systematisation of data on the components is given in Table B.1.

V. Yu. Topolov et al., *Piezo-Active Composites*,
Springer Series in Materials Science 185, DOI: 10.1007/978-3-642-38354-0,

Table B.1 Electromechanical constants of components at room temperature

Component	Composition	Set of constants	Table number
SC	PMN–0.33PT[a]	s^E_{ab}, d_{ij} and ε^σ_{pp}	1.1
	PMN–0.33PT[b]	s^E_{ab}, d_{ij} and ε^σ_{pp}	2.1
	PMN–0.33PT[a]	c^E_{ab}, e_{ij} and ε^ξ_{pp}	5.2
	PMN–0.30PT[a]	s^E_{ab}, d_{ij} and ε^σ_{pp}	1.1
	PMN–0.28PT[a]	s^E_{ab}, d_{ij} and ε^σ_{pp}	1.1
	PMN–0.28PT[a,b,c]	s^E_{ab}, d_{ij} and ε^σ_{pp}	3.2
	PZN–0.12PT[b]	s^E_{ab}, d_{ij} and ε^σ_{pp}	2.2
	PZN–0.08PT[a]	s^E_{ab}, d_{ij} and ε^σ_{pp}	1.1
	PZN–0.07PT[a]	s^E_{ab}, d_{ij} and ε^σ_{pp}	1.1
	PZN–0.07PT[c]	s^E_{ab}, d_{ij} and ε^σ_{pp}	3.6
	PZN–0.045PT[a]	s^E_{ab}, d_{ij} and ε^σ_{pp}	1.1
	PIN–0.24–0.49[b]	s^E_{ab}, d_{ij} and ε^σ_{pp}	2.3
	PIN–0.27–0.40[b]	s^E_{ab}, d_{ij} and ε^σ_{pp}	2.3
	PIN–*x*–*y*[b]	s^E_{ab}, d_{ij} and ε^σ_{pp}	2.3
	$PbTiO_3$[b]	s^E_{ab}, d_{ij} and ε^σ_{pp}	1.1
FC	Compositions with perovskite-type structure ($BaTiO_3$, PZT, PCR, ZTS, modified $PbTiO_3$, PMN–0.35PT, *etc*.)	s^E_{ab}, d_{ij} and ε^σ_{pp}	1.2
	Modified $PbTiO_3$	c^E_{ab}, e_{ij} and ε^ξ_{pp}	5.1
	ZTS-19	c^E_{ab}, e_{ij} and ε^ξ_{pp}	5.1
	PMN–0.35PT	c^E_{ab}, e_{ij} and ε^ξ_{pp}	5.2
Polymer	Araldite	s_{ab} and ε_{pp}	3.1
	Araldite	c_{ab} and ε_{pp}	5.2
	Polyurethane	s_{ab} and ε_{pp}	3.1
	Elastomer	s_{ab} and ε_{pp}	3.1
	PVDF	s^E_{ab}, d_{ij} and ε^σ_{pp}	3.3
	VDF-TrFE	c^E_{ab}, e_{ij} and ε^ξ_{pp}	5.2

[a] $[001]_c$-poled domain-engineered SC
[b] Single-domain SC
[c] $[011]_c$-poled domain-engineered SC

About the Authors

Vitaly Yuryevich Topolov was born in Rostov-on-Don, Russia (former USSR) on November 8th, 1961. He received the qualification "Physicist. Educator" (honours degree) in 1984 along with the degrees "Candidate of Sciences (Physics and Mathematics)" and "Doctor of Sciences (Physics and Mathematics)" in 1987 and 2000, respectively, all from the Rostov State University, Russia. From 1987 to 1991, he worked as a research scientist of the Institute of Physics at the Rostov State University. From 1991 to 2000, he worked as a Senior Lecturer (1991–1992) and an Associate Professor (1992–2000) of the Department of Physics at the Rostov State University. Since 2000, he has been Professor of the same Department. Since December 2006, after reforming the Rostov State University, he is Professor of the Department of Physics at the Southern Federal University (Rostov-on-Don, Russia).

Dr. V. Yu. Topolov was also a visiting scientist at the Moscow State University, Russia (former USSR, 1989), University of Saarland, Germany (1994–1995), Aachen University of Technology–RWTH Aachen, Germany (1998), Karlsruhe Research Center, Germany (2002 and 2003–2004), University of Bath, UK (2006, 2007, 2012, and 2013), and University of Rome "Tor Vergata", Italy (2008). His research interests include heterogeneous ferroelectrics, smart materials, domain and heterophase structures, as well as electromechanical effects in ferroelectrics and related materials. He earned the special award from the International Science Foundation (1993) and the Soros Associate Professor title and awards from the International Soros Science-Educational Program and the Open Society Institute (1997, 1998, 2000, and 2001). He presented the best poster at the International Symposium on Ferroelectric Domains (China, 2000), the best oral report at the International Conference on Relaxation Phenomena in Solids (Russia, 2010), the best training aids in the Department of Physics, Southern Federal University (Russia, 2006 and 2011), and the best research works in the Department of High Technologies, Southern Federal University (Russia, 2008 and 2011). He is author of two monographs published at *Springer* (London, UK, 2009, and Berlin, Heidelberg, Germany, 2012), four chapters in monographs published at *Nova Science Publishers* (New York, USA, 2010–2012), and over 350 scientific papers, reviews, conference proceedings, and abstracts. Dr. V. Yu. Topolov has been included in the list of Active Russian Scientists five times: his papers have

V. Yu. Topolov et al., *Piezo-Active Composites*,
Springer Series in Materials Science 185, DOI: 10.1007/978-3-642-38354-0,

been cited over 100 times in periodicals from 2000 to 2006, from 2001 to 2007, from 2002 to 2008, from 2003 to 2009, and from 2005 to 2011.

Honorary co-worker of Higher Professional Education of the Russian Federation (Ministry of Education and Science of the Russian Federation, Moscow, Russia, 2009). Member of the International Biographical Centre Top 100 Educators (Cambridge, UK, 2010) and Top 100 Scientists (Cambridge, UK, 2012). Biographical data by Dr. V. Yu. Topolov have been published in "Dictionary of International Biography" (*IBC*, Cambridge, UK), "2000 Outstanding Intellectuals of the 21st Century" (*IBC*, Cambridge, UK) and "Who's Who in the World" (*Marquis*, New Providence, USA).

Paolo Bisegna was born on June 13th, 1968. He received the M.Sc. degree in engineering from the University of Naples "Federico II", Naples, Italy, in 1991, and the M.Sc. degree in mathematics from the University of Rome "Tor Vergata", Rome, Italy, in 1994, where he received the M.D. degree from the School of Medicine in 2006. From 1992 to 1994 he worked as a research assistant for the Italian National Research Council. From 1994 to 2000 he worked as an Assistant Professor in the Department of Civil Engineering, University of Rome "Tor Vergata". Since 2001, he has been Professor of Mechanics of the same Department. Since 2012, after reforming the University of Rome "Tor Vergata", he is Professor of the Department of Civil Engineering and Computer Science. In 2000 he has been visiting scholar, Department of Mathematics, Northwestern University, Evanston, IL, USA. Since 2001, he has been yearly visiting scholar at the Department of Mathematics, Vanderbilt University, Nashville, TN, USA. Since 2011, he is Program Director of the Biomedical Engineering Program, University of Rome "Tor Vergata", and Director of the Structural Engineering Doctoral Program, University of Rome "Tor Vergata" (Italy). He served as a Reviewer for over 30 international journals. He is a Member of the Editorial Board for *Annals of Solid and Structural Mechanics* (*Springer*).

His research interests are concerned with piezoelectric composites, smart materials, ferroelectric ceramics and composites for modern sensors and actuators. Additional research interest includes: finite elements, mechanics of materials, structural dynamic, biomechanics, biomedical engineering, biomathematics. He has published over 120 journal papers, chapters in monographs, and articles in conference proceedings. His research activity is currently funded by national and international institutions, including Italian Department of University Research and 7th Framework Programme, SME-2011 (DIMID, Grant Agreement No. 286692).

Christopher Rhys Bowen was born on January 18th, 1968 and grew up in Beddau, South Wales (UK). He earned a BSc (First Class) in Materials Science at the School of Materials, University of Bath, UK in 1990 and worked on his DPhil thesis in ceramic manufacture under the supervision of Prof. Brian Derby in the Department of Materials, University of Oxford, UK in 1990–1993 (PhD awarded in 1994). In 1993 – 1994, he worked as a Researcher in the Advanced Ceramics Group at the Technical University of Hamburg-Harburg (TUHH), Germany under the supervision of Prof. Nils Claussen. From 1994 to 1996, he was research fellow at the School of Materials, University of Leeds, UK working with Prof. Ron Stevens. From 1996 to

1998, he was a Senior Scientist at the Defence Evaluation and Research Agency (DERA), Functional Materials Group, UK working on ferroelectric ceramics and composites. He joined the University of Bath, UK in August 1998 and is now a Professor at the same University.

The research interests of Dr. C. R. Bowen are concerned with functional ceramics, including ferroelectric ceramics and composites for modern sensors and actuators, as well as with manufacturing and characterisation of these materials. Additional interest includes the use of piezoelectric materials combined with structural composites, such as bistable laminates, for energy harvesting and shape changing applications. He earned the Thornton and Hazelwood prizes for academic work (1986–1990), Institute of Materials National Lecture Competition award (1993), SET award (2002), and John Willis award for excellence in research and teaching (2003). Dr. C. R. Bowen has published over 200 scientific papers, conference proceedings, and abstracts. He has recently been awarded an ERC Advanced Fellowship in Novel Energy Materials, Engineering Science and Integrated Systems (NEMESIS, Grant Agreement No. 320963), and this support is greatly acknowledged.

Index

V. Yu. Topolov et al., *Piezo-Active Composites*,
Springer Series in Materials Science 185, DOI: 10.1007/978-3-642-38354-0,